Site directed molecular design and performances of Interferon-α2a and Interleukin-4 bioconjugates with PEG alternative polymers

Dissertation zur Erlangung des naturwissenschaftlichen Doktorgrades der

Julius-Maximilians-Universität Würzburg

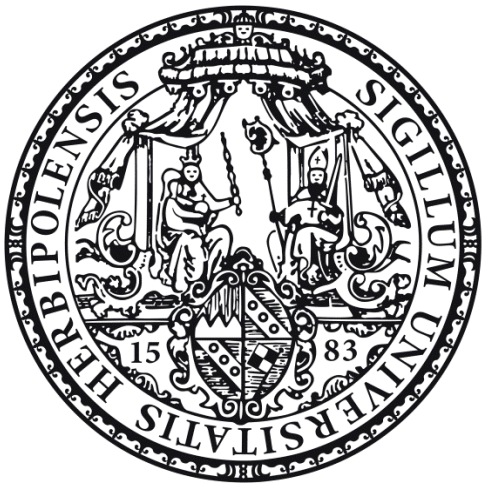

vorgelegt von

Niklas Hauptstein

aus Bad Laer

Würzburg 2022

Eingereicht bei der Fakultät für Chemie und Pharmazie am

Gutachter der schriftlichen Arbeit

1. Gutachter: Prof. Dr. Dr. Lorenz Meinel

2. Gutachter:

Prüfer des öffentlichen Promotionskolloquiums

1. Prüfer: Prof. Dr. Dr. Lorenz Meinel

2. Prüfer:

3. Prüfer:

Datum des öffentlichen Promotionskolloquiums:

Doktorurkunde ausgehändigt am:

Die vorliegende Arbeit wurde in der Zeit von Januar 2018 bis Juli 2022 am Institut für Pharmazie und Lebensmittelchemie der Bayerischen Julius-Maximilians-Universität Würzburg unter der Anleitung von Herrn Prof. Dr. Dr. Lorenz Meinel und Frau Prof. Dr. Tessa Lühmann angefertigt.

Inhaltsverzeichnis

Summary

Serum half-life elongation as well as the immobilization of small proteins like cytokines is still one of the key challenges for biologics. This accounts also for cytokines, which often have a molecular weight between 5 and 40 kDa and are therefore prone to elimination by renal filtration and sinusoidal lining cells. To solve this problem biologics are often conjugated to poly(ethylene glycol) (PEG), which is the gold standard for the so called PEGylation. PEG is a synthetic, non-biodegradable polymer for increasing the hydrodynamic radius of the conjugated protein to modulate their pharmacokinetic performance and prolong their therapeutic outcome. Though the benefits of PEGylation are significant, they also come with a prize, which is a loss in bioactivity due to steric hindrance and most often the usage of heterogeneous bioconjugation chemistries. While PEG is a safe excipient in most cases, an increasing number of PEG related side-effects, such as immunological responses like hypersensitivity and accelerated blood clearance upon repetitive exposure occur, which highlights the need for PEG alternative polymers, that can replace PEG in such cases.

Another promising method to significantly prolong the residence time of biologics is to immobilize them at a desired location. To achieve this, the transglutaminase (TG) Factor XIIIa (FXIIIa), which is an important human enzyme during blood coagulation can be used. FXIIIa can recognize specific peptide sequences that contain a lysine as substrates and link them covalently to another peptide sequence, that contains a glutamine, forming an isopeptide bond. This mechanism can be used to link modified proteins, which have a N- or C-terminal incorporated signal peptide by mutation, to the extracellular matrix (ECM) of tissues.

Additionally, both above-described methods can be combined. By artificially introducing a TG recognition sequence, it is possible to attach an azide group containing peptide site-specifically to the TG, recognition sequence. This allows the creation of a site-selective reactive site at the proteins N- or C-terminus, which can then be targeted by cyclooctyne functionalized polymers, just like amber codon functionalized proteins.

This thesis has focused on the two cytokines human Interferon-α2a (IFN-α2a) and human, as well as murine Interleukin-4 (IL-4) as model proteins to investigate the above-described challenges. IFN-α2a has been chosen as a model protein because it is an approved drug since 1986 in systemic applications against some viral infections, as well as several types of cancer. Furthermore, IFN-α2 is also approved in three PEGylated forms, which have different molecular weights and use different conjugation techniques for polymer attachment. This turns it into an ideal candidate to compare new polymers against the gold standard PEG. Interleukin-4 (IL-4) has been chosen as the second model protein due to its similar size and biopotency. This allows to compare found trends from IFN-α2a with another bioconjugate platform and distinguish between IFN-α2a specific, or general trends. Furthermore, IL-4

is a promising candidate for clinical applications as it is a potent anti-inflammatory protein, which polarizes macrophages from the pro-inflammatory M1 state into the anti-inflammatory M2 state.

Chapter 1 – gives an overview of the currently available IFN drugs as well as their clinical usage. Additionally, standard bioconjugation techniques that are used by the pharmaceutical industry to produce PEGylated IFNs are described, including the consequential influences on the bioconjugate. Finally, this chapter gives an overview of the different routes of IFN application and finishes with an outlook on the future potential of IFNs and IFN bioconjugates.

Chapter 2 – investigates 10 kDa linear polyglycerol (LPG) and poly-(2-ethyl-2-oxazoline) (PEtOx) as PEG alternative polymers for bioconjugation. For this approach, IFN-α2a has been site-specifically functionalized with an azide group by using the amber codon expansion technology to create a potent cytokine that can be easily conjugated by copper free click chemistry to cyclooctyne functionalized polymers. This results in homogenous bioconjugates. The study highlights the impact of the polymer's different hydrophilicities, regarding their *in vitro* potencies and thermal stability, which is achieved by using *in vitro* and *in silico* methods. Finally, the interaction of the polymers with the proteins surface is investigated by using a limited proteolysis approach and *in silico* calculations.

Chapter 3 – continues the research of chapter 2 but has put a focus on longer LPGs and PEG polymers with molecular weights between 20 and 40 kDa, which are required for a therapeutically relevant half-life. It uses the same azide functionalized IFN-α2a protein as in chapter 2 for conjugation to guarantee comparability. The study characterizes the bioconjugates in detail with respect to the bioconjugates hydrodynamic size, hydrophilicity, and thermal stability, as well as the sole polymers. Furthermore, the study investigates important biologic parameters, including the bioconjugates, *in vitro* potencies, as well as their pharmacokinetic profile in an *in vivo* mice study.

Chapter 4 – completes the work of chapter 2 and 3 by investigating longer cyclooctyne functionalized PEtOx polymers of up to 25 kDa, using the same IFN-α2a azide mutant to create hydrodynamic radii balanced bioconjugates for acute virus infections, which are analyzed with similar experiments as in chapter 3. The resulting PEtOx bioconjugates yield lasting exposure in mice and disease-modifying effects in IAV-infected ferrets, in contrast to their PEG counterparts, highlighting their potential in future medical applications.

Chapter 5 – investigates similar aspects, which are already discussed in chapter 2 and 3 for IFN-α2a, but uses human IL-4 as a model protein. In contrast to chapter 2 and 3 a wildtype protein was used and a site-specific modification was achieved by reductive alkylation, utilizing the higher pka value of a proteins N-terminus compared to side chain amines for site specific modification. As performed in chapter 2 and 3, the bioconjugates are characterized in detail and important biological, as well as physico- chemical parameters are investigated. This includes their hydrodynamic size, human serum albumin (HSA) binding affinity and *in vitro* bioactivity. Additionally, LPGs antigenicity to PEG IgG

antibodies is investigated for the polymers and bioconjugates by surface plasmon resonance spectroscopy and ELISA.

Chapter 6 – uses an enzymatic approach for the conjugation of polymers. In this study, murine IL-4 was C-terminally elongated with a TG recognition sequence. This TG recognition sequence was recognized by FXIIIa to covalently attach an azide bearing peptide. The azide bearing peptide can then be targeted as a reactive group by cyclooctyne modified polymers, like it was already performed in chapter 2, 3 and 4. The compared polymers are PEG and PEtOx. The protein and resulting bioconjugates were characterized for their physico-chemical and biological properties, similar to the previous chapters. Additionally enzymatic functionalization by FXIIIa was optimized.

Chapter 7 – utilizes FXIIIa for the enzymatic immobilization of modified IFN-α2a on cell surfaces. For this purpose, two IFN-α2a mutants were designed that are recognized by FXIIIa and can be immobilized on extra cellular matrix (ECM). The mutants were characterized for their *in vitro* bioactivity, their ability to be immobilized by FXIIIa on ECM and their ability to be cleaved at an artificially inserted sensitive linker by the matrix metallopeptidase 9 (MMP-9) in solution and after being immobilized on ECM. MMP-9 is secreted by immune cells like macrophages and neutrophils upon stimulation, which occurs after pathogen infiltration of tissues.

In summary, the presented work gives a detailed comparison of LPG and PEtOx attributes in comparison to PEG as alternatives for bioconjugation. This detailed characterization allows a precise evaluation of these two PEG alternative polymers and rates them in the tested areas to be mostly similar in performance. Therefore, LPG and PEtOx are two reasonable PEG alternative polymers, which should be considered for medical application.

Additionally, a novel IFN-α2a mutant is described, that can be immobilized on tissue surfaces by FXIIIa and can be released by MMP-9. The described mutant shows promising results for the intended pulmonic application by nebulization and will be tested *in vivo* in the close future.

Zusammenfassung

Die Verlängerung der Serum-Halbwertszeit sowie die Immobilisierung kleiner Proteine wie Zytokine ist nach wie vor eine der größten Herausforderungen für Biologika. Dies gilt auch für Zytokine, die häufig ein Molekulargewicht zwischen 5 und 40 kDa haben und daher leicht durch die Nierenfiltration und sinusoidale Endothelzellen eliminiert werden können. Um dieses Problem zu lösen, werden Biologika häufig an Poly(ethylenglykol) (PEG) konjugiert, das den Goldstandard für die so genannte PEGylierung darstellt. PEG ist ein synthetisches, biologisch nicht abbaubares Polymer, das den hydrodynamischen Radius des konjugierten Proteins vergrößert, um die pharmakokinetische Leistung zu modulieren und die therapeutische Wirkung zu verlängern. Obwohl die Vorteile der PEGylierung beträchtlich sind, haben sie auch ihren Preis, nämlich einen Verlust an Bioaktivität aufgrund sterischer Hindernisse und meist die Verwendung heterogener Biokonjugationstechniken. Obwohl PEG in den meisten Fällen ein sicherer Hilfsstoff ist, treten immer mehr PEG-bedingte Nebenwirkungen auf, wie z. B. immunologische Reaktionen wie Überempfindlichkeit und beschleunigter Abbau bei wiederholter Exposition, was den Bedarf an alternativen PEG-Polymeren unterstreicht, die PEG in solchen Fällen ersetzen können.

Eine weitere vielversprechende Methode, um die Verweildauer von Biologika deutlich zu verlängern, besteht darin, sie an einem gewünschten Ort zu immobilisieren. Dazu kann die Transglutaminase (TG) Faktor XIIIa (FXIIIa) verwendet werden, die ein wichtiges menschliches Enzym bei der Blutgerinnung ist. FXIIIa kann bestimmte Peptidsequenzen, die ein Lysin enthalten, als Substrate erkennen und sie kovalent an eine andere Peptidsequenz, die ein Glutamin enthält, binden, wobei eine Isopeptidbindung entsteht.

Dieser Mechanismus kann benutzt werden um modifizierte Proteine, welche durch Mutation ein N- oder C-terminal eingebautes Signalpeptid besitzen, mit der extrazellularen Gewebematrix (ECM) zu verknüpfen.

Diese Arbeit konzentriert sich auf die beiden Zytokine humanes Interferon-α2a (IFN-α2a) und humanes sowie murines Interleukin-4 (IL-4) als Modellproteine, um die oben beschriebenen Herausforderungen zu untersuchen. IFN-α2a wurde als Modellprotein ausgewählt, weil es seit 1986 ein zugelassenes Medikament für die systemische Anwendung gegen einige Virusinfektionen und verschiedene Krebsarten ist. Darüber hinaus ist IFN-α2 auch in drei PEGylierten Formen zugelassen, die unterschiedliche Molekulargewichte haben und verschiedene Konjugationstechniken für die Polymeranbindung verwenden. Dies macht es zu einem idealen Kandidaten für den Vergleich neuer Polymere mit dem Goldstandard PEG. Interleukin-4 (IL-4) wurde als zweites Modellprotein gewählt, da es eine ähnliche Größe und Biopotenz aufweist. Dies ermöglicht es, die von IFN-α2a gefundenen Trends mit einer anderen Biokonjugat-Plattform zu vergleichen und zwischen IFN-α2a-spezifischen und allgemeinen Trends zu unterscheiden. Darüber hinaus ist IL-4 ein vielversprechender Kandidat für

klinische Anwendungen, da es ein starkes entzündungshemmendes Protein ist, das Makrophagen vom entzündungsfördernden M1-Zustand in den entzündungshemmenden M2-Zustand polarisiert.

Kapitel 1 – gibt einen Überblick über die derzeit verfügbaren IFN-Medikamente und ihre klinische Verwendung. Darüber hinaus werden Standard-Biokonjugationstechniken beschrieben, die von der pharmazeutischen Industrie zur Herstellung von PEGylierten IFNs verwendet werden, einschließlich der sich daraus ergebenden Einflüsse auf das Biokonjugat. Schließlich gibt dieses Kapitel einen Überblick über die verschiedenen Wege der IFN-Anwendung und schließt mit einem Ausblick auf das künftige Potenzial von IFNs.

Kapitel 2 – untersucht 10 kDa lineares Polyglycerin (LPG) und Poly-(2-ethyl-2-oxazolin) (PEtOx) als alternative PEG-Polymere für die Biokonjugation.Für diesen Ansatz wurde IFN-α2a mit Hilfe der Amber-Codon-Expansionstechnologie ortsspezifisch mit einer Azidgruppe funktionalisiert, um ein potentes Zytokin zu entwickeln, das durch kupferfreie Click-Chemie leicht an Cyclooctin-funktionalisierte Polymere konjugiert werden kann. Dies führt zu homogenen Biokonjugaten. Die Studie beleuchtet die Auswirkungen der unterschiedlichen Hydrophilie der Polymere auf ihre *In-vitro*-Potenz und ihre thermische Stabilität, die mit Hilfe von *In-vitro*- und *In-silico*-Methoden ermittelt wird. Schließlich wird die Wechselwirkung der Polymere mit der Oberfläche der Proteine mit Hilfe eines limitierten Proteolyse-Ansatzes und *In-silico*-Berechnungen untersucht.

Kapitel 3 – setzt die Forschungsarbeiten aus Kapitel 2 fort, konzentriert sich aber auf längere LPGs und PEG-Polymere mit Molekulargewichten zwischen 20 und 40 kDa, die für eine therapeutisch relevante Halbwertszeit erforderlich sind. Für die Konjugation wird dasselbe azidfunktionalisierte IFN α2a-Protein wie in Kapitel 2 verwendet, um die Vergleichbarkeit zu gewährleisten. In der Studie werden die Biokonjugate im Hinblick auf ihre hydrodynamische Größe, Hydrophilie und thermische Stabilität sowie die alleinigen Polymere detailliert charakterisiert. Darüber hinaus werden in der Studie wichtige biologische Parameter, einschließlich der *In-vitro*-Potenzen der Biokonjugate, sowie ihres pharmakokinetischen Profils in einer *In-vivo*-Studie an Mäusen untersucht.

Kapitel 4 – vervollständigt die Arbeit von Kapitel 2 und 3 durch die Untersuchung längerer Cyclooctin-funktionalisierter PEtOx-Polymere von bis zu 25 kDa unter Verwendung derselben IFN-α2a-Azid-Mutante zur Herstellung von Biokonjugaten mit angepassten hydrodynamischen Radien für akute Virusinfektionen, die mit ähnlichen Experimenten wie in Kapitel 3 analysiert werden. Die resultierenden Biokonjugate führen zu einer dauerhaften Stimulierung bei Mäusen und zu krankheitsmodifizierenden Effekten bei IAV-infizierten Frettchen, im Gegensatz zu den PEG Biokonjugaten, was ihr Potenzial für zukünftige medizinische Anwendungen unterstreicht.

Kapitel 5 – untersucht ähnliche Aspekte, die bereits in Kapitel 2 und 3 für IFN-α2a erörtert wurden, verwendet jedoch menschliches IL-4 als Modellprotein. Im Gegensatz zu Kapitel 2 und 3 wurde ein Wildtyp-Protein verwendet und eine ortsspezifische Modifikation durch reduktive Alkylierung erreicht,

wobei der höhere pka-Wert des N-Terminus eines Proteins im Vergleich zu Seitenkettenaminen für die ortsspezifische Modifikation genutzt wurde. Wie in Kapitel 2 und 3 ausgeführt, werden die Biokonjugate detailliert charakterisiert und wichtige biologische sowie physikalisch-chemische Parameter untersucht. Dazu gehören die hydrodynamische Größe, die Bindungsaffinität an humanes Serumalbumin (HSA) und die *in vitro* Bioaktivität. Zusätzlich wird die Antigenität der LPGs gegenüber PEG-IgG-Antikörpern für die Polymere und Biokonjugate mittels Oberflächenplasmonen-resonanzspektroskopie und ELISA untersucht.

Kapitel 6 – verwendet einen enzymatischen Ansatz für die Konjugation von Polymeren. In dieser Studie wurde murines IL-4 mit einer TG-Erkennungssequenz C-terminal verlängert. Diese TG-Erkennungssequenz wurde von FXIIIa erkannt, um ein azidhaltiges Peptid kovalent zu binden. Das Azid-tragende Peptid kann dann als reaktive Gruppe durch Cyclooctin-modifizierte Polymere angegriffen werden, wie es bereits in Kapitel 2, 3 und 4 durchgeführt wurde. Die verglichenen Polymere sind PEG und PEtOx. Das Protein und die resultierenden Biokonjugate wurden auf ihre physikalisch-chemischen und biologischen Eigenschaften hin charakterisiert, ähnlich wie in den vorherigen Kapiteln. Zusätzlich wurde die enzymatische Funktionalisierung durch FXIIIa optimiert.

Kapitel 7 – nutzt FXIIIa für die enzymatische Immobilisierung von modifiziertem IFN-α2a auf Zelloberflächen. Zu diesem Zweck wurden zwei IFN-α2a-Mutanten entwickelt, die von FXIIIa erkannt werden und auf extrazellulärer Matrix (ECM) immobilisiert werden können. Die Mutanten wurden hinsichtlich ihrer *In-vitro*-Bioaktivität, ihrer Fähigkeit, von FXIIIa auf der ECM immobilisiert zu werden, und ihrer Fähigkeit, an einem künstlich eingefügten empfindlichen Linkem von der Matrix-Metallopeptidase 9 (MMP-9) in Lösung und nach Immobilisierung auf der ECM gespalten zu werden, charakterisiert. MMP-9 wird von Immunzellen wie Makrophagen und Neutrophilen sezerniert, wenn sie nach dem Eindringen von Pathogenen in das Gewebe stimuliert werden.

Zusammenfassend enthält die präsentierte Arbeit einen detaillierten Vergleich zwischen den Eigenschaften von LPG und PEtOx im Vergleich zu PEG als Alternativen für die Biokonjugation. Die detaillierte Charakterisierung erlaubt eine präzise Evaluation dieser zwei PEG alternativen Polymere und stuft diese in den getesteten Bereichen als sehr ähnlich zu PEG ein. Daher sind LPG und PEtOx zwei aussichtsreiche PEG alternative Polymere, welche für die medizinische Anwendung in Betracht gezogen werden sollten.

Darüber hinaus wird eine neuartige IFN-α2a-Mutante beschrieben, die durch FXIIIa auf Gewebeoberflächen immobilisiert und durch MMP-9 freigesetzt werden kann. Die beschriebene Mutante zeigt vielversprechende Ergebnisse für die beabsichtigte pulmonale Anwendung durch Vernebelung und soll in naher Zukunft *in vivo* getestet werden.

Chapter 1 - Bioconjugation strategies and clinical implications of Interferon-bioconjugates

Niklas Hauptstein, Lorenz Meinel, Tessa Lühmann*

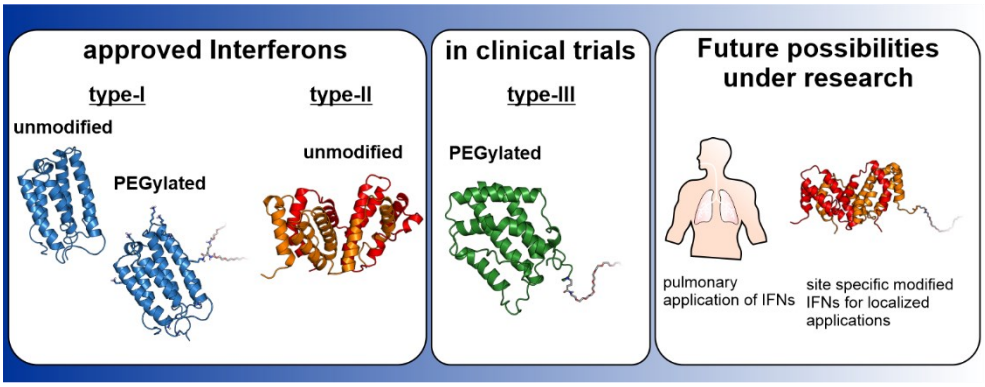

Keywords: Interferon; bioconjugation; lung delivery; PEGylation; protein-engineering

Reprinted (adapted) with permission from: Hauptstein, N.; Meinel, L.; Lühmann, T., Bioconjugation strategies and clinical implications of Interferon-bioconjugates. Eur. J. Pharm. Biopharm. 2022, 172, 157-167, DOI: 10.1016/j.ejpb.2022.02.006. Copyright 2022, Elsevier.

Abstract

Interferons (IFN) are immunomodulating, antiviral and antiproliferative cytokines for treatment of multiple indications, including cancer, hepatitis, and autoimmune disease. The first IFNs were discovered in 1957, first approved in 1986, and are nowadays listed in the WHO model list of essential Medicines. Three classes of IFNs are known; IFN-α2a and IFN-β belonging to type-I IFNs, IFN-γ a type-II IFN approved for some hereditary diseases and IFN-λs, which form the newest class of type-III IFNs. IFN-λs were discovered in the last decade with fascinating yet under discovered pharmaceutical potential. This article reviews available IFN drugs, their field and route of application, while also outlining available and future strategies for bioconjugation to further optimize pharmaceutical and clinical performances of all three available IFN classes.

Overview of Interferon pharmacology

Interferons (IFNs) are a group of small proteins (19-33 kDa of the class II cytokine family) [2]. Three IFN classes are known, referred to as type-I, type-II and type-III, respectively [3, 4]. Within these classes, 22 different IFNs (17 x type-I, 1x type-II and 4x type-III IFNs) are known, acting through three different heterodimeric receptors.

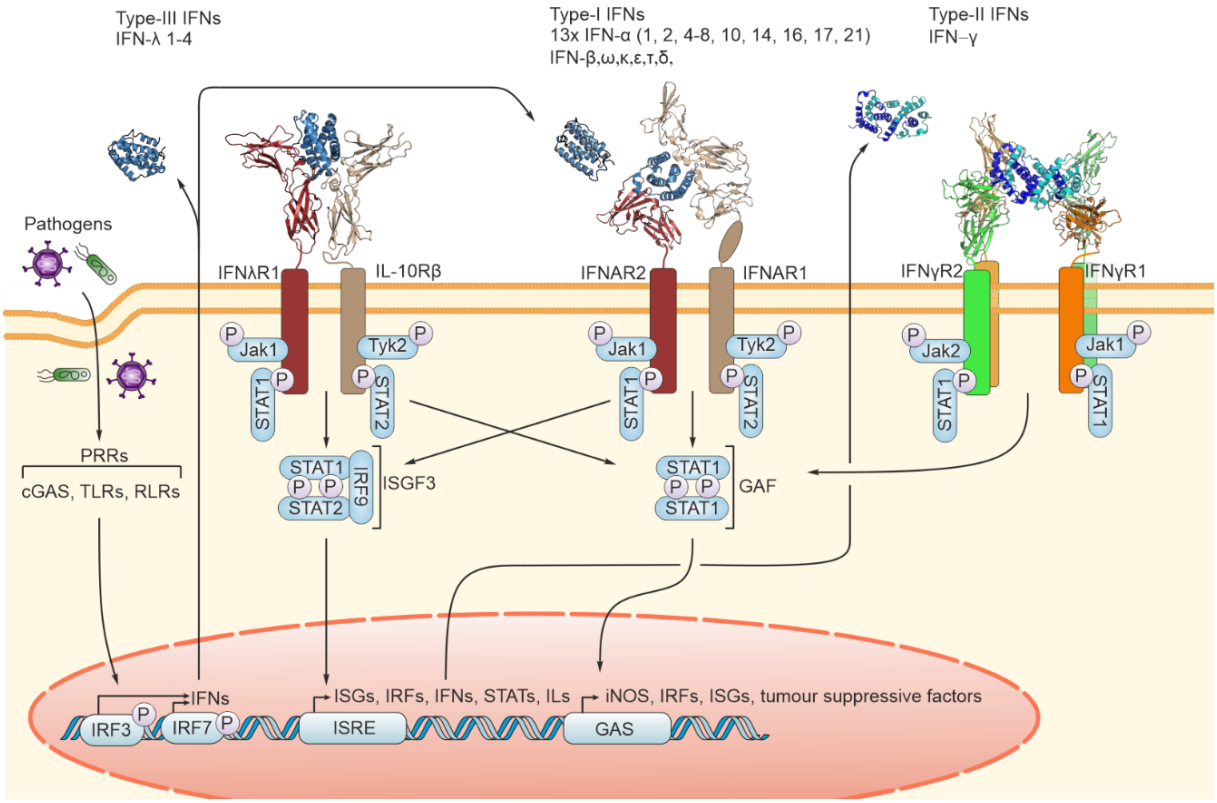

Figure 1: Simple schematic presentation of IFN signalling pathways. Initially pathogens are recognised by PRRs that stimulate the release of type-I and type-III IFNs. These translocate to the intercellular space where they bind and stimulate the activation of the innate immune system, including the expression of type-II IFN, which stimulates immune cells and initiates the activation of the adaptive immune system. A detailed review to type I and type-III signalling can be found elsewhere,[5] as wells as for type-II IFN [6]. Used PDB structures (left to right): 5T5W [7], 3SE3 [8], 6E3K [9].

There is one receptor pair for each IFN class (type-I: IFNAR1 and IFNAR2, type-II: IFNγR1 and IFNγR2, type-III: IFNλR1 and IL-10Rβ) (**Figure 1, Figure 2**) and all receptor activation triggers Janus kinase/signal transducer and activator of transcription (JAK-STAT) signalling pathways, respectively (**Figure 1**). IFNs have important function and are used therapeutically in (i) viral infection [5, 10], (ii) autoimmune disease [11-14], (iii) myeloproliferative neoplasms [15-19] (iv) cancer [10, 20-23] and (v) some hereditary diseases that affect immune defence [24] (**Table 1**). For anti-viral treatment, type-I IFNs are applied to activate the innate immune system [5, 10]. Type-I and type-III IFNs have similar functions and share pathways but with different tissue specificity [4, 25]. Whereas type-I IFN receptors are ubiquitously present, type-III IFNs are predominantly produced in epithelial cells modulating the crosstalk between barrier cells and the innate immune system, but without triggering inflammatory responses [26-31]. In contrast to type-I and III, type-II IFN consists only of IFN-γ. IFN-γ release stimulates the adaptive immune response of antigen presenting cells, including macrophages [32]. This results in the commitment of naïve T helper cells towards the Th1 state, and not Th2 state, which results in antigen presenting cell activation. The production of IFN-γ is therefore a hallmark of the Th1 response [21].

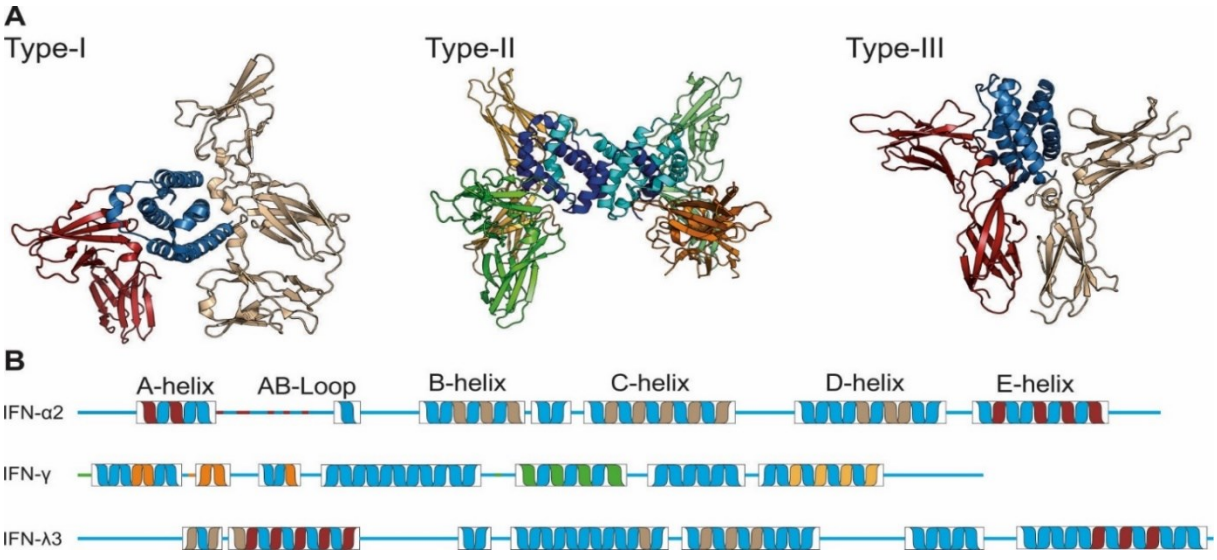

Figure 2: (A) Overview of IFN receptor complexes. Type-I IFN ternary complex: IFNAR2 is displayed in red, IFN-α2a is displayed in blue, IFNAR1 is displayed in beige (PDB: 3SE3). Type-II IFN hexameric complex: IFNγR1 is displayed in orange and light orange, IFN-γ homodimer is displayed in dark and light blue, IFNγR2 is displayed in green and light green (PBD: 6E3K). Type-III IFN ternary complex: IFNλR1 is displayed in red. IFN-λ3 is displayed in blue, IL10βR is displayed in beige (PDB: 5T5W). (B) Schematic display of selected IFN proteins with their most important secondary structure motifs from N- to C-terminus. Alpha helices are displayed as ribbons in boxes. Important areas for receptor binding are displayed in the same colour as the receptors in (A) [7-9].

Table 1: classification of approved IFN drugs, with their respective modifications and most important diseases of application

Type	Subtype	Approved Drug	manufacturer	Year of approval (FDA or EMA)	Type of modification	HBV	HCV [#5]	HCL	CML	CT-CL	PV	MS	SG	OP	source
Type-I	IFN-α-2a	Roferon A®[#1]	Roche	1986	---	x	x	x	x	x					51, 54
		Pegasys®	Roche	2002	Branched NHS-mPEG 2x 20 kDa[#3]	x	x								51-53
	IFN-α-2b	Intron A®	MSD	1986	---	x	x	x	x						50
		PegIntron®	MSD	2001	SC-mPEG 12 kDa		x[#6]								47-49
		Besremi®	AOP	2019	Branched CHO-mPEG 2x 20 kDa[#3]						x				17, 43-46
	IFN-β-1a	Avonex®(i.m.), Rebif®(s.c.)	Biogen, Merck	1996 2002	---							x			41 42
		Plegridy®	Biogen	2014	CHO-mPEG 20 kDa[#4]							x			11, 12
	IFN-β-1b [#2]	Betaferon®, Extavia®	Bayer, Novartis	1993 2009	---							x			39 40
Type-II	IFN-γ-1b	Imukin®, Actimmune®	Boehringer, Vidara	1997 1999	---								x	x	38
Type-III	IFN-λ-1a		Eiger Bio Pharma.	Phase III started (2021)	CHO-mPEG 20 kDa[#4]	x*[7]	x								34-37

HBV: hepatitis B virus, *HCV*: hepatitis C virus *HCL*: hairy cell leukemia, *CML*: chronic myeloid leukemia, *CTCL*: cutaneous T-cell lymphoma, *PV* polycythemia vera (only without symptomatic splenomegaly), *MS*: multiple sclerosis, *SG*: septic granulomatosis, *OP*: malignant osteopetrosis

[#1]production stopped in 2019, [#2] only one natural IFN-β variant exists termed IFN-β-1a, IFN-β-1b is recombinantly produced in *E. coli*, lacks Met1 has a C17S mutation, and lacks glycosylation (Drugbank: DB00068)[33]

[#3] see figure 4 for more details on modification-chemistry. [#4] Uses a similar chemistry to Besremi®

[#5]: in combination with Ribavirin

[#6]: in combination with Ribavirin and Boceprevir (also approved with HIV co-infection)

[#7]: Phase IIb study finished in combination with entecavir for HBV treatment. In phase III for treatment of chronic hepatitis D (HDV), as monotherapy and in phase II in combination with Lonafarnib and Ritonavir. HDV can propagate only in the presence of HBV infection

Drug delivery of Interferons

Pharmacokinetic and pharmacodynamic properties of therapeutic IFNs are impacted by rapid disposition kinetics resulting from short serum half-lives primarily excreted renally ($t_{1/2}$ between 2-8 hours for human IFN-α2a) and the route of administration [55]. By changing the route of administration from i.v. to i.m. or s.c. injection, the t_{max} value can be increased from 0.67 to 3.7 h for i.m. and 7.3 h for s.c, resulting in higher serum concentrations after 3h, when compared to i.v. injection [56]. For this reason, all approved IFN drugs (type-I and type-II) are applied by default s.c. to extend the therapeutic outcome as the continued release after s.c. injection leads to more stable serum levels (**Table 2**). To further address these challenges, IFNs have been biotechnologically modified and/or conjugated to the hydrophilic polymer methoxy-polyethylene glycol (mPEG). mPEG is a synthetic, non-biodegradable polymer for increasing the hydrodynamic radius of the conjugated protein to modulate PK performances and prolong therapeutic outcome [57, 58].

After their administration, unmodified IFNs are majorly catabolised via the kidney, where they are degraded in tubular cells after reabsorption [59-61]. This proportion is reduced for PEGylated IFNs (30 % for PEGIntron® (IFN-α2b 12 kDa mPEG), 42 % Plegridy® (IFN-β1a 20 kDa mPEG) ,<5 % for Pegasys® ((IFN-α2a 2x 20 kDa mPEG)) and shifts to hepatic elimination via nonspecific proteases [62-64]. In this paragraph we first discuss the evolution of approved IFN drugs and highlight the biotechnological and pharmaceutical progress for advanced IFN function and delivery.

Table 2: Pharmacokinetic parameters of approved IFN drugs

Approved Drug	Serum half life	Peak	Dose (s.c.)	interval (per week)	bioavailability	source
Roferon A®	3.7-8.5 h (i.v.)	3.8 h (i.m.), 7.3 h (s.c)	18 mio I.E. (67 µg)	3x	80 % (i.m., s.c.)	54-56
Pegasys®	60-80 h (i.v.) 160 h (s.c.)	72-96 h (s.c.)	180 µg	1x	84 % (s.c.)	52
Intron A®	7-9 (i.v. / s.c.)	6-8 h (s.c.)	10 mio I.E. (38 µg)	3x	100 % (i.m., s.c.)	50, 63
PegIntron®	40±13.3 h (s.c)	15-44 h (s.c.)	80 µg	1x	---	47
Besremi®	144-240 h (s.c.)	72-144 h (s.c.)	350 µg	0.5	80 %*	17
Avonex®, Rebif®	10h(i.m.) 50-60h (r.s.c.)	5-15h (i.m., s.c.) 8h (r.s.c)	30 µg, 44 µg	1x 3x	40 % (s.c.) ---	41, 65 42
Plegridy®	78±15 h (s.c.)	24-36h (s.c.)	125 µg	0.5x	---	11
Betaferon®, Extavia®	5 h (s.c.)	1-8 h (s.c.)	250 µg	3x	50 % (s.c.)	39
Imukin®, Actimmune®	11h (s.c.)	8 h (s.c.) 4h (i.m.)	50 µg/m^{2**}	3x	89 % (s.c.)	38

*was tested in apes only, **body surface. If body surface is < 0.5 m^2, dosing is changed to 1.5 µg/kg.

Approved IFNs drugs: From 1st to 3rd generation

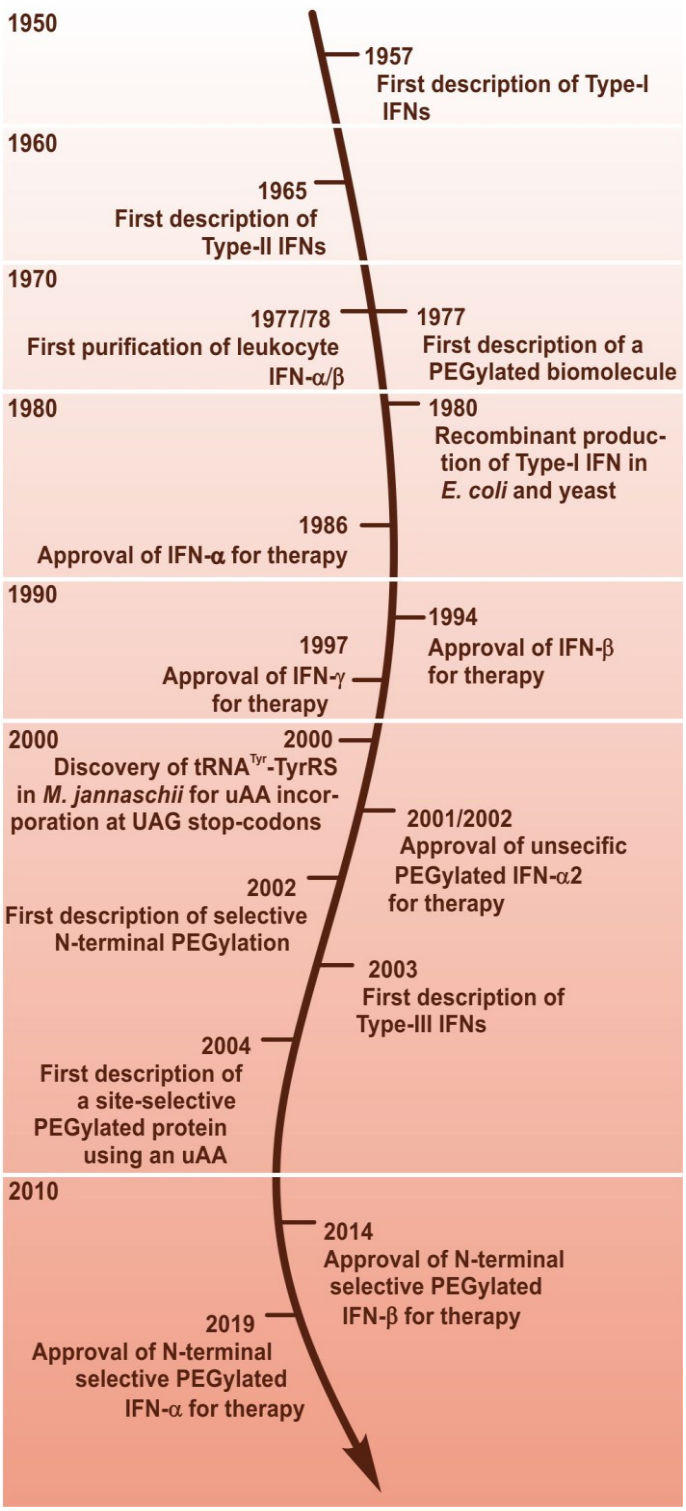

Figure 3: IFN drugs with important scientific breakthroughs and first-time approvals by the FDA or EMA, with additional key technologies for future development [11, 17, 38, 41, 52, 66-76].

Recombinant wild type human IFN was first approved in 1986 for CML, HCL and HCV treatment (**Figure 3, Table 1**). Due to its early clinical use, IFN-α was one of the first biologicals to be modified with mPEG, resulting in the second generation with Pegasys® and PegIntron®, amending pharmacokinetic properties of IFN (**Figure 3 and Table 1**) [77].

Pegasys® and PegIntron® rely on N-hydroxysuccinimidyl (NHS) chemistry for attachment of two 20 kDa branched mPEGs for Pegasys®, or a single 12 kDa mPEG in case of PegIntron® (**Table 1 and Figure 4A**). NHS reacts selectively with primary amines (and histidine residues, depending on the used specific NHS) to target lysine residues and the N-terminus of the protein. This chemistry therefore yields into a mixture of monomeric isomers (one mPEG is conjugated to one differing residue) and partially oligomers (more than one PEG is conjugated to the same protein on two different residues). After conjugation, the mono PEGylated-IFNs are separated from unreacted educts and oligo PEGylated IFNs by ion exchange chromatography [77]. This mixture of mono PEGylated IFNs can be further purified by excessive ion exchange chromatography on a laboratory scale to isolate the different isomers, but is not performed for Pegasys® in industrial-scale production (**Figure 4B**) [53]. PEG bioconjugation resulted in a 25-fold increase (Pegasys®) of renal clearance (10-fold increase for PegIntron®) after subcutaneous administration (**Table 2**), achieving better patience compliance with one injection per week [52].

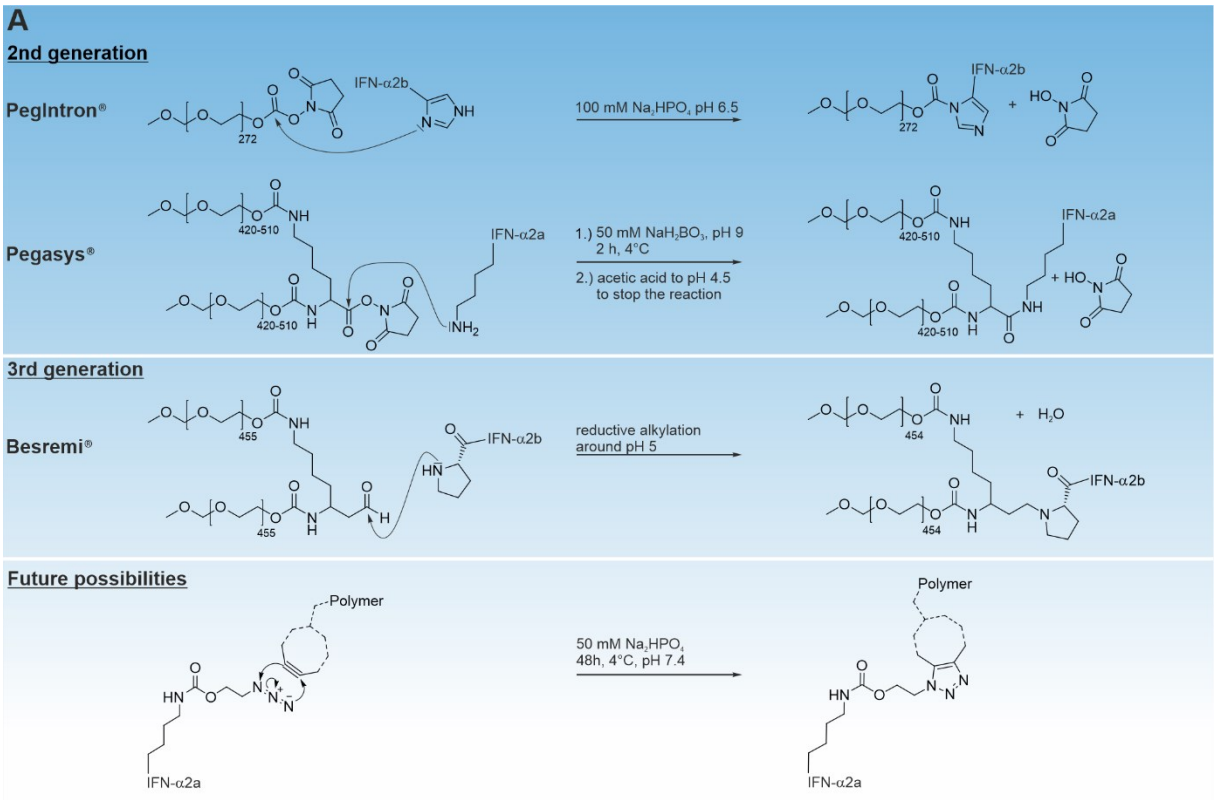

B

drug	residue	degree of modification
Pegasys®	K121	32.3 %
	K164	6.6 %
	K31	15.9 %
	K134	18.7 %
	K131	18.6 %
	K70/83	5.5 %
	K49	1.4 %
	K112	0.8 %
PegIntron®	C1	13.2 %
	H34	47.8 %
Besremi®	P0	90 %

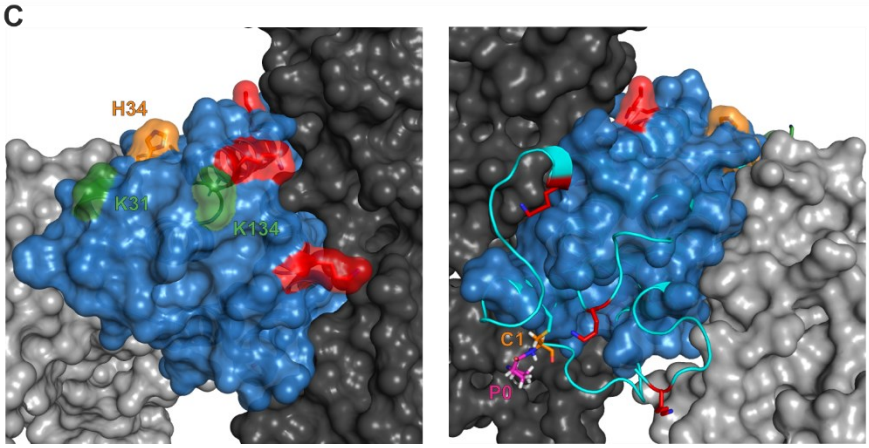

Figure 4: (A) PEGylation strategies of approved IFN-α drugs [46, 48, 49, 53, 77]. (B) Most abundant PEGylation sites on IFN-α´s residues,[48, 53] estimated for Pegasys® from [53]. Purified Pegasys® isomers are highlighted in red and green. Residues that are highlighted in red have a lower potency than the Pegasys® mixture, green marked residues have a higher potency than the Pegasys® mixture, showing that most PEGylation sites are not suitable for PEGylation [53]. Lysine Isomers from PEGIntron® have similar modification sites as Pegasys®, but to a different degree of modification [48]. Additional important modification sites are highlighted in orange, whereby C1 is conjugated via the N-terminus. The main modification site of Besremi® is highlighted in magenta as P0 as a mutationally introduced proline residue. (C) Superimposition of IFN-α2a in its ternary complex (PDB:3SE3) and IFN-α2a in its free form (1ITF). IFNAR1 is displayed in black, IFNAR2 is displayed in grey, bound IFN-α2a is displayed in blue and superimposed with an NMR-structure of IFN-α2a, displayed in cyan, to display the approximate positions of residues and secondary structures that are not resolved in the ternary complex crystal structure 3SE3. P0 was introduced artificially. Colors from side residues are displayed as given in panel B.

However, these pharmacokinetic benefits come with a prize. Potency of PEGylated biologicals is often diminished due to steric hindrance with receptor surfaces and heterogeneous bioconjugation chemistries [78]. Potency reduction was 93 % for Pegasys® and 72 % for Pegintron®, respectively [48, 77]. Balancing the loss of potency, a nearly 3-fold higher dosage of Pegasys® is applied compared to Roferon-A, with respect to the active protein component (**Table 2**), though the applied IFN has a longer serum-half life,

which results in a similar amount of applied IFN on a weekly scale. The loss in potency may be explained by (i) the size of conjugated mPEG itself and (ii) existing amounts of PEGylated IFN with reduced or lost receptor affinity (**Figure 4B and C**).

To address the heterogeneity of the second generation of IFN drugs, more site-specific aldehyde coupling has been reported, called reductive alkylation [46]. This type of bioconjugation chemistry is based on the N-terminal nucleophilic activity at acidic pH (≈ 4-5), exceeding the nucleophilicity of ε-amine groups of lysine within the protein backbone. In the presence of reducing agents, the primary amine of the N-terminus reacts spontaneously with aldehydes, resulting in a stable C-N bond (**Figure 4A**) [73]. As the N-terminus is favoured for this reaction, a higher product homogeneity as compared to NHS chemistry is achieved for IFN, as demonstrated with Besremi® compared to Pegasys® and PEGIntron®. Product homogeneity can be further tailored by genetic introduction of an artificial proline at the protein`s N-terminus for enhancement of the inductive effect on the primary amine. This underlying bioconjugation strategy has been applied to produce Besremi®, a 90 % mono-PEGylated N-terminal IFN-α2b conjugate (**Figure 4B**) [46]. Interestingly, no statistical differences in pharmacokinetic properties were monitored between the third generation IFN drug Besremi® in comparison to the second generation IFN drug Pegasys® (**Table 2**). The dose that needs to be applied is still comparable to the one of Pegasys®, but product homogeneity reduces drug side effects (rash symptoms in 7 % of patients of Besremi® compared to 36.8 % in Pegasys® treated patients) and an optimised application profile of 350 ug every two weeks (Pegasys® 180 ug once a week) accelerated response rates in HBV to 24 instead of 48 weeks [43, 48].

Site-selective bioconjugation strategies

Site-selective conjugated bioconjugates benefit from modifications at a preselected location and therefore result in homogeneous products. Through site selective conjugation strategies heterogeneity and loss of potency can be significantly addressed [72, 79-85]. A simple technique for site-selective conjugation is the introduction of an additional cysteine residue. This additional cysteine residue must be placed at a position, where it does neither affect protein folding (e.g. by forming an unwanted disulphide bridge) nor its potency. A challenge is keeping the cysteine reduced, which can be achieved by adding low concentrations of reducing agents (like dithiothreitol, or TCEP) and by keeping the pH above neutral [86, 87]. After a successful purification, the additional free cysteine residue can be targeted by several chemistries such as Michael addition by reactive maleimide groups as performed for IFN-α2 [87, 88]. This attempt resulted in an IFN-α2-PEG 40 kDa bioconjugate which had a Q5C mutation, a 4-fold reduction in potency and a 40-fold increased serum half-life after subcutaneous administration in rats [87]. Another approach tested on IFN-α2 was performed by exchanging a short AA sequence (3-4 AA) of the protein with a small histidine tag (HGH) at different sites, enabling the use of bis-sulfone as a linker to conjugate mPEG [89]. For effective conjugation bis-sulfone needs to react with two nucleophilic residues in proximity, which are either His, Cys or Lys. The preferred residue and therefore conjugation site can

be influenced by pH, favouring His at slightly acidic pH (5-6). Though the selective incorporation at different engineered sites was demonstrated, reaction conditions needed to be highly optimized, regarding educt concentration and protein to bis-sulfone-polymer ratio to yield mainly mono-PEGylated bioconjugates, which were successfully purified afterwards. Apart from technical optimisation, the bioactivity of the produced bioconjugates resulted in comparable bioactivities to mutation studies previously performed on identical sites [87].

A more versatile technique for the site-selective modification of proteins is the codon expansion technology. Codon expansion technology grew rapidly in diversity and application for biologicals, ranging from newly functionalized antibodies, over engineered enzymes to potent vaccines [72, 79-85]. Generally, the codon expansion technique allows for the incorporation of an unnatural amino acid (uAA) with a selective reactive group to a preselected position during recombinant protein synthesis, by recognition of an amber stop codon and a tRNA/amino acyl tRNA synthetase pair [79-81, 90]. The unnatural incorporation can be performed in *E. coli* as well as in yeast and mammalian cell systems, depending on the used tRNA/amino acyl tRNA synthetase pair [91]. The site-selective reactive group is coupled to a polymer or another reactive carrier, yielding homogeneous conjugates as it has been well demonstrated in literature with various biologicals [92-97]. This approach has also been shown to lead to more potent PEGylated IFNs with increased *in vitro* potency compared to available IFNs [98]. We recently reported that site specific IFN-α2a bioconjugates originated from PEG and PEG alternative polymers performed equally with respect to biological performances. Polymer interactions with IFN-α2a were further studied via a limited proteolysis (LIP) assay, suggesting weak interactions of each type of polymer with the protein′s surface. The codon expansion technology goes generally in hand with an overall lower protein expression, higher production costs due to synthesis of the needed uAA, and optimization for large scale production. Moreover, clinical trials are necessary to evaluate the safety of uAAs incorporated in biologicals for use in patients. Currently, several clinical phase I trials are ongoing with a focus on site-specific engineered antibody drug conjugates, that bear an unnatural amino acid, which release conjugated payloads (mostly cytotoxic) upon target binding [99, 100].

IFN fusion proteins

Fusion of a long circulating protein is one alternative strategy to modulate pharmacokinetic properties of short-half-life biologicals. In this regard Albinterferon® was recombinantly expressed as a fusion protein consisting of IFN-α2b and human serum albumin (HSA) fused to the N-terminus [101]. Although several drugs have been approved as fusion protein, this approach is general limited to the N-or C-terminus due to the recombinant expression technology. The pharmacokinetic profile of Albinterferon® was comparable to the one of Pegasys® with comparable low potencies [102, 103]. Compared to Pegasys®, no significant benefits were achieved. Ultimately, Albinterferon® development was stopped. In contrast to albumin fusion, aldehyde coupling as strategy for N-terminal modification (Besremi®) was more

promising as the mPEG polymer proved to be more flexible than the N-terminally fused globular albumin.

Other traditionally used fusion proteins are antibody fragments, which have also been performed for type-I IFN [104, 105]. Another interesting IFN fusion protein under development is SL335-IFN-β-1a. SL335 is a human Fab antibody (23 kDa) recognizing HSA [106]. SL335 is N-terminally fused through a short 8 amino acid long peptide linker to IFN-β-1a. Recombinant expression of this fusion protein is facilitated as IFN-β is prone to aggregation [107]. These aggregates are likely to promote neutralizing antibody formation against IFN-β, which makes a proper formulation even more important [107]. Its pharmacokinetic and pharmacodynamic properties were found to be at least twice as good as IFN-β (Rebif®) as assessed in rats and cynomolgus monkeys [105, 108]. Additionally, other IFN fusion proteins with the same purpose were tested [104].

Apart from IFN fusion proteins, that focus on a serum-half life extension, several other studies were done with IFN fusion proteins in animal models to increase the specificity and potency against certain cancers. These include the fusion of epitope specific antibodies (Ab) to specifically target certain cancer cells, or the vascularization of cancers [109-111]. In one study murine IFN-α and IFN-β were fused to a CD-20 specific Ab fragment [110]. The proteins were tested for treatment in mice challenged with murine B cell lymphoma [110]. Both fusion proteins had a superior antiproliferative performance versus their natural counterparts and CD-20-IFN-β was superior to CD-20-IFN-α. The survival rate was also better in B-cell lymphoma cells, which are more sensitive to type-I IFNs [109, 110]. In contrast to disseminated tumors like B-cell lymphomas, an Ab-IFN-α specific therapy against a solid teratocarcinoma had no beneficial effect, that could be correlated to the fused Ab fragment [109]. The fusion protein was directed against the extra domain B of fibronectin, a splice variant of fibronectin, which is expressed in various solid tumors, but rarely in adults, during epithelial to mesenchymal transition and neovascularization [109, 112]. Similar studies were earlier performed with an Ab-IFN-γ fusion protein, targeting the same fibronectin domain, with varying doses against different tumors. The outcome depended strongly on the tumor type and was most often enhanced when combined with other Ab-cytokine fusion proteins and chemotherapeutic agents [111].

Artificially designed IFNs

Artificial IFN-α mutants were produced with higher activities than type-I IFNs by an artificial design technology combining DNA-shuffling and High Throughput Screening (HTS) [113]. By this approach, the IFN-α2 drug Novaferon was developed with 29 mutations, to increase its antiproliferative potency, but without targeting pharmacokinetic properties [8, 113]. The 29 mutations occurring in Novaferon are majorly a combination of natural occurring mutations from two other type-I IFNs, that have higher binding affinities than the natural ligand IFN-α2 [114, 115]. Designed IFNs with an improved affinity profile may be a promising future therapy to combat IFN led resistances 116, 117.

Pulmonary and nasal administration of IFN

Pulmonary application of type-I and type-III IFNs against viral diseases is of specific interest as the respiratory tract is one of the primary gateways for pathogens to enter human circulation [118]. Several studies and reviews have already been published [29, 119-121]. Some viral pathogens, including coronaviruses, have learned to delay the initial IFN type-I/III response, which results in unhampered virus replication, an inflammatory response and lung immunopathology with diminished survival [122-124]. Therefore, delivery of type-I/III IFNs should target the very early stages of infection to combat viral replication. This is further supported by recent findings, where a significant number of patients with severe symptoms that were infected with SARS-CoV2 had neutralizing immunoglobulin G (IgG) auto-antibodies against type-I IFNs (majorly against all IFN-α and/or IFN-ω, but only few against IFN-β), or a genetic disorder in one type-I IFN regulator [116, 117]. Therefore, administration of type-I/III IFNs may contribute to decrease the number of severe infections and support patient recovery, as demonstrated for IFN-β1a [119]. It must also be noted that recent findings have pointed out that type-I IFN response can boost inflammatory responses. The timing of type-I IFN is crucial, as a delayed, but strong type-I IFN response leads often to hyper inflammation, causing severe symptoms, but an early type-I/III IFN response controls viral replication [121, 122, 125-128]. Nebulized type-I/III IFNs may therefore be used as a therapy to fight respiratory virus infections. It is likely that type-I and type-III IFNs are suited for this type of therapy, though the application of type-III IFNs is likely to be less risky due to their local effect and earlier time of onset during viral infection [29, 127]. Furthermore, no hyper inflammation using type-III IFNs has been yet reported. This trend towards type-III IFNs is supported by a recently published study by Davidson et al. showing, that mild Covid is characterized by high levels of type-III IFN, but not type-I IFN in the upper airways [129]. These efficiently induce an antiviral response, that leads to a more rapid elimination of the virus, limiting its viral spread to the lower airways.

This route of administration can be further tailored when IFNs are artificially modified with PEG. In this case medium long PEGs (10-20 kDa) may be optimal to increase the therapeutic effect of type-I/III IFNs as reported from animal studies [29, 130]. In one study [29] murine PEGylated IFN-λ2 (likely 20 kDa as donated from the same company that runs clinical trials on 20 kDa PEGylated IFN-λ1a, though not explicitly stated) was administered intranasally 1-2 days post lethal Influenza A virus infection, resulting in a significantly higher survival and less symptoms compared to saline treatment. In another study, human IFN-α2, PEGIntron® and Pegasys® were administered via intratracheal instillation to compare their pharmacokinetics to i.v. administration [130]. The plasma levels after i.t. instillation were overall significantly lower for PEGIntron® and Pegasys® over 48 h, in contrast to IFN-α2 where similar plasma levels were measured after 2 hours. It was concluded that the tested 12 kDa PEG chain is the best tradeoff between an enhanced retention (the drug stays longer in the lung and can longer stimulate cells) and a decrease in biological activity, which decreases with increasing PEG chain length. In this study the bioavailability of unmodified IFN-α2 was 15 % (5.5 % for PEGIntron® and <0,4 % for Pegasys®), but

may be significantly increased (up to 10-fold), when administered as an aerosol as shown for other proteins [131-133].

Depots for controlled IFN delivery

Based on pharmacokinetic properties of IFN drugs, drug delivery platforms were developed to release IFNs in a constant manner. For example, elastin like polypeptides (ELPs) were used as fusion proteins to IFN. ELPs are polypeptides that undergo a reversible phase separation above a characteristic transition temperature [134, 135]. This transition temperature can be fine-tuned by alternating the polypeptide length and amino acid sequence. As they are polypeptides, they can only be fused to the N or C-terminus of a protein. Due to ELPs ability to aggregate above a certain temperature (like 37°C), they can quickly form solid depots and micelles, when injected that dissolve slowly over time. This leads to improved pharmacokinetic profiles, by stabilising plasma levels and can result in a constant drug release over several weeks, as well as increased proteolytic stability [136-138].

Safety of IFN application

As type-I and type-II IFNs act systemically, there are several adverse events that go in hand with IFN therapy. Reported adverse effects for type-I IFNs are related to flu like symptoms (fever, vomiting, fatigue, weight loss). These have been accompanied by more severe reactions, ranging from psychological disorders (severe depression, suicidal thoughts) to anaemia, neutrophil reduction, hypertension and organ disorders (liver insufficiency, gastrointestinal bleeding, etc.) [52, 54]. type-II IFNs provoke similar adverse reactions [38]. Other reported effects are on upregulated liver enzyme concentrations and on gastrointestinal disorders (vomiting, diarrhoea, pain) [38]. To date there are only clinical phase two studies available for type-III IFN. In these studies, type-III IFN was tested for hepatitis B, C and D treatment (Table 1). Based on these results, therapeutic intervention of type-III IFN seem to be less critical on the hematopoietic system as compared to type-I IFNs but has otherwise similar side effects [34-37].

Safety issues need to be considered when patients have an impaired renal function as this results in elevated IFN plasma concentrations after single and multiple applications up to 2-fold higher serum concentrations and serum half-life times for unmodified IFN-α2 and PEGIntron® [60, 139-141]. This effect reduces for IFNs with longer mPEG chain modifications as their proportional elimination is shifted towards the liver the longer the PEG chain is. Additionally, this effect is reduced when the application interval is rarer (PEGIntron® is applied 1x weekly, Plegridy® is applied 1x every other week) (**Table 2**). Furthermore, haemodialysis needs to be considered too, as it reduces IFN plasma levels [60, 140-142]. Hemodialysis results for PEGIntron® in a dose reduction of 25 % for patients with moderate renal insufficiencies (50 % in patients with severe renal insufficiencies), but no recommended dose reduction for Plegridy® [60, 142].

Other safety issues were discovered during recent COVID-19 research, where 10.2 % of patients with severe COVID-19 had neutralising immunoglobulin G (IgG) auto-antibodies against type-I IFNs (majorly against all IFN-α and/or IFN-ω, but only few against IFN-β) [116]. Noteworthy is, that these patients were majorly male (94 %).

Conclusion and Outlook

IFNs are powerful therapeutics due to their antiviral and antiproliferative effects in many different diseases. Despite over 30 years of research, type-I interferons (IFN)s are still improved by bioconjugation strategies to reduce frequent administrations. Furthermore, their anti-viral potential recently became relevant for local treatment of COVID19 by exploiting novel routes of administration (pulmonary, nasal delivery). However, each novel site of administration needs a new safety assessment.

Type-II IFN (IFN-γ) are particularly difficult to modify at the N-terminal site as it binds the receptor as a homodimer and the N-terminus is located between both IFNγRs. Garcia et al. already described that two IFN-γ molecules can be expressed as a fusion protein, featuring a protease sensitive linker that can be cleaved after dimerization. This approach may be combined with site-selective functionalization to yield homogeneously functionalized IFN-γ [9]. Using modified IFN-γ in cancer therapy might be reasonable, but is highly cancer dependent as IFN-γ can have pro- and anti-tumorigenic effects [21]. On the one hand IFN-γ is critical for immune cells migrating to the tumor and can also inhibit angiogenesis, but on the other hand tumors with IFN-γ dysregulations can lead to immune evasion [143-145]. To avoid the side-effects of IFN-γ therapy, a localized administration is advisable due to the nature of IFN-γ´s local secretion and diffusion to the surrounding tissues. There are several ongoing clinical trials with IFN-γ as an adjuvant in cancer therapy [21, 146]. Additionally, a higher dose seems to be critical for a positive response to inhibit tumor progression, as low dosages enhance tumor survival, as well as ongoing dosage, due to the nature of IFN self-regulating negative feedback loops [22]. A functionalized IFN-γ can help to stabilize high local concentrations, by a covalent attachment to carrier systems, like PEG, hydrogels, Ab-fragments, or else, which have yet been partially successful in cancer models [111, 147, 148].

Likely more potential lies in the development of type-III IFNs as a therapeutic. To date there is no FDA/EMA approved type-III IFN drug on the market, though one PEGylated type-III IFN is in clinical trials for treatment of hepatitis. The selectively expressed IFNλR1 is a challenging target regarding the use of type-III IFNs as a potent type-I IFN alternative. The IFNλR1 cell selective expression in epithelial tissues is on the one hand its biggest advantage, as it minimizes side effects, but also its biggest weakness as the reduced receptor frequency correlates with a reduced downstream activation of its antiviral and anti- proliferative potency. As the potency of type-III IFNs is already limited by IFNλR1 frequency it is reasonable to suppose that a clinical application will be focused on a localized type-III IFN therapy, such as pulmonary administration, although a recent clinical trial has also shown its effectiveness in HBV therapy [36]. Type-III IFNs may be used to upregulate the antiviral potencies of epithelial tissues (lung and gastrointestinal tract), as type-III IFNs usability is inferior for ongoing systemic infections

compared to type-I IFNs but induces no detrimental inflammatory effects [120, 128, 149, 150]. This would also most likely reflect their natural role in the immune system to prime epithelial tissues for pathogens, without activating the rest of the immune system. Regarding their possible modifications, it seems likely that N- and C-terminal modifications can be easily achieved as the termini are likely distant enough to the receptors, which facilitates their mutational possibilities.

Conclusively IFNs are still a promising class of cytokines to target diseases even if they are already established since more than 30 years. Additionally, the vast amount of research that has been performed with IFNs turns them into perfect model proteins. Their key role in the innate and adaptive immune response turns them into viable first line treatment options against viral diseases, when more specific therapies are not available. Advanced engineering of yet to come IFNs is desirable to minimize the shortcomings of the currently used 3rd generation of approved mPEGylated IFNs. These are currently limited to N-terminal conjugation and subcutaneous injection. Especially the potential of type-III IFNs, as well as the use of type-II IFN in cancer research has yet to be discovered and will likely result in new IFN drugs to complement the range of application of these versatile and essential class of cytokines.

Acknowledgements

This work was supported by the Bundesministerium für Bildung und Forschung (grant “Next-PEG; number 13XP5049B).

Chapter 2 - Molecular insights into site-specific interferon-α2a bioconjugates originated from PEG, LPG and PEtOx

Niklas Hauptstein‡, Paria Pouyan‡, Josef Kehrein, Michael Dirauf, Marc D. Driessen, Martina Raschig, Kai Licha, Michael Gottschaldt, Ulrich S. Schubert, Rainer Haag, Lorenz Meinel, Christoph Sotriffer, Tessa Lühmann*

‡ These authors contributed equally to this work.

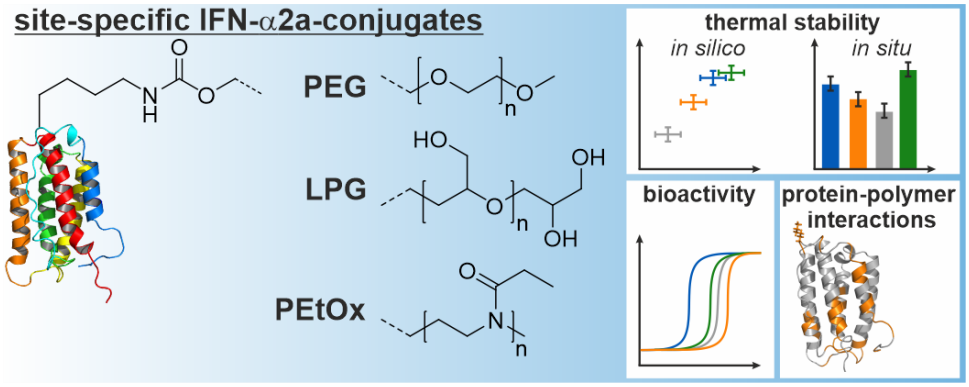

Keywords: site-specific conjugation, PEG, polyglycerol, poly(2-ethyl-2-oxazoline), IFN-α2a, genetic code expansion

Reprinted (adapted) with permission from: Hauptstein, N.; Pouyan, P.; Kehrein, J.; Dirauf, M.; Driessen, M. D.; Raschig, M.; Licha, K.; Gottschaldt, M.; Schubert, U. S.; Haag, R.; Meinel, L.; Sotriffer, C.; Lühmann, T., Molecular Insights into Site-Specific Interferon-α2a Bioconjugates Originated from PEG, LPG, and PEtOx. Biomacromolecules 2021, 22, (11), 4521-4534. DOI: 10.1021/acs.biomac.1c00775. Copyright 2021, American Chemical Society.

Abstract

Conjugation of biologics with polymers modulates their pharmacokinetics, with polyethylene glycol (PEG) as the gold standard. We compared alternative polymers and two types of cyclooctyne linkers (BCN/DBCO) for bioconjugation of interferon-α2a (IFN-α2a) using 10 kDa polymers including linear mPEG, poly(2-ethyl-2-oxazoline) (PEtOx) and linear polyglycerol (LPG). IFN-α2a was azide functionalized *via* amber codon expansion and bioorthogonally conjugated to all cyclooctyne linked polymers. Polymer conjugation did not impact IFN-α2a's secondary structure and only marginally reduced IFN-α2a's bioactivity. In comparison to PEtOx, the LPG polymer attached via the less rigid cyclooctyne linker BCN was found to stabilize IFN-α2a against thermal stress. These findings were further detailed by molecular modeling studies which showed a modulation of protein flexibility upon PEtOx conjugation and a reduced amount of protein native contacts as compared to PEG and LPG originated bioconjugates. Polymer interactions with IFN-α2a were further assessed *via* a limited proteolysis (LIP) assay, which resulted in comparable proteolytic cleavage patterns suggesting weak interactions with the protein`s surface. In conclusion, both PEtOx and LPG bioconjugates resulted in similar biological outcome and may become promising PEG alternatives for bioconjugation.

Introduction

Biologics are conjugated for modulating stability or pharmacokinetic properties.[151] The most frequently used conjugation is with polyethylene glycol (PEG), known as PEGylation, which was first introduced in 1977.[152, 153] PEG is a non-toxic, highly flexible, and hydrophilic polymer. However, PEGylation might reduce the bioactivity of biologics and transport characteristics, as of reduced receptor affinity and loss of intracellular sequestration, respectively.[154-156] In spite of the use of PEG to reduce frequency of administration of biologicals, recent studies have linked complement activation to PEG due to anti-PEG neutralizing antibodies.[157-161] Therefore, PEG alternative polymers are being thoroughly studied in the biomedical field.

A promising PEG alternative polymer class are LPGs (linear polyglycerols), which are biocompatible, water-soluble and flexible polyols, based on a PEG-like polyether backbone.[162, 163] LPG has been successfully synthesized with molecular weights up to 100 kDa (hyperbranched PG up to 540 kDa) with potential for biomedical and antifouling application.[58, 163-165] Linear and branched polyglycerols have been recently conjugated *via* aldehyde coupling to the N-terminus of the protein inhibitor anakinra and bioconjugates showed similar pharmacokinetic performances as the PEGylated counterpart.[166]

Poly(2-ethyl-2-oxazolines) (PEtOx) are another PEG alternative polymer class and have been intensively studied for biomedical purposes due to their thermoresponsivity and biocompatibility,[167, 168] ranging from the delivery of hydrophobic drugs, proteins, and nucleic acids[169-174] to antifouling surfaces.[58, 175-183] Moreover, different protein bioconjugates have been successfully produced with polyoxazoline (POx) as a PEG alternative polymer.[177, 184, 185] POx based rotigotine conjugates recently demonstrated potential for treatment of Parkinson`s disease in a clinical study.[186]

PEGylated Interferon-α2a (IFN-α2a) was one of the first bioconjugates entering the market, demonstrating potent immune-modulating, antiviral and antiproliferative properties for use in hepatitis or cancer therapy.[184, 187-191]

Strategies for site-specific bioconjugation yield homogenous PEGylation products with precise spatial control of the modification site within the protein sequence. Thereby, heterogenous product qualities are avoided as resulting from more widely used syntheses including carboxyl-reactive or sulfhydryl-reactive crosslinking, respectively.[192] One successful strategy for site-specific decoration of biologics is the integration of functionalized unnatural amino acids (uAA) into the primary structure at predefined positions using genetic code expansion during protein translation. Genetic code expansion was effective in a wide range of expression systems, including *Escherichia. coli*, [92, 97, 184] yeast, [91, 193] and mammalian cells. [79, 194]

In this study, we recombinantly expressed a human IFN-α2a mutein with an azide-bearing unnatural amino acid by amber codon expansion, enabling bioorthogonal bioconjugation to PEG and PEG alternative polymers using strain-promoted alkyne-azide cycloaddition (SPAAC). All bioconjugates were analysed for biological activity, secondary structure, and performances against thermal stress. Finally, computational and experimental approaches were combined to elucidate how PEG and PEG alternative polymers interact with the protein`s surface.

Experimental section

Materials:

A detailed description of materials and the synthesis of all presented polymers is given in the supporting information.

Boc-protected L-lysine was from P3 BioSystems LLC (Shelbyville, KY, US). 2-Bromoethanol, triphosgene, sodium azide, HCl in diethyl ether, 1,4-dithiothreitol (DTT), carbenicillin, chlorampenicol, isopropyl-β-D-1-thiogalactopyranoside (IPTG), penicillin-streptomycin, phenylmethylsulfonyl fluoride (PMSF), guanidine hydrochloride, primer, NDSB-201, L(+)-arabinose, lysozyme, DNAse I, triton X-100, acetonitrile HPLC grade, ethyl acetate, chloroform and trifluoracetic acid were purchased from Sigma Aldrich (Schnelldorf, Germany). PageRuler™ Prestained Protein Ladder, Coomassie Brilliant Blue G250, NuPAGE LDS sample buffer (4X), slide-a-lyzer, Dulbeco's Modified Eagle's Medium (DMEM), Gibco-FBS-HI (Origin Brasil) BCA assay, synthesized IFN-α2a genes, *E.coli* BL21(DE3)Star bacteria, MagicMedia™ *E. coli* Expression Medium, Pierce C18 Tips, SYPRO™ Orange Protein Gel Stain, tris-(2-carboxyethyl)-phosphine (TCEP), iodacetamide (IAA) and formic acid MS grade were ordered from Thermo Fisher Scientific Germany (Darmstadt, Germany). BioPro IEX SmartSep S20 1 mL and 5 mL were ordered from YMC Europe (Dinslaken, Germany). XK16/600 Superdex 75 pg column was ordered from Cytiva Life Sciences (Freiburg, Germany). Zorbax 300SB-CN column was ordered from Agilent (Waldbronn, Germany). Vivaspin centrifugal concentrators were ordered from Sartorius AG (Göttingen, Germany). Spectra/Por 1 Dialysis Membrane Standard RC tubing was ordered from Repligen (Ravensburg, Germany). ROTIPHORESE® NF-Acrylamide/Bis-Solution 30 (29:1) was ordered from carl roth gmbh (Karlsruhe, Germany). HEK-Blue™ IFN-α/β Cells, blasticidin and zeocin were ordered from Invivogen (Toulouse, France). Proteinase K was ordered from Promega (Walldorf, Germany). Strata™-X 33 µm Polymeric Reversed Phase syringe columns were ordered from Phenomenex (Aschaffenburg, Germany). Pre columns and columns for LC-MS/MS analysis were ordered from PepSep (Marslev, Denmark). ReproSil-Pur 120 C18-AQ, 1.9 µm was ordered from Dr. Maisch (Ammerbuch-Entringen, Germany). Bovine serum albumin standard for MALDI-MS calibration were purchased from Bruker (Bremen, Germany) DBCO-PEG_4-5/6-Carboxyrhodamine 110 was purchased from Jena bioscience (Jena, Germany). Sep-Pak C18 1 cc Vac Cartridge from Waters were ordered from VWR (Darmstadt, Germany).

Expression of IFN-α2a, IFNK31N_3 and IFNK134N_3

All used IFN-α2a genes were cloned into pET21a(+) vectors with an ampicillin resistance between the NdeI and BamHI restriction sites. The correct insertion was verified by Sanger DNA sequencing (Eurofins genomics). Each vector was transformed into competent *E. coli* BL21(DE3)Star bacteria. If an amber codon was present in the coding sequence the pEVOL-pylRS vector, which was kindly donated by Prof. Dr. Edward A. Lemke (Johannes Gutenberg University of Mainz/Ruprecht-Karls-University of Heidelberg, Germany), was cotransformed, containing a chloramphenicol resistance.[195, 196] For protein

expression an *E. coli* BL21(DE3)Star glycerol stock was plated on an agar plate containing the needed antibiotics and incubated overnight at 37 °C. On the next day, one colony was picked and inoculated at 37 °C overnight in LB medium containing the needed antibiotics. At the following day, a desired amount of culture was transferred into TB-medium yielding a starting OD_{600} of 0.08 and was grown to an OD_{600} of 0.7. At this point IFN-α2a WT was induced with 1 mM IPTG and left for 8 h at 37 °C, 120 rpm (2-inch rotation radius). Mutants were collected at an OD_{600} of 0.7 and centrifuged at 3000 × g, 20 °C for 20 min. The supernatant was discarded and the bacteria pellet was resuspended in 1:10 magic media, containing 20 mM of the used unnatural amino acid, 0.4 % (w/v) L(+)-arabinose and 0.2 mM IPTG (pH was corrected before use with NaOH to 7.4 due to the acidic uAA), yielding a 10-fold condensed culture. The culture was put back into the incubator at 37 °C, 120 rpm for 16 h. Afterwards the culture was harvested, cooled down on ice and centrifuged at 5000 × g, 4 °C for 20 min. The supernatant was discarded, and the pelleted bacteria were resuspended to an OD_{600} of 100 in buffer A (50 mM Tris–HCl pH 8.0, 200 mM NaCl).

Cell lysis, inclusion body isolation and refolding of IFN-a2a WT and its azide functionalized mutants IFNK31N_3 and IFNK134N_3

Cell lysis was done using a high-pressure homogenizer (Emulsiflex C5, Avestin Europe GmbH, Mannheim, Germany). The resuspended bacteria were lysed in 3 cycles at 15 000 to 20 000 psi. Directly after the first lysis 1 mM PMSF, 25 µg/mL lysozyme and 10 µg/mL DNAse I was added, and the lysate was left on ice for 1 h. Afterwards the remaining 2 lysis cycles were performed. The lysed cells were centrifuged in an ultracentrifuge at 100 000 × g, 30 min at 4 °C and the pellet was resuspended in buffer A + 1% Triton X-100. The solution was centrifuged again and the Triton X-100 step was repeated once. Afterwards the pellet was resuspended with buffer A and centrifuged again. The resulting pellet was resuspended in 5 mL per 1 g wet pellet in buffer A + 7 M guanidinium hydrochloride and was vortexed intensely to solubilise the pellet. Afterwards, the solution was ultra-centrifuged for 45 min, 4 °C at 100 000 × g and the pellet discarded. The protein concentration of the supernatant was determined by BCA Assay. Afterwards, the supernatant containing the dissolved IFN-α2a was added dropwise to the ice-cold refolding buffer (Buffer A + 1 M 3-(1-Pyridinio)-1-propanesulfonate (also known as NDSB-201) + 2 mM β-mercaptoethanol) up to a final protein concentration of 150 µg/mL and was stirred for 5 more minutes and incubated overnight at 4 °C under constant stirring at 100 rpm. At the next day the refolding buffer was centrifuged at 5000 × g 4 °C for 5 min.[197]

Purification of IFN-α2a by ion exchange chromatography

The supernatant containing the refolded IFN-α2a was dialysed three times for 3 hours in dialysis buffer (20 mM Tris-HCl pH 8.0) against a 30-fold volume of the refolding buffer at 4 °C. The solution was centrifuged again at 5000 × g 4 °C for 5 min and sterile filtered afterwards. The dialysed sample was used for anion exchange chromatography on an FPLC system (Äkta Pure, Cytiva, Freiburg, Germany) using 2x BioPro IEX SmartSep 5 mL columns. (A: 20 mM Tris-HCl pH 8.0, B: 20 mM Tris-HCl pH

8.0, 2 M NaCl). A single step elution was performed using 15% B over 5 column volumes. All IFN-α2a containing fractions were pooled and dialysed against a 100-fold excess of 25 mM NaOAc pH 4.5 overnight. The solution was sterile filtered and used for cation exchange chromatography using a BioPro IEX SmartSep S20 1 mL column in a linear gradient from 0-50% in 25 column volumes (A: 25 mM NaOAc pH 4.5, B: 25 mM NaOAc pH 4.5 + 2 M NaCl). IFN-α2a containing fractions were pooled, concentrated to a final volume of 1 mL, 5 mg/mL and used for size exclusion chromatography using a XK16/600 Superdex 75 pg column. An isocratic elution was run (25 mM NaH_2PO_4 pH 7.4 + 150 mM NaCl) over 1.5 column volumes. Clean IFN-α2a samples were pooled concentrated to 1 mg/mL, snap frozen in liquid nitrogen and stored at -80 °C.

In-gel digest of proteins and protein fragment extraction with MS/MS analysis

In-gel digest of proteins followed by MS/MS analysis was performed as described before.[198]

Strain promoted alkyne-azide Huisgen cyclo-addition (SPAAC)

IFNK31N_3, or IFNK134N_3 and a 20-fold molar excess of BCN or DBCO functionalized polymer were mixed. The click reaction was performed at 4 °C for at least 48 h in PBS at pH 7.4. Afterwards the sample was dialysed overnight at 4 °C against a 100-fold excess of buffer (25 mM NaOAc pH 4.5) and purified from unreacted educts using cation exchange chromatography as described above.

SDS-PAGE

SDS PAGE was performed using standard Tris-glycine buffer systems. Tris-HCl 37.5 mM + 1 g/L SDS were used as final concentrations for stacking (pH 6.8) and separating gel (pH 8.8). Acrylamide concentrations ranged from 10-15%. 25 mM Tris + 192 mM glycine + 1 g/L SDS was used as a running buffer. The run was started at 80 V until samples reached the separating gel, afterwards voltage was increased to 120 V.

Native-PAGE

Native PAGE was performed on a 7.5-12% gradient gel (Tris-HCl 37.5 mM pH 7.5). 25 mM Tris-HCl pH 7.5 + 192 mM glycine was used as a running buffer. PAGE took place at 4 °C for 4 h, 160 V under constant additional chamber cooling using ice.

Circular dichroism spectroscopy

IFN samples were dialysed against 20 mM sodium phosphate buffer pH of 7.4, with the identical buffer serving as a blank. CD spectra were recorded at 37 °C on a spectropolarimeter (J715 spectropolarimeter, Jasco Labor- and Datentechnik GmbH, Groß-Umstadt, Germany). Protein solutions had final concentrations of 0.18 - 0.2 mg/mL in a 1 mm path length cell with the following parameters: 100 mdeg sensivity, 0.1 nm step resolution, 50 nm min^{-1} scan speed from 250 - 190 nm, 2 s time constant. Three accumulations per scan were averaged.

RP-HPLC analysis

RP-HPLC analysis was performed on an HPLC-System, equipped with a VWD detector (Agilent 1260 Infinity II Agilent Technologies Deutschland GmbH, Waldbronn, Germany). The wavelength was set to 214 nm and column oven temperature to 30 °C. 5 µg of protein were applied to a ZORBAX 300SB-CN column (4.6 x 150 mm, particle size = 5 µm) with an autoinjector. Proteins were eluted by a linear gradient of 5-70% eluent B over 35 min, flow = 1 mL/min with eluent A = Water + 0.1% TFA and eluent B = ACN + 0.1% TFA.

MALDI-TOF MS

The samples were desalted using Pierce C18 –tips following the manufacturer's instructions. Matrix-assisted laser desorption ionization (MALDI) mass spectra were acquired in the linear positive mode (UltrafleXtreme mass spectrometer equipped with a 355 nm smartbeam-II™ laser, Bruker Daltonics, Bremen, Germany). Mass spectra were calibrated with bovine serum albumin.

HEK Blue IFNα/β cell culture assay

The cell culture assay was performed in HEK-Blue™ IFN-α/β Cells according to the manufacturer's instructions.

Differential scanning fluorimetry

DSF was performed on a Real Time PCR machine (Agilent Stratagene Mx3005P, Agilent Technologies, Waldbronn, Germany) equipped with a SYPRO Orange filter with an excitation wavelength of 492 nm and an emission wavelength of 610 nm. The filter set gain multiplier was set to x4 for SYPRO Orange. A temperature step gradient was run with 1 °C increments and 1 min steps from 25-95 °C. The protein concentration was set to 8 µM in 25 µL buffer (100 mM Na_2HPO_4 pH 7.4, 150 mM NaCl). The buffer also contained SYPRO Orange with a final 5x concentration of SYPRO Orange. SYPRO Orange was diluted from a 5000x stock in DMSO. Normalisation was performed as described before, but no smoothing was performed.[199] Half maximal denaturation (HMD) method was used to determine the melting points as it did represent the measured data better than the first derivative method (FD method).

Limited Proteolysis Assay (LIP)

For Each experiment 30 µg of IFN-α2a WT, or IFNK31N_3 coupled to BCN polymers of PEG, LPG and PEtOx) were diluted to 570 µL with digestion Buffer (25 mM Tris, 150 mM KCl, 10 mM $CaCl_2$) and warmed to 37 °C. The assay was started by adding 30 µL of a 10 ng/µL (total 300 ng) Proteinase K solution (diluted with digestion buffer from stock solution), this equals a 1:100 ratio of protease/protein. Digestion was performed at 37 °C under constant shaking at 750 rpm. After digestion times of 1, 3, 5, 10 and 30 minutes each time 120 µL of the sample were removed and digestion was stopped by addition of the sample to a 2 mL tube containing 94 mg of solid guanidine hydrochloride (final concentration ~ 8.2 M) and 10 µL of PMSF (200 mM in DMSO), leading to a final concentration of ~16,5 mM PMSF. Each sample was briefly vortexed and frozen in liquid nitrogen.

For analysis, samples were heated to 95 °C for 8-10 minutes, briefly centrifuged and then reduced and alkylated. In brief, while still warm, TCEP was added to a final concentration of ~ 33,3 mM (10 µL of 0,5 M stock), after 15-20 minutes and cooling to RT, 60 µL of 0.2 M iodacetamide in water were added, alkylation was allowed to proceed for 20 min in the dark. Immediately afterwards polymers were extracted by ethyl acetate, or chloroform. For this, 800 µL of organic solvent were added to the tube, and then the organic phase was acidified with 25% TFA (1/25 of the total volume). The samples were vortexed and then shaken for 5 minutes, followed by centrifugation at 16 000 × g for 10 minutes. The supernatant was removed carefully with a pipet. This procedure was repeated three times, but acidification was only performed twice. The remaining volume was vacuum centrifuged at 37 °C for 30 minutes to remove remaining solvent. Immediately afterwards, the samples were loaded on 1 mL Strata X33 syringe columns (when extracted with ethyl acetate), or 1 mL C18 syringe columns (when extracted with chloroform). These columns were washed and eluted using only gravitational flow. Washing: 5-7 mL of 0.4% formic acid (FA) in water; elution: 2x 0.8 mL 0.4% formic acid in 80% acetonitrile/water). Samples were then freeze dried overnight and then resuspended in 30 µL of 0.2% FA, 2% acetonitrile in water for immediate LC-MS analysis.

Analysis of LIP (LC-MS / Data Analysis)

NanoLC-MS/MS analyses were performed on a LTQ-Orbitrap Velos Pro (Thermo Fisher Scientific, Darmstadt, Germany) equipped with a PicoView Ion Source (New Objective, Littleton, USA) and coupled to an EASY-nLC 1000 (Thermo Fisher Scientific, Darmstadt, Germany). Peptides were loaded on a precolumn (trap column, 2 cm x 150 µM ID) packed with 3 µm C18 ReproSil and then eluted to capillary columns (30 cm x 150 µm ID) self-packed with ReproSil-Pur 120 C18-AQ, 1.9 µm and separated with a 30-minute linear gradient from 3-30% acetonitrile and 0.1% formic acid and a flow rate of 500 nL/min.

MS scans were acquired in the Orbitrap analyzer with a resolution of 30,000 at m/z 400, MS/MS scans were acquired in the Orbitrap analyzer with a resolution of 7500 at m/z 400 using HCD fragmentation with 30% normalized collision energy. A TOP5 data-dependent MS/MS method was used; dynamic

exclusion was applied with a repeat count of 1 and an exclusion duration of 7 seconds; singly charged precursors were excluded from selection. Minimum signal threshold for precursor selection was set to 50,000. Predictive automatic gain control (AGC) was used with AGC target a value of $1x10^6$ for MS scans and $5x10^4$ for MS/MS scans. Lock mass option was applied for internal calibration in all runs using background ions from protonated decamethylcyclopentasiloxane (m/z 371.10124). Data analysis was performed using PMi-Byos (Protein Metrics inc., Cupertino United states). All datafiles were searched at the same time, with the following settings:

Precursor Tolerance of 6 ppm, fragment mass tolerance of 20 ppm, unspecific digestion, carboxymethyl @ C as fixed modification, Gln to pyro-Glu @ peptide N-terminus Q, Glu to pyro-Glu @ peptide N-terminus E, both as common and last oxidation @ M,W; Deamidation @ N,Q; ammonia loss @ N; Dioxidation @ W all as rare modifications in addition a wildcard search for masses between 100-120 @ K was allowed. With total common and rare max to 1 each. Data was searched against custom database containing the WT sequence, decoys were added. Results were filtered and only peptide matches with a scoring of >100 were considered.

Molecular modeling

Atom types and force field parameters were assigned on the basis of the AMBER14ffSB[200] and GAFF2[201] force fields using *antechamber* and *parmchk2* from AmberTools18.[202] RESP partial charges for the systems were derived using Gaussian 09 Rev. C.01[203] (Hartree-Fock level of theory, 6-31G* basis set). During charge derivation, monomers were capped with residues of the same type, the N-termini of the K31-BCN and the K31-DBCO amino acid backbones with acetyl groups and their C-termini with *N*-methylamide groups. Initial straight polymer conformations were generated using *tleap*.[202] Subsequently, K31 conjugates of the IFN-α2a WT NMR structure (PDB: 1ITF)[204] were built using MOE[205] (Molecular Operating Environment 2019.01). Protonation states were not altered, as applying Epik within Maestro 2018-1[206, 207] at pH 7.4 did not lead to changes thereof.

Ten different starting structures were generated for each 10 kDa BCN and DBCO polymer conjugate by first modelling IFNα-2a with stretched out linkers and polymers, which were then initially energy minimized within MOE. Polymers were oriented into different directions and then subjected to short initial simulations in MOE, using the Nosé-Poincaré-Andersen approach[208, 209] with the Generalized Born implicit solvent model[210] and the Amber14:EHT force field[200, 211] while holding the positions of all other residues fixed. This led to compact starting structures with different regions of the protein being covered by the respective polymer. These were then solvated with TIP3P water[212] in octahedral simulation boxes with a distance of the solutes of at least 15 Å to the box borders. After an initial energy minimization of 10,000 steps systems were heated up from 100 to 300 K over 500 ps. Initial harmonic constraints on the bioconjugates were applied and gradually released over an additional 1.6 ns. NVT ensembles were ensured via Langevin dynamics before collecting statistics on the energy potential in a 20 ns long NPT equilibration via application of the Nosé-Hoover Langevin piston method (2 ns

conventional MD and 18 ns Gaussian accelerated MD (GaMD)),[213, 214] as required for the GaMD approach. For each structure, a 150 ns GaMD production run was then performed with a dual-boost scheme (dihedral and total potential boost), setting the user-specified upper limits σ_{0D} and σ_{0P} for the standard deviation of the boost potential ΔV to 6.0 kcal/mol. Thus, for each 10 kDa polymer conjugate a total of 1.5 µs of simulation data was collected. For an equal simulation length of conventional MD of the IFN-α2a WT, the first ten structures of the NMR conformational ensemble of PDB file 1ITF were each solvated with TIP3P water[212] in a rectangular box with a minimum distance of the protein to the border of 10 Å. Analogous energy minimization and NVT equilibration with harmonic constraints were applied as described above. A subsequent 1 ns NPT equilibration was then performed before conducting a 150 ns long production run for each of the ten structures. All simulations were performed with NAMD 2.13.[215] Periodic boundary conditions were applied along with the particle mesh Ewald method[216] with a cutoff of 1.2 nm.

Analyses were conducted with *cpptraj*[217] and images were produced using PyMOL 2.2.3.[218] Backbone heavy atom RMSF values (atoms C_α, N, C and O) were calculated as squared atomic positional fluctuations (multiplied by $8\pi^2/3$) in relation to the average structure of the respective simulation replica. Native contacts analysis was performed for all protein atoms (except for the K31 conjugation site and the flexible termini C1 – L9 and N156 – E165) in relation to the respective NMR structure by calculating the average fraction of frames in which these contacts occurred (using the *native contacts* command of *cpptraj* with a distance cutoff of 4.5 Å). Polymer densities were calculated using the *grid* command. Constrained network analysis was performed by writing out PDB files without solvent for every 0.1 nanoseconds of our GaMDs and IFN-α2a WT simulations. These ensembles were then used to perform a thermal unfolding simulation within CNA 2.0.[219-225] The unfolding was observed over an energy cutoff range from -10 to 0 kcal/mol with 0.05 kcal/mol steps (E = -10 0 0.05). For hydrophobic constraints, the standard distance cutoff of 0.25 Å (+ the corresponding Van der Waals radii, c = 0.25) between any carbon-carbon, carbon-sulfur or sulfur-sulfur atom (H = 1) was used and the strength was not altered at higher temperatures (TUS = 1). Melting temperatures were assessed with CNA using a spline fit, based on the cluster configuration entropy type 2 (CCE2). Linker atoms were treated as part of the amino acid K31, whereas monomers of the polymer were treated as ligand heteroatoms, meaning that only non-covalent interactions of the polymer with the protein were considered.

Results and Discussion

Synthesis and functionalization of polymers

LPG was synthesized by monomer-activated anionic ring-opening polymerization based on a previously reported protocol as shown before with modification (**Scheme 1A, S1-3**).[226, 227] In brief, the hydroxyl group of glycidol was protected with an acetal group prior to polymerization, which thereafter was deprotected in slightly acidic media to yield the linear backbone with respective free hydroxyl groups.[226] The desired molar mass with narrow dispersity was confirmed by SEC characterization (**Table 1**).

Table 1: Molar masses (kDa) and polydispersity values of the used polymers as analyzed by MALDI-TOF MS, SEC, and NMR.

	Molar mass [a]	$\overline{M_n}$	PDI [b]
BCN-PEG	10.7	10[b]	1.04
DBCO-PEG	10.9	10[b]	1.04
BCN-LPG	11.4	11.6[b]	1.23
DBCO-LPG	11.4	10.5[b]	1.32
BCN-PEtOx	8.4	8.1[c]	1.1
DBCO-PEtOx	8.1	8.1[c]	1.08

[a] by MALDI-TOF MS, calculated from bioconjugates, [b] by SEC in water, [c] by NMR.

To enable strain-promoted azide-alkyne cycloaddition (SPAAC), the bromide group was substituted by an azide group followed by reduction to a primary amine (**Figure S1**). In the next step the amine was modified with a cyclooctyne (BCN-NHS or DBCO-NHS) *via* carbamate formation, as shown before with modification.[228] Successful functionalization of the chain-ends was confirmed by ^{1}H-NMR spectroscopy (**Figure S2 and S3**).

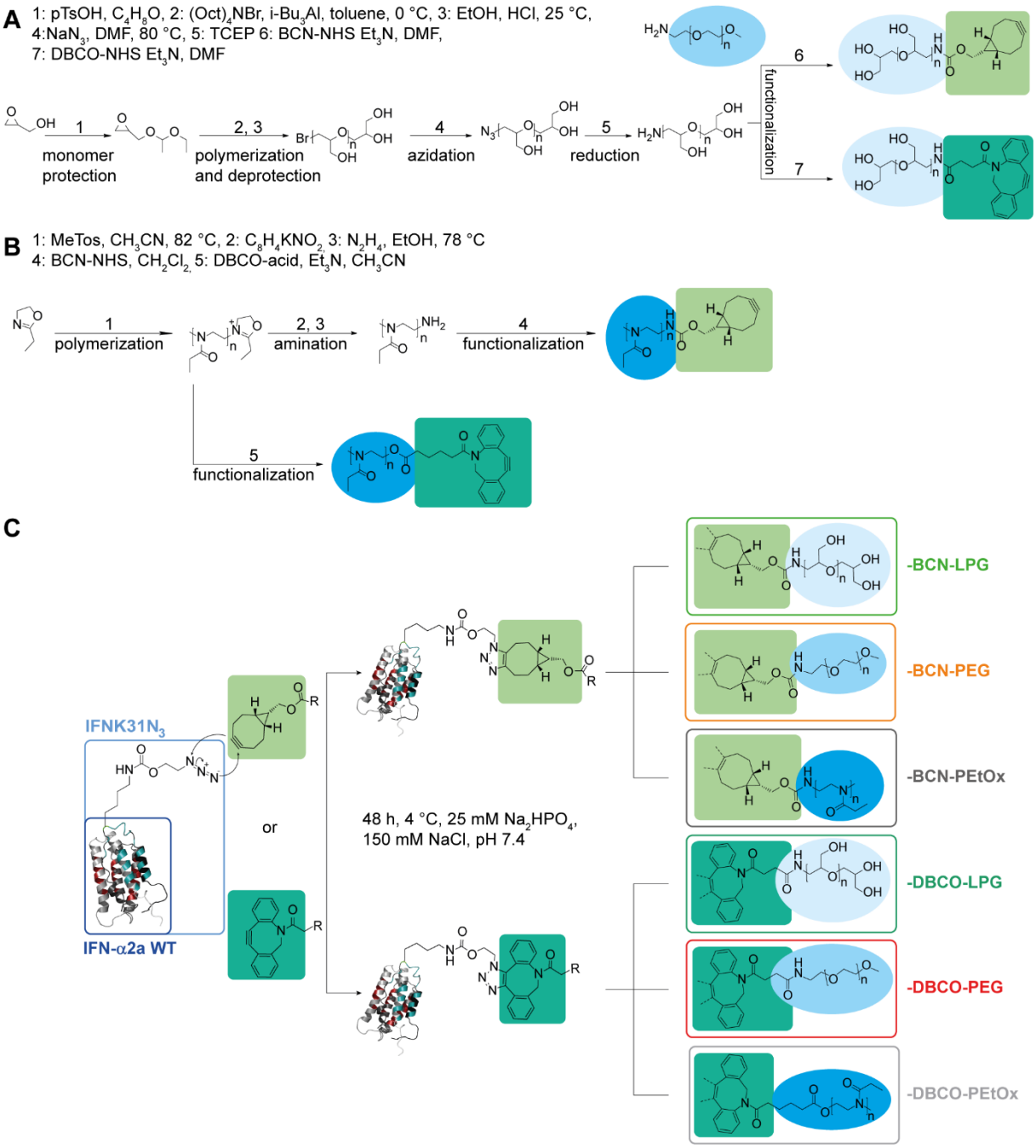

Scheme 1: (A) Synthesis and chain-end modification of LPG via anionic ring opening polymerization. Structure of commercial mPEG-NH_2 is displayed, its modification to cyclooctyne groups was done under the same conditions as shown for LPG-NH_2. (B) Synthesis of PEtOx via cationic ring-opening polymerization and its chain-end modification strategies. (C) SPAAC reaction of NAEK with BCN or DBCO functionalized polymer and used reaction conditions for the site-specific modification of IFN-α2a. The resulting IFN-α2a bioconjugates are displayed.

To compare the linker chemistry of our IFN-α2a bioconjugates, commercial mPEG-NH_2 was modified with BCN and DBCO applying the same conditions as for LPG-NH_2 (**Scheme 1A, Figure S4 and S5**). PEtOx was synthesized by cationic ring-opening polymerization (CROP) of 2-ethyl-2-oxazoline. The reactive cyclooctyne moieties were introduced by two different synthetic strategies (**Scheme 1B and Figure S6-10**). Here, DBCO was introduced by direct addition of the respective DBCO-acid in presence of triethylamine.[229] Alternatively, the living oxazolinium ω-chain-end was further functionalized with

phthalimide and subsequently deprotected by hydrazinolysis yielding the ω-amino PEtOx.[183] The insertion of the cyclooctyne moiety was performed as for the LPGs utilizing the BCN-NHS ester.[230] The successful modifications were demonstrated by ^{1}H-NMR spectroscopy. The molar masses as well as dispersity values were determined by SEC (**Figure S9, S10 and Table 1**).

Expression and characterization of azide functionalized IFN-α2a

We engineered two mutants of IFN-α2a by amber codon (UAG) suppression using a pyrrolysyl-tRNA synthethase/tRNAPyl CUA pair originating from *Methanosarcina barkeri* and as demonstrated before.[92-97, 184, 231-233] Positions #31 or #134 were chosen for mutation as these lysine residues are surface-accessible for bioconjugation as demonstrated in the IFN-α2a tertiary structure (**Figure 1A and S11**).

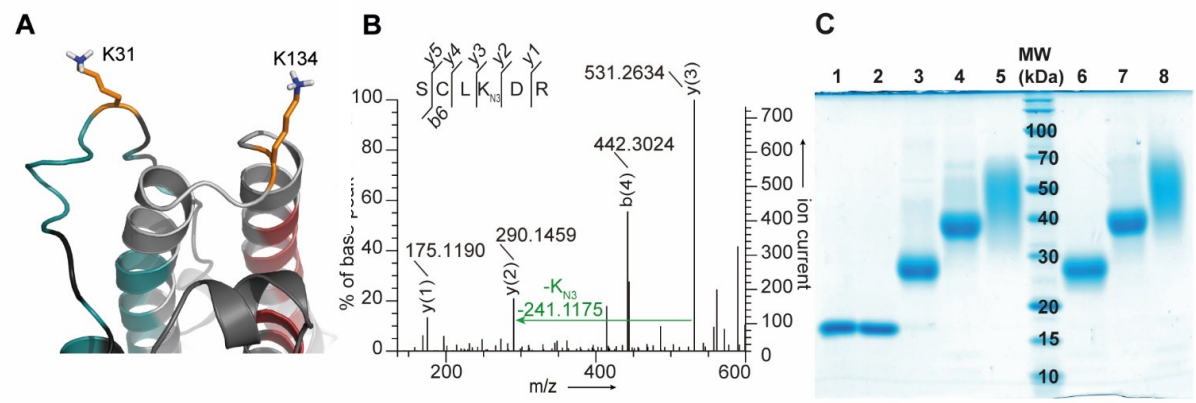

Figure 1: (A) NMR structure of IFN-α2a WT displaying the tertiary structure close to the chosen mutation sites K31 and K134 highlighted in orange. IFNAR1 binding domain is highlighted in red, IFNAR2 binding domain in petrol. (PDB: 1ITF).[204] (B) Exemplary MS/MS spectrum of IFNK31N$_3$ displaying the correct incorporation of NAEK (KN$_3$) at amino acid position #31 in a successive Y-Ion series. KN$_3$-H$_2$O = 241.1133 (C) 10–15% SDS-PAGE of IFN-α2a WT (1) IFNK31N$_3$ (2) IFNK31N$_3$-BCN-PEtOx 8.4 kDa (3) IFNK31N$_3$-BCN-PEG 10.7 kDa (4) IFNK31N$_3$-BCN-LPG 11.4 kDa (5) IFNK31N$_3$-DBCO-PEtOx 8.1 kDa (6) IFNK31N$_3$-DBCO-PEG 10.9 kDa (7) IFNK31N$_3$-DBCO-LPG 11.4 kDa (8).

Moreover, IFN-α2a-PEG isomers present in the marketed product Pegasys® that are modified at #31 or #134 revealed to have the highest bioactivity compared to all other IFN-α2a PEG isomers that are present in Pegasys®. These two sites were previously suggested as ideal mutation sites.[234] Therefore, we engineered two mutants, each of which replacing either K31 or K134 by the unnatural amino acid (uAA) NAEK ((*N*^{6}-((2-azidoethoxy)carbonyl)-L-lysine) (**Scheme 1C**). Integration of NAEK was by IPTG induced expression in Escherichia coli *BL21(DE3)Star*, using a condensed culture technique to maximize the overall protein yield of IFN-α2a K31N$_3$ to 20 – 30 mg purified protein per liter condensed culture (**Figure S12A**).[235] The incorporation of the uAA at the intended positions #31 or #134 was confirmed by trypsin in-gel digest followed by ESI MS/MS (**Figure 1B and S13**).

Functionality of the incorporated azide was demonstrated by a fluorescent, alkyne-functionalized dye, followed by SDS-PAGE (**Figure S12B**).

IFN-α2a binds to the interferon α/β receptor, being composed of IFNAR1 and IFNAR2. Our HEK-293 cell line reports IFN-α/β stimulation by an inducible secreted embryonic alkaline phosphatase gene (SEAP) reporter gene being under control of the ISRE (interferon sensitive response element) ISG54-

promotor.[236] Introduction of the azide functionality into IFN-α2a at position #31 or #134 resulted in a 2-fold reduced bioactivity compared to IFN-α2a WT (**Figure S14**). We finally selected the mutant IFN-α2a with NAEK at position #31 due to its higher protein expression yield.

Bioconjugation of polymers to azide functionalized IFN-α2a and characterization

Bioconjugation of PEG, PEtOx and LPG was performed at 4 °C in PBS buffer at pH 7.4 for 48 h (**Scheme 1C**), starting off previous protocols.[237] All bioconjugates were analyzed by SDS-PAGE (**Figure 1C**). Here, the type of polymer impacted the retention of the bands, which is why further characterization was done by native PAGE. All types of IFN-α2a bioconjugates resulted in comparable outcome (**Figure S12C**). The differences between SDS-PAGE and native PAGE results reflect the interaction particularly of the PEG and LPG polymers with SDS, as reported before for PEG.[238] All bioconjugates were determined by MALDI-TOF MS (**Figure S15**) confirming the correct and expected molecular masses (**Table 1**).

IFN-α2a bioconjugates were further studied by RP-HPLC analysis (**Figure S16**). Both types of LPG conjugated IFN-α2a (BCN and DBCO) showed a reduction in retention time (r.t.) by 1.1 min compared to unconjugated IFNK31N_3. In contrast, PEG conjugation to IFN-α2a marginally reduced the r.t., whereas PEtOx conjugated IFN-α2a showed the highest r.t. shift (30 min BCN-PEtOx and 30.1 min DBCO-PEtOx), as expected for PEtOx being the most hydrophobic polymer in this study.

Secondary structure of IFN-α2a WT, IFNK31N_3 and bioconjugates was investigated by CD-spectroscopy (**Figure 2A**), with a strong α-helical signal as expected for IFN-α2a.[239] Comparable spectrograms were recorded for all groups, indicating that neither the genetically introduced unnatural amino acid nor its conjugation to any of the polymers impacted secondary structure.

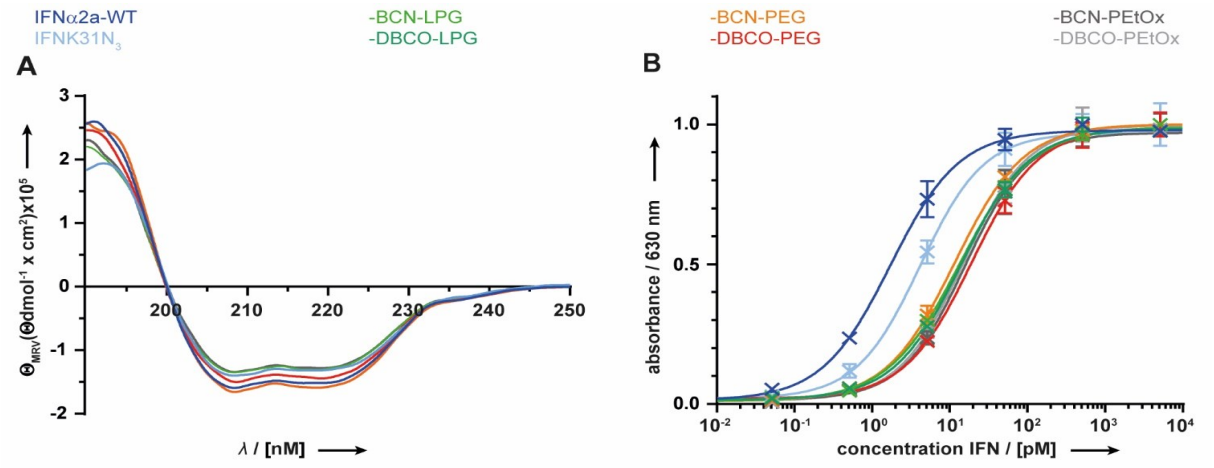

Figure 2: (A) CD spectra of IFN-α2a, IFNK31N_3 and IFN-α2a bioconjugates. α-helical minima are at 209 and 220 nm. α-helical maxima are at 192 nm. (B) Secreting alkaline phosphatase assay of HEKBlue 293 IFN-α/β cells after 20 h of stimulation with IFN-α2a WT, IFNK31N_3 and IFN-α2a bioconjugates (mean ± standard deviation, n = 3). (WT = blue, N_3 = light blue, BCN-LPG = light green, DBCO-LPG = dark green, BCN-PEG = orange, DBCO-PEG = red, BCN-PEtOx = dark grey, DBCO-PEtOx = light grey).

To evaluate the influence of the type of conjugated polymer and linker chemistry (BCN/DBCO) on biological performances, all IFNK31N_3 bioconjugates were compared to the unconjugated mutant and IFN-α2a WT counterpart in the SEAP reporter assay. IFN-α2a bioconjugates showed a 3-fold reduction in biological activity compared to IFNK31N_3, with no significant differences among each of the different polymers or linkers (**Figure 2B and Table 2**).

Table 2: Bioactivity and melting points of tested IFN-α2a and bioconjugates, given as EC50 values in 95% confidence intervals.

	EC50 [pM]	T_m [°C]
WT	1.5-2.0	64.7-65.3
N_3	3.5-5.0	62.3-63.0
BCN-PEG	10.7-12.5	60.9-61.7
DBCO-PEG	16.7-21.6	60.5-61.2
BCN-LPG	12.3-14.6	62.0-63.1
DBCO-LPG	12.6-15.7	60.6-61.2
BCN-PEtOx	13.1-18.6	59.8-60.2
DBCO-PEtOx	12.9-17.3	59.6-60.3

Next, we analyzed the thermal stability of all IFN-α2a bioconjugates to determine the impact of PEG, PEtOx and LPG and cyclooctyne linker type on thermally induced unfolding (**Figure 3 and Table 2**). As PEtOx is a thermoresponsive polymer and might therefore interfere with the differential scanning fluorimetry assay, we first determined the critical solution temperature as analyzed by turbidity analysis. A 3-fold higher concentration relative to the differential scanning fluorimetry assay was tested, but no significant turbidity increase was detected between the chosen temperature range from 5 °C to 85 °C (**Figure S17**). Both, DBCO-PEtOx and BCN-PEtOx had a significant destabilising effect resulting in -2.7 °C in T_m, followed by DBCO-PEG with -1.8 °C and BCN-PEG with -1.4 °C as compared to IFNK31N_3. In contrast, BCN-LPG and DBCO-LPG differed significantly in their thermal stability. BCN-LPG retained the thermal stability, yielding a T_m difference of -0.1 °C in contrast to DBCO-LPG, with a T_m difference of -1.8 °C, when compared to IFNK31N_3. Therefore, PEtOx conjugation promoted unfolding at lower temperatures compared to thermal unfolding of unconjugated IFNK31N_3. This polymer order (bioconjugates of PEtOx, PEG, and LPG) correlated with the order of increasing polymer hydrophilicity (**Figure 3A**).

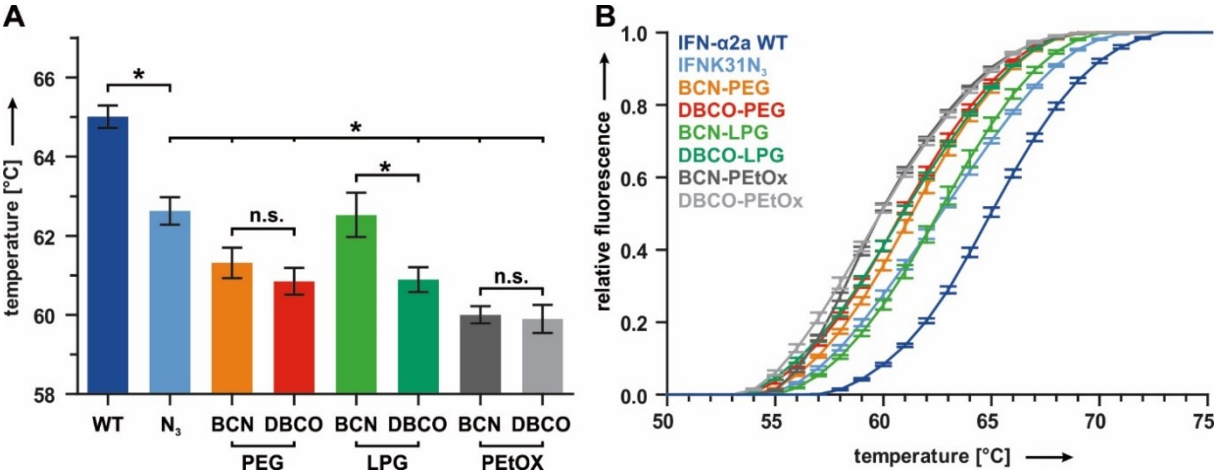

Figure 3: Differential scanning fluorimetry of bioconjugates (A) Measured melting points of bioconjugates (n = 5). 95% CIs are stated with error bars. The colour code is also displayed in Scheme 1 (WT = blue, N_3 = light blue, BCN-LPG = light green, DBCO-LPG = dark green, BCN-PEG = orange, DBCO-PEG = red, BCN-PEtOx = dark grey, DBCO-PEtOx = light grey) significant p-values < 0.05 compared to IFNK31N_3 and between bioconjugates are indicated. (B) Normalised, averaged fluorescence of the differential scanning fluorimetry assay with IFN-α2a WT, IFNK31N_3 and its BCN bioconjugates (n = 5). The lowest value of each measurement was set to 0 as well as all values below this temperature. The highest value of each measurement was set to 1 as well as all values above this temperature. The normalized values were averaged, and adjacent points connected. Standard deviations are indicated with error bars.

Molecular modeling of IFN bioconjugates

To further detail thermal stability and interaction profiles of the polymers and both cyclooctyne linkers on a molecular level, we conducted classical molecular dynamics simulations (cMDs) of the IFN-α2a WT and Gaussian accelerated MDs (GaMDs)[213, 214] of IFNK31N_3 10 kDa BCN/DBCO bioconjugates. Similar to a previously published study,[240] we modeled ten different starting structures of each variant in which the polymers covered different areas of the protein surface, followed by constrained network analyses (CNA) in which body-and-bar networks were generated from these structural ensembles.[219-225, 241] Constraints based on covalent and non-covalent interactions were evaluated to assess protein rigidity and, by successively releasing the ones resulting from hydrogen bonds and salt-bridges, unfolding temperatures were predicted. The output agreed with experimental findings (**Figure 4A**).

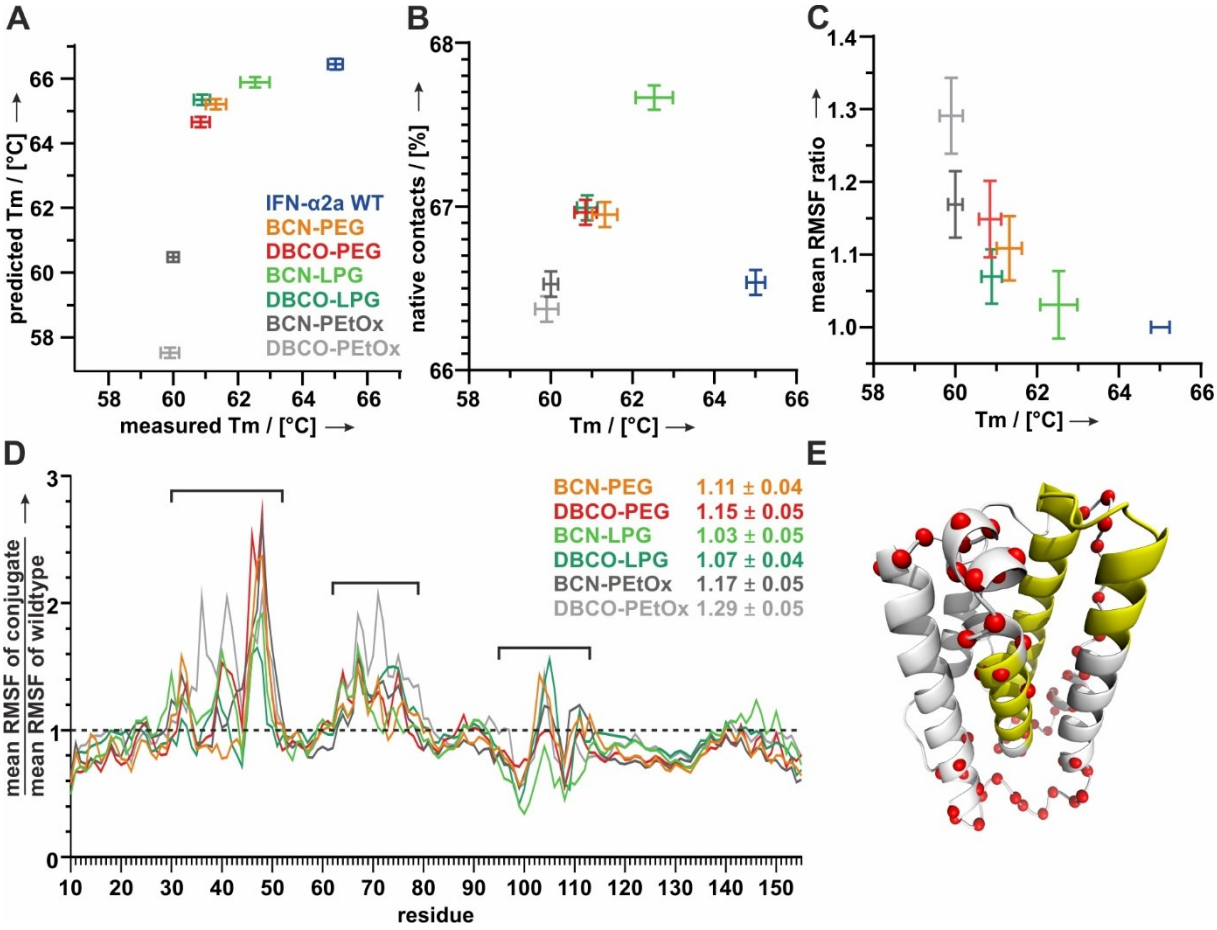

Figure 4: (A) Correlation between CNA-based and experimentally determined melting temperatures. The color code is displayed in Scheme 1 (WT = blue, BCN-LPG = light green, DBCO-LPG = dark green, BCN-PEG = orange, DBCO-PEG = red, BCN-PEtOx = dark grey, DBCO-PEtOx = light grey). (B) Correlation between the amount of native contacts and melting temperatures. (C) Correlation between the RMSF ratios (mean values in the top right of D) and melting temperatures (D) Residue-wise plotting of backbone RMSF ratios between the bioconjugates and the WT (mean value for all replicas) for residues G10 to T155 (excluding flexible termini). The largest differences are seen for residues of the flexible loops between the helices and some residues of helices 2 and 3 (L30 - T52, Q62 - T79 and L95 - E113, shown as red spheres in E and indicated with black brackets in the graph; the mean values for these residues are shown at the top right). (E) Tertiary structure of IFN-α2a WT (PDB:1ITF) highlighting the regions with the highest RMSF differences, which are displayed in D, as red spheres. Regions of interest regarding local rigidity indices (see Figure 5) are colored in yellow. Errors for all calculations represent standard errors of the mean.

The BCN-LPG bioconjugate was predicted to have the highest unfolding temperature, the DBCO-PEtOx conjugate the lowest, suggesting that a protein rigidity modulation upon conjugation might impact thermal stability, as previously reported for protein PEGylation.[242-244] Additionally to the network analysis, the number of native contacts was also the highest for the BCN-LPG and lowest for the DBCO-PEtOx bioconjugate (**Figure 4B**). This analysis showed a good correlation with regard to the thermal stability of the conjugates, thereby also detecting DBCO-LPG to be the only DBCO variant with a significantly reduced melting temperature compared to its BCN counterpart. A reduced protein rigidity compared to IFN-α2a WT is further supported by measurements of root-mean-square fluctuations (RMSF) of the protein backbone (**Figure 4C, D and E**). Increased RMSF values for residues of the non-structured loops between the helices and some residues of helices 2 and 3 of the bioconjugates were in

agreement with the lower melting temperatures. This increase in flexibility is, once again, smallest for the BCN-LPG conjugate and highest for the DBCO-PEtOx variant.

Looking more in-depth into the percolation indices of type 2 from our constrained network analyses, we found that certain areas of helices 2, 4 and 5 (V55 – N65, R125 – T155) were more flexible for the destabilized PEtOx conjugates (**Figure 5A**).

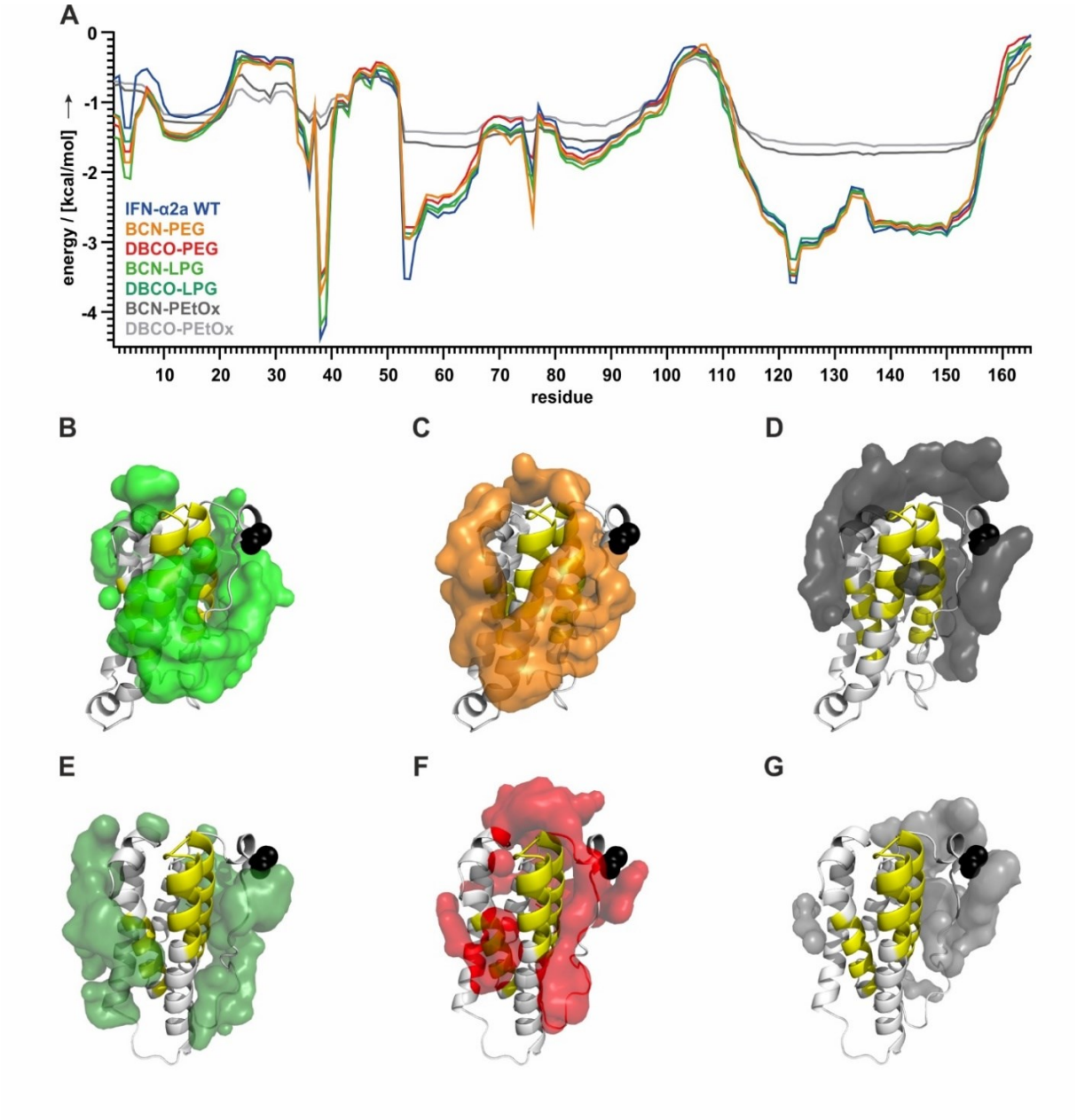

Figure 5: Energy cutoffs for percolation indices (type 2) per residue (WT = blue, BCN-LPG = light green, DBCO-LPG = dark green, BCN-PEG = orange, DBCO-PEG = red, BCN-PEtOx = dark grey, DBCO-PEtOx = light grey). Underneath, polymer densities from our simulations (analogously to Figures S20 and S21) are shown, with residues V55 – N65 and R125 – T155 depicted in yellow ((B) = BCN-LPG, (C) = BCN-PEG, (D) = BCN-PEtOx, (E) = DBCO-LPG, (F) = DBCO-PEG, (G) = DBCO-PEtOx).

This local rigidity index describes the energy cutoff during the thermal unfolding simulation of the applied CNA program, at which point a residue is removed from the largest rigid cluster and becomes flexible. Hence, less negative cutoff values correspond to residues becoming flexible early on due to hydrogen bonds and salt bridges (resembling constraints in the body and bar network) breaking up at lower temperatures. This may result from fewer protein-polymer interactions, as corresponding polymer densities around these areas are lower for both analyzed PEtOx conjugates (**Figure 5B-G**).

Taken together, all three prediction methods (CNA, native contacts and RMSF ratios) were in line with the experimentally determined thermal stability ranking of the conjugates (LPG > PEG > PEtOx) for both linker types, BCN and DBCO, respectively. With regard to the CNA based calculation, the observed overestimation of predicted PEG und LPG bioconjugate melting temperatures might reflect an overvaluation of the hydrogen bond acceptor capability of the polymer ether oxygen atoms, which are only present in PEG and LPG, but not PEtOx. Generally, melting temperatures obtained by this method should only be compared relatively between similar systems.[221]

The protein-polymer interaction profiles (**Figures S18 and S19**) from our simulations differed for the type of polymer and type of linker. With regard to BCN variants, PEG preferentially wrapped around positively charged lysines and arginines, as similarly observed before. [240] In contrast, LPG was often situated near serines and methionines, whereas the hydrophobic PEtOx more readily interacted with aromatic residues (F, Y, H). Polymer conformations sterically interfering with the IFNAR1 and IFNAR2 binding sites were found for all variants, which may explain the decreased bioactivity across all tested bioconjugates (**Figure S20 and S21**). Identified density hotspots and the amount of covered protein surface area for BCN-PEG were similar to results for a less bulkier aldehyde linker at the respective position (**Figure S22**).

The described protein-polymer interactions may only be very weak and transient though. This is reflected by the overall small melting temperature differences obtained from differential scanning fluorimetry (around 2.7 °C) and results from our limited proteolysis assay (*vide infra*).

Therefore, we hypothesize that these polymer-bioconjugates attain a dumbbell configuration, meaning the polymer more likely forms a random coiled structure adjacent to the globular IFN-α2a rather than being continuously adhered to it (shroud model).[245]

Limited proteolysis of IFN bioconjugates

To further evaluate the positioning of the polymers and their interplay with the IFN-α2a protein surface we conducted a limited proteolysis (LIP) experiment starting off previously published protocols.[246, 247] We therefore digested the IFN-α2a WT and all BCN-polymer conjugates with the protease Proteinase K and collected aliquots at different time points of digest. The used protocol of the LIP assay allowed for qualitative analysis of proteolytic events as of different extraction conditions of the polymers and varying ion suppression for different IFN-α2a BCN polymers.

An increasing number of cleavage sites was observed over time for the IFN-α2a WT and its PEGylated bioconjugate (**Figures 6 and S23)**. At the final time point, the cleavage sites were evenly spread across the whole protein sequence of IFN-α2a WT (**Figure S23C**). The cleavage sites were similar for the WT and the PEGylated protein, indicating no specific protection of IFN-α2a by PEG against the protease Proteinase K. The slightly delayed appearance of cleavage events from BCN-PEG 10 kDa compared to the WT is probably reflecting lower signal coverage caused by sample processing necessary for removal of polymer conjugates before the measurement. The resulting cleavage patterns over time were similar for LPG and PEtOx, respectively (**Figure 6, Figure S23**).

Regarding the outcome of the LIP analysis, we hypothesize that the probabilities of presence of the polymers around the protein are quite similar for all types and rather widespread, thus indicating only weak interactions and transient coverage of the protein surface. However, the current data lack quantitative information of the proteolytic events on the protein surface, which is subject to ongoing studies in our lab.

The performed LIP analysis was conducted on a minute time scale, thereby complementing the information from our 1.5 μs long *in silico* analysis of each bioconjugate (*vide supra*). Without resorting to less detailed coarse-grained models, the latter can only capture protein-near conformations of the polymers on relatively short time scales

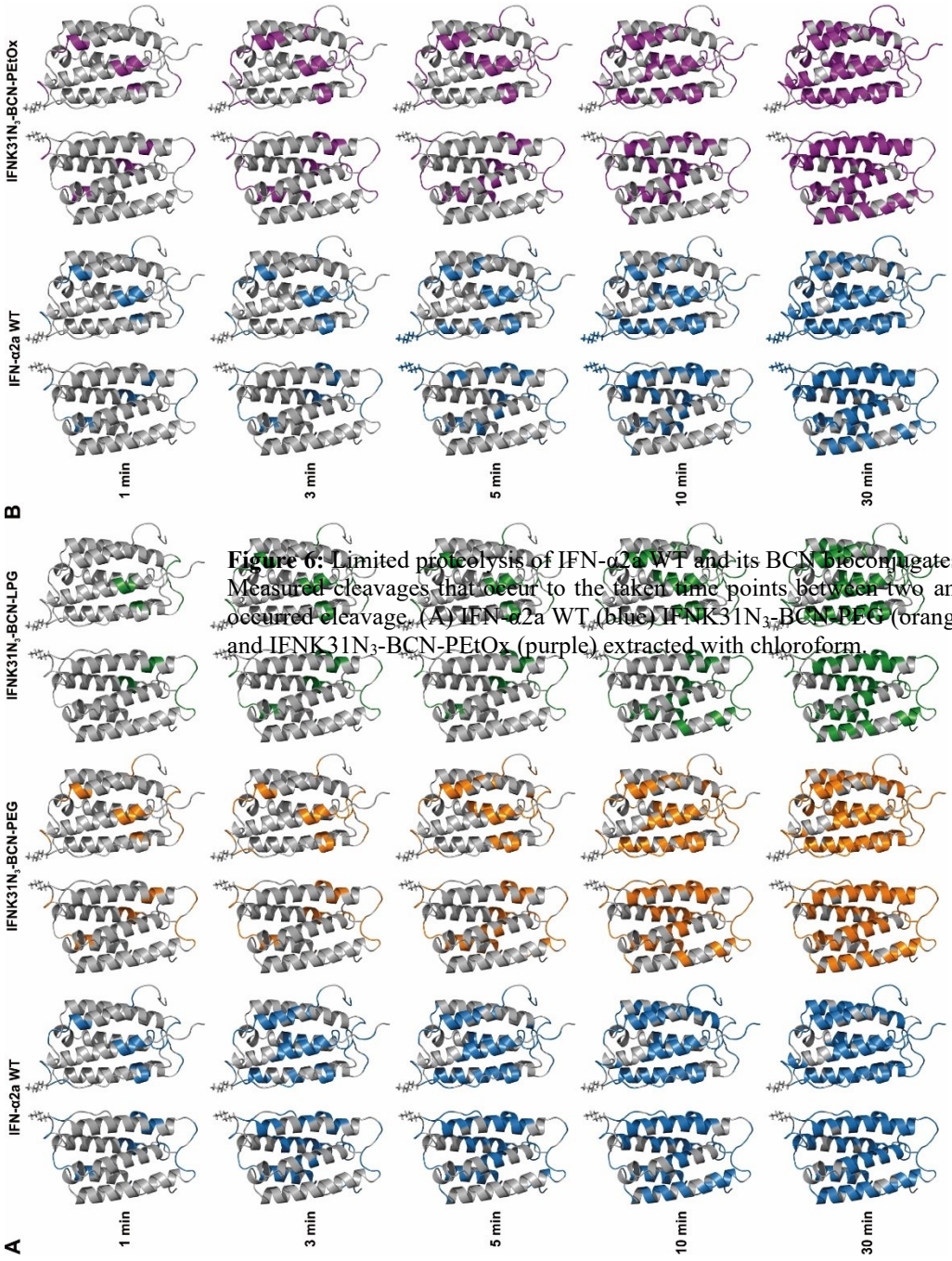

Figure 6: Limited proteolysis of IFN-α2a WT and its BCN bioconjugates with Proteinase K. The tertiary
Measured cleavages that occur to the taken time points between two amino acids are indicated, whereb
occurred cleavage. (A) IFN-α2a WT (blue) IFNK31N_3-BCN-PEG (orange) and IFNK31N_3-BCN-LPG (gr
and IFNK31N_3-BCN-PEtOx (purple) extracted with chloroform.

Conclusions

In this work, we demonstrated the synthesis of cyclooctyne functionalized linear mPEG, LPG and PEtOx polymers that were site-specifically conjugated to an azide functionalized IFN-α2a *via* SPAAC, deploying both BCN- and DBCO-linkers. All bioconjugates were compared to PEG regarding physico-chemical and biological properties. Thermal stability of IFN-α2a bioconjugates was highest for BCN-LPG and lowest for DBCO-PEtOx. Molecular modelling studies suggested destabilizing effects on IFN-α2a protein rigidity upon conjugation for the PEtOx polymer. Polymer choice also impacted interactions with IFN-α2a, although these may be overall very weak and only transient.

In conclusion, our presented experimental and computational data on IFN-α2a suggested that LPG and PEtOx are promising PEG alternative polymers for bioconjugation. Further studies using the IFN-α2a conjugates with polymer molecular weights up to 40 kDa are currently under pharmacokinetic investigation.

Acknowledgements

We would like to acknowledge the group of Dr. Andreas Schlosser (Rudolf-Virchow-Zentrum, University of Würzburg, Germany) for their help in MS/MS analysis, the group of Prof. F. Würthner (Institute of Organic Chemistry, University of Würzburg) for their help in MALDI-TOF MS analysis of bioconjugates and Dr. Anabel Pacios from the group of Prof. Dr. Schindelin (Rudolf- Virchow-Zentrum, University of Würzburg, Germany) for her help with differential scanning fluorimetry assays. We also thank Dr. Rahul Nair from the group of Prof. Dr. Kisker (Rudolf-Virchow-Zentrum, University of Würzburg, Germany) for his help with CD measurements. We further thank Prof. Dr. Edward A. Lemke from the Johannes Gutenberg University of Mainz/EMBL Heidelberg for donating the pEVOL-pylRS vector. The authors would like to acknowledge the Core Facility BioSupraMol (Freie Universität Berlin) for assistance with NMR and MS measurements. We would like to thank Daniel Kutifa for assistance with polymerizations and Cathleen Hudziak for GPC measurements. We gratefully acknowledge the Rechenzentrum of the University of Würzburg for providing computing time on the Julia High Performance Computing Cluster. The project is a collaborative work between Freie Universität Berlin (FKZ: 13XP5049A), Julius-Maximillians University Würzburg (FKZ: 13XP5049B) and Friedrich-Schiller-University Jena (FKZ: 13XP5049C) in the framework of Next-PEG and we would like to thank the Federal Ministry of Education and Research (BMBF) of Germany for funding.

Supporting Information

Supporting information 1: Detailed description of material and methods for synthesis and characterization of investigated polymer structures. Synthesis of N^6-((2-azidoethoxy)carbonyl)-L-lysine. Supporting results and discussion include: Site selection of mutation sites, expression of IFN-α2a and mutants, incorporation of NAEK into IFNK134N_3, comparison of IFNK31N_3 and IFNK134N_3 mutants and their DBCO-PEG 10 kDa bioconjugates, MALDI-TOF analysis, RP-HPLC analysis, turbidity measurements of the clickable PEtOx polymers, density and interaction analysis of simulations, limited proteolysis peptide sequence coverage.

Supporting information 2: raw MS data of LIP measurements

Supporting Information to Chapter 2

Experimental

Materials for polymer synthesis

Methyl tosylate (97%), potassium phthalimide (99%), triethylamine (anhydrous, ≥ 99%), (1R,8S,9s)-bicyclo[6.1.0]non-4-yn-9-ylmethyl *N*-succinimidyl carbonate (BCN-NHS), dibenzocyclooctyne-acid (95%), dichloromethane (anhydrous, ≥ 99.8%) and hydrazine monohydrate (64-65% N_2H_4, 98%), dibenzocyclooctyne-acid (95%), dichloromethane (anhydrous, ≥ 99.8%) and hydrazine monohydrate (64-65% N_2H_4, 98%) was purchased from Sigma Aldrich (Schnelldorf Germany). 2-ethyl-2-oxazoline was obtained from TCI (98%).

Anhydrous solvents (dimethylformamide and toluene), benzoylated cellulose dialysis tubes (2000 Da, 32 mm width), (1R,8S,9S)-bicyclo[6.1.0]non-4-yn-9-ylmethyl *N*-succinimidyl carbonate (BCN) and dibenzocyclooctyne-*N*-hydroxysuccinimidyl ester (DBCO-NHS), were purchased from Merck (Darmstadt, Germany).

Tetra-*N*-octyl ammonium bromide (98%) was purchased from Fisher Scientific (Schwerte, Germany) and used as received.

Bariumoxide (BaO) (90%) was purchased from Fisher Scientific (Schwerte, Germany) Acros Organics brand.

10 kDa α-methoxy-ω-amino-poly(ethylene glycol) (PEG-NH_2) (Rapp POLYMERE, Tübingen, Germany) was used as received.

All other chemicals were bought from Merck (Darmstadt, Germany) unless stated otherwise and used without further purification.

The following chemicals were processed before usage:

2-Ethyl-2-oxazoline (EtOx) (TCI, 98%) was pre-dried over BaO (90%) and distilled under inert conditions. Methyl tosylate (97%) (MeTos) was dried over CaH_2, distilled under reduced pressure and stored under argon atmosphere. Acetonitrile was dried in a solvent purification system

(SPS, Pure solv EN, InnovativeTechnology, Oldham, United Kingdom).

Instrumentation for characterization of LPG

^{1}H-NMR spectra were recorded on a Bruker AMX 500, or a Bruker Avance III 700 (Bruker Corporation, Billerica, USA) or Jeol ECP 500 (JEOL GmbH, Freising, Germany). Chemical shifts (δ) are reported in ppm *via* the deuterated solvent peak as the standard. IR measurements were done on a Nicolet AVATAR

320 FT_IR 5 SXC (Thermo Fisher Scientific, Darmstadt, Germany) with a detector range of 4000 to 650 cm^{-1}. Spectra Manager software (Jasco Labor- and Datentechnik GmbH, Groß-Umstadt, Germany) was applied to process the obtained infrared spectra.

SEC measurements in water were performed with an Agilent 1100 equipped with an automatic injector, isopump, and Agilent 1100 differential refractometer (Agilent Technologies, Santa Clara, CA, USA). The PSS Suprema (pre-column, 1x with pore size of 30 Å, 2x with pore size of 1000 Å (all of them with a particle size of 10 µm) column, was calibrated against pullulan standards prior to measurements. The SEC measurements in THF were done with an Agilent SECurity (1200 Serie) (Agilent Technologies, Waldbronn, Germany), equipped with automatic injector, isopump and UV and RI detector. The separation was done via a PL gel from Agilent (1x pre-column, 3x Mixed-C with a particle size of 5 µm) which was calibrated against polystyrene standards.

Instrumentation for characterization of PEtOx

All PEtOx polymers were measured on a SEC system (Agilent Technologies, Waldbronn, Germany) equipped with a PSS degasser, a G1310A pump, a G1329A autosampler and a techlab oven (40 °C) was used. The signals were detected using a G7162A RI detector. As an eluent, 0.21 wt% LiCl in *N,N*-dimethylacetamide (DMAc) was applied. A column set consisting of a PSS GRAM 30 Å and 1,000 Å (10 µm particle size) placed in series was utilized for separation. The flow rate was set constant as 1 mL min^{-1} and the molar masses were estimated using PS standards (ca. 400 – 1,000,000 g mol^{-1}) from PSS. All nuclear magnetic resonance (NMR) spectra of the PEtOx based polymers were measured on a 300 MHz spectrometer (Bruker Corporation, Billerica, USA) equipped with an Avance I console, a dual ^{1}H and ^{13}C sample head and a 120 × BACS automatic sample changer. All shifts are given in ppm using the residual non-deuterated solvent signal as a reference.

Polymer Synthesis and characterization

Synthesis of ethoxyethyl glycidyl ether (EEGE)

The acetal protection of glycidol was done slightly modified to a reported protocol.[226] In summary in an ice bath, glycidol (70 mL, 1.052 mol, 1eq) was mixed under stirring with divinyl ether (403.3 mL, 4.21 mol, 4 eq) and *p*-TsOH•H_2O (2 g, 0.0105 mol, 0.01 eq) was slowly added to the mixture. After 4 hours the reaction was quenched and washed with saturated $NaHCO_3$ solution. The organic phase was dried over sodium sulfate and concentrated under reduced pressure. The crude product was dried over CaH_2 and distilled under vacuum over a preheated molecular sieve and stored under argon in freezer until further use. Due to storage under dry and inert conditions, weighing of the final product was not possible and complete conversion of starting material is assumed.

^{1}H-NMR (500 MHz, $CDCl_3$): δ [ppm] = 4.69 (td, J = 5.5, 0.8 Hz, 1H), 3.86 – 3.22 (m, 4H), 3.14 – 2.97 (m, 1H), 2.73 (dd, 1H), 2.61 – 2.46 (m, 1H), 1.25 (m, 3H), 1.13 (t, 3H).

Synthesis of linear poly(ethoxyethyl glycidyl ether) (PEEGE)

The polymerization was done according to a reported protocol.[227] In a flame dried Schlenk flask, Oct_4NBr (267 mg, 0.479 mmol, 0.0073 eq) was dried under high vacuum and dissolved in 60 mL dry toluene. Afterwards EEGE (10 mL, 65.6 mmol, 1eq) was added under argon atmosphere to the solution. The mixture was cooled in an ice bath to 0 °C and *i*-Bu_3Al (2.2 mL, 2.4 mmol, 36.4 eq) was added all at once under argon atmosphere and strong stirring. The reaction proceeded overnight and was subsequently quenched by addition of 1 mL ethanol. The crude product was dissolved in cold Et_2O to precipitate the excess *i*-Bu_3Al. The product was dialyzed in acetone (MWCO: 2 kDa) for further purification. After drying, the product was obtained as 8.38 g colorless viscous oil (87%).

^{1}H-NMR (500 MHz, $CDCl_3$): δ [ppm] = 4.71 (m, 1H), 3.86 – 3.35 (m, 7H, monomer unit), 1.30-1.26 (m, 3H, acetal), 1.28 – 1.11 (m, 3H, acetal).

Synthesis of linear polyglycerol (LPG)

5.1 g PEEGE was dissolved in 52 mL ethanol. Thereafter, 4.21 mL HCl 37% (3% v/v) was added to the solution. The mixture was stirred overnight and purified via dialysis in water (MWCO: 2 kDa). The product was obtained as 2.1 g colorless viscous oil (82.5%).

For BCN modification: SEC (Water, 0.1 M $NaNO_3$, RI-detection, pullulan-calibration): Mn = 11.587g mol-1; Đ = 1.22

For DBCO modification: SEC (Water, 0.1 M $NaNO_3$, RI-detection, pullulan-calibration): Mn = 10.518 g mol-1; Đ = 1.32

Synthesis of α-azido-linear polyglycerol (LPG-N_3)

LPG (909 mg, 0.009 mmol, 1 eq) was dissolved in 5 mL dry DMF and heated to 80 °C. Then NaN_3 (29.8 mg, 0.4 mmol, 5 eq) was added to the mixture. The reaction was allowed to run under reflux for 72 hours. Afterwards DMF was removed and the product was purified by dialysis against water. The successful modification was proven by IR spectroscopy as appearance of a band at ca. 2100 cm^{-1} (93%).
IR (dry film): $\tilde{\nu}$ = 3362 (w, -OH), 2330 (m, -CH), 2102 (w, N_3), 1618.9 (s, C=O) cm^{-1}

Synthesis of α-amino-linear polyglycerol (LPG-NH_2)

LPG-N_3 (861 mg, 0.007 mmol, 1 eq) was dissolved in 17 mL H_2O and TCEP (27.8 mg, 0.111 mmol, 1.5 eq.) was added. The progress of reaction was controlled with IR-spectroscopy until disappearance of the N_3 peak. After completion of reaction, the polymer was dialyzed in water (MWCO: 2 kDa) (100%).

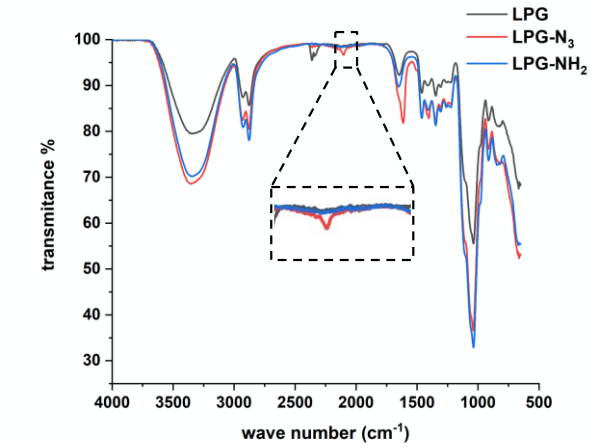

Figure S1: Overlay of the IR spectra of LPG (grey), LPG-N_3 (red) and LPG-NH_2 (blue).

Synthesis of α-cyclooctyne- linear polyglycerol (LPG-BCN)

LPG-NH_2 (394.1 mg, 0.033 mmol, 1 eq) was dissolved in 12 mL dry DMF. Afterwards Et_3N (14.1 µL, 0.01 mmol, 3 eq) and BCN (14.74 mg, 0.05 mmol, 1.5 eq) were added to the solution. The reaction was stirred overnight at RT. DMF was removed and the crude product was dialyzed against water (MWCO: 1 kDa) for purification. Because the product is prone to crosslinking in the dry state, full conversion of the product is assumed.

^{1}H-NMR (700 MHz, D_2O): δ [ppm] = 4.11 – 3.33 (m, backbone), 2.51 – 2.05 (m, 4H, BCN), 1.41 – 1.12 (br, 4H, BCN), 1.07 – 0.81 (br, 3H, m BCN).

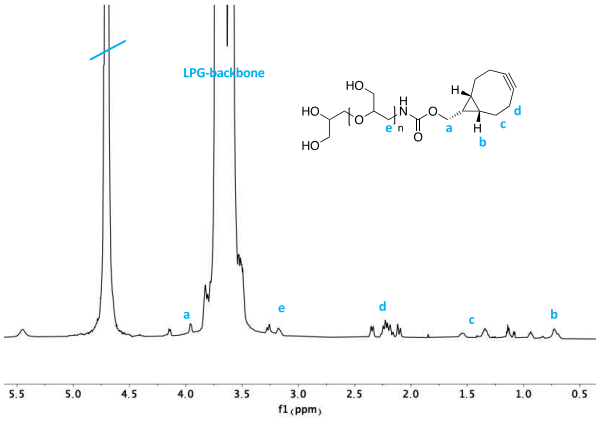

Figure S2: Characterization of LPG-BCN with ^{1}H-NMR spectroscopy (700 MHz, D_2O)

Synthesis of α-dibenzocyclooctyne- linear polyglycerol (LPG-DBCO)

LPG-NH_2 (331.3 mg, 0.033 mmol, 1 eq) was dissolved in 10 mL dry DMF and Et_3N (13.8 µL, 0.099 mmol, 3 eq) and DBCO (20 mg, 0.049 mmol, 1.5 eq) were added to the solution. The mixture was stirred overnight. DMF was removed and the crude product was dialyzed against water: acetone (1:1) for one day and then water for one day (MWCO: 2 kDa). As the product is prone to crosslinking in dry state, full conversion of the product is assumed. ^{1}H NMR (700 MHz, D2O): δ [ppm] = 7.83 – 7.24 (m, 8H), 4.20 – 3.13 (LPG-backbone), 2.43 – 2 – 10 (m, 2H), 1.53 – 1.01 (m, 1H), 0.91 – 0.66 (m, 1H).

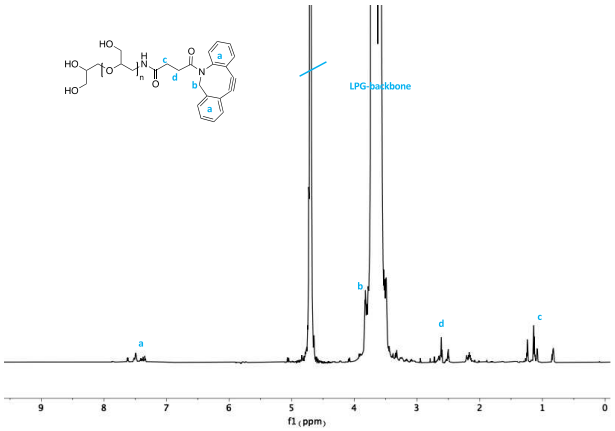

Figure S3: Characterization of DBCO-BCN with ^{1}H-NMR spectroscopy (700 MHz, D_2O).

Synthesis of α-methoxy-ω-cyclooctyne- poly(ethylene glycol) (PEG-BCN)

mPEG-NH_2 (506 mg, 0.05 mmol, 1 eq.) was dissolved in 14 mL dry DMF. Et_3N (22 µL, 0.151 mmol, 3 eq.) and BCN (22.1 mg, 0.007 mmol, 1.5 eq.) were added to the solution and stirred overnight. Then the DMF was evaporated and product was dialyzed against water (MWCO: 1 kDa). Product was obtained as 416 mg white solid (86%).

^{1}H-NMR (700 MHz, D_2O): δ [ppm] = 4.22 (d, 1H, $OCOCH_2$), 4.03 (d, 1H, $OCOCH_2$), 3.87 – 3.60 (PEG-backbone), 3.44 – 3.32 (m, 2H, $OCONH\text{-}CH_2$), 2.51 – 2.15 (m, 4H, BCN), 1.73 – 1.54 (br, 4H, BCN), 1.07 – 0.72 (br, 3H, BCN).

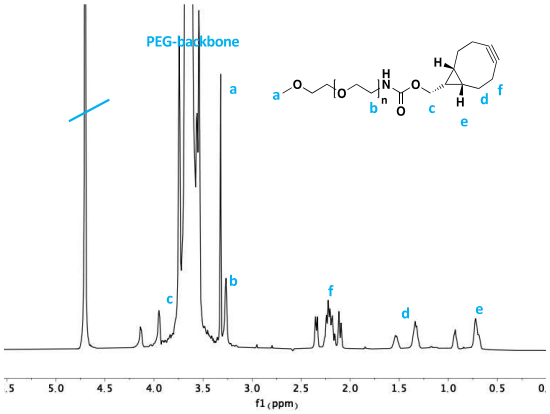

Figure S4: Characterization of PEG-BCN with ^{1}H-NMR spectroscopy (700 MHz, D_2O).

Synthesis of α-methoxy-ω-dibenzocyclooctyne poly(ethylene glycol) (PEG-DBCO)

PEG-NH_2 (343.1 mg, 0.034 mmol, 1 eq) was dissolved in 10 mL dry DMF and Et_3N (14.5 µL,1.043 mmol, 3 eq) and DBCO (21 mg, 0.052 mmol, 1.5 eq) were added to the solution. DMF was removed and the crude product was dialyzed in water: acetone (1:1) for one day and only water for one day changing the dialysate twice per day (MWCO: 1 kDa). 313 mg obtained product were solved in 5 mL water as a stock solution (91.2%).

^{1}H-NMR (600 MHz, D2O): δ [ppm] = 7.69 – 7.29 (m, 8H), 5.10 (dd, 2H), 3.89-3.55 (PEG-backbone), 3.48 – 3.32 (m, 2H, OCONH-CH_2), 2.64 – 2.44 (m, 2H), 2.30-2.20 (m, 1H), 217-2.11 (m, 1H) ppm.

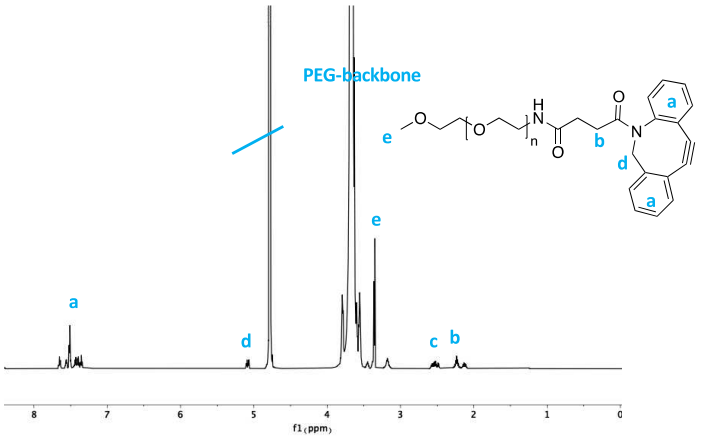

Figure S5: Characterization of PEG-DBCO with ^{1}H-NMR spectroscopy (700 MHz, D_2O).

Synthesis of ω-dibenzocyclooctyne poly(2-ethyl-2-oxazoline) (PEtOx-DBCO)

A pre-heated Schlenk flask was cooled to room temperature by a continuous argon stream. Methyl tosylate (30.5 µL, 0.2 mmol, 1 eq.), 2-ethyl-2-oxazoline (2036 µL, 20 mmol, 100 eq.) and 3 mL dry acetonitrile were added. The flask was connected to a findenser under argon atmosphere. The mixture was heated to reflux and was allowed to stir for 5 h. After cooling to room temperature, a solution of DBCO acid (73.5 mg, 0.22 mmol, 1.1 eq.) in 2 mL dry acetonitrile and triethylamine (60 µL, 2.15 eq.) were added under argon atmosphere *via* syringe. The reaction was stirred at room temperature for 19 h. Subsequent to removal of an aliquot for the determination of the monomer conversion by means of ^{1}H-NMR and the molar mass distribution by means of SEC, the mixture was diluted with dichloromethane, washed with a sat. aq. $NaHCO_3$ solution twice and once with a sat. aq. NaCl solution. The organic layer was dried over Na_2SO_4, filtered and the volatiles were removed under reduced pressure at a water bath temperature of 30 °C. The residue was re-dissolved in a small amount of dichloromethane and precipitated from –22 °C diethyl ether. The process was repeated once in order to remove residual monomer. The solid was collected, dried *in vacuo* and stored at –22 °C. Yield: 1.05 g (48%). Conversion: 77%. DPNMR = 77. DFNMR = 64%. Mn, NMR = 7,800 g mol^{-1}. ^{1}H-NMR (300 MHz, $CDCl_3$): δ [ppm] = 0.79 – 1.52 (br, 231H, CH_3 sidechain), 2.16 – 2.62 (br, 154H, CH_2 sidechain), 2.92 – 3.10 (br, 3H, α-CH_3), 3.10 – 3.89 (br, 308H, CH_2 backbone), 4.03 – 4.28 (br, 2H, CH_2-O-(CO)), 5.09 – 5.24 (d, 1H,

CH_2-N cyclooctyne), 7.63 – 7.74 (d, 1H, CH-aromat). SEC (DMAc, 0.21 wt% LiCl, RI-detection, PS-calibration): $M_{n,\,SEC}$ = 12,500 g mol^{-1}; Đ = 1.18.

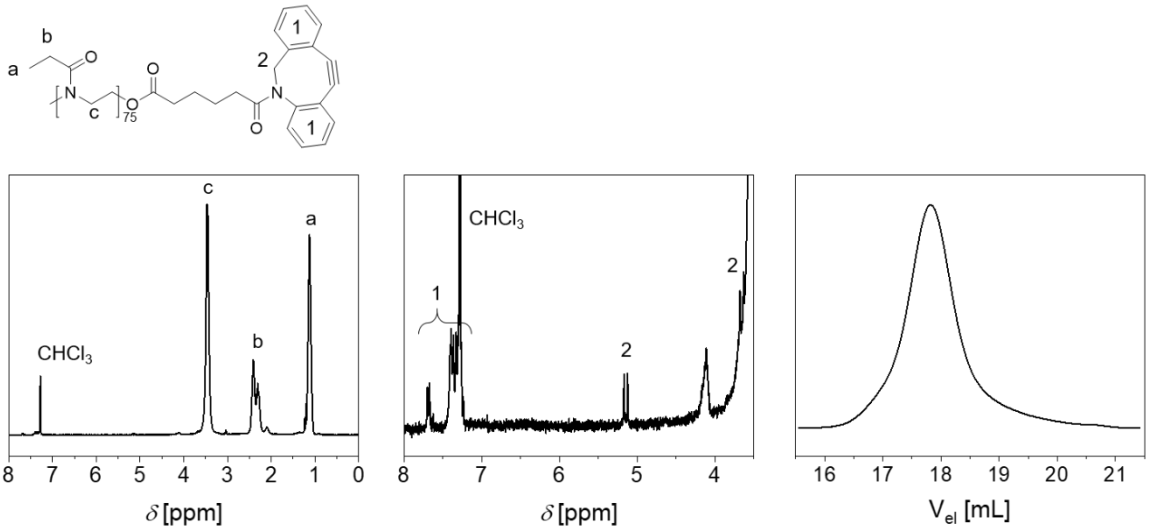

Figure S6: Left: Full ^{1}H-NMR spectrum (300 MHz, $CDCl_3$). Middle: Zoom into the ^{1}H-NMR spectrum into a region displaying the ω-end group signals. Right: SEC elugram (DMAc, 0.21 wt% LiCl, RI-detection).

Synthesis of PEtOx-phthalimide

A pre-heated two-neck flask was connected to a findenser with T-piece. The setup was evacuated, heated and flushed with argon thrice. Then, methyl tosylate (305 µL, 2.02 mmol, 1 eq.), 2-ethyl-2-oxazoline (20 mL, 19.64 mmol, 99 eq.) and 30 mL acetonitrile were added. The mixture was refluxed for 5 h. The reaction was terminated by addition of solid potassium phthalimide (1 g, 5.4 mmol, 2.7 eq.). The oil bath temperature was adjusted to 70 °C and the reaction was allowed to stir for 15 h under a gentle argon stream. After removal of an aliquot for ^{1}H-NMR and SEC analysis, the mixture was filtered, diluted with chloroform and washed with a sat. aq. $NaHCO_3$ solution twice and once with a sat. aq. NaCl solution. The organic layer was dried over Na_2SO_4, filtered and the volatiles were removed under reduced pressure. The residue was dissolved in dichloromethane and precipitated from –22 °C diethyl ether and dried *in vacuo* (40 °C), yielding PEtOx-phthalimide as a colorless solid. Yield: 13.46 g (67%). Conversion: 80%. DP_{NMR} = 80. DF_{NMR} = 90%. $M_{n,\,NMR}$ = 8,100 g mol^{-1}. ^{1}H-NMR (300 MHz, CD_2Cl_2): δ [ppm] = 0.86 – 1.55 (br, 240H, CH_3 sidechain), 1.94 – 2.78 (br, 160H, CH_2 sidechain), 2.92 – 3.06 (br, 3H, α-CH_3), 3.06 – 4.04 (br, 320H, CH_2 backbone), 7.61 – 7.98 (br, 4H, $CH_{phthalimide}$). SEC (DMAc, 0.21 wt% LiCl, RI-detection, PS-calibration): $M_{n,\,SEC}$ = 13,400 g mol^{-1}; Đ = 1.08.

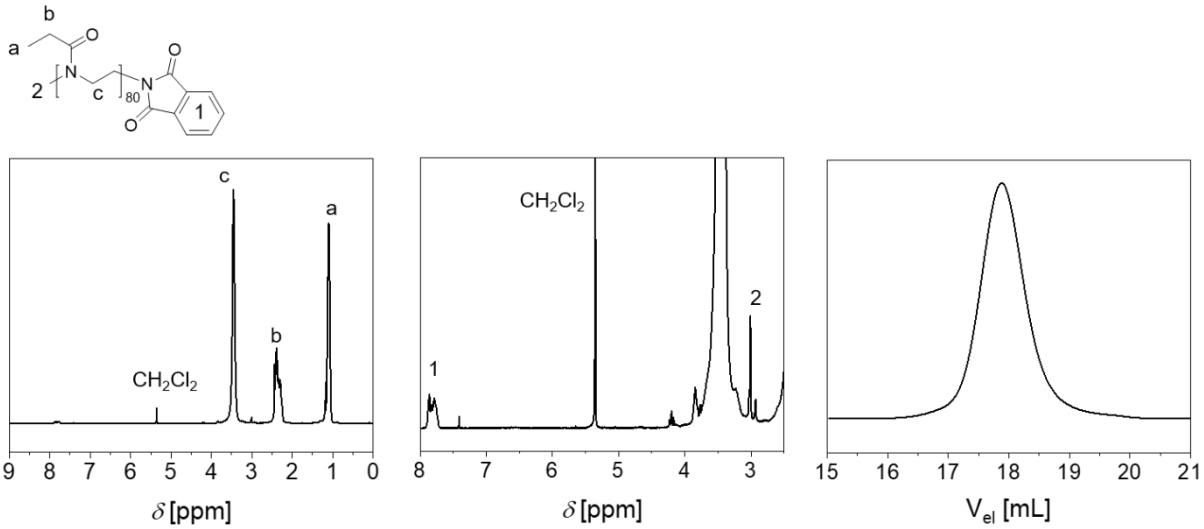

Figure S7: Characterization of the phthalimide decorated PEtOx and assignment of characteristic ^{1}H-NMR signals to its schematic representation. Left: Full ^{1}H-NMR spectrum (300 MHz, CD_2Cl_2). Middle: Zoom into the ^{1}H-NMR spectrum into a region displaying the ω-end group signals. Right: SEC elugram (DMAc, 0.21 wt% LiCl, RI-detection).

Synthesis of PEtOx-NH_2

PEtOx-phthalimide (13.06 g, 1.6 mmol, 1 eq.) was dissolved in 48 mL ethanol. Hydrazine monohydrate (1 mL, 20.6 mmol, 12.8 eq.) was added and the mixture was stirred at reflux temperature for 20 h, leaving a pink solution with minor amounts of colorless precipitate. After cooling to room temperature, the suspension was acidified to pH = 2 by addition of diluted aq. HCl. Subsequent to filtration, the pH value was re-adjusted to pH = 9 by addition of diluted aq. NaOH. The mixture was extracted with chloroform thrice. It should be noted that the phase separation upon the first extraction was accomplished overnight due to slow de-mixing of the solvents. The combined organic phases were dried

over Na_2SO_4, filtered and the volatiles were removed under reduced pressure. The residue was re-dissolved in chloroform, precipitated from –22 °C diethyl ether and dried *in vacuo* (40 °C). Yield: 12.02 g (93%). DF_{NMR} = quant. $M_{n,\,NMR}$ = 8,000 g mol^{-1}. ^{1}H-NMR (CD_2Cl_2): δ [ppm] = 0.80 – 1.38 (br, 240H, CH_3 sidechain), 2.13 – 2.58 (br, 160H, CH_2 sidechain), 2.68 – 2.87 (br, 2H, CH_2-NH_2), 2.87 – 3.12 (br, 3H, α -CH_3), 3.12 – 3.92 (br, 320H, CH_2 backbone). SEC (DMAc, 0.21 wt% LiCl, RI-detection, PS-calibration): $M_{n,\,SEC}$ = 13,200 g mol^{-1}, Đ = 1.08.

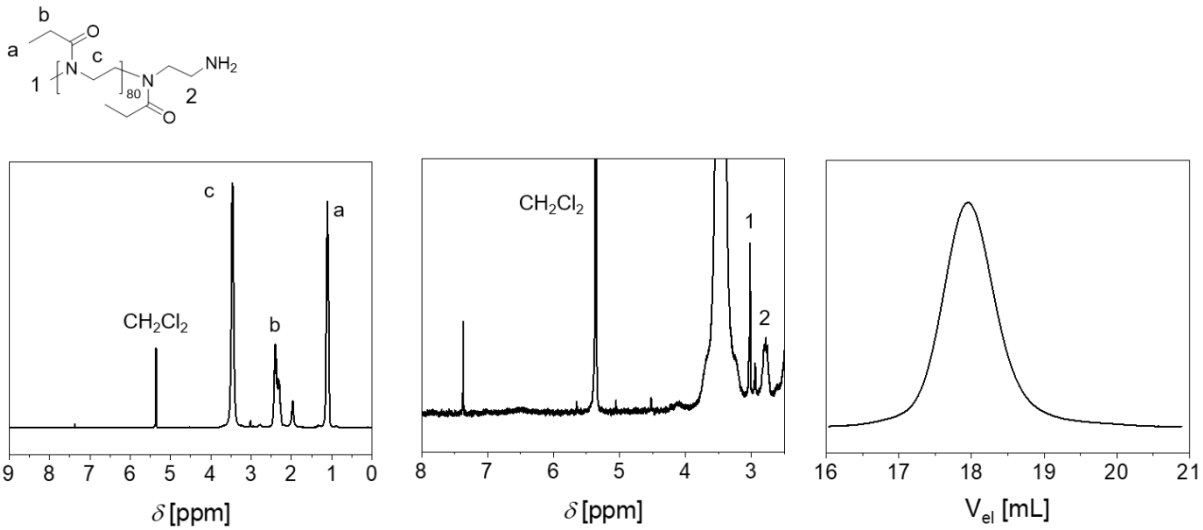

Figure S8: Characterization of the amine decorated PEtOx and assignment of characteristic 1H-NMR signals to its schematic representation. Left: Full ^{1}H-NMR spectrum (300 MHz, CD_2Cl_2). Middle: Zoom into the ^{1}H-NMR spectrum into a region displaying the ω-end group signals. Right: SEC elugram (DMAc, 0.21 wt% LiCl, RI-detection).

Synthesis of PEtOx-BCN

The synthesis was performed as recently described.[248] A pre-heated vial was cooled to room temperature by a continuous argon stream. It was charged with PEtOx-NH_2 (255 mg, 0.032 mmol, 1 eq.) and 1.5 mL dry dichloromethane. Then, triethylamine (10 µL, 0.072 mmol, 2.3 eq.) was added via a syringe. BCN-NHS (10.5 mg, 0.036 mmol, 1.1 eq.) was dissolved in 0.5 mL dry dichloromethane and added to the polymer solution. The mixture was stirred at room temperature for 17 h. Subsequent to dilution with dichloromethane, it was washed with sat. aq. $NaHCO_3$ solution twice and once with sat. aq. NaCl solution. The organic layer was dried over Na_2SO_4, filtered and concentrated under reduced pressure. The residue was re-dissolved in small amounts of dichloromethane, precipitated from –22 °C diethyl ether and dried *in vacuo*. Yield: 175 mg (67%). $M_{n,\,NMR}$ = 8,100 g mol^{-1}. ^{1}H-NMR (CD_2Cl_2): δ [ppm] = 0.83 – 1.39 (br, 240H, CH_3 sidechain), 2.03 – 2.70 (br, 160H, CH_2 sidechain), 2.91 – 3.08 (br, 3H, α -CH_3), 3.12 – 3.90 (br, 320H, CH_2 backbone), 4.02 – 4.29 (br, 2H, CH_2-carbamate). SEC (DMAc, 0.21 wt% LiCl, RI-detection, PS-calibration): $M_{n,\,SEC}$ = 13,900 g mol^{-1}, Đ = 1.10.

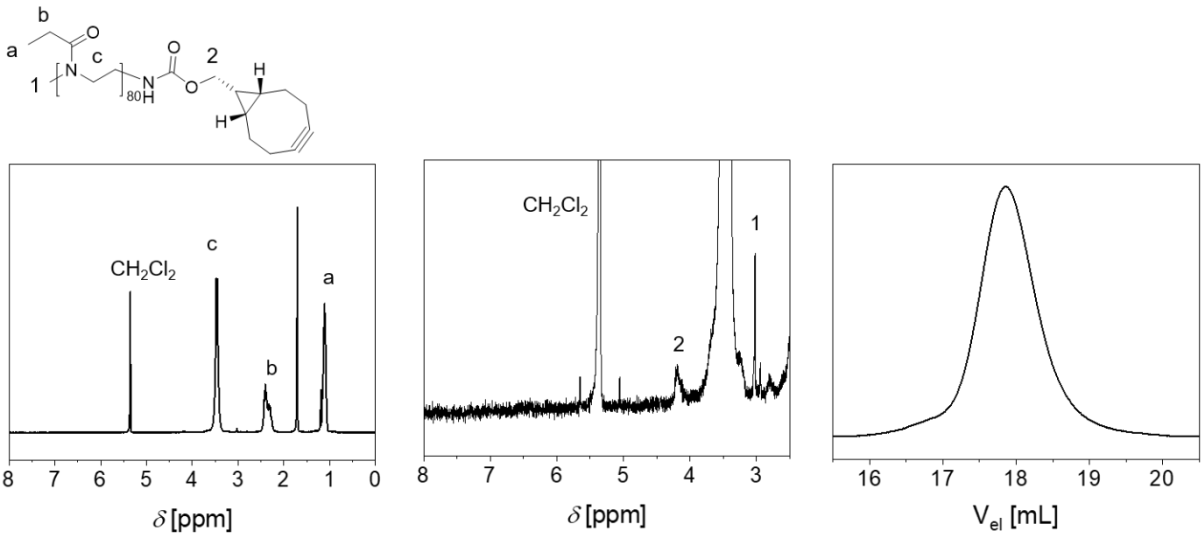

Figure S9: Characterization of the BCN decorated PEtOx and assignment of characteristic ^{1}H-NMR signals to its schematic representation. Left: Full ^{1}H-NMR spectrum (300 MHz, CD_2Cl_2). Middle: Zoom into the ^{1}H-NMR spectrum into a region displaying the ω-end group signals. Right: SEC elugram (DMAc, 0.21 wt% LiCl, RI-detection).

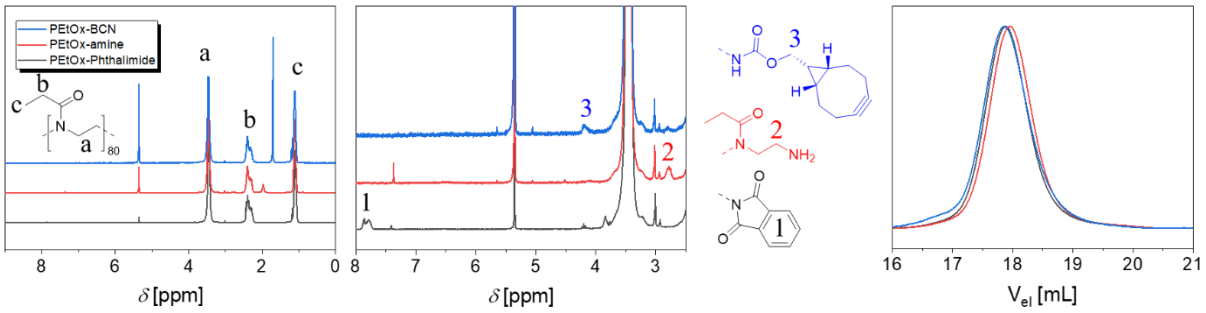

Figure S10: Characterization of the PEtOx-BCN as well as all intermediate polymer species. Left: Overlay of the full ^{1}H-NMR spectra (300 MHz, CD_2Cl_2). Middle: Zoom into regions displaying signals derived from the respective ω-end groups. Right: Overlay of the SEC elugrams (DMAc, 0.21 wt% LiCl, RI-detection).

Synthesis of N^{6}-((2-azidoethoxy)carbonyl)-L-lysine (NAEK):

NAEK was prepared as HCl-salt following procedures described by Spieler *et al.*[233]

Results and discussion

Site selection of mutation sites

For site selection of mutation sites the NMR structure 1ITF and the crystal structure 3SE3 were used (**Figure 1A and Figure S11**). K31 and K134 are freely accessible at the protein surface and are not involved into any molecular interactions that are important for the binding of IFN-α2a WT to IFNAR1 or 2, or for the proteins tertiary structure (**Figure S11A**). Our simulations of the wild type affirm this, showing the side chains of these residues mostly oriented away from the binding regions, thus being potentially suited for polymer attachment and not crucial for the binding event of IFNAR1 and IFNAR2. K31 is mainly interacting with the side chain of the neighboring D32, K134 remains solvent-exposed and is only briefly addressing the backbone carbonyl group of E132. Both D32 and E132 are not situated in the direction of the binding sites. Figure S11 shows the dynamics of these side chains for one of our wild type replicas. The mean distance for the K31 side chain nitrogen to the nearest IFNAR2 heavy atom (β-C-atom of P49 from crystal structure 3SE3) is 11.48 Å (taking into account every nanosecond), whereas the nitrogen of K134 shows a mean distance of 16.69 Å to the nearest heavy atom of IFNAR1 (γ-O-atom of S64).

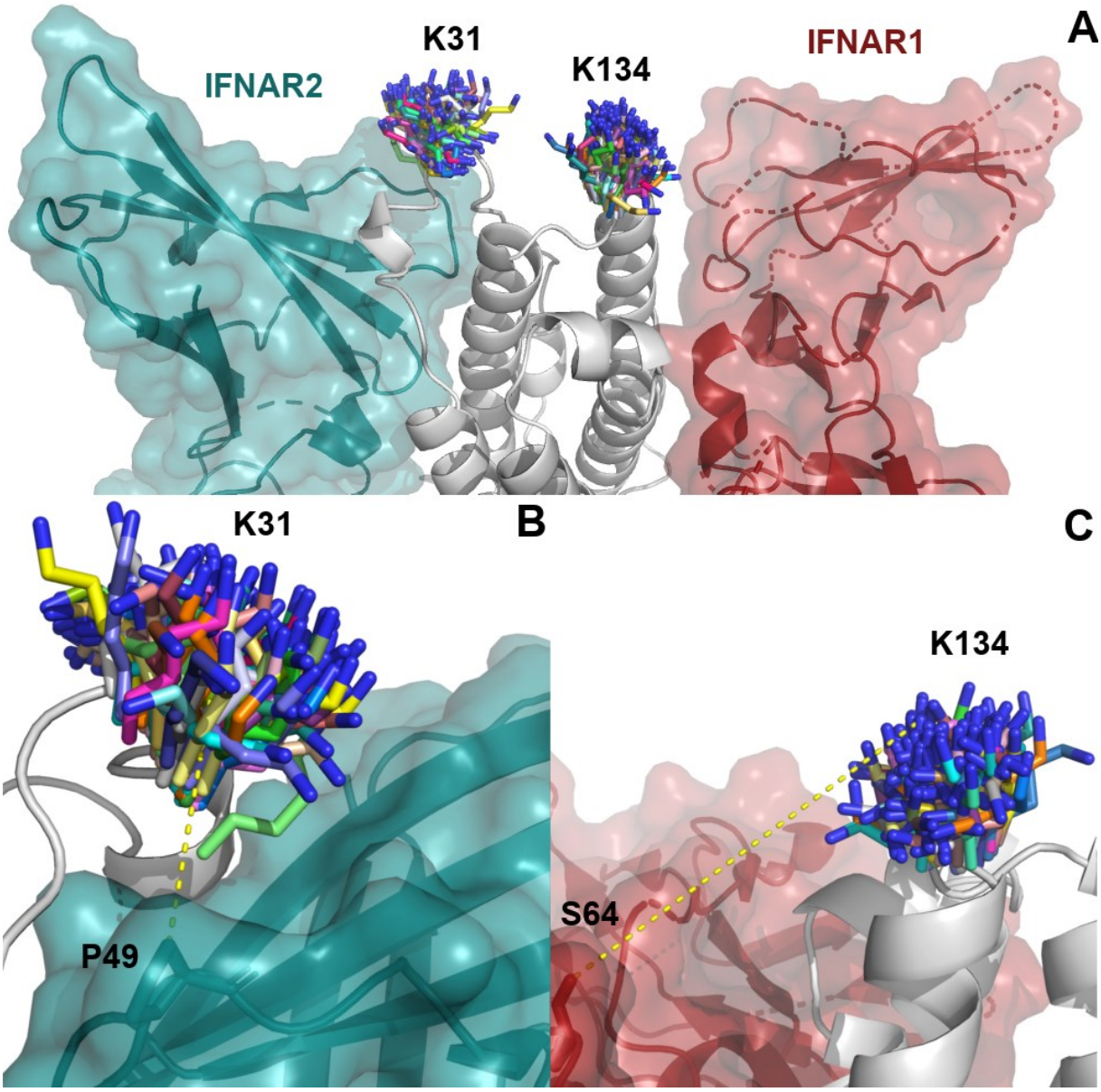

Figure S11: (A) Snapshots of one of our IFN-α2a WT simulations after alignment of the backbone to the crystal structure 3SE3 (shown in gray). The side chains of K31 and K134 are shown for every nanosecond. In (B) and (C), the distances described in the text are illustrated going from the receptor atom of interest to the lysine side chain nitrogen of a single snapshot. The receptors IFNAR1 and IFNAR2 from crystal structure 3SE3 are illustrated in red and petrol.

Expression of IFN-α2a and mutants

IFN-α2a was expressed as described above. As shown in figure S12 IFN-α2a accumulates in inclusion bodies in the pellet, but can be refolded in sufficient amounts. Mutants were expressed with an efficiency of up to 70% compared to the WT (data not shown). Exemplary steps during protein purification are displayed.

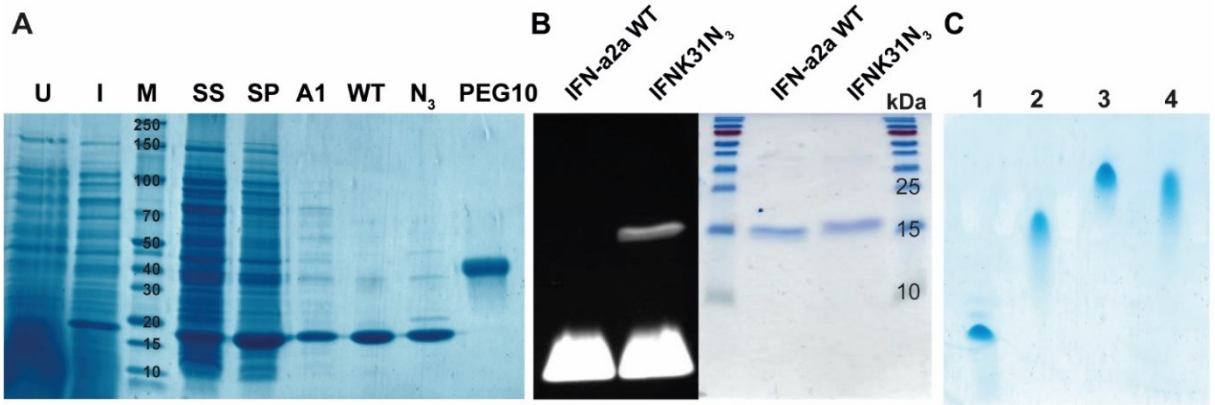

Figure S12: (A) 10-15% SDS PAGE of IFN-α2a WT purification. U=uninduced, I=induced with IPTG, M=MW marker in kDa, SS = sonication supernatant, SP=sonication pellet, A1=After first IEX purification, WT= purified WT protein, N_3 = purified IFNK31N_3 mutant, PEG10=purified IFNK31N_3-DBCO-PEG protein polymer conjugate (B) Strain promoted azide-alkyne Huisgen cycloaddition (SpAAC) of IFNK31N_3 with DBCO-PEG$_4$-5/6-Carboxyrhodamine 110 and IFN-α2a WT as a negative control. Right: Coomassie stained 15% polyacrylamide SDS-Gel. Left: Image of the right side, before Coomassie staining took place, exposed to UV light. (C) 7.5-12% native PAGE of IFNK31N_3 (1), IFNK31N_3-DBCO-PEtOx 8.1 kDa (2), IFNK31N_3-DBCO-PEG 10.9 kDa (3), IFNK31N_3-DBCO-LPG 11.4 kDa (4).

IFNK134N_3 analysis

IFNK134N_3 was analyzed by MS/MS fragmentation like IFNK31N_3 after trypsin in gel digestion to validate the correct incorporation of NAEK at position 134. This was proven in a successive b-ion series (**Figure S13**).

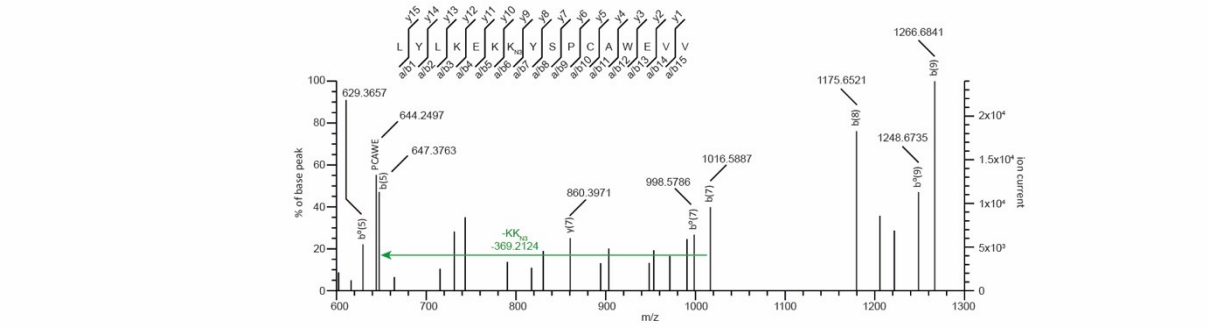

Figure S13. Exemplary MS/MS spectra of IFNK134N_3 displaying the correct incorporation of NAEK at amino acid position 134 in a successive b-ion series. Molecular mass of KKN_3-2*$H_2$0 = 369.2074.

Comparison of IFNK31N_3 and IFNK134N_3 mutants and their conjugates

IFNK31N_3 and IFNK134N_3 were compared for their bioactivity and coupling efficiency (**Figure S14**). As mentioned, the bioactivity of IFNK134N_3 and IFNK31N_3 are similar. Regarding coupling efficiency IFNK31N_3 had an efficiency of around 75% and IFNK134N_3 of around 40%.

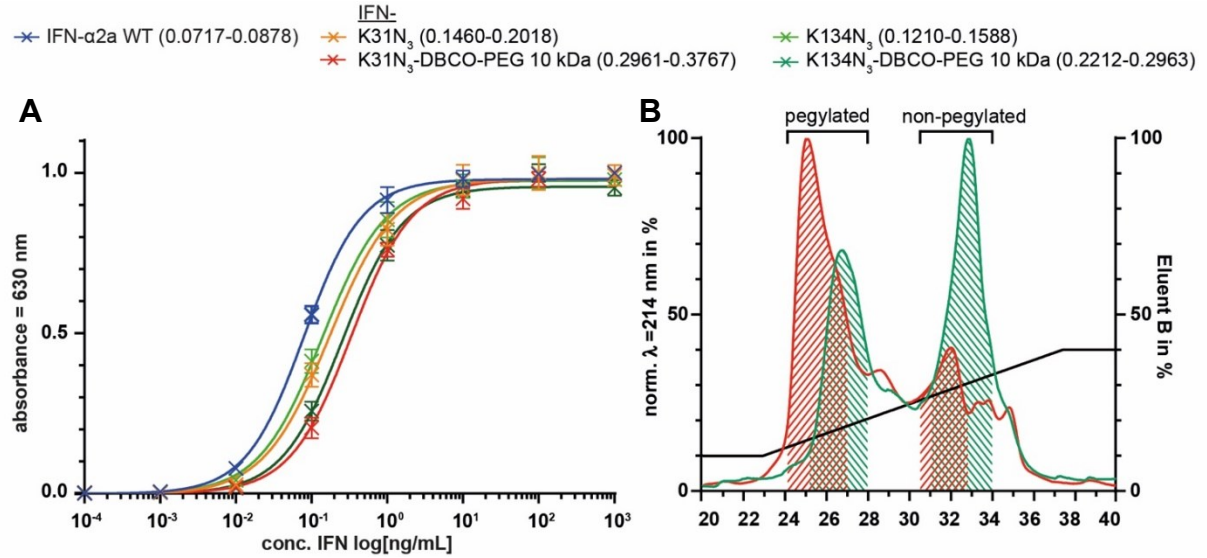

Figure S14. (A) Secreting alkaline phosphatase assay of HEKBlue 293 IFNα/β cells after 20 h of stimulation with IFN-α2a WT, IFNK31N_3, IFNK134N_3 and its DBCO-PEG 10 kDa conjugates (mean ± standard deviation, n = 3). 95%CI values [ng/mL] are stated in brackets. (B) IEX purification of IFNK31N_3 and IFNK134N_3 after PEGylation with DBCO-PEG 10 kDa for 48 h, 4 °C at pH 7.4. Areas, containing coupled IFNK31N_3, which was used for the SEAP assay were marked as well as uncoupled IFNK31N_3.

MALDI-TOF Analysis

MALDI-TOF MS was performed for all proteins and bioconjugates. For all used conjugates the [M+H^+] peak was clearly identified, as well as the [M+2H^+] peak for most (**Figure S15**). The measured molecular weights of conjugated polymers are in good agreement with the results acquired by SEC and NMR (**Table 1**).

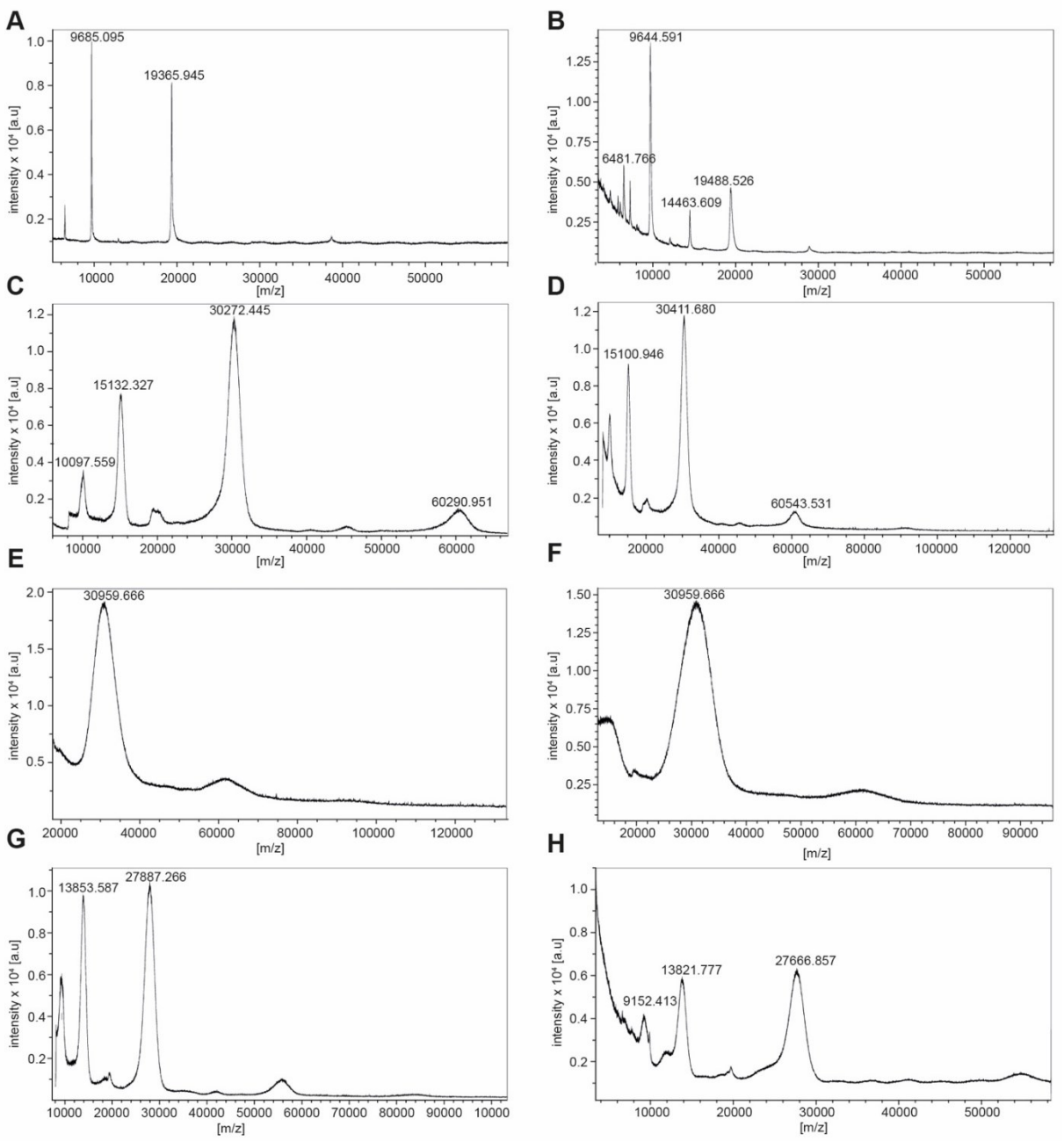

Figure S15. MALDI-TOF mass spectra of (A) IFN-α2a-WT (expected mass: 19372.30 Da), (B) IFNK31N_3 (expected mass: 19485.37), (C) IFNK31N_3-BCN-PEG 10.7 kDa, (D) IFNK31N_3-DBCO-PEG 10.9 kDa, (E) IFNK31N_3-BCN-LPG 11.4 kDa, (F) IFNK31N_3-DBCO-LPG 11.4 kDa, (G) IFNK31N_3-BCN-PEtOx 8.4 kDa, (H) IFNK31N_3-DBCO-PEtOx 8.1 kDa.

RP-HPLC analysis

IFN-α2a WT, its mutant and bioconjugates were analyzed by RP-HPLC using a CN column that is specifically designed for the separation of biomacromolecules and is highly sensitive to different hydrophilicities. As shown in figure S16, the mutant has a slightly higher retention time than the IFN-α2a WT. Depending on the conjugated polymer the retention time is drastically affected. As mentioned, the influence of retention time correlates with the polymer's hydrophilicity. This behavior was also observed on a standard C18 matrix (data not shown) even if the retention time shifts were strongly reduced. IFNK31N_3-BCN-PEtOx showed a pattern of four closely appearing peaks. As no four distinct species could be identified neither by SDS-PAGE nor by MALDI-TOF this was attributed to the high-resolution separating properties of the used CN column and a somewhat more distinctive distribution of the polymer conjugated polymer.

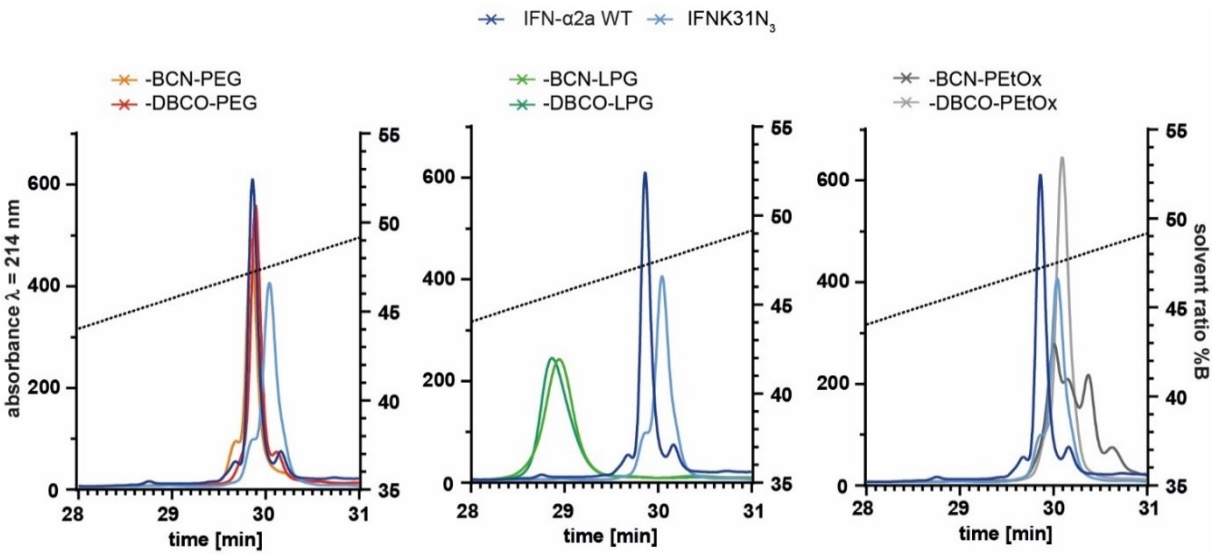

Figure S16. RP-HPLC analysis of purified IFN-α2a WT, IFNK31N_3 and its mutant protein polymer conjugates.

Turbidity measurements of the clickable PEtOx polymers

The polymers were dissolved in deionized water (PEtOx-DBCO: c = 0.185 mg mL^{-1} (24 µmol mL^{-1}), PEtOx-BCN: c = 0.064 mg mL^{-1} (8 µmol mL^{-1})). The vials were subjected to three consecutive heating/cooling cycles from 5 to 85 °C in a Crystal16 device, to investigate the LCST behaviour of the polymers at the concentration range applied in the differential scanning fluorimetry assay. The polymers did not show temperature induced turbidity (**Figure S17**), thus no LCST behaviour among these measurements. Therefore, an influence on the assay can be certainly excluded.

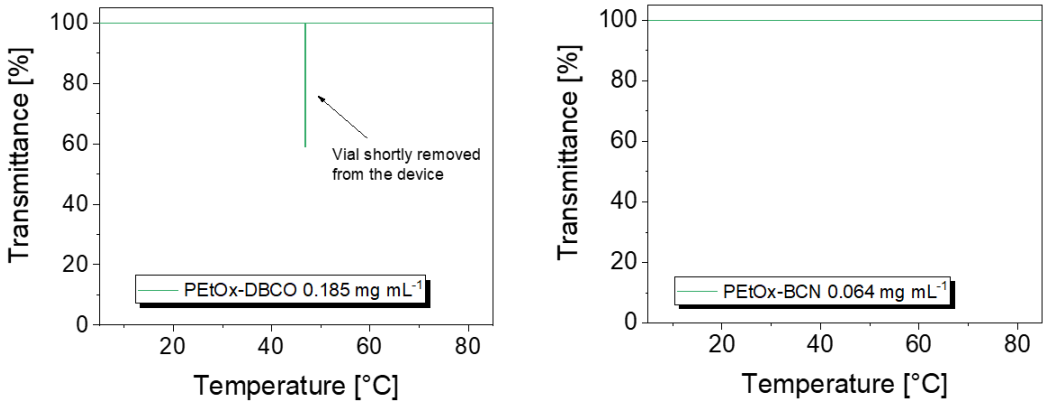

Figure S17. Turbidity measurements of the clickable PEtOx polymers. Left: PEtOx-DBCO. Right: PEtOx-BCN.

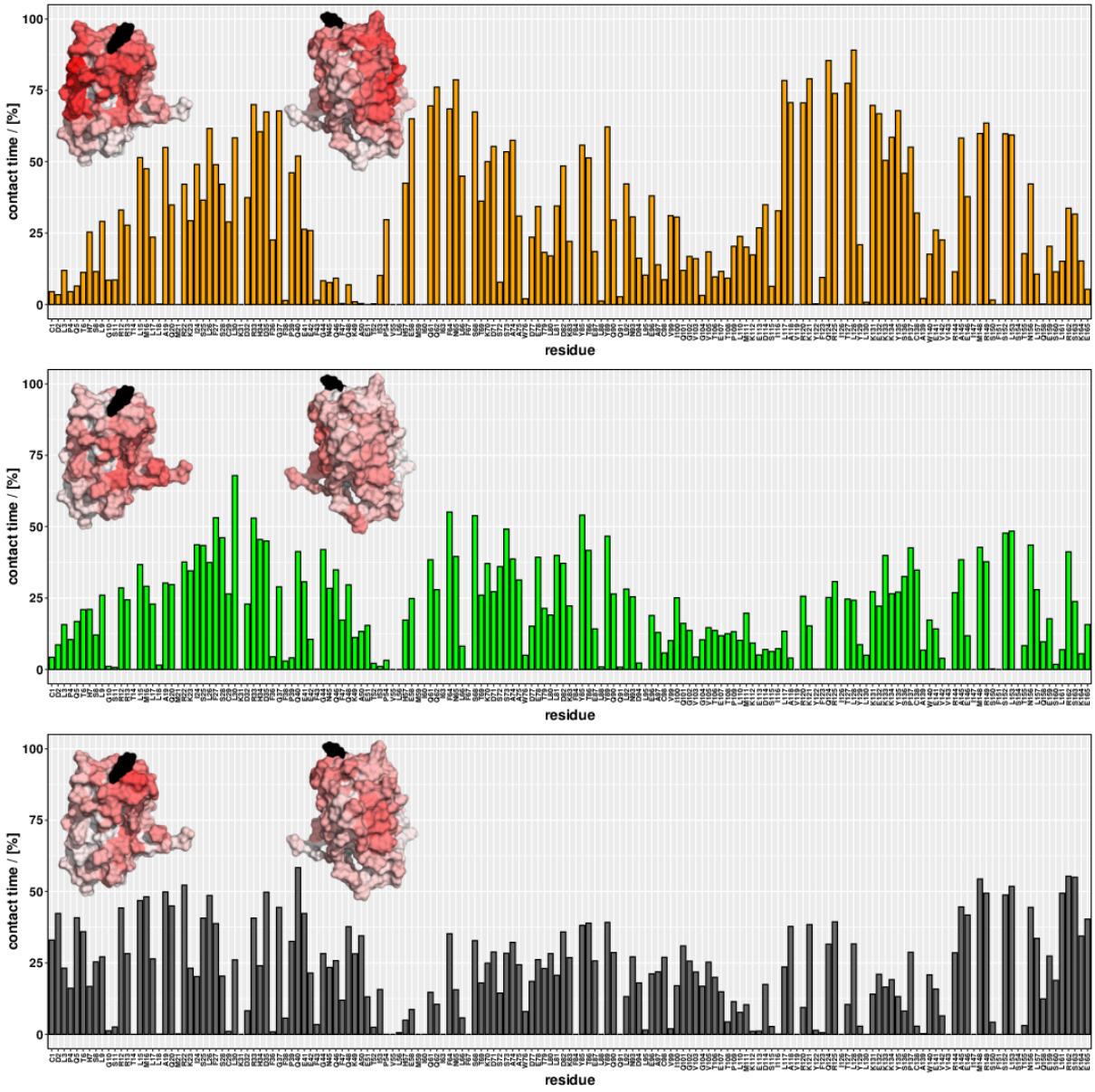

Figure S18: Percentage of simulation time in which polymer atoms are situated within 5 Å of any residue, shown for BCN conjugates (BCN-PEG = orange, BCN-LPG = green, BCN-PEtOx = dark gray). In the top left of each plot, the protein surface is shown from two different angles and colored according to these values (white = 0%, red = 100%, conjugation site = black).

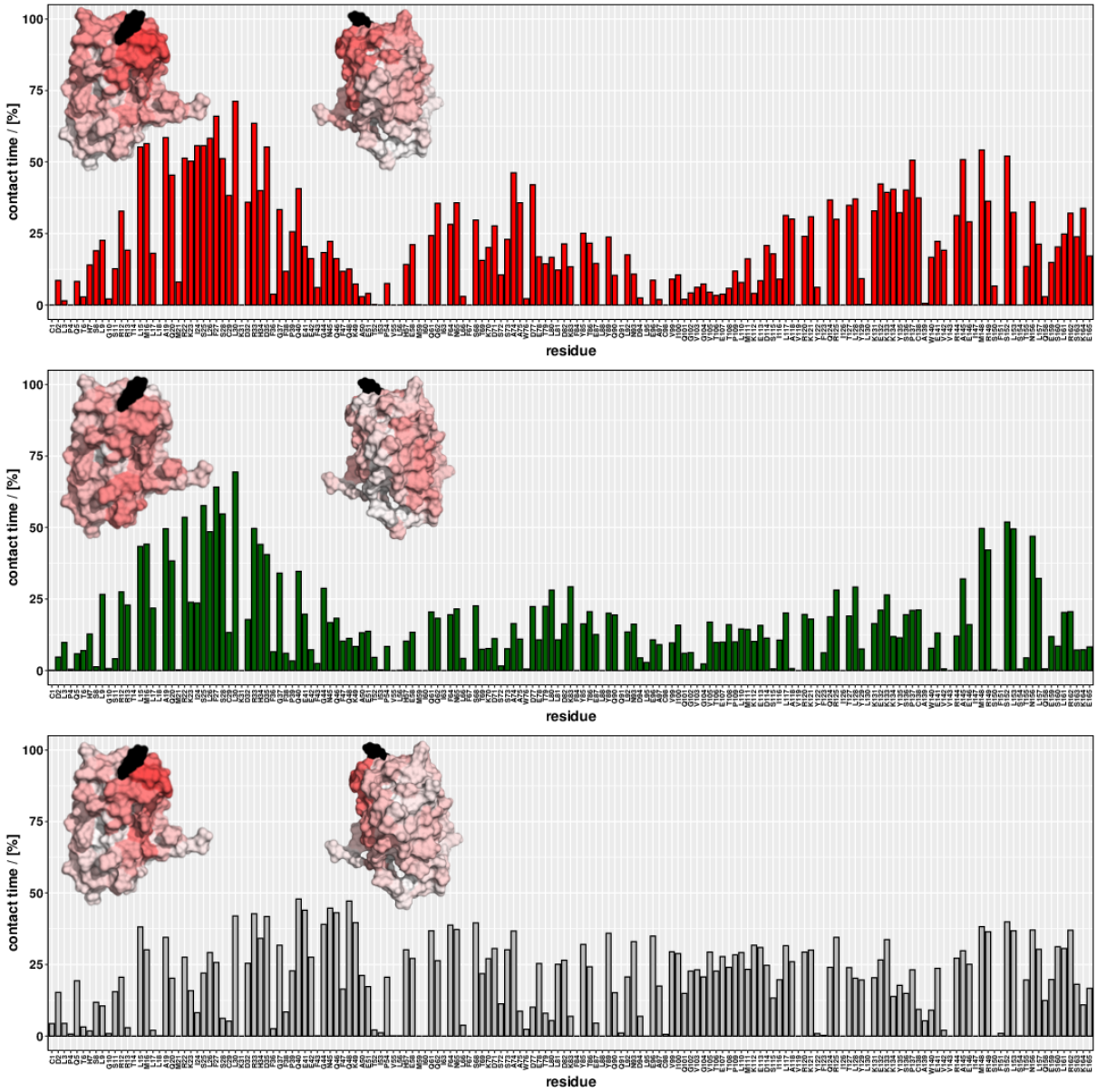

Figure S19: Percentage of simulation time in which polymer atoms are situated within 5 Å of any residue, shown for DBCO conjugates (DBCO-PEG = red, DBCO-LPG = dark green, DBCO-PEtOx = light gray). In the top left of each plot, the protein surface is shown from two different angles and colored according to these values (white = 0%, red = 100%, conjugation site = black).

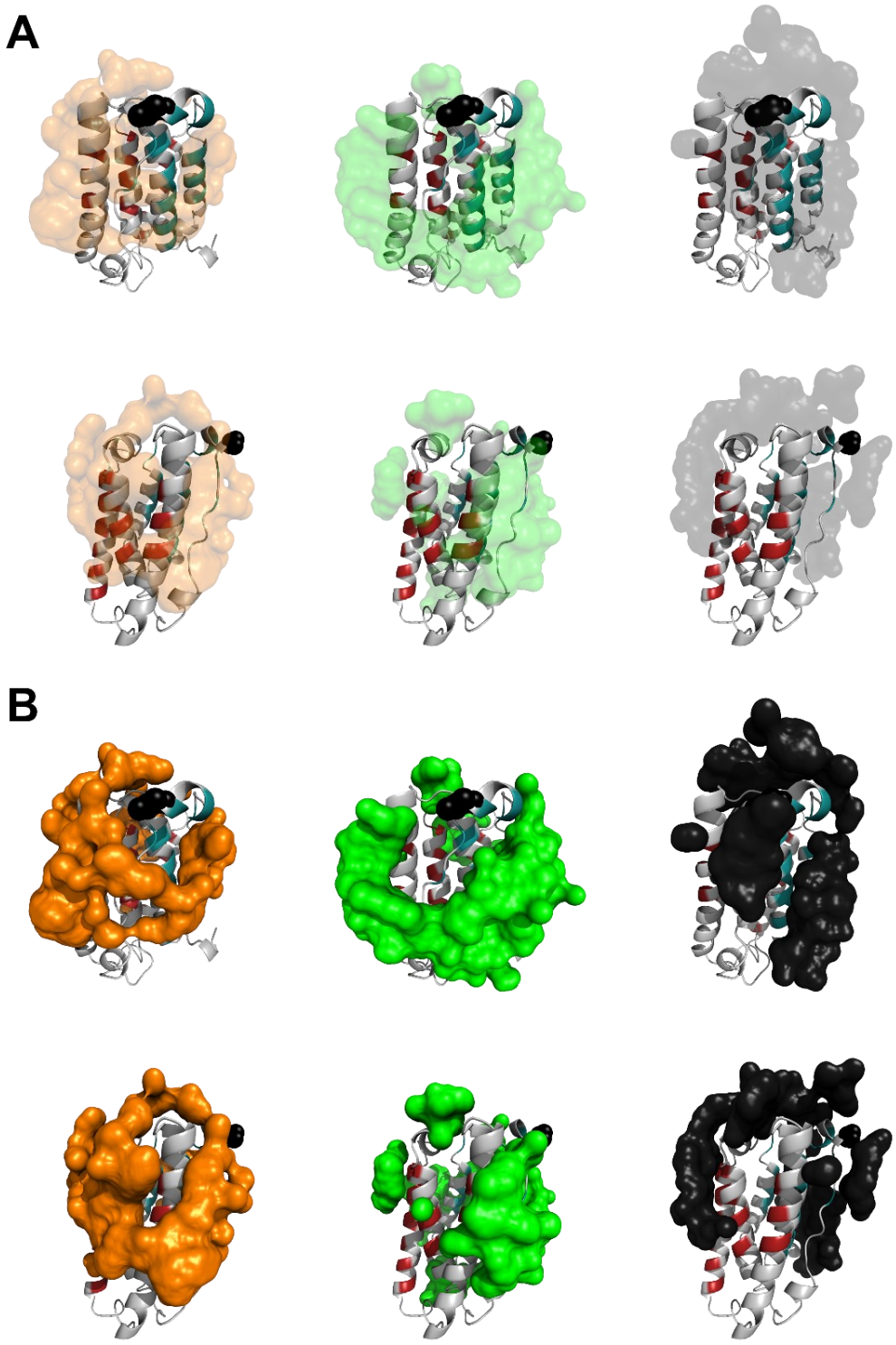

Figure S20: Polymer density hotspots for the 10 kDa BCN-PEG (orange), BCN-LPG (green), and BCN-PEtOx (black) conjugates. Densities for polymer heavy atoms (excluding BCN) are shown as (A) transparent and (B) opaque coloured surfaces from two different view angles. They represent all grid points with a density greater than 30% of the maximum grid value observed. The first snapshot of the first replica of each polymer, onto which all successive frames and replicas were aligned before grid calculation, is shown as light-grey cartoon, with residues of the IFNAR1 binding region coloured red and residues of the IFNAR2 binding site coloured petrol. Backbone heavy atoms of the conjugation site K31 are illustrated as black spheres.

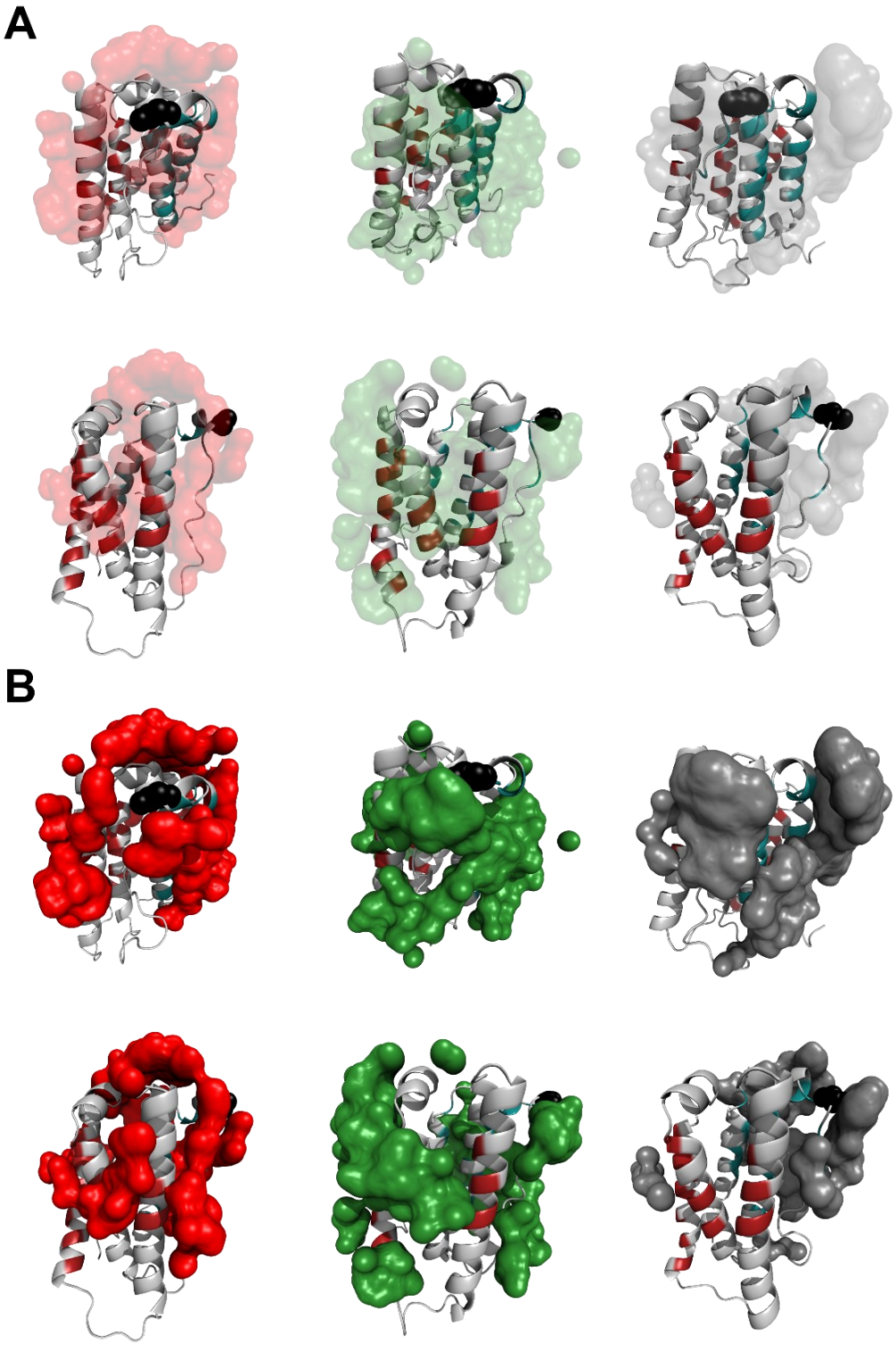

Figure S21: Polymer density hotspots for the DBCO-PEG (red), 10 kDa DBCO-LPG (dark green), and DBCO-PEtOx (grey) conjugates. Densities for polymer heavy atoms (excluding DBCO) are shown as (A) transparent and (B) opaque coloured surfaces from two different view angles. They represent all grid points with a density greater than 30% of the maximum grid value observed. The first snapshot of the first replica of each polymer, onto which all successive frames and replicas were aligned before grid calculation, is shown as light-grey cartoon, with residues of the IFNAR1 binding region coloured red and residues of the IFNAR2 binding site coloured petrol. Backbone heavy atoms of the conjugation site K31 are illustrated as black spheres.

Comparability of the rigidity of BCN and aldehyde linkers with respect to polymer protein surface interaction.

While BCN and DBCO linkers resemble inherently more rigid structures compared to a simple peptide bond, our simulations suggest that they do not prevent the polymer from addressing the protein surface. For a direct comparison, we exchanged the attachment site in one of our IFNK31N_3-BCN-PEG starting conformations with an acylated PEG at #K31 and conducted an analogous simulation (**Figure S22**). A great overlap of density hotspots between these two cases can be found, indicating that exchanging a simple peptide bond with a bulkier cyclooctyne linker does not prevent interactions of the polymer with the protein. The mean protein surface areas buried by PEG in these 150 ns replicas are nearly identical: 21.98 +/- 0.05% for the K31-BCN-PEG conjugate, compared to 20.84 +/- 0.10% for the acylated variant.

While the acylated lysine is sometimes stretched out towards the solvent (in contrast to the BCN linker which remains directly on top of the protein surface most of the time), the amino acids addressed by the first PEG monomers are largely the same. PEG initially wraps around residues K121 and R149, in the case of K31-BCN-PEG also around R125. PEG wrapping around positively charged lysine groups has been reported previously.[240]

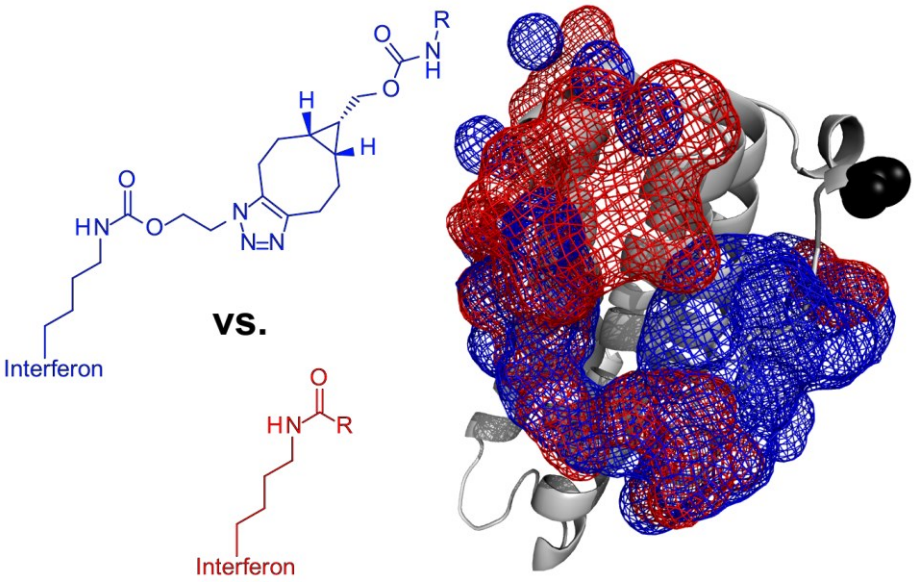

Figure S22: Polymer density hotspots (analogous calculation as for Figure S20, but shown as meshes) for the simulations of the K31-BCN-PEG (blue) and the acyl-linked K31 (red) variant. The first snapshot of the former is shown as gray cartoon, backbone heavy atoms of the conjugation site K31 are illustrated as black spheres.

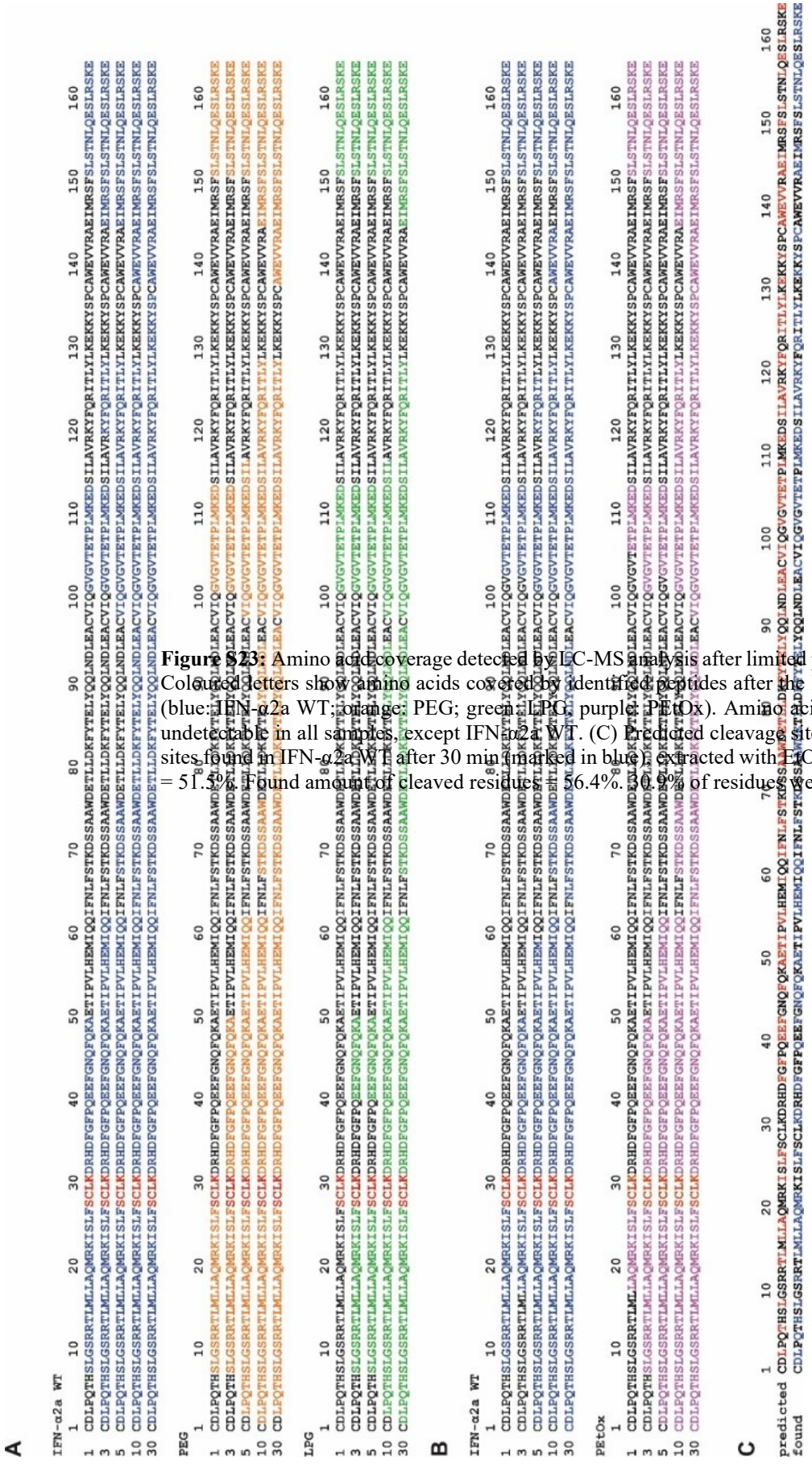

Figure S23: Amino acid coverage detected by LC-MS analysis after limited proteolysis of the WT and polymer con
Coloured letters show amino acids covered by identified peptides after the labelled time points (1, 3, 5, 10 and 30
(blue: IFN-α2a WT; orange: PEG; green: LPG; purple: PEtOx). Amino acids 28-31 are labelled red, as, due to th
undetectable in all samples, except IFN-α2a WT. (C) Predicted cleavage sites of Proteinase K (marked in red) bas
sites found in IFN-α2a WT after 30 min (marked in blue), extracted with EtOAc. Coloured amino acid residues are
= 51.5%. Found amount of cleaved residues: 56.4%. 30.9% of residues were correctly predicted and detected.

Chapter 3 – Polymer selection impacts the pharmaceutical profile of site specifically conjugated Interferon-α2a

Niklas Hauptstein‡, Paria Pouyan‡, Kevin Wittwer, Gizem Cinar, Oliver Scherf-Clavel, Martina Raschig, Kai Licha, Tessa Lühmann, Ivo Nischang, Ulrich S. Schubert, Christian K. Pfaller, Rainer Haag, Lorenz Meinel*

‡ These authors contributed equally to this work

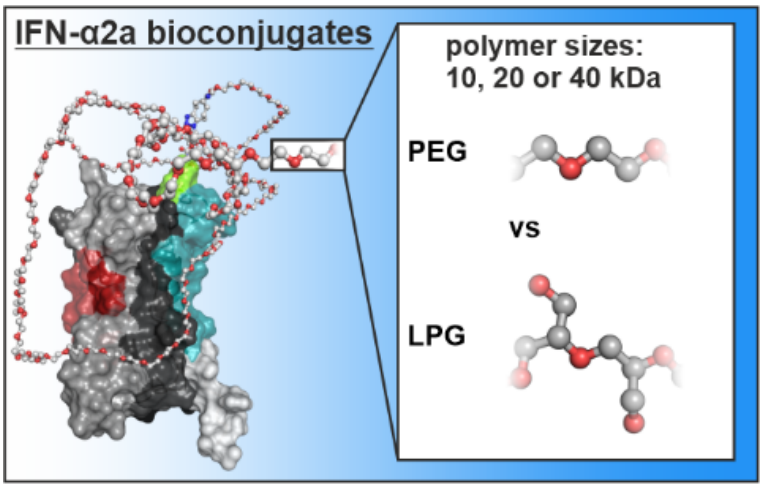

Keywords: bioconjugate; genetic code expansion; polyglycerol; poly(ethylene glycol); analytical ultracentrifugation; pharmacokinetic

Reprinted (adapted) with permission from: Hauptstein, N.; Pouyan, P.; Wittwer, K.; Cinar, G.; Scherf-Clavel, O.; Raschig, M.; Licha, K.; Lühmann, T.; Nischang, I.; Schubert, U. S.; Pfaller, C. K.; Haag, R.; Meinel, L., Polymer selection impacts the pharmaceutical profile of site-specifically conjugated Interferon-α2a. J. Controlled Release 2022, *348*, 881-892. DOI: 10.1016/j.jconrel.2022.05.060, Copyright 2022, Elsevier.

Abstract

Conjugation of poly(ethylene glycol) (PEG) to biologics is a successful strategy to favorably impact the pharmacokinetics and efficacy of the resulting bioconjugate. We compare bioconjugates synthesized by strain-promoted azide-alkyne cycloaddition (SPAAC) using PEG and linear polyglycerol (LPG) of about 20 kDa or 40 kDa, respectively, with an azido functionalized human Interferon-α2a (IFN-α2a) mutant. Site-specific PEGylation and LPGylation resulted in IFN-α2a bioconjugates with improved *in vitro* potency compared to commercial Pegasys. LPGylated bioconjugates had faster disposition kinetics despite comparable hydrodynamic radii to their PEGylated analogues. Overall exposure of the PEGylated IFN-α2a with a 40 kDa polymer exceeded Pegasys, which, in return, was similar to the 40 kDa LPGylated conjugates. The study points to an expanded polymer design space through which the selected polymer class may result in a different distribution of the studied bioconjugates.

Highlights

- IFN-α2a bioconjugates with linear polyglycerols (LPG) and linear PEGs were designed.
- Pharmacokinetics of the 40 kDa PEG-IFN-α2a matched the marketed product, Pegasys.
- LPG-IFN-α2a had faster disposition kinetics at comparable radii when compared to PEG-IFN-α2a.
- The study points to an expanded polymer design space for bioconjugate synthesis.

Introduction

PEGylation, the attachment of poly(ethylene glycol) (PEG) to a biologic, may improve various pharmaceutical aspects of the resulting bioconjugates, including stability, solubility, and pharmacokinetics [69, 70, 116]. PEGylation increases a drug's hydrodynamic volume and may, at proper overall size, reduce drug disposition by decreasing glomerular filtration [57, 58]. Another aspect of PEG, known as "stealth-effect", shields PEGylated biologics from phagocytic cells, thereby reducing elimination [69, 70]. Both factors contribute to longer half-lives and have been reported for PEGylated Interferon-α2a (IFN-α2a), which is the starting point of our study [249, 250]. IFN-α2a, a cytokine with potent, antiviral, immune-modulating, and antiproliferative properties, is used for hepatitis and cancer therapy since 1980s [251]. We selected IFN-α2a for its wealth of available information [8, 10, 13, 44, 48, 49, 62, 77, 87, 115, 130, 141, 189, 249-252]. Today IFN-α2a is marketed as a PEGylated biologic [252]: One IFN-α2a carrying a 40 kDa branched PEG (Pegasys) [77, 253], one IFN-α2b carrying a 12 kDa linear PEG (PegIntron) [254], or one IFN-α2a carrying a branched 40 kDa PEG which is N-terminally linked (Besremi) [255].

To date, there are more than 20 FDA-approved PEGylated proteins and drugs on the market [256]. The first PEGylated bioconjugates, which were approved around 20 years ago, are challenged by at least two aspects, firstly, the missing control of the modification site at the biologic and secondly, immunological

challenges regarding PEG [155, 234, 257-259], but also the immunogenicity of the protein itself. However, unspecific multi- PEGylation may actually be advantageous in specific cases, for example immunogenic enzymes of non-human origin (e.g. cyanobacterial (Palynziq)[259], bovine (Adagen)[260], etc.)), and similar enzymes [259-262]; their functionality is not substantially impacted by non-specific PEGylation [263]. Such design aspects are already discussed elsewhere [264, 265]. However, these non-targeted PEGylation approaches are inappropriate for receptor interacting proteins like cytokines.

Improved conjugation techniques have overcome the challenges of unspecific conjugation. Site-specific strategies pointing in this direction include the targeting of amino acids (cysteines[87, 88], tyrosines[266], arginines [267], histidines[89]), the N-terminus [166, 268, 269] and C-terminus [269, 270], site directed enzymatic conjugation by e.g. sortase A [269, 271] and transglutaminases [270, 272-275], or by glycoPEGylation [276, 277]. These methods have been reviewed before [252, 265, 278-281] and are already integrated in FDA approved PEGylated drugs (Besremi (N-terminal 20 kDa PEGylated IFN-α2b), Neulasta (N-terminal 20 kDa PEGylated G-CSF), Lonquex (20 kDa glycoPEGylated G-CSF), Refixia (glycoPEGylated factor IX), etc.). Alternatively, as performed in this study, genetical introduction of unnatural amino acids guarantees polymer decoration at that preselected site [92, 93, 95, 97, 98, 166, 184, 198, 233, 268, 282-288].

As to the second, immunological challenges of PEGylated biologics, recent reports point to possible side-effects including hypersensitivity,[289, 290] and immunological responses, [154, 155, 259] which are at least in part driving accelerated plasma clearance after repetitive dosing [259, 291]. Hence, expanding the polymer space beyond PEGylation is of interest and linear polyglycerol (LPG) has been discussed in this context before [98, 166, 268, 288].

Therefore, we recently synthesized bioconjugates through strain-promoted azide-alkyne cycloaddition (SPAAC), starting off a genetically engineered, azido-IFN-α2a mutant and functionalized PEG, and LPG polymers of about 10 kDa, respectively [98]. All products were generally comparable across the two polymer chemistries reported here, including their preferential interaction sites with the protein surface. We are now expanding to bioconjugates with higher polymer molecular weights of about 20 and 40 kDa as required for a therapeutically relevant half-life and compare the outcome to the commercial PEGylated IFN-α2a bioconjugate, Pegasys [77, 253].

Materials and methods

Materials. Boc-protected L-lysine was from P3 BioSystems LLC (Shelbyville, KY). 2-bromoethanol, triphosgene, sodium azide, HCl in diethyl ether (c = 2 mol · L^{-1}), 1,4-dithiothreitol (DTT), carbenicillin, chlorampenical, isopropyl-β-D-thiogalactopyranosid (IPTG), penicillin-streptomycin, phenylmethylsulfonyl fluoride (PMSF), guanidine hydrochloride, primer, NDSB-201, L-(+)-arabinose, lysozyme, DNAse I, triton X-100, acetonitrile HPLC grade, ethylacetate, trifluoracetic acid, human plasma, phosphate buffered saline (PBS), potassium phthalimide (99%), hydrazine monohydrate (64-65% N_2H_4, 98%), (1*R*,8*S*,9s)-bicyclo[6.1.0]non-4-yn-9-ylmethyl *N*-succinimidyl carbonate (BCN-NHS), dichloromethane (anhydrous, ≥ 99.8%), and triethylamine (anhydrous, ≥ 99%) were purchased from Sigma Aldrich (Schnelldorf, Germany). PageRuler™ Prestained Protein Ladder, PageRuler™ Unstained Broad Range Protein Ladder, Coomassie Brilliant Blue G250, slide-a-Lyzer, Dulbecco's Modified Eagle's Medium (DMEM), Gibco-FBS-HI (Origin Brasil), BCA assay, synthesized IFN-α2a genes, *E. coli* BL21(DE3) Star bacteria, MagicMedia™ *E. coli* Expression Medium, Pierce C18 Tips, SYPRO™ Orange Protein Gel Stain, IFN-α Human Instant ELISA™ Kit (BMS216INST) were received from Thermo Fisher Scientific Germany (Darmstadt, Germany). BioPro IEX SmartSep S20 1 mL and 5 mL were obtained from YMC Europe (Dinslaken, Germany). XK16/600 Superdex 75 pg column was received from Cytiva Life Sciences (Freiburg, Germany). Zorbax 300SB-CN column was ordered from Agilent (Waldbronn, Germany). Vivaspin centrifugal concentrators were obtained from Sartorius AG (Göttingen, Germany). Spectra/Por 1 Dialysis Membrane Standard RC tubing was ordered from Repligen (Ravensburg, Germany). ROTIPHORESE® NF-Acrylamide/Bis-Solution 30 (29:1) was obtained from Carl Roth GmbH (Karlsruhe, Germany). HEK-Blue™ IFN-α/β Cells, blasticidin and zeocin were ordered from Invivogen (Toulouse, France). Bovine serum albumin standard for MALDI-MS calibration was purchased from Bruker (Bremen, Germany).

Synthesis of polymers. Polymer synthesis of LPG and PEG was performed as described previously [98]. In brief, LPG was synthesized by monomer-activated anionic ring-opening polymerization. Prior to polymerization, the glycidols' hydroxyl groups were protected by acetal groups, which were removed in acidic media afterward, yielding the linear deprotected backbone. For functionalization, the terminal bromide group was reduced to an amine and functionalized using BCN-NHS, yielding the terminally functionalized LPG. PEG was bought as PEG-amine and directly functionalized with BCN-NHS.

Analytical ultracentrifugation. A stock solution of each polymer was prepared and diluted with water to obtain concentrations of approximately 0.25 mg mL^{-1} and 0.75 mg mL^{-1}, respectively. The aqueous solutions of the protein IFNK31N_3 and the bioconjugates were diluted with 10 mM phosphate-buffered saline (PBS, pH = 7.4) to obtain a sample concentration of approximately 0.75 mg mL^{-1}. Sedimentation velocity experiments were performed with an Optima Analytical Ultracentrifuge (Beckman Coulter Instruments, Brea, CA) by utilizing double-sector Epon centerpieces with a 12 mm solution optical path length. The cells were placed in an An-50 Ti eight-hole rotor. The cells were filled with 420 µL sample solution in diluent and with 440 µL water (polymers) or water / PBS buffer (10 mM) mixture (IFNK31N_3

and bioconjugates) as the reference. All samples were measured by using the interference optical detection module (refractive index (RI)) for observation of sedimentation boundaries in respect to time. For the protein and bioconjugates, additionally the absorbance detection module at λ = 280 nm was used. All measurements were performed at 20 °C and at a rotor speed of 42 000 rpm for up to 48 hours, depending on the sample. A three-minute (polymers) or five-minute (IFNK31N_3 and bioconjugates) time interval between each scan was used. Analysis of a suitable selection of scans was used for data evaluation with Sedfit [292]. Viscosity and density measurements of the solvents were performed at the accurate compositions utilized for the experiments with a DMA4100 densimeter (Anton Paar, Graz, Austria) at 20 °C. For viscosity measurements of the exact same solvents, an Automated Microviscometer (AMVn, Anton Paar, Graz, Austria) at 20 °C was used (**Table S1**). The instrument was operated with a capillary / ball combination. Sedimentation velocity analytical ultracentrifugation (AUC) data were evaluated by numerical solution of the Lamm equation via Sedfit making use of the c(*s*) model, returning differential distributions of sedimentation coefficients, *s*, and weight average translational frictional ratios, f/f_{sph} [292, 293]. Here, *f* is the translational friction coefficient of the investigated macromolecules and f_{sph} the translational friction coefficient of a spherical particle with the same anhydrous volume and mass [294]. Numerical estimates of signal (weight) average values of *s* and the f/f_{sph} values from sedimentation-diffusion analysis are summarized in Table S2. The used partial specific volumes, υ, for the c(*s*) model, allowing numerical solution of the Lamm equation, were taken from the literature (υ = 0.83 cm^3 g^{-1} for PEGs)[178, 294]. For the LPG polymers, a partial specific volume of υ = 0.73 cm^3 g^{-1} was taken based on unpublished previous experimental results. For the IFNK31N_3, we utilized a typical value for proteins (υ = 0.73 cm^3 g^{-1}) as reported in the literature [295, 296], and also in line with previous studies of a related protein [297]. υ for the PEG conjugate was calculated by use of υ of PEGs and the protein weighed by mass fractions of components in the conjugate (as known from separate AUC investigations of PEG polymer and protein), resulting in υ = 0.76 cm^3 g^{-1}. υ for the LPGs and protein had similar values and, therefore, were also taken for the conjugate (υ = 0.73 cm^3 g^{-1}). The intrinsic sedimentation coefficients, *[s],* were calculated by $[s] = s\eta_0/(1-\upsilon\rho_0)$ with the solvent viscosity, η_0, and solvent density, ρ_0. Molecular weights by AUC (**Table S2**) were calculated from the lowest investigated polymer concentration being closest to solution ideality by utilizing the modified Svedberg equation: $M_{s,f} = 9\pi\sqrt{2}N_A([s](f/f_{sph}))^{3/2}\sqrt{\upsilon}$ with N_A being the Avogadro constant [178, 294].

Size exclusion chromatography of polymers. Size exclusion chromatography (SEC) of polymers was performed as described previously [98]. In brief, SEC of LPG polymers was performed in pure water with an Agilent 1100 SEC system (Agilent Technologies, Santa Clara, CA, USA), equipped with an automatic injector, isocratic pump and an Agilent 1100 diffractometer. As a column, a PSS Suprema column (pre-column, 1x with pore size of 30 Å, 2x with pore size of 1000 Å, all of them with a particle size of 10 µm) was used with a flow rate of 1 mL/min. Calibration was performed with pullulan standards prior to measurements. Molecular weight of the PEG used for conjugation was taken as provided by the manufacturer.

Expression and purification of IFN-α2a and mutant. Expression of IFN-α2a and IFNK31N$_3$ was performed as described before [98]. In brief, expression was in *E. Coli* (BL21) DE3 bacteria with IPTG induction. For the mutant, expression of the pyrrolysyl-tRNA synthethase/tRNA^{Pyl} CUA pair was done by co-induction with L(+)-arabinose of a pEVOL-pylRS vector containing a chloramphenicol resistance cassette, which was kindly donated by Prof. Dr. Edward A. Lemke from the Johannes Gutenberg University of Mainz/EMBL Heidelberg [195, 196]. After expression, inclusion bodies were isolated and refolded. The refolded protein was purified by anion and cation exchange chromatography, followed by SEC.

Strain promoted azide-alkyne Huisgen cyclo-addition. Strain promoted azide-alkyne Huisgen cyclo-addition (SPAAC) was performed as described previously [98]. In brief, the protein was mixed with a 20-fold excess of activated polymer in 25 mM phosphate buffer pH 7.4 + 150 mM NaCl at a concentration of approximately 500 µg/mL and incubated for 48 h under gentle stirring at 4 °C in a borosilicate glass vessel. For the 40 kDa polymers, the SPAAC reaction was allowed for a timescale of 72 h. To account for differences in polymer activation, the amount of used polymer was adapted based on the activation of the used polymer (**Table S1**).

Sodium dodecyl sulphate polyacrylamide gel electrophoresis. Sodium dodecyl sulphate polyacrylamide gel electrophoresis (SDS-PAGE) was performed as described previously using standard Tris-glycine buffer systems. For samples with a molecular weight up to 40 kDa (up to 20 kDa bioconjugates) 10 to 15% SDS-Gels were used. For samples with a molecular weight above 40 kDa 5 to 15 % SDS-Gels were used.

Reversed phase high pressure liquid chromatography analysis. Reversed phase high pressure liquid chromatography (RP-HPLC) analysis was performed as described previously [98]. In brief, an Agilent Zorbax 300SB-CN (4.6 x 150 mm, 5 µm particle) column was used for analysis, using a linear gradient of 5 to 70% eluent B (%, v/v) within 35 min at a constant flow of 1 mL/min. Eluent A = Water + 0.1% TFA and eluent B = ACN + 0.1% TFA, λ = 214 nm.

Dynamic light scattering. Dynamic light scattering (DLS) was performed as described previously with adaptions [268]. DLS was performed on a Malvern Zetasizer ZS (Malvern Panalytical, Herrenberg, Germany). Measurements were performed at 25 °C in 100 mM phosphate buffer pH 7.2 + 150 mM NaCl (c[Protein] = 0.4 mg/mL) after sterile filtration. Three measurements were performed of each sample, whereby three acquisitions were averaged per measurement. Results are reported as intensity value as shown in the Zetasizer software (version 7.13).

HEK Blue IFNα/β cell culture assay. The cell culture assay was performed in HEK-Blue™ IFN-α/β cells according to the manufacturer's instructions. In brief, 50 000 cells were seeded at day 1 in a 96-well plate (280 000 cells/mL) in each well and stimulated with IFN bioconjugates starting at a concentration of 1 µg/mL, followed by eleven 10-fold dilutions. On day 2, 20 µL of the supernatants

were mixed with 180 µL of Quanti-Blue™ and analyzed at λ = 630 nm after 120 min of incubation at 37 °C. The potency of 10 kDa bioconjugates was reported previously [98] and were measured again on the same plates here along with the other molecular weight bioconjugates for comparability purposes.

Differential scanning fluorimetry. Differential scanning fluorimetry (DSF) was performed as described previously [98]. In brief, bioconjugates were analyzed at a final concentration of 8 µM protein equivalents over a range of 25 to 95 °C using a heating ramp of 1 °C/min, whereby SYPRO Orange was used at a 5-fold concentration. Normalization was performed as described before, without smoothing of data [199].

***In vivo* pharmacokinetic study in mice.** Animal experiments were carried out in compliance with the regulations of the German animal protection laws and authorized by the responsible state authority (Regierungspräsidium Darmstadt, Dezernat V54 - Veterinärwesen und Verbraucherschutz). Male and female transgenic C57BL/6 B6.Tg(ISRE-eGFP)Tovey mice [298] between 8 and 18 weeks of age were divided into groups of 15 animals for each interferon conjugate (mean group age 10 to 13 weeks). Mice were weighed, interferon conjugates were diluted in sterile PBS and 3 µg/kg bodyweight of IFN-α2a-WT equivalents (therefore the protein amount was always the same) of the respective dilution were administered intravenously in the tail vein. For blood sampling, groups were divided into three subgroups of five animals each. In each subgroup, blood was taken at two time points, respectively (time points 1+4, 2+5, 3+6 as reported in **Scheme 1**). At the first time point, mice were anesthetized using isoflurane, and 100 µL blood was taken from the retro-orbital vein plexus. At the second time point, animals were anesthetized by intraperitoneal injection of Ketamine/Xylazine (100 mg/10 mg per kg bodyweight) and exsanguinated via cardiac heart puncture. Serum was obtained by blood centrifugation at 14.000 x g at 4 °C for 10 min. The serum was then snap-frozen in liquid nitrogen, followed by storage at -80 °C until further analysis. After thawing on ice, the collected serum samples were diluted appropriately and analyzed by ELISA (see below for details) according to the manufacturer's instructions. The primary data set was fitted using non-linear least squares fits using RStudio (version 4.0.5) [299].

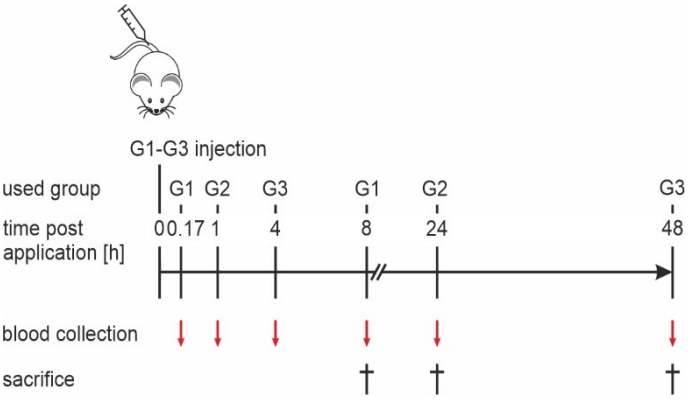

Scheme 1: Protocol of the *in vivo* pharmacokinetic study. G1= group 1, G2 = group 2, G3 = group 3 (n = 5).

Plasma stability of Interferon-α2a and bioconjugates. IFN-α2a WT and its bioconjugates were spiked into plasma to a final concentration of 1 ng/mL. The plasma was incubated at 37 °C at 300 rpm for up to 48 h. Samples were taken at 0,1,3,7,24, and 48 h and snap frozen in liquid nitrogen until further analysis. IFN concentrations of the samples were analyzed by ELISA (see below for details) setting the averaged concentration of IFN-α2a WT at 0 h as the 100% reference.

Enzyme-linked immunosorbent assay. Samples of plasma stability and serum samples from the *in vivo* pharmacokinetic study were analyzed by enzyme-linked immunosorbent assay (ELISA). Samples taken for plasma stability were directly used. Samples taken from the *in vivo* study were 25-fold diluted using the kits dilution buffer, except from IFN-α2a WT, setting the maximum expected concentration to 2 ng/mL. IFN-α2a WT was only diluted 2-fold as an initial trial did show too low detectable concentrations indicating a rapid decay. To account for polymer specific decreased antibody binding, every bioconjugate, as well as the WT was analyzed with a calibration curve established by the pure bioconjugate as the reference. For the calibration curve, the same concentrations were used as the supplied standard calibration concentrations (39 to 2500 pg/mL+ blank). The lower limit of detection was 3.3 pg/mL, according to the manufacturer.

Stimulation of B6.Tg(ISRE-eGFP) Tovey mice bone marrow cells followed by fluorescent activated cell sorting analysis. Animals were sacrificed by intraperitoneal anesthesia (Ketamine/Xylazine (100 mg/10 mg per kg bodyweight)) and exsanguination. Femoral bones were dissected, flushed with RPMI (10% FBS, 1% L-glutamine, 1% P/S, 1% Na-pyruvate) and 10^6 bone marrow cells were seeded in a 24-well plate. Human IFN-α2a WT (1000 ng/ml) or murine IFN-α2a WT (1000 U/ml) was added and plates were incubated for 24 hours at 37°C. The next day, cells were washed twice with PBS (1% FBS, 0.1% NaN_3). PBS supplemented with 1% paraformaldehyde was used to re-suspend the cell pellet and GFP expression was determined using a CytoFLEX flow cytometer (Beckman Coulter, Krefeld, Germany).

Statistical analysis. Statistical analysis was performed with Graphpad Prism 6. Results were compared by one-sided ANOVA, followed by Tukey *post hoc* test for pair-wise comparison; $p < 0.05$ was considered statistically significant.

Results

Polymer synthesis and characterization

The synthesis of PEG and LPG polymers started off previous protocols with adaptations as required for the longer polymer chains (**Figures 1A, B, Scheme S1, Figures S1-3**)[98, 227, 300]. LPG was synthesized by anionic ring-opening polymerization of the acetal protected glycerol with $(Oct)_4NBr$ in toluene in presence of $(i\text{-}Bu)_3Al$ as activator (**Scheme S1**). After polymerization, the acetal protected backbone was treated in slightly acidic media and the respective LPG with free hydroxyl moieties was obtained (data not shown)[98]. To introduce the cyclooctyne group for SPAAC, the bromide at the chain-end was substituted with an azide group with NaN_3 (data not shown)[98]. In a subsequent step, the azide was reduced to a primary amine which was then modified with BCN-NHS (**Table S1, Figure S1**). SEC measurements confirmed LPG polymers with similar molecular weights to theoretical values (**Table 1, Figure S2**). The commercial PEG-NH_2 was modified with BCN-NHS and analogous to the synthesis with LPG-NH_2 (**Table S1, Figure S3**).

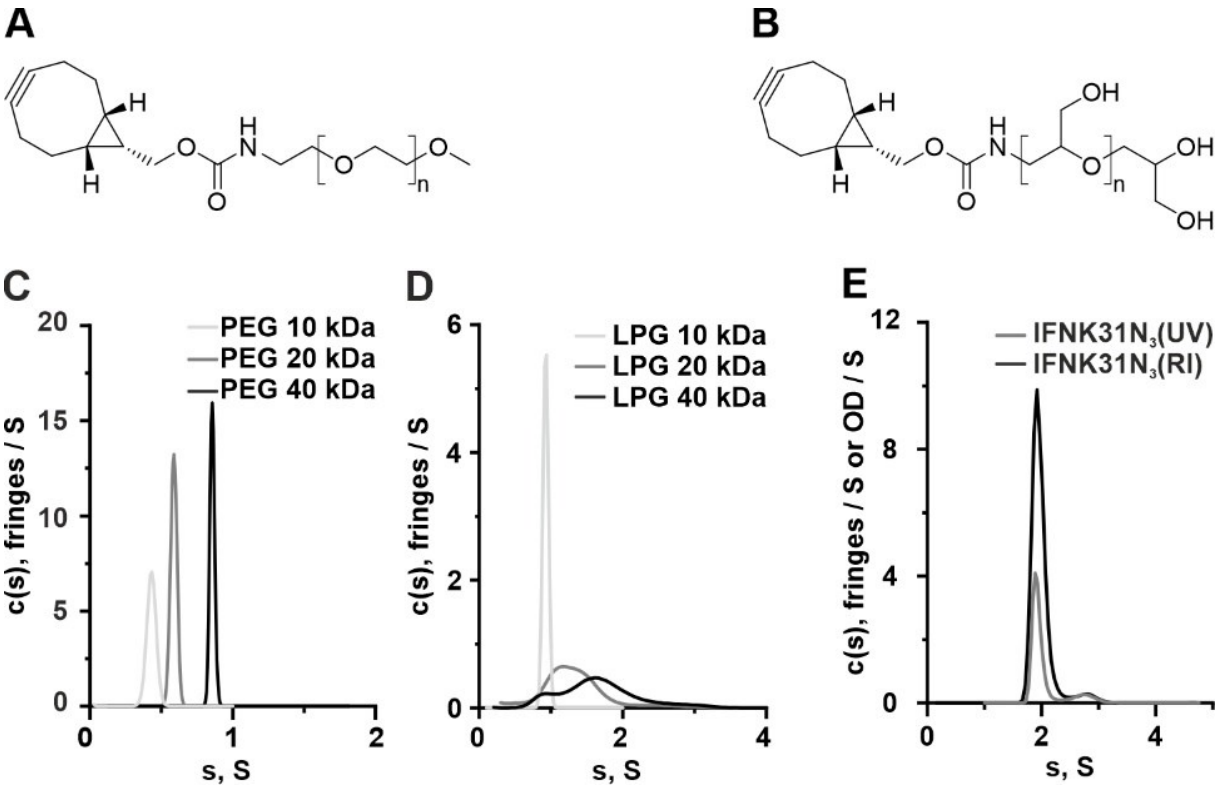

Figure 1: (A) Chemical structure of BCN-PEG and (B) BCN-LPG. Differential distributions of sedimentation coefficients, c(*s*), of (C) NH_2-PEG polymers (c ≈ 0.26 mg mL^{-1}), (D) N_3-LPG polymers (c ≈ 0.25 mg mL^{-1}) of different molecular weights, and (E) $IFNK31N_3$ (c ≈ 0.75 mg mL^{-1}). The latter results were obtained from RI (in terms of interference fringes) and absorbance detection (in terms of optical density (OD) at λ = 280 nm). AUC measurements and evaluation of polymers that are displayed in C and D were also performed at a higher concentration, results which are displayed in Figure S4.

All polymers were characterized by AUC as amino-, or as azide intermediates (**Scheme S1, Tables 1, S2, S3, Figures 1C, D, S4**) and by SEC for comparison (**Table 1, Figure S2**). Results from both analyses were in the same order of magnitude with lower apparent molecular weight values obtained by AUC compared to calibrated SEC against standards and in line with previous reports [178, 294]. The larger LPGs

had broader differential distributions of sedimentation coefficients, c(*s*), as compared to PEG (**Figure 1C and D, S4A-C**). The signal (weight) average sedimentation coefficients, *s*, obtained by integration of the entire differential distributions, increased from *s* = 0.43 S (Svedberg) to *s* = 0.59 S and *s* = 0.86 S for the 10 kDa, 20 kDa, and 40 kDa PEG (**Figures 1C, S4, Table S3**), and from *s* = 0.93 S to *s* = 1.35 S and *s* = 1.66 S for the 10 kDa, 20 kDa, and 40 kDa LPGs (**Figures 1D, S4, Table S3**). This LPG inhomogeneity translated into quite challenging disadvantages on the level of the bioconjugate and concerning overall yield. Rigorous cutting of the fractions was required for the LPG bioconjugates to obtain fractions comparable to the PEGylated counterparts and as detailed in the next paragraph (**Figure S5**).

Table 1: Polymer characterization by SEC, AUC, and by MALDI-TOF MS for the resulting IFNK31N_3 bioconjugates.

Method	SEC (kDa, Đ)	AUC (kDa)	MALDI-TOF MS (kDa)	AUC (kDa)
Sample	Polymer	Polymer	Bioconjugate or protein	Bioconjugate or protein**
PEG 10 kDa	10.0, 1.04 [98]	7.9	30.3* [98]	27.7
PEG 20 kDa	23.3, 1.04 [a]	14.9	40.5	---
PEG 40 kDa	40, 1.08 [a]	47.6	60.2	---
LPG 10 kDa	11.6, 1.23 [98]	9.0	32.0* [98]	30.4
LPG 20 kDa	22.1, 1.22 [b]	19.8	44.6	---
LPG 40 kDa	54.8, 1.5 [b]	37.8	n.d.	---
IFNK31N_3	---	---	19.5* [98]	19.7

[a] M_p according to manufacturer, [b] measured in H_2O by SEC calibrated with pullulan standards. *the value was published previously in the indicated reference. **Average from RI and absorbance detection. n.d. = not determinable

Conjugation, purification, and analysis of bioconjugates

Sedimentation-diffusion analysis, c(*s*), of IFNK31N_3 displayed a major species and a second less abundant species, both identified by data from the interference and absorbance detection module. The sedimentation coefficient for the monomer from both detector principles averaged to *s* = 1.95 S (**Figure 1E and S4D, Table S3**), which is in agreement with a recent study of recombinant human IFN-α2a in a nonrelated study[301]. Average molecular weights were calculated to be 19.7 kDa as an average based on absorbance and RI detection (**Tables 1 and S3**), comparable to the MALDI-TOF MS results (**Table 1**) [98]. Next to the IFNK31N_3 monomer, the second species at *s*-values of ca. 2.8 S, presumably originates from a discernable existence of reversibly associated protein dimers, which has been reported previously for IFN-α2 at neutral pH [301-304]. The BCN functionalized polymers were conjugated with azide functionalized IFN-α2a (IFNK31N_3; **Scheme 2**) and purified by FPLC (**Figure S5, Table S4**).

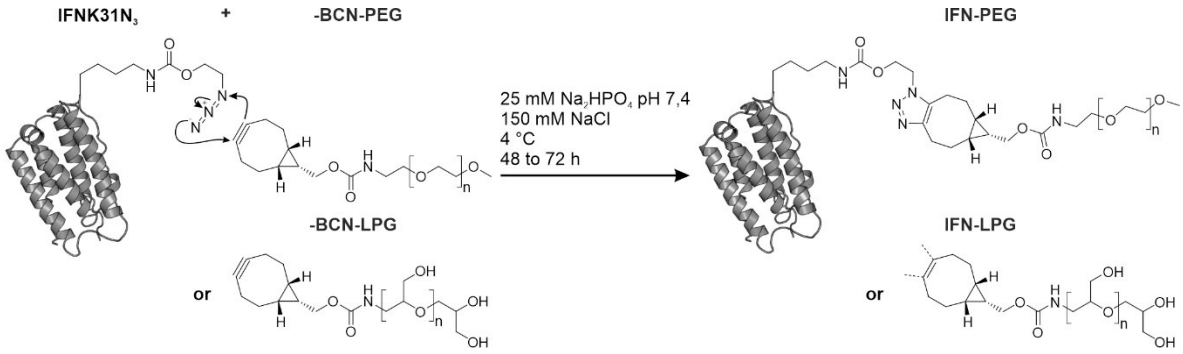

Scheme 2: Schematic representation of the BCN functionalized polymer conjugation to IFNK31N_3.

As mentioned for LPG, the product yield decreased with increasing molecular weight of the polymer(**Figure S5, Table S4**). The higher dispersity of LPG polymers reduced the collected fractions and, hence, lowered the yield (**Figure S5, Table S4**). The resulting molecular weights of 20 and 40 kDa PEG and 20 kDa LPG bioconjugates were confirmed by MALDI-TOF MS. The LPG 40 kDa bioconjugate could not be measured by MALDI-TOF MS, possibly reflecting its higher dispersity. The calculated molecular weights of the conjugated polymers were in good agreement with SEC outcome after subtracting the mass of IFNK31N_3 from the measured mass of the bioconjugate, via MALDI-TOF MS, or AUC. Calculated molecular weights from AUC had the same tendency to slightly lower molecular weights, as did the sole polymers. SDS-PAGE analysis resulted in defined single bands for IFNK31N_3, IFN-α2a WT, and all bioconjugates except for the 40 kDa LPG (**Figures 2A, B**).

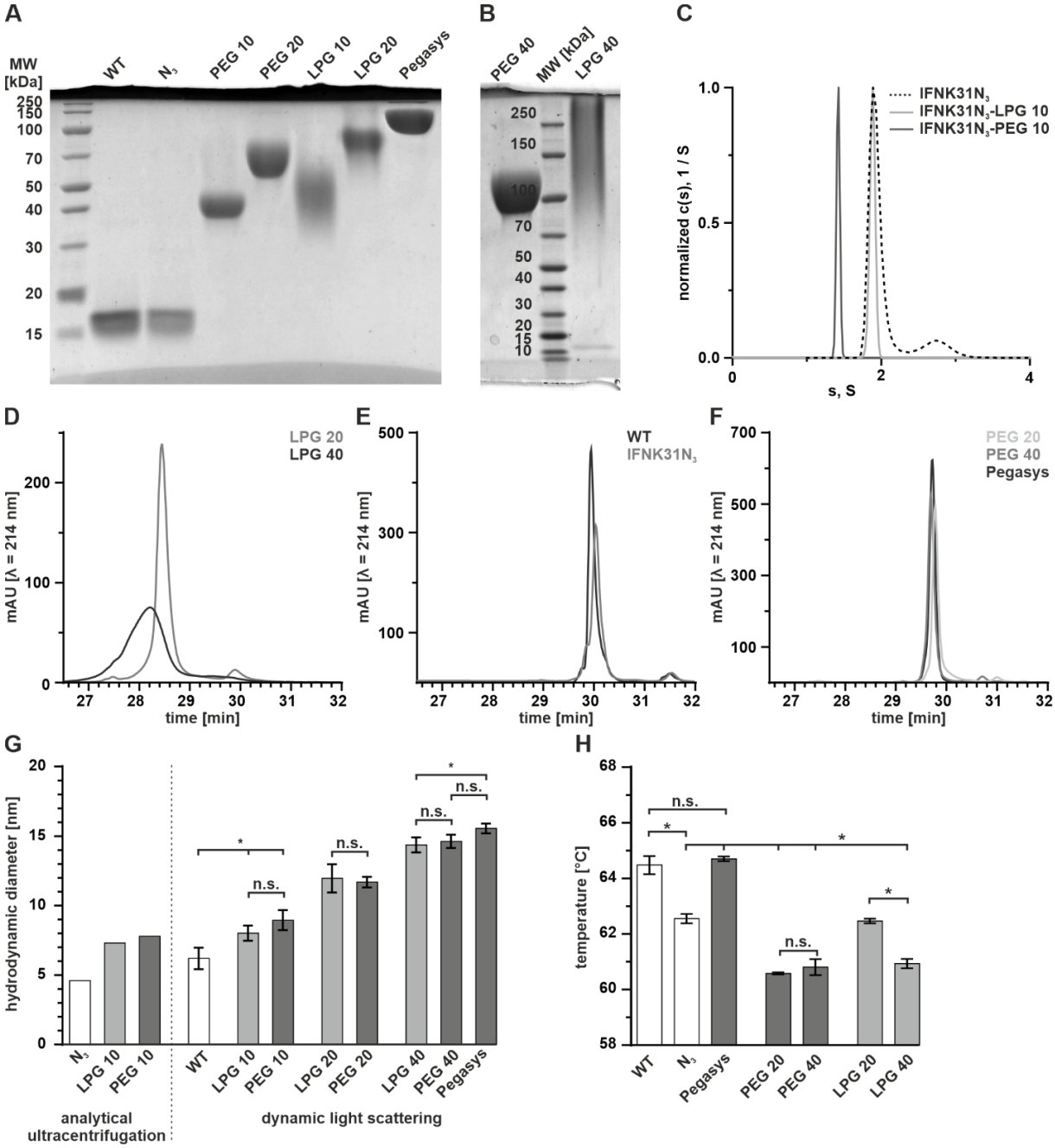

Figure 2: SDS-PAGE of (A) IFN-α2a WT (WT), IFNK31N$_3$ (N$_3$), IFNK31N$_3$-PEG 10 kDa (PEG 10), IFNK31N$_3$-PEG 20 kDa (PEG 20), IFNK31N$_3$-LPG 10 kDa (LPG 10), IFNK31N$_3$-LPG 20 kDa (LPG 20) and Pegasys, (B) IFNK31N$_3$-PEG 40 kDa (PEG 40) and IFNK31N$_3$-LPG 40 kDa (LPG 40). (C) Normalized differential distributions of sedimentation coefficients, c(*s*), of 10 kDa bioconjugates by absorbance detection in terms of OD at λ = 280 nm (c(*s*) of IFNK31N$_3$, which is displayed in Figure 1E is displayed again for comparative purposes). Magnification of RP-HPLC chromatograms of (D) LPG-bioconjugates, (E) IFN-α2a WT and IFNK31N$_3$ and (F) PEG-bioconjugates (for full chromatograms please see Figure S7). (G) Hydrodynamic diameter of IFN-α2a WT and its bioconjugates (AUC n = 1; DLS n = 3; mean ± standard deviation; analysis for differences by one-sided ANOVA test followed by Tukey *post hoc* test for pair-wise comparison; $p < 0.05$ was considered statistically significant and selected differences as relevant for this study were marked by asterisks). (H) Melting points of bioconjugates determined by differential scanning fluorimetry (n ≥ 4; mean ± standard deviation; one-sided ANOVA test followed by Tukey *post hoc* test for pair-wise comparison; $p < 0.05$ was considered statistically significant and selected differences as relevant for this study were marked by asterisks).

The 40 kDa LPGylated bioconjugate was less defined (**Figure 2B**), which was further reflected by its broader peak in the HPLC chromatogram (**Figures 2D, S7**). Furthermore, polymer hydrophilicity of the conjugated PEG and LPG polymers impacted the hydrophilicity of the resultant bioconjugates. These showed an altered hydrophilicity when compared to the unconjugated IFNK31N_3 mutant. This effect was more pronounced for the LPG conjugates than for the PEG conjugates (**Figure 2D-F, S7**).

Additionally, the 10 kDa PEG and LPG bioconjugates were analyzed by AUC (**Figure 2C and S4D**). The conjugation of PEG reduced the sedimentation velocity of the bioconjugate when compared to the protein monomer (despite higher overall molecular weights), resulting in a sedimentation coefficient of 1.42 S. The conjugation of LPG appeared not to significantly change the sedimentation velocity of the bioconjugate when compared to the protein monomer (despite higher overall molecular weights). It only led to a slight decrease to a sedimentation coefficient of 1.87 S. The conjugation of PEG and LPG to IFNK31N_3 did not show an apparent indication of dimers or higher aggregates, likely an effect of the polymeric stealth entity (**Figures 1E, 2C and S4D**). Data based on universal RI detection indicate the absence of free polymer while absorbance detection data are coherent with RI detection data for the bioconjugate (**Figure S4D**). Associated to sedimentation-diffusion analysis, we realized that the conjugated polymer (though of lower molecular weight than the protein) translated its much larger translational frictional properties to the protein, i.e., the bioconjugate (**Table S3**). Calculated molecular weights for the protein and bioconjugates by sedimentation-diffusion analysis, c(*s*), followed the anticipations of conjugation in concert to MALDI-TOF MS. Again, the decreased sedimentation coefficients of the PEG bioconjugates compared to the protein, despite their higher molecular weights compared to the protein, is known in the scientific literature, [297, 305-307] also coined as a “parachute” like effect. This is understandable by the altered translational friction properties of the bioconjugates compared to the parent protein. Apparently also, this effect is much reduced when using LPG conjugation as indicated here, though still being present. Bioconjugation significantly increased the hydrodynamic diameter of the IFNK31N_3 mutant for all polymers as observed by dynamic light scattering (DLS) and calculated from AUC data, i.e., the polymer contributes pronouncedly to the measured and calculated hydrodynamic equivalent spherical size estimates (**Figure 2G, Table S5**). DLS and AUC data correlated to each other, as exemplarily compared for IFN-α2a itself and the 10 kDa bioconjugates of PEG and LPG, respectively. The LPG and PEG polymers had overall comparable sizes among the 10, 20 or 40 kDa polymer group. The hydrodynamic diameter of the PEG 40 kDa bioconjugate was comparable to the Pegasys conjugates, in contrast to all other bioconjugates which were smaller in hydrodynamic equivalent spherical size estimates. The unfolding temperature of all bioconjugates was comparable for all bioconjugates and significantly reduced as compared to IFN-α2a WT, or Pegasys (**Figure 2H, S8, Table S5**).

Potency of bioconjugates

All bioconjugates had reduced potency as compared to IFN-α2a WT or the IFNK31N_3 mutant (**Figures 3A, S9, Table S5**) and bioconjugates performed similar within groups, and significantly different between groups of 10, 20, and 40 kDa bioconjugates. All groups performed significantly better than Pegasys. In general, an increasing hydrodynamic diameter inversely correlated with potency regardless of the polymer class used for conjugation following, *e.g.*, a third order polynomial regression for all bioconjugates other than Pegasys (**Figure 3B**).

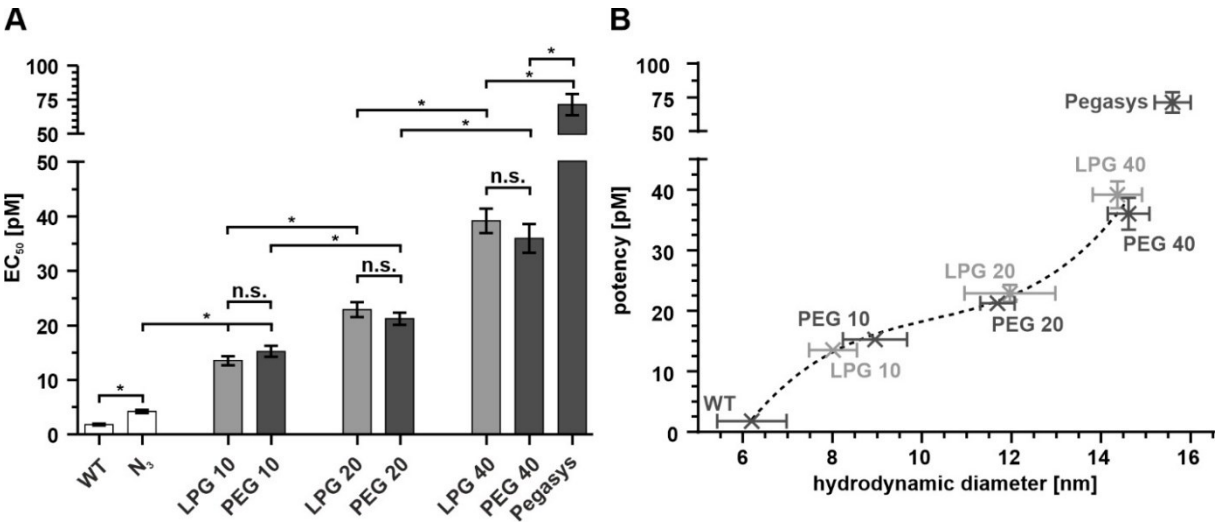

Figure 3: (A) EC_{50} values of bioconjugates ($n \geq 3$; mean ± standard deviation; analysis for differences by one-sided ANOVA test followed by Tukey *post hoc* test for pair-wise comparison; $p < 0.05$ was considered statistically significant and selected differences as relevant for this study were marked by asterisks. (B) Correlation of hydrodynamic diameter (data taken from Figure 2G) and potency (data taken from panel A of this figure).

Pharmacokinetics

IFN-α2a WT and all bioconjugates were stable in plasma throughout 48 hours (**Figure S10**). We further confirmed human IFN-α2a binding to the murine Interferon receptors by fluorescence-activated cell sorting (FACS) analysis of primary murine bone marrow cells (**Figure S11**). Resulting *in vivo* pharmacokinetics (PK) were mono-exponential for human IFN-α2a WT and PEG 20 kDa, and biphasic for all other bioconjugates. PK profiles for the human IFN-α2a WT were characterized by rapid disposition with a slope of about 9 h^{-1} ($t_{1/2} \approx 4$ min). The slope of the initial (distribution) phase indicated substantially slower distribution for the 20 kDa and 40 kDa LPG bioconjugates with 1.3 h^{-1} ($t_{1/2} \approx 32$ min) and 1.1 h^{-1} ($t_{1/2} \approx 39$ min), respectively, as compared to the wild type (**Figure 4, Table 2 and S6**).

Table 2: Calculated *in vivo* elimination constants (α and β), calculated initial concentrations of bioconjugates (CP_a and CP_b), terminal disposition rate constant (λ_Z), serum half-life ($t_{1/2}$), apparent total body clearance (CL), area under the curve values till infinity ($AUC_{0-\infty}$) and mean residence time till infinity (MRT_∞) of bioconjugates.

Compound	α [h^{-1}]	β [h^{-1}]	CP_a [ng/mL]	CP_b [ng/mL]	λ_Z [h^{-1}]	$t_{1/2}$ [h]**	CL [L/h · kg^{-1}]	$AUC_{0-\infty}$ [h · ng/mL]	MRT_∞ [h]
WT*	9.319	-	9.66	-	9.319	0.07	2.237	1.341	0.074
PEG 20*	0.208	-	32.95	-	0.217	3.2	0.0189	158.97	4.36
LPG 20	1.249	0.120	32.09	6.56	0.311	2.23	0.039	76.28	2.91
PEG 40	0.174	0.018	27.93	18.73	0.0277	25.0	0.0029	1043.51	31.9
LPG 40	1.059	0.058	30.88	16.32	0.0469	14.8	0.0085	354.28	17.68
Pegasys	0.139	0.015	27.95	7.50	0.0357	19.4	0.0048	620.73	23.9

Mono-exponential PK: $Conc(t) = CP_a \cdot e^{-\alpha \cdot t}$, Biphasic PK: $Conc(t) = CP_a \cdot e^{-\alpha \cdot t} + CP_b \cdot e^{-\beta \cdot t}$

* no distribution phase, mono-exponential PK, ** based on λ_Z

The distribution pharmacokinetics of the PEGylated bioconjugates and Pegasys was in the range of several hours, ranging from 0.2 to 0.14 h^{-1} ($t_{1/2} \approx 3$ h to 6 h). Terminal half-lives were some minutes for the IFN-α2a WT, and clustered between 2 hours and 4 hours for all 20 kDa bioconjugates. Substantially longer half-lives were recorded for the LPG 40 kDa, Pegasys, and PEG 40 kDa bioconjugates with 15, 19, and 25 hours, respectively. The rapid initial disposition of the LPG bioconjugates as compared to the PEGylated bioconjugates, resulted in an overall lower exposure (area under the curve) and was, in case of LPG 40 kDa, about half the amount when compared to Pegasys. Both were lower than the PEG 40 kDa bioconjugate.

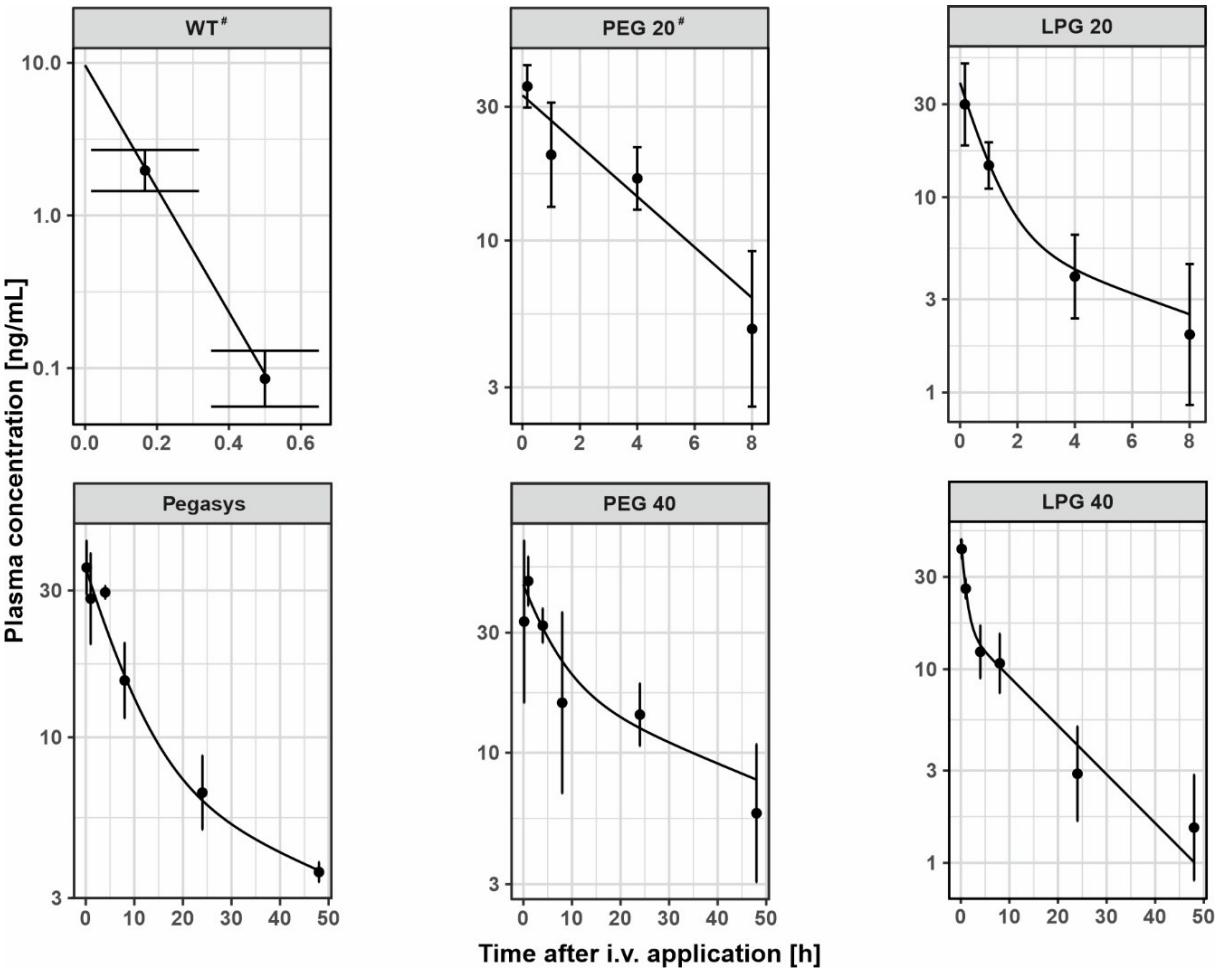

Figure 4: Pharmacokinetics of the human IFN-α2a WT and its bioconjugates (mean ± standard deviation, n ≥ 4). Mono-exponential pharmacokinetic were found for the human IFN-α2a WT and PEG 20 bioconjugate, respectively, and highlighted by a hashtag. All other profiles followed a biphasic pattern.

A faster distribution rate constant of LPGylated bioconjugates as compared to PEGylated bioconjugates was found although they had comparable hydrodynamic diameters (**Figure 5**).

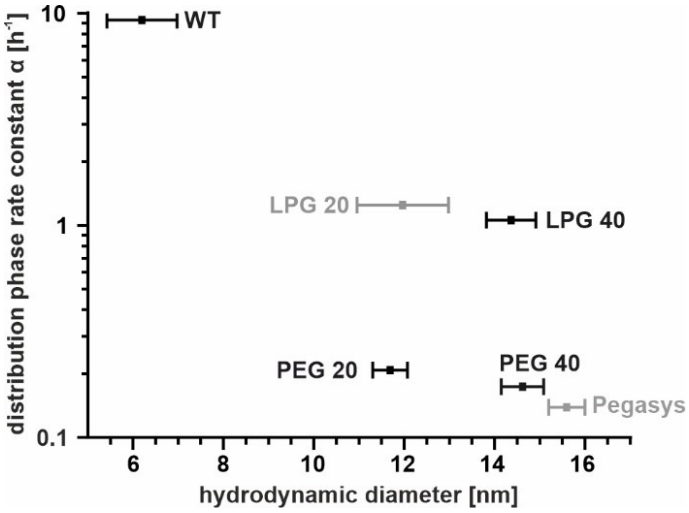

Figure 5: Hydrodynamic diameter (taken from Figure 2H, Table S5) and the initial rate/distribution rate constant (taken from Table 2). The PEG20 bioconjugate group followed mono-exponential kinetics (i.e. no distribution phase was distinguished).

Discussion

IFN-α2a mutants with a genetically introduced unnatural azide-carrying amino acid (IFNK31N_3) were manufactured and successfully conjugated with poly(ethylene glycol) (PEG) and linear polyglycerol (LPG) each with molecular weights of 20 or about 40 kDa (**Figure 2**). All bioconjugates had reduced potency as compared to IFN-α2a WT and its mutant, but higher potency as compared to the commercial product, Pegasys. The hydrodynamic diameter of the conjugates, but not their chemical nature negatively correlated with potency (**Figure 3**). Overall exposure of the 40 kDa PEG bioconjugate exceeded those seen for Pegasys. A faster initial disposition was observed for the LPGylated bioconjugates as compared to the PEGylated bioconjugates, respectively, despite comparable hydrodynamic diameters (**Figure 5**).

Pegasys, among the first PEGylated biologics on the market, was selected as an exemplary starting point for systematically expanding the polymer space for cytokine bioconjugates [98]. A recent publication using the same polymers with lower molecular weight, detailed optimal chemical linker structures between the biologic and the polymers as well as interaction patterns of the polymer-biologic interface [98]. This study now translates these findings to polymers with molecular weights targeting the colloidal dimensions of Pegasys and as required to lastingly modulate IFN-α2a pharmacokinetics for therapeutic use. Though only two time points were captured for IFN-α2a WT, which would generally jeopardize PK analysis, the resulting outcome was in line with previous results from experiments in mice and rats [77, 130, 136, 308, 309]. IFN-PEG 20 kDa showed a mono exponential decay, though biphasic decays for similar bioconjugates were reported previously [310-312]. Interestingly, the LPGylated bioconjugates had a faster initial disposition from blood serum as compared to the PEGylated counterparts with otherwise comparable hydrodynamic radii and potency (**Figure 3**). This provided evidence that these differences were not related to renal excretion. Furthermore, binding to serum components cannot explain these differences as supporting earlier reports indicate that albumin binding was not different for similar sized PEGylated or LPGylated human Interleukin-4 [268]. Hence, these differences in disposition kinetics from blood serum are likely reflecting different distribution characteristics for LPGylated bioconjugates as compared to PEGylated bioconjugates. Interestingly, these at present unknown sinks for LPGylated bioconjugates were rapidly saturated and the following patterns in the terminal phase were comparable for LPGylated and PEGylated equivalents. Further studies, *e.g.*, bioimaging studies, are required to detail these findings, *e.g.,* comparing uptake phenomena in the liver or spleen for LPGylated and PEGylated bioconjugates and possibly binding studies in whole blood can detail potential binding to cellular components during circulation. Detailing these findings might in fact be particularly interesting for IFN-α2a bioconjugates. For example, previous studies indicated that prolonged exposure, as seen for Pegasys in comparison to the unconjugated wild type, shifted elimination from renal excretion to hepatic elimination [249]. Hence, different elimination routes and different organ distributions may result from different polymers and different sizes of conjugated polymers used for bioconjugation.

Similar outcome was obtained for the molecular weights of the polymers by SEC, AUC, and MALDI-TOF MS. While being in the same order of magnitude (**Table 1**), AUC analysis, though being performed from a limited amount of measurements, resulted in smaller molecular weights of the polymers, except for PEG 40 kDa. These effects were also found when calculating the molecular weight of the polymers by subtracting the mass of the protein from the AUC analysis outcome for the respective bioconjugates. Furthermore, the calculated and measured molecular weights of the bioconjugates by AUC and MALDI-TOF MS were not contrasting each other. An interesting aspect found in the sedimentation velocity data was re-affirmation of a "parachute" like effect on protein hydrodynamics for PEG conjugates,[297, 305, 306] observed also for LPG conjugates, but according to our present results to a much lower extend. This effect was coined down to originate from increased translational frictional ratios, f/f_{sph}, templated from the synthetic polymers on the biologic. Notwithstanding, AUC data unveiled rather accurate calculation of molecular weights of bioconjugates, since the methods of hydrodynamics inherently consider variations of translational friction properties associated to sedimentation and diffusion (the latter through translational frictional ratios, f/f_{sph}) in molecular weight estimations [307].

Potency negatively correlated with the hydrodynamic parameter (doubling diameter approximately reduced the potency four-fold; **Figure 3**) and was qualitatively reported for 10 kDa polymers before [98]. The measured hydrodynamic diameters of the protein and diameter increase of bioconjugates were in line with previous measurements performed by DLS for Anakinra (17.3 kDa), as well as Interleukin-4 (15.1 kDa) and their 10 to 40 kDa PEG and LPG bioconjugates [166, 268]. Nevertheless, melting temperature, which is regularly used as a predictor of secondary structure stability, was identical for Pegasys and IFN-α2a WT and in the range of previously reported results [98, 313]. The IFNK31N_3 mutant had significantly lower melting temperatures than IFN-α2a WT as had all other bioconjugates except for the LPG 20 kDa bioconjugate which had a melting temperature similar to the IFNK31N_3 mutant (**Figure 2H**). The data set does not allow to assess possible confounding effects of (i) shifting from IFN-α2a (Pegasys) to the IFNK31N_3 mutant (all other bioconjugates reported here), (ii) site directed conjugation or random conjugation (a total of eight lysines is target for random PEGylation in Pegasys; **Figure S12**; [252]), or (iii) polymer choice. However, the differences in melting temperature may be put into perspective with respect to previous studies by others. For example, the thermal stability of IFN-α2b at neutral pH could be improved by 2.6 °C just by changing the protein concentration and by 2.2 °C at increasing the ionic strength of the formulation [313]. To which extent these small differences are pharmaceutically relevant requires further real-time stability studies.

Conclusion

In conclusion, LPGylation is complementing bioconjugation possibilities beyond PEGylation with similar outcome in terms of the stability of the secondary structure (melting temperatures), and potency. Site specific polymer attachment may further increase the quality of the resulting bioconjugates. Differences were observed in terms of the pharmacokinetics, with faster initial distribution being

observed for LPGylated as compared to PEGylated variants. At present the cause of these differences is unclear, but may point to LPG specific targeting mechanisms, possibly distinguishing this polymer from PEG.

Acknowledgements

We acknowledge the help of Dr. Andreas Schlosser, Juliane Adelmann, and Antje Gerlinde Heckmann with mass spectrometry and Nicole Bader with differential scanning fluorimetry assays (University of Würzburg). We further acknowledge Prof. Dr. Edward A. Lemke from the Johannes Gutenberg University of Mainz / EMBL Heidelberg for donating the pEVOL-pylRS vector. We further thank the Core Facility BioSupraMol for NMR measurements, Daniel Kutifa for assistance with polymerization reactions and Cathleen Hudziak for SEC measurements (Freie Universität Berlin). The project was funded within the framework 'Next-PEG' by the Federal Ministry of Education and Research (BMBF) of Germany (# 13XP5049), the "Thüringer Aufbaubank (TAB)", and the "Europäischer Fonds für regionale Entwicklung (EFRE)" (2018FGI0025). G.C. acknowledges support from the Free State of Thuringia and the European Social Fund (2019SD0129).

Supporting Information

Supporting results include results of size exclusion chromatography, NMR of polymers, additional AUC results, full chromatograms of RP-HPLC analysis, SDS-PAGE of 20 and 40 kDa bioconjugate purifications, MALDI-TOF MS results, potency stimulation curves, additional DSF data, results of human plasma stability and FACS analysis of IFN-α2a stimulated murine bone marrow cells.

Author Information

Corresponding author

Prof. Dr. Dr. Lorenz Meinel, Institute of Pharmacy and Food Chemistry, University of Würzburg, Am Hubland, DE-97074 Würzburg, Germany, lorenz.meinel@uni-wuerzburg.de, Tel.: +49 931 3185471

Notes

N. Hauptstein and P. Pouyan have contributed equally to this work.

Declaration of interest

None

Supporting Information to Chapter 3

Experimental

Synthesis of linear polyglycerol (LPG)

The polymers were synthesized based on our recently published protocol [98]. In this work, 40 kDa LPG was purified via tangential flow filtration (TFF) in water using a 30 kDa regenerated cellulose cassette (Millipore) in a cassette holder (Sartorius). The flow was enabled by a peristaltic pump (minipuls 3).

Results

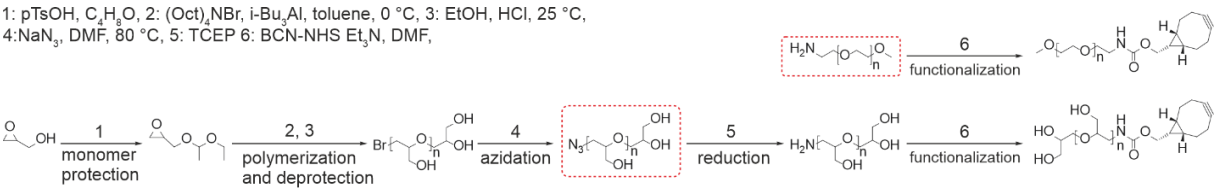

Scheme S1: Schematic representation of the synthesis of BCN functionalized LPG and PEG polymers. The synthesis of functionalized BCN-PEG and BCN-LPG was performed as previously reported [98]. Red circeled intermediates were used for analytical ultracentrifugation, which is displayed in Figure 1 and Figure S4.

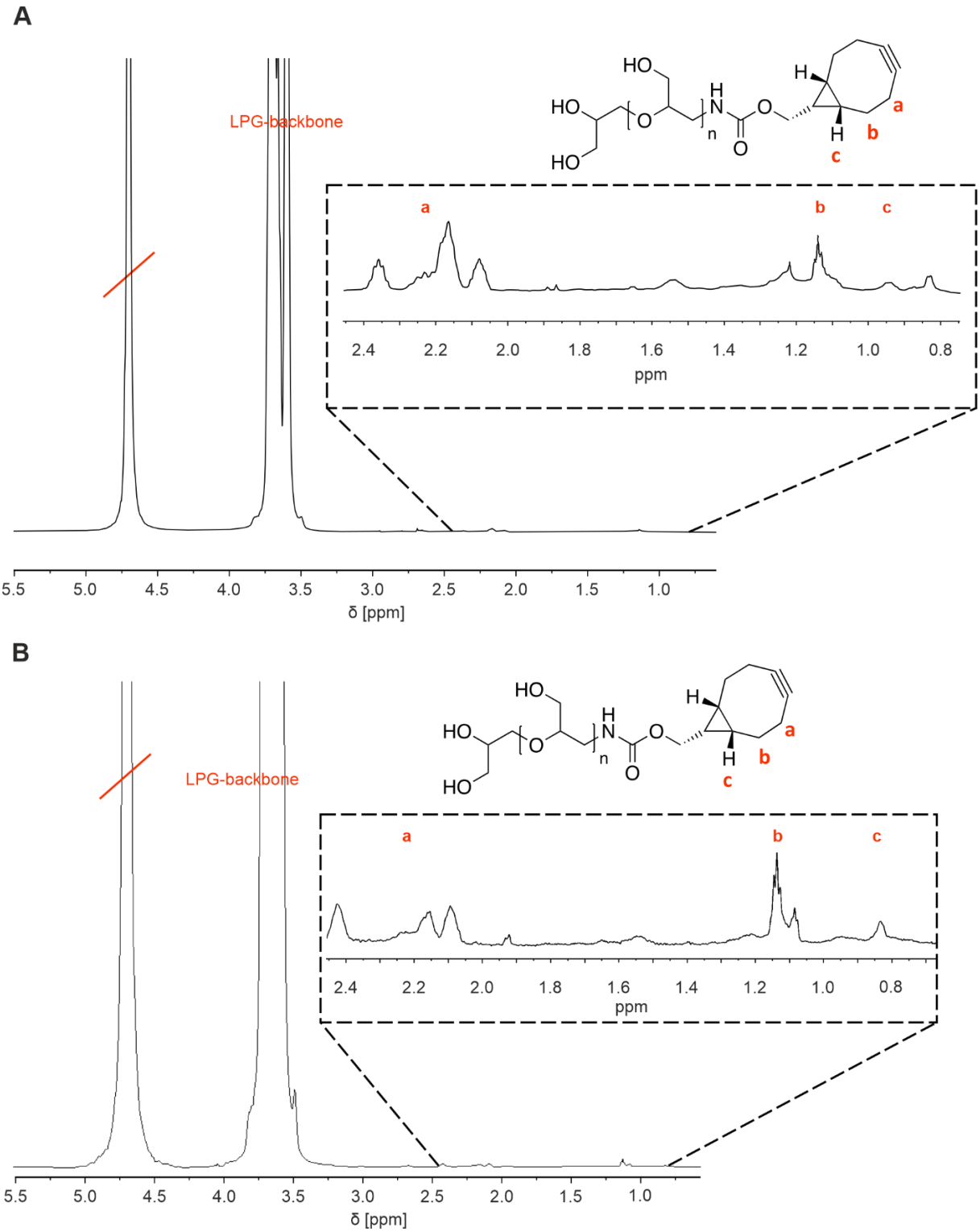

Figure S1: ^{1}H NMR of (A) BCN-LPG 20 kDa and (B) BCN-LPG 40 kDa.

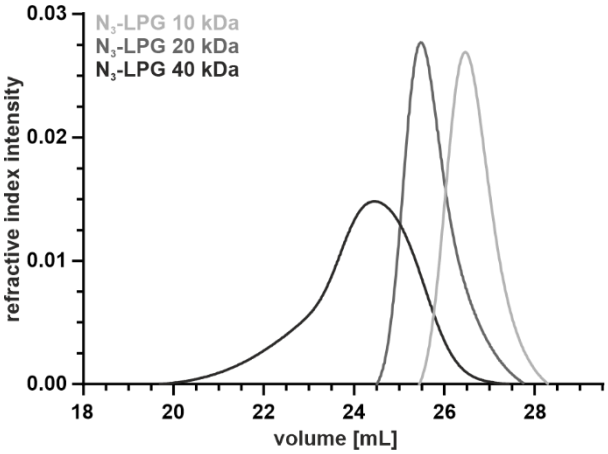

Figure S2: Overlay of SEC chromatograms of used LPGs in H_2O.

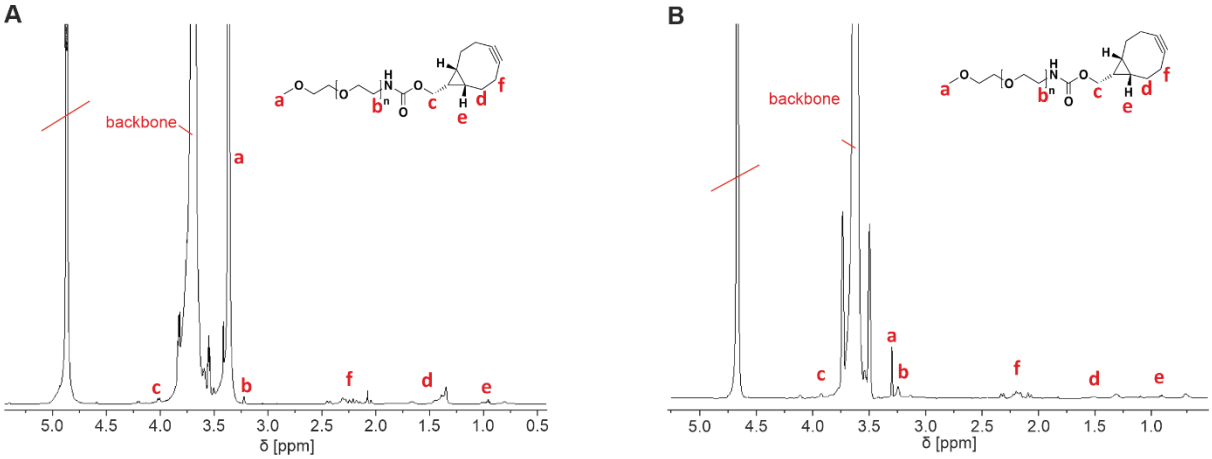

Figure S3: ^{1}H NMR of (A) BCN-PEG 20 kDa and (B) BCN-PEG 40 kDa.

Table S1: Degree of functionalization of used polymers.

Polymer	degree of functionalization (%)
PEG-BCN 10 kDa	30
PEG-BCN 20 kDa	48
PEG-BCN 40 kDa	41
LPG-BCN 10 kDa	15
LPG-BCN 20 kDa	10
LPG-BCN 40 kDa	19

Analytical ultracentrifugation (AUC)

Table S2: Absolute densities, ρ_0, and viscosities, η_0, of the H_2O / PBS buffer mixture used as solvent for the protein or bioconjugates and water used for the polymers, all measured at 20 °C.

Liquid	ρ_0 [g · cm^{-3}]	η_0 [mPa · s]
H_2O / PBS buffer mixture (approx. 46 w% / 54 w%)	1.0050	1.0436
H_2O	0.9982	1.002

Table S3: Hydrodynamic properties determined from sedimentation-diffusion analysis of sedimentation velocity AUC experiments. Signal (weight) average sedimentation coefficients, *s,* and weight-average translational frictional ratios, *f/fsph*, were determined by data from RI detection and / or absorbance detection in terms of OD at λ = 280 nm. Utilized sample concentrations were approx. 0.25 mg mL^{-1} (polymers) or approx. 0.75 mg mL^{-1} (IFNK31N_3 and bioconjugates).

Sample	*s, S*	f/f_{sph}
IFNK31N_3	1.96/1.93*	1.21/1.34*
IFNK31N_3-PEG 10 kDa	1.42/1.42*	1.93/1.92*
IFNK31N_3-LPG 10 kDa	1.88/1.87*	1.77/1.76*
PEG 10 kDa	0.43	1.97
PEG 20 kDa	0.59	2.19
PEG 40 kDa	0.86	3.27
LPG 10 kDa	0.93	1.68
LPG 20 kDa	1.35	1.96
LPG 40 kDa	1.66	2.45

*Based on sedimentation-diffusion analysis of either absorbance detection in terms of OD at λ = 280 nm (protein and conjugates) / RI detection based on interference fringes (polymers).

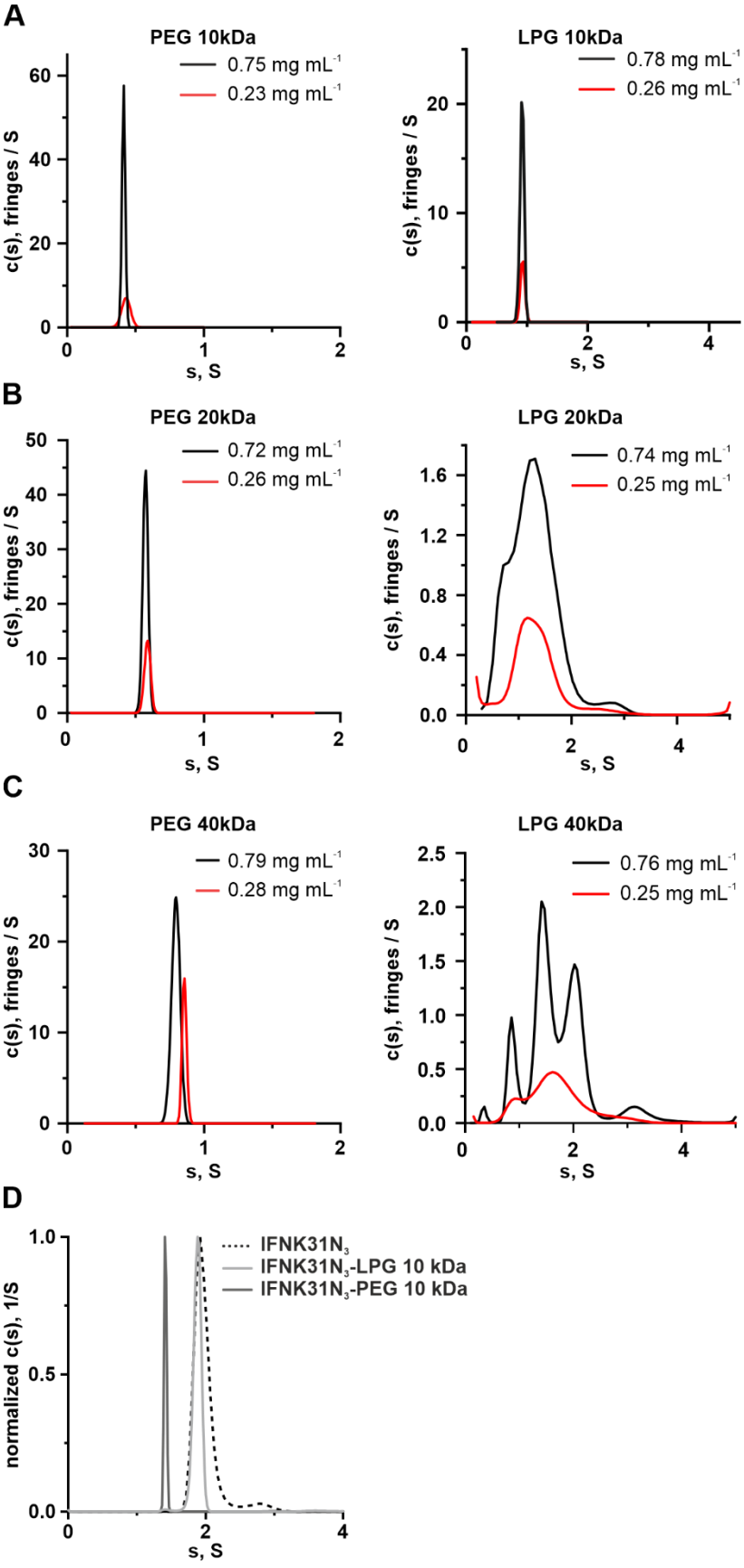

Figure S4: Differential distributions of sedimentation coefficients, c(s), by using the RI detection of (A) 10 kDa polymers, (B) 20 kDa polymers, (C) 40 kDa polymers and (D) normalized for proteins and bioconjugates. The analyzed polymer intermediates, which were used for AUC are depicted in Scheme S1. Distributions obtained from lower concentrations (red lines) are identical to the ones, which are displayed in Figure 1C and D.

Bioconjugate coupling

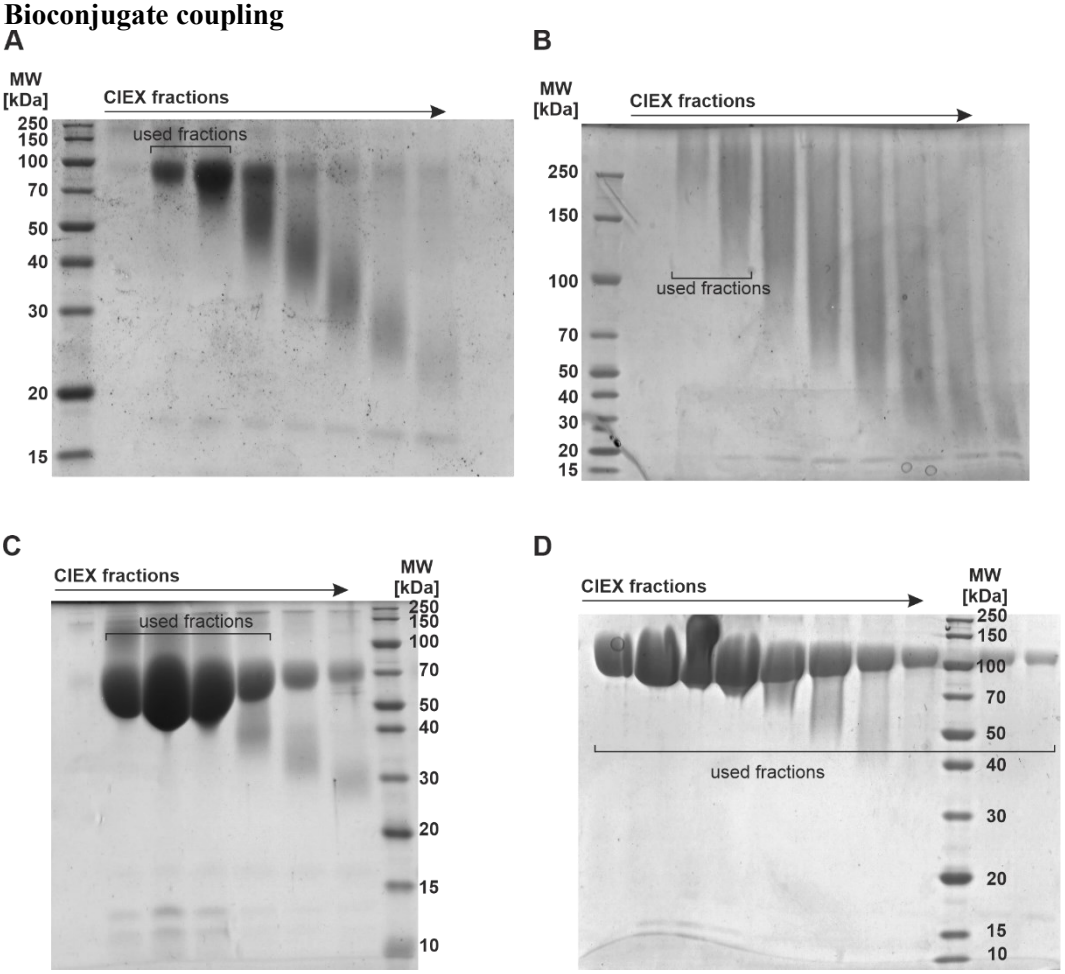

Figure S5: Exemplary SDS-PAGE of fractions from CIEX purification of (A) IFNK31N_3-LPG 20 kDa, (B) IFNK31N_3-LPG 40 kDa, (C) IFNK31N_3-PEG 20 kDa and (D) IFNK31N_3-PEG 40 kDa. Used and pooled fractions for the presented experiments are indicated.

Table S4: Conjugation efficiencies of used polymers displayed in Figure S6 in relation to the used protein educt and the total yield of selected fractions in relation to the used protein educt.

Compound	total product yield [%]	yield of selected fractions [%]
PEG 20 kDa	60	55
PEG 40 kDa	50	50
LPG 20 kDa	49	15
LPG 40 kDa	33	11

Table S5: Important biological and chemical parameters of IFN-α2a and its bioconjugates. Mean values are indicated with standard deviations.

Compound	Hydrodynamic diameter [nm] [a]	T_M[°C]	EC_{50} [pM]
IFN-WT	6.2 ± 0.8 / 4.6	64.5 ± 0.3	1.8 ± 0.2
N_3	n.d.	62.6 ± 0.2	4.2 ± 0.3
Pegasys	15.6 ± 0.4	64.7 ± 0.1	71.4 ± 7.8
PEG 10 kDa*	9.0 ± 0.7 / 7.8	n.d.*	15.3 ± 1.0
PEG 20 kDa	11.7 ± 0.4	60.6 ± 0.1	20.3 ± 1.7
PEG 40 kDa	14.6 ± 0.5	60.8 ± 0.3	36.0 ± 2.6
LPG 10 kDa*	8.0 ± 0.5 / 7.3	n.d.*	13.5 ± 0.8
LPG 20 kDa	12.0 ± 1.0	62.5 ± 0.1	22.9 ± 1.4
LPG 40 kDa	14.4 ± 0.6	60.9 ± 0.2	39.2 ± 2.2

n.d. = not determined, t_1= half-life slow, t_2= half-life fast, [a] analyzed by dynamic light scattering / calculated from AUC by making use of $d_h = 3\sqrt{2}\sqrt{([s]\,\upsilon)}(f/f_{sph})^{3/2}$,[307] with the partial specific volume, υ, for polymers / bioconjugates.* The approximately 10 kDa molar mass bioconjugates were presented in a previous contribution[98], however, the data reported here is either new (hydrodynamic diameter) or was measured again to obtain comparable data among all polymers (EC_{50} [pM]). T_M values were already determined previously and were not remeasured.

MALDI-TOF MS

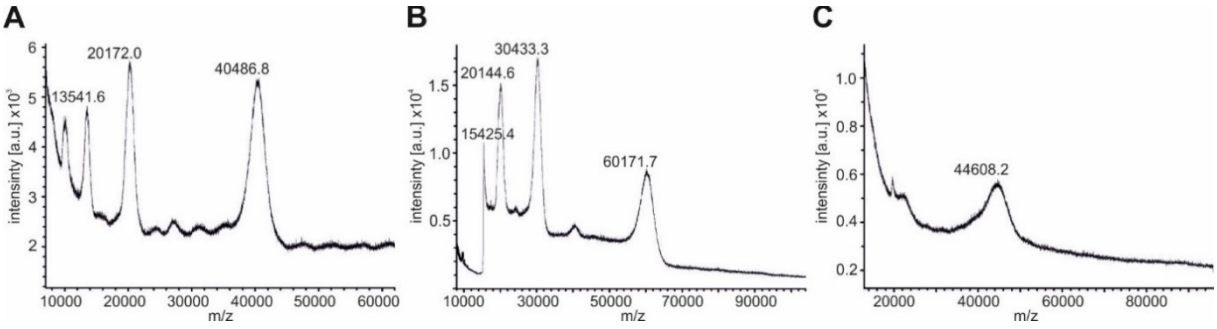

Figure S6: MALDI-TOF mass spectra of (A) IFNK31N_3-PEG-20 kDa (b) IFNK31N_3-PEG-40 kDa (C) IFNK31N_3-LPG-20 kDa. Additionally assigned peaks in A and B are multicharged species of the tested compounds.

RP-HPLC analysis

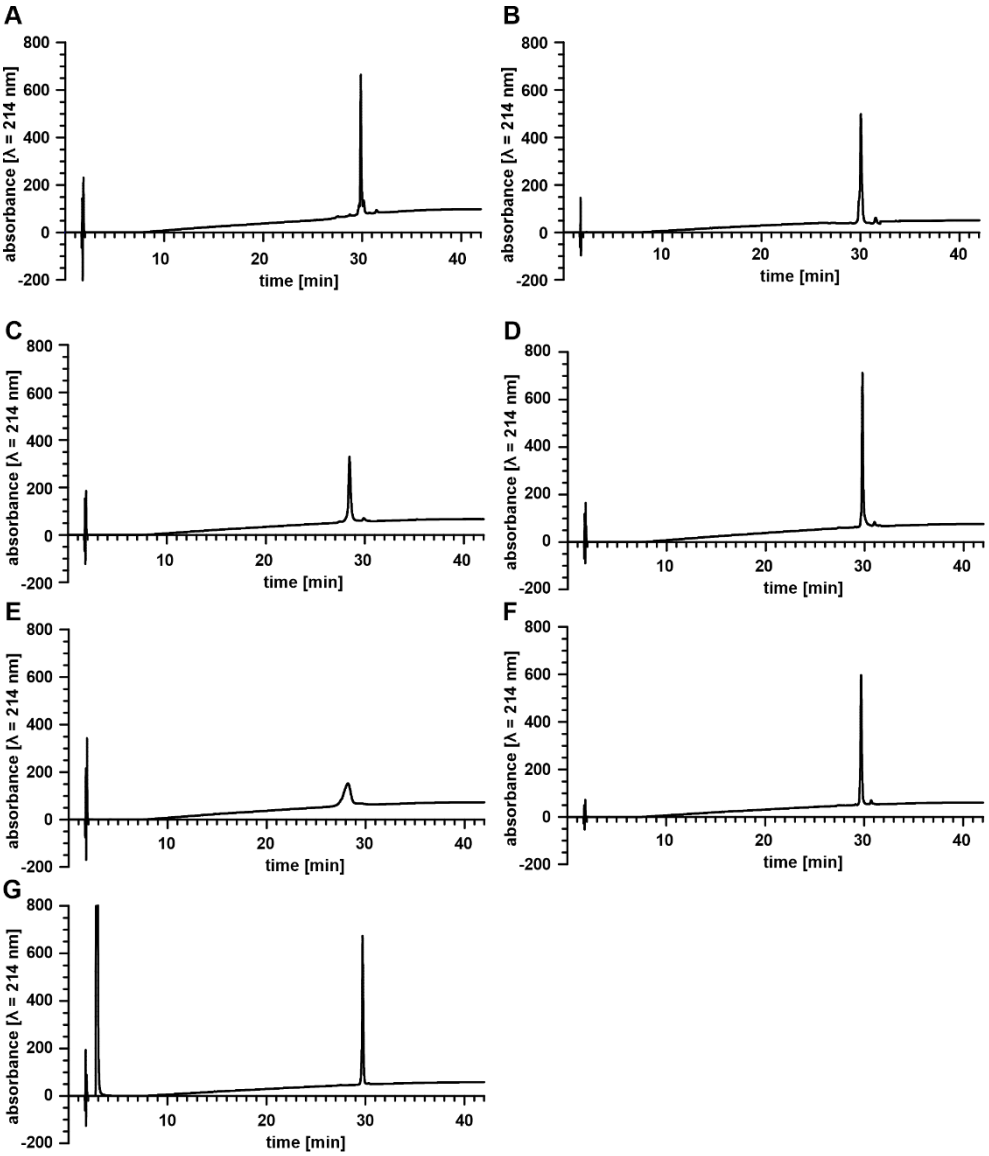

Figure S7: RP-HPLC analysis of (A) IFN-α2a WT, (B) IFNK31N_3, (C) IFNK31N_3-LPG 20 kDa, (D) IFNK31N_3-PEG 20 kDa, (E) IFNK31N_3-LPG 40 kDa, (F) IFNK31N_3-PEG 40 kDa, (G) Pegasys. The displayed graphs are the same measurements that are displayed in Figure 2D-F.

Differential scanning fluorimetry

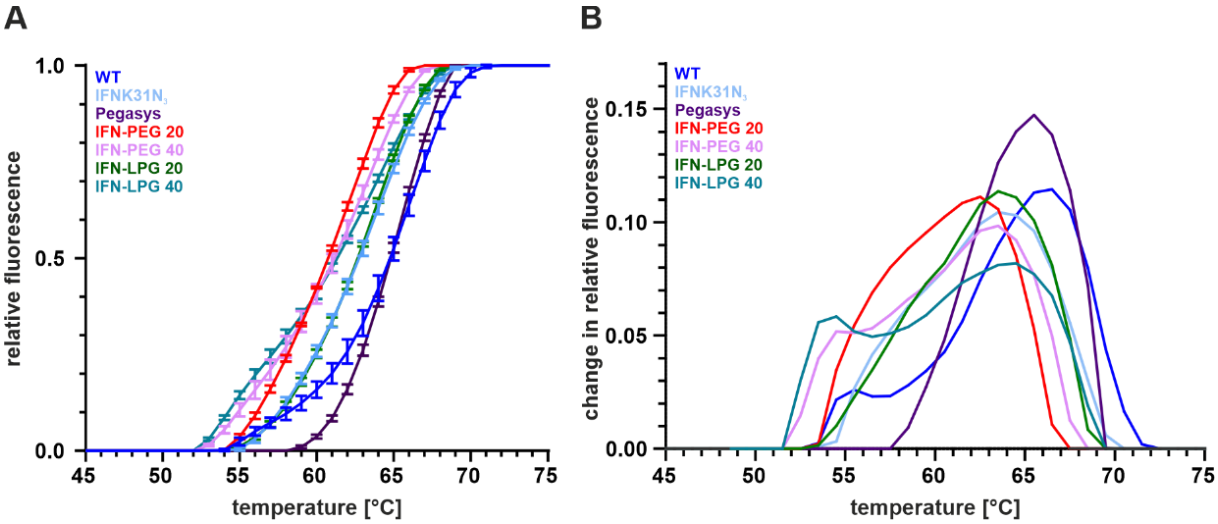

Figure S8: (A) Normalized, averaged fluorescence of the Differential scanning fluorimetry assay with IFN-α2a WT, IFNK31N_3 and its bioconjugates (n = 5). The lowest value of each measurement was set to 0 as well as all values below this temperature. The highest value of each measurement was set to 1 as well as all values above this temperature. The normalized values were averaged, and adjacent points connected. Standard deviations are indicated with error bars. (B) Averaged smoothed first derivate plot of A.

Potency

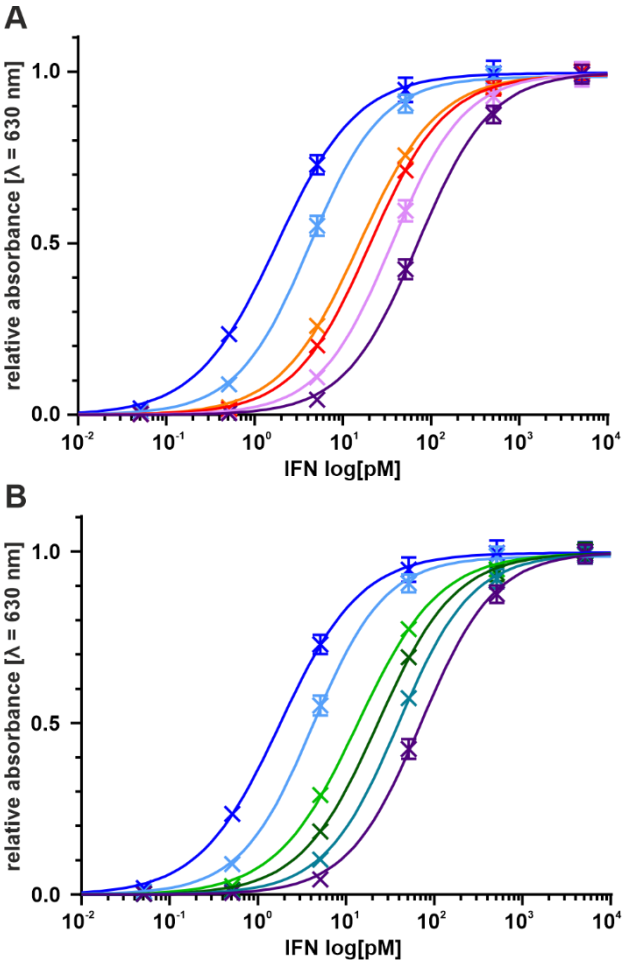

Figure S9: Secreting alkaline phosphatase assay of HEKBlue 293 IFN-α/β cells after 20 h of stimulation with IFN-α2a, IFNK31N_3 and IFN-α2a bioconjugates (mean ± standard deviation, n≥3). Colours of bioconjugates are displayed in A-C as followed: (WT=blue, N_3=light blue, LPG 10 kDa = light green, LPG 20 kDa = dark green, LPG 40 kDa = petrol, PEG 10 kDa = orange, PEG 20 kDa = red, PEG 40 kDa = rose, PEtOx 8 kDa = light grey, PEtOx 20 kDa = grey, PEtOx 35 kDa = dark grey, Pegasys = purple). (A) Stimulation curve of HEKBlue 293 IFN-α/β cells after IFN-α stimulation with PEG bioconjugates. (B) Stimulation curve of HEKBlue 293 IFN-α/β cells after IFN-α stimulation with LPG bioconjugates.

Human plasma stability analysed by ELISA

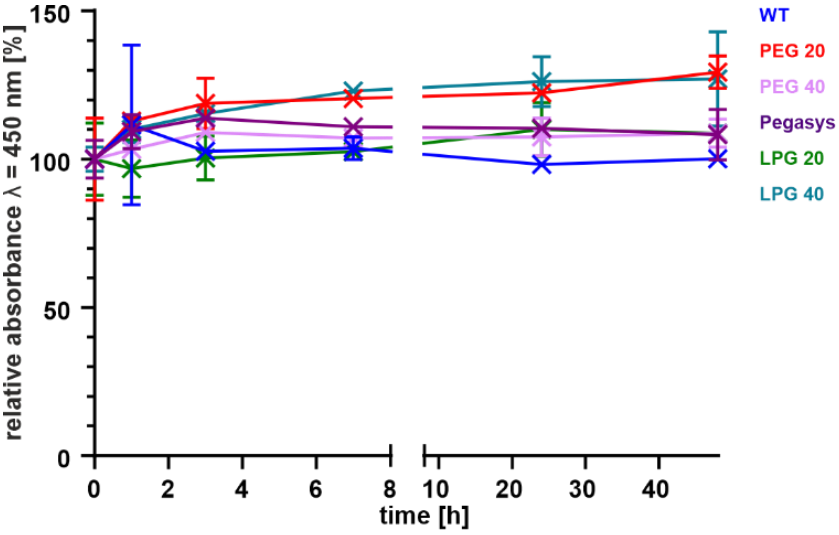

Figure S10: plasma stability of IFN-α2a and bioconjugates, tested over 48 h (mean ± standard deviation, n = 3).

Activation of murine bone marrow cells by IFN-α2a

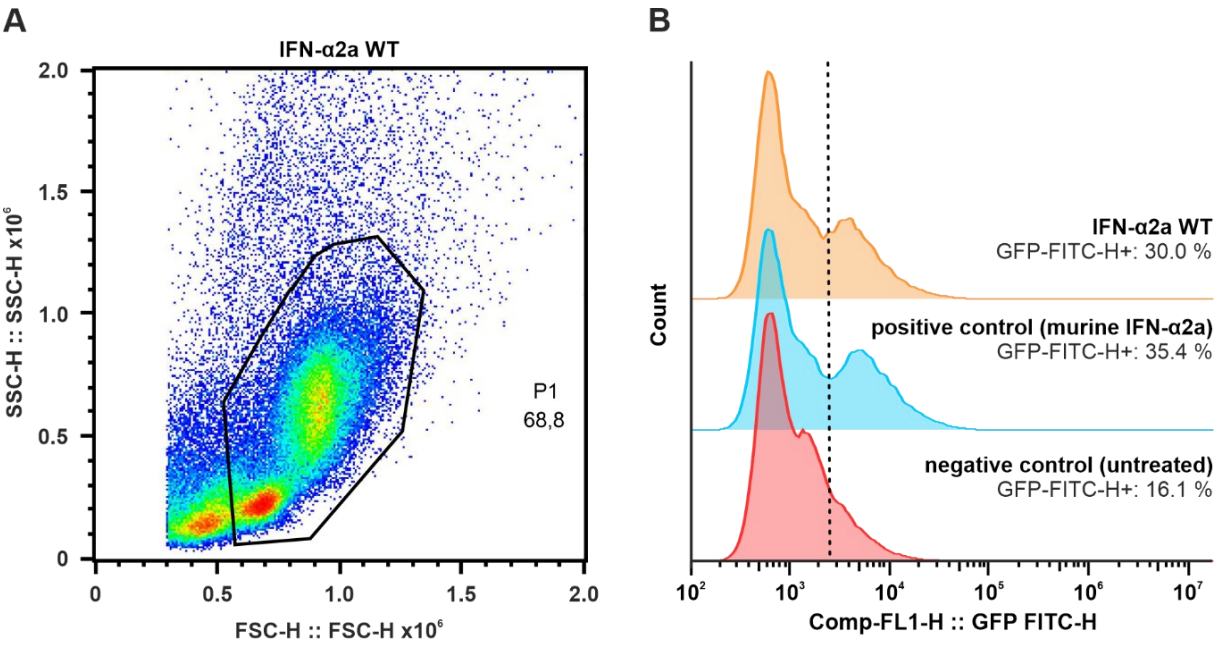

Figure S11: Bone marrow from B6.Tg(ISRE-eGFP) Tovey mice was isolated and *ex vivo* incubated with human IFN-α2a WT, murine IFN-α2a WT or left untreated. After 24 hours incubation time, cells were subjected to flow cytometry to measure GFP expression. (A) Exemplary gating strategy for isolated murine bone marrow cells after *ex vivo* incubation over 24 hours. (B) Determination of GFP^+ cell population under human IFN-α2a WT (orange), or murine IFN-α2a (blue) treatment or for untreated cells (red).

In vivo pharmacokinetic study

Table S6: Calculated *in vivo* apparent volume of distribution during terminal phase (V_Z) and at equilibrium determined after intravenous administration (Vss), area under the curve values till last time point ($AUC_{0\text{-tlast}}$), area under the first moment curve till last time point ($AUMC_{0\text{-tlast}}$) and mean residence time till last time point (MRT_{Last}) of bioconjugates.

Compound	[L · kg^{-1}]	V_{ss} [L · kg^{-1}]	$AUC_{0\text{-tlast}}$ [h · ng/mL]	$AUMC_{0\text{-tlast}}$ [h² · ng/mL]	MRT_{Last} [h]
WT	0.240	0.165	1.331	0.0928	0.070
PEG 20	0.087	0.082	133.50	371.79	2.78
LPG 20	0.127	0.115	68.19	131.61	1.93
PEG 40	0.104	0.092	802.67	13008.9	16.2
LPG 40	0.181	0.150	316.99	3677.13	11.6
Pegasys	0.135	0.116	518.75	7096.80	13.7

PEGylated sites in Pegasys

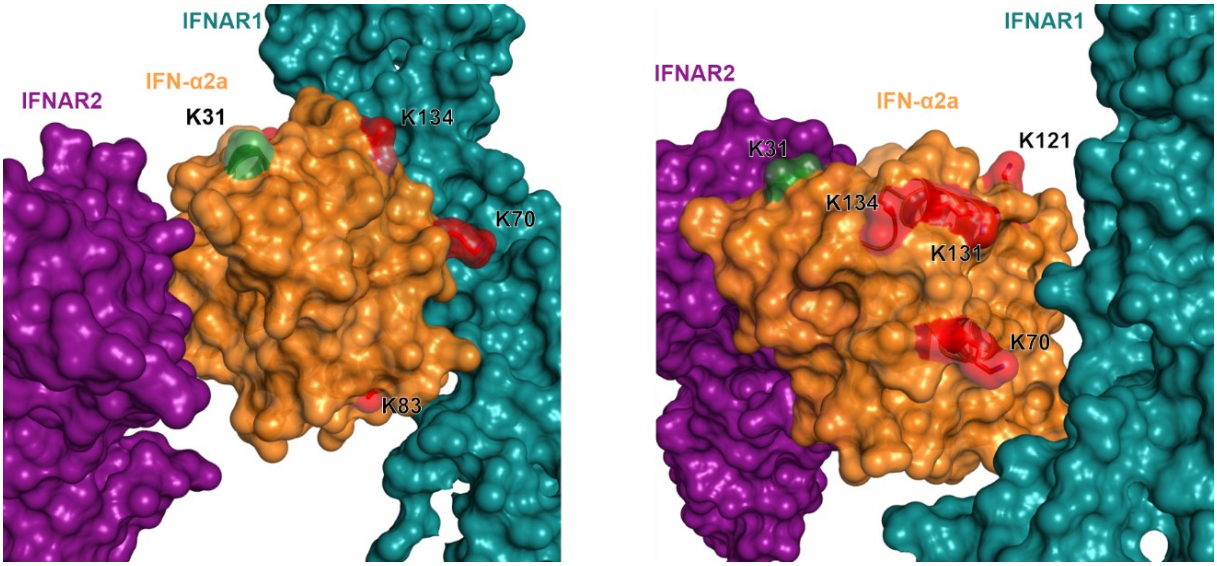

Figure S12: IFN-α2a (orange) in its ternary receptor binding complex with IFNAR1 (petrol) and IFNAR2 (purple) (pdb:3SE3). Receptors were slightly detached from IFN-α2a artificially. Lysine residues, which are PEGylated in Pegasys are highlighted on IFN-α2a´s surface, whereby the chosen mutation site of this study #K31 is marked in green (which is also modified in Pegasys) and other sites are marked in red (#K70, 83, 121, 131, 134) [252, 297]. #K49, 112 and 164, which are also PEGylated in Pegasys are not highlighted, as they are not resolved in this crystal structure.

Chapter 4 – PEtOxylated Interferon-α2a bioconjugates addressing H1N1 influenza A virus infection

Niklas Hauptstein, Michael Dirauf, Kevin Wittwer, Gizem Cinar, Oliver Siering, Martina Raschig, Tessa Lühmann, Oliver Scherf-Clavel, Bevan Sawatsky, Ivo Nischang, Ulrich S. Schubert, Christian K. Pfaller, Lorenz Meinel*

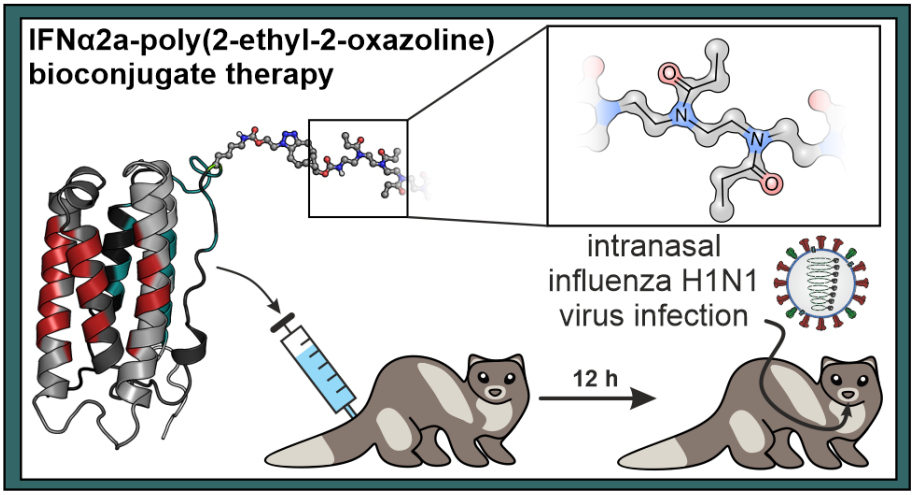

Keywords: Interferon alpha 2a; poly(2-ethyl-2-oxazoline); H1N1; ferret; genetic codon expansion

Reprinted (adapted) with permission from: Hauptstein, N.; Dirauf, M.; Wittwer, K.; Cinar, G.; Siering, O.; Raschig, M.; Lühmann, T.; Scherf-Clavel, O.; Sawatsky, B.; Nischang, I.; Schubert, U. S.; Pfaller, C. K.; Meinel, L., PEtOxylated Interferon-α2a Bioconjugates Addressing H1N1 Influenza A Virus Infection. Biomacromolecules 2022, DOI: 10.1021/acs.biomac.2c00358. Copyright 2022, American Chemical Society.

Abstract

Influenza A viruses (IAV), including the pandemic 2009 (pdm09) H1N1 or avian influenza H5N1 virus, may advance into more pathogenic, potentially antiviral drug-resistant strains (including loss of susceptibility against oseltamivir). Such IAV strains fuel the risk of future global outbreaks, to which this study responds by re-engineering Interferon-α2a (IFN-α2a) bioconjugates into influenza therapeutics. Type-I interferons such as IFN-α2a play an essential role in influenza infection and may prevent serious disease courses. We site-specifically conjugated a genetically engineered IFN-α2a mutant to poly(2-ethyl-2-oxazoline)s (PEtOx) of different molecular weights by strain-promoted azide-alkyne cyclo-addition. The promising pharmacokinetic profile of the 25 kDa PEtOx bioconjugate in mice echoed an efficacy in IAV infected ferrets. One intraperitoneal administration of this bioconjugate, but not the marketed IFN-α2a bioconjugate, changed the disease course similar to oseltamivir, given orally twice every study day. PEtOxylated IFN-α2a bioconjugates may expand our therapeutic arsenal against future influenza pandemics, particularly in light of rising first-line antiviral drug resistance to IAV.

Introduction

Three IFN-α2a (IFN) PEG bioconjugates are marketed in the U.S. today, and none has a marketing authorization for influenza treatment.[17, 52, 252, 254] Prima facie, this counters the central, antiviral role of type-I interferons, including IFN-α2a.[5, 118, 187, 314, 315] IFN-α2a quickly suppresses viral replication by regulating innate and adaptive immune responses and impacts pro-inflammatory (fever, tissue destruction) and anti-inflammatory (promote healing) cytokines in the airway cells.[122, 125, 126, 252, 314] Marketed IFN-α2a bioconjugates were not developed for (acute) IAV infections or to reach the lungs rapidly, the clinically relevant site of IAV replication. Quite contrarily, these were optimized for treating (chronic) viral conditions and long-lasting persistence in the circulation, achieved by conjugating IFN-α2a to high molecular weight, 40 kDa PEGs.[10, 62, 77, 249, 316, 317] These designs delay the onset of IFN signalling after subcutaneous (s.c.) injection.[62, 77] Contrarily, acute virus infections require a fast type-I IFN immune response after infection, as a delayed immune response, initialized by a delayed type-I activation, can result in hyperinflammation.[122]

We hypothesize that effectiveness against influenza viruses is directly linked to the hydrodynamic radii of IFN-α2a bioconjugates. These radii should delay rapid elimination of IFN bioconjugates (e.g., glomerular filtration), while allowing disposition into tissues such as the lungs. Previous studies deciphered the relationship between PEG molecular weight/hydrodynamic diameter and pulmonary exposure following intravenous (i.v.) or s.c. administration. These studies detailed that 10-25 kDa PEGs are a good trade-off between tissue permeability, potency, and serum half-life. [130, 318-321] Such results guided us to design and test IFN-PEtOx bioconjugates with PEtOx polymers ranging between 10 and 25 kDa. An azido functionalized IFN mutant was used for site-specific PEtOxylation to control the decoration site and yield homogenous product outcomes.[98] The plasma concentration profiles of the

bioconjugates were recorded over time in mice. One bioconjugate was selected and tested against marketed IFN-α2a PEG bioconjugates (Pegasys) in ferrets infected with the influenza A virus strain H1N1pdm09, the subtype responsible for the 2009 swine flu pandemic.[322]

Materials and Methods

Materials. potassium phthalimide (99%), hydrazine monohydrate (64-65% N_2H_4, 98%) potassium phthalimide (99%), (1*R*,8*S*,9s)-bicyclo[6.1.0]non-4-yn-9-ylmethyl *N*-succinimidyl carbonate (BCN-NHS), dichloromethane (anhydrous, ≥ 99.8%), tetrafluoroboric acid (48 wt% in H_2O), triethylamine (anhydrous, ≥ 99%) and 3-amino-9-ethylcarbazole were purchased from Sigma Aldrich (Schnelldorf, Germany). MagicMedia™ E. coli Expression Medium, PageRuler™ Prestained Protein Ladder, PageRuler™ Unstained Broad Range Protein Ladder, Gibco-FBS-HI (Origin Brasil), IFN-α Human Instant ELISA™ Kit (BMS216INST) were received from Thermo Fisher Scientific Germany (Darmstadt, Germany). BioPro IEX SmartSep S20 1 mL and 5 mL were obtained from YMC Europe (Dinslaken, Germany). XK16/600 Superdex 75 pg column was received from Cytiva Life Sciences (Freiburg, Germany). Zorbax 300SB-CN column was ordered from Agilent (Waldbronn, Germany).
2-Ethyl-2-oxazoline (EtOx, TCI, 98%) was distilled from BaO (Acros Organics, 90%) under argon atmosphere into a silanized Schlenk flask and stored under argon. 2-Phenyl-2-oxazoline (PhenOx, 99%, Sigma Aldrich) was purified by fractional distillation under reduced pressure. Chlorobenzene was purified in a solvent purification system (SPS, Pure solv EN, innovative technology).

Methods.

Polymer characterization of 15 and 25 kDa BCN-PEtOx.

Synthesis of poly-(2-ethyl-2-oxazoline). Prior to usage, the distillation apertures as well as the glassware used for the CROP were silanized by treatment with chloroform containing 5 vol% trimethylsilyl chloride. Shortly, the glassware was filled with the solution, turned upside down once in order to ensure that the entire surface was in contact with it and left opened for one hour. Subsequent to removal of the mixture, the glassware was rinsed with chloroform, acetone, water and acetone (twice with each solvent), and finally dried by a continuous argon stream.

Synthesis of the 2-phenyl-2-oxazolinum tetrafluoroborate ($HPhenOx^+BF_4^-$) initiator. The compound was synthesized according to the literature.[323] In brief 10 mL PhenOx was used as a starting material, yielding 4.7 g (26%) of $HPhenOx^+BF4^-$ as colorless crystals, which were stored in a Schlenk flask under argon atmosphere. ^{1}H NMR (CD_3CN, 300 MHz): δ [ppm] = 4.25 (t, 2H, =N-CH_2-), 5.15 (t, 2H, -CH_2-O-), 7.59 – 8.08 (m, 5H, CH_{Aromat}).

General procedure for the synthesis of 15 and 25 kDa PEtOx polymers. The synthesis of high molecular weight PEtOx was performed as recently reported with adaptions, [323] whereby reaction steps

were investigated by NMR (**Figure S1 and S2**). Briefly, the appropriate amount of $HPhenOx^+BF4$ was transferred to a Schlenk tube, which was subsequently sealed, evacuated and backfilled with argon thrice. While evacuated, the crystalline initiator $HPhenOx^+BF4^-$ was molten by gentle heating with a heat gun in order to remove residual trapped solvents. EtOx and chlorobenzene (c(EtOx) = 3.2 mol L^{-1}) were added under argon atmosphere and the Schlenk tube was sealed, immersed in an oil bath at a temperature of 40 °C and allowed to stir for pre-determined times, dependent on the intended chain-lengths. The reaction was terminated by addition of potassium phthalimide and subsequently heated to 70 °C overnight. The reaction mixture was cooled to room temperature, diluted with dichloromethane or chloroform and washed with a sat. aq. $NaHCO_3$ solution twice and once with a sat. aq. NaCl solution. The organic layer was dried over Na_2SO_4, filtered, and the volatiles were removed under reduced pressure. The residue was precipitated into cold diethyl ether (–26 °C), collected and dried *in vacuo*.

Phthalimide-PEtOx 15kDa: 3.0 g EtOx (30.26 mmol, 230 eq.), 31 mg $HPhenOx^+BF4^-$ (0.13 mmol, 1 eq.), 6.4 mL chlorobenzene and 85 mg potassium phthalimide (0.46 mmol, 3.5 eq) were used. The polymerization proceeded for 10 days. A sample was removed after 6 d to determine the monomer conversion by ^{1}H NMR.

Conversion (EtOx) = 90%. Yield: 1.77 g (58%). SEC (DMAc, 0.21 wt% LiCl, RI-det., PS-calibration): M_n = 21,200 g mol^{-1}, Đ = 1.27. ^{1}H NMR (CD_2Cl_2, 300 MHz): δ [ppm] = 0.65 – 1.45 (br, CH_3 side chain), 1.96 – 2.81 (br, CH_2 side chain), 2.94 – 3.99 (br, CH_2 backbone), 7.65 – 8.01 (br, $CH_{Phthalimide}$).

Phthalimide-PEtOx 25kDa: 3.0 g EtOx (30.26 mmol, 418 eq.), 17 mg $HPhenOx^+BF4^-$ (0.072 mmol, 1 eq.), 6.4 mL chlorobenzene and 49 mg potassium phthalimide (0.26 mmol, 3.6 eq) were used. The polymerization proceeded for 20 days.

Conversion (EtOx) = 89%. Yield: 2.38 g (78%). SEC (DMAc, 0.21 wt% LiCl, RI-det., PS-calibration): M_n = 29,100 g mol^{-1}, Đ = 1.39. ^{1}H NMR (CD_2Cl_2, 300 MHz): δ [ppm] = 0.77 – 1.40 (br, CH_3 side chain), 1.98 – 2.66 (br, CH_2 side chain), 3.07 – 3.91 (br, CH_2 backbone), 7.68 – 7.97 (br, $CH_{Phthalimide}$).

Post-polymerization modifications. PEtOx-NH_2 and PEtOx-BCN were synthesized according to our previously published procedure.[98]

NH_2-PEtOx 15kDa: 1.52 g Phthalimide-PEtOx 15kDa (1 eq.) and 45 µL hydrazine monohydrate (12.5 eq.) were used. Yield: 1.22 g (80%). SEC (DMAc, 0.21 wt% LiCl, RI-det., PS-calibration): M_n = 21,800 g mol^{-1}, Đ = 1.25. ^{1}H NMR (CD_2Cl_2, 300 MHz): δ [ppm] = 0.69 – 1.44 (br, CH_3 side chain), 1.99 – 2.74 (br, CH_2 side chain), 3.01 – 4.02 (br, CH_2 backbone).

NH_2-PEtOx 25kDa: 2.01 g Phthalimide-PEtOx 25kDa (1 eq.) and 40 µL hydrazine monohydrate (15 eq.) were used. Yield: 1.60 g (80%). SEC (DMAc, 0.21 wt% LiCl, RI-det., PS-calibration): M_n = 30,300 g mol^{-1}, Đ = 1.32. ^{1}H NMR (CD_2Cl_2, 300 MHz): δ [ppm] = 0.79 – 1.38 (br, CH_3 side chain), 2.01 – 2.68 (br, CH_2 side chain), 2.98 – 4.20 (br, CH_2 backbone).

BCN-PEtOx 15kDa: 0.99 g NH_2-PEtOx 15kDa (1 eq.) and 16.7 mg BCN-NHS (1.5 eq.) were used. Yield: 0.90 g (90%, minor amounts of residual diethyl ether were evident from the NMR spectrum). SEC (DMAc, 0.21 wt% LiCl, RI-det., PS-calibration): M_n = 21,300 g mol^{-1}, Đ = 1.26. ^{1}H NMR (CD_2Cl_2, 300 MHz): δ [ppm] = 0.83 – 1.37 (br, CH_3 side chain), 2.10 – 2.56 (br, CH_2 side chain), 3.06 – 3.97 (br, CH_2 backbone).

BCN-PEtOx 25kDa: 0.99 g NH_2-PEtOx 25kDa (1 eq.) and 9.1 mg BCN-NHS (1.15 eq.) were used. Yield: 0.85 g (85%, minor amounts of residual diethyl ether were evident from the NMR spectrum). SEC (DMAc, 0.21 wt% LiCl, RI-det., PS-calibration): M_n = 30,600 g mol^{-1}, Đ = 1.34. ^{1}H NMR (CD_2Cl_2, 300 MHz): δ [ppm] = 0.82 – 1.42 (br, CH_3 side chain), 2.13 – 2.58 (br, CH_2 side chain), 3.06 – 3.84 (br, CH_2 backbone).

Analytical ultracentrifugation. Analytical ultracentrifugation (AUC) was performed as described previously.[324] A stock solution of all three polymers was prepared and diluted with water to obtain concentrations of approximately 0.25 mg mL^{-1} and 0.75 mg mL^{-1}, respectively. Sedimentation velocity experiments were performed with an Optima Analytical Ultracentrifuge (Beckman Coulter Instruments, Brea, CA) by utilizing double-sector Epon centerpieces with a 12 mm solution optical path length. The cells were filled with 420 µL sample solution in water and with 440 µL water as the reference and placed in an An-50 Ti eight-hole rotor. Sedimentation velocity data were recorded using the interference optical detection module (refractive index (RI)). All measurements were performed at 20 °C and at a rotor speed of 42 000 rpm for at least 24 hours. A three-minute time interval between scans was used. Analysis of a suitable selection of scans was used for data evaluation with Sedfit [57]. Viscosity and density of the water are known literature values (η_0 = 1.002 mPas, ρ_0 = 0.9982 g cm^{-3}). Sedimentation velocity experiments were analyzed by numerical solution of the Lamm equation, c(s), with literature known values of the partial specific volume (υ = 0.84 cm^3 g^{-1} for PEtOx).[178] This analysis results in differential distributions of sedimentations coefficients and weight average translational frictional ratios f/f_{sph}. Here, f is the translational friction coefficient of the investigated macromolecules and f_{sph} the translational friction coefficient of a spherical particle with the same anhydrous volume and mass.[294] Numerical estimates of signal (weight) average values of s from differential distributions of sedimentations coefficients and the f/f_{sph} values from sedimentation-diffusion analysis are summarized in **Table S1**. The intrinsic sedimentation coefficients, $[s]$, were calculated by $[s] = s\eta_0/(1- \upsilon\rho_0)$ with the solvent viscosity, η_0, and solvent density, ρ_0. Molecular weights by AUC (**Table 1**) were calculated from the lowest investigated polymer concentration being closest to solution ideality by utilizing the modified Svedberg equation: $M_{s,f} = 9\pi\sqrt{2}N_A([s](f/f_{sph}))^{3/2}\sqrt{\upsilon}$ with N_A being the Avogadro constant.[178, 294]

Size exclusion chromatography coupled to multi-angle laser light scattering (SEC-MALLS). SEC-MALLS was performed as described recently.[178] In brief, we utilized a mobile phase of 0.1 M NaCl + 0.3% trifluoroacetic acid (TFA) with a PSS, NOVEMA MAX column (10 µm particle size, 30 nm pore size, dimensions: 300 mm length × 8 mm i.d.). The oven temperature was set to T = 25°C, and 50 µL of

a 2 mg mL^{-1} concentrated polymer solution was injected. The isocratic flow of 1 mL min^{-1} was controlled with the tip pump of an asymmetrical flow field-flow fractionation system from Postnova Analytics GmbH (Landsberg, Germany). The elutions were detailed *via* the RI as a concentration-sensitive detector and MALLS detector as a mass-sensitive detector. Values for the refractive index increment in the run solvent were taken from reference 178, as dn/dc = 0.1614 mL g^{-1}. Molecular weight data are reported at recoveries of approximately 90 %.

Expression and purification of IFN-α2a WT and mutant. Expression of IFN-α2a WT and IFNK31N_3 was performed as described before.[98] Protein expression was performed in *E. Coli* (BL21) DE3 star bacteria after induction with IPTG and L(+)-arabinose, to express the mutant protein and the additional $tRNA^{pyl}$/aaRS pair. The used pEVOL-pylRS vector was kindly donated by Prof. Dr. Edward A. Lemke from the Johannes Gutenberg University of Mainz/EMBL Heidelberg.[195, 196] For protein expression, *E. Coli* (BL21) DE3 star bacteria were cotransformed with an IFN-α2a or mutant gene containing pET21a plasmid, and in case of the azide mutant the pEVOL-pylRS plasmid containing the $tRNA^{pyl}$/aaRS pair. A four-step procedure was used for expression of the mutant protein. At first, a glycerol stock of the transformed bacteria was plated on an antibiotic containing agar plate at 37 °C overnight. Secondly, one colony was picked and inoculated overnight at 37 °C in antibiotic containing LB medium. Thirdly, on the next day the overnight culture was transferred into TB-medium (always with needed antibiotics) having a starting OD_{600} of 0.08-0.1. The culture was grown to an OD_{600} of 0.7 at 37 °C and 120 rpm (2 in. rotation radius). At last, IFN-α2a WT cultures were induced at this point with 1 mM IPTG and were incubated for 8 h under the same conditions as before being harvested. Mutants were collected and centrifuged at 3000 × g, 20 °C, 20 min and the supernatant discarded afterwards. The bacteria pellet were resuspended in 1:10 (v/v) of Magic Media™, supplemented with 20 mM of the unnatural amino acid N^6-((2-azidoethoxy)carbonyl)-L-lysine, 0.4% L-(+)-arabinose and 0.2 mM IPTG (pH adjusted with NaOH to 7.4 after supplementation), resulting in a 10-fold condensed culture having an $OD_{600} \approx 4$ to 5. The culture was incubated for 12 to 16 h at 37 °C, 120 rpm and harvested afterwards by centrifugation, 5000 × g, 4 °C. 20 min.

Cell lysis, inclusion body isolation and refolding. Inclusion bodies were isolated and refolded after expression as described previously.[98] Cell lysis was performed with a high-pressure homogenizer (Emulsiflex C5, Avestin Europe GmbH, Mannheim, Germany) in 3 cycles at 15000 to 20000 psi, whereby 1 mM PMSF, 25 µg/mL lysozyme and 10 µg/mL DNase I were added after the first lysis and left on ice for 1 h. Cells were resuspended for lysis in 50 mM Tris pH 8.0 + 200 mM NaCl (lysis buffer). Lysed cells were ultracentrifuged at 100000 × g, 30 min, 4 °C. Pellet washing was performed once with lysis buffer containing 1% Triton X-100 and once with lysis buffer containing 1% Triton X-100 and 1 M urea. Unfolding of the harvested pellet was done with lysis buffer containing 7 M guanidinium hydrochloride. Refolding was performed by dropwise addition to ice cold refolding buffer (lysis buffer + 1 M 3-(1-Pyridinio)-1-propanesulfonate and 2 mM β-mercaptoethanol)[197] to a final protein

concentration of 150 µg/mL and left under slight constant stirring overnight at 4 °C. Precipitated protein was removed by centrifugation at 4 °C at the next day.

Purification of IFN. Excipients were removed before ion exchange chromatography by dialysis (8 kDa MWCO) against 10 volumes of 20 mM Tris-HCl pH 8.0 at 4 °C for 3 h, which was repeated thrice, as previously described.[98] After centrifugation and sterile filtration, the dialysed IFN was catched and eluted on an FPLC system (Äkta Pure, Cytiva, Freiburg, Germany) using 2x BioPro IEX SmartSEP 5 mL columns and a single step elution at 15% B over 5 column volumes (Buffer A: 20 mM Tris-HCl pH 8.0, Buffer B: 20 mM Tris-HCl pH 8.0 + 2 M NaCl). Sample loading was performed at 4 °C to avoid precipitation. IFN containing fractions were pooled and dialysed against a 100-fold excess of 25 mM NaOAc pH 4.5 overnight. At the next day, cation exchange chromatography was performed using a BioPro IEX SmartSep S20 1 mL column. A linear gradient from 0% to 50% in 25 column volumes was used (Buffer A: 25 mM NaOAc pH 4.5, B: 25 mM NaOAc pH 4.5 + 2 M NaCl). IFN containing fractions were pooled and the concentration adjusted to 5 mg/mL. At last size exclusion chromatography was performed using a XK16/600 Superdex 75 pg column and an isocratic elution over 1.5 column volumes with 25 mM NaH_2PO_4 pH 7.4 + 150 mM NaCl as eluent, whereby 5 mg of protein were injected in each run. For IFNK31N_3, a final yield of 20-30 mg per liter condensed culture was achieved. For IFN-WT a yield of 5-8 mg per liter TB medium culture was achieved.

Strain promoted azide-alkyne Huisgen cyclo-addition. Strain promoted azide-alkyne Huisgen cyclo-addition (SPAAC) was performed as described previously.[98] In brief, the mutant, having a final concentration of about 500 µg/mL, was mixed with a 20-fold molar excess of BCN-PEtOx polymer in 25 mM sodium phosphate buffer pH 7.4 + 150 mM NaCl and incubated for at least 48 hours under gentle stirring at 4 °C. The solution was then dialyzed (8 kDa MWCO) against a 100-fold excess of 25 mM NaOAc pH 4.5 overnight at 4 °C. Excess polymer was then removed by cation exchange chromatography using the same procedure as described above, whereby PEtOx does not bind to the matrix and IFN-PEtOx bioconjugates elute earlier than unreacted IFNK31N_3, due to a reduced matrix affinity.

Reversed-phase high performance liquid chromatography analysis. Reversed-phase high performance liquid chromatography (RP-HPLC) analysis was performed as described previously.[98] In brief, an Agilent Zorbax 300SB-CN (4.6 x 150 mm, 5 µm particle) column was used**.** For separation, a linear gradient of 5 to 70% eluent B (%, v/v) within 35 min at a constant flow of 1 mL/min was used**.** Eluent A = Water + 0.1% TFA and eluent B = CH_3CN + 0.1% TFA, λ = 214 nm.

Dynamic light scattering. Dynamic light scattering (DLS) was performed as described previously with adaptions.[268] DLS was performed on a Malvern Zetasizer ZS (Malvern Panalytical, Herrenberg, Germany). Measurements were performed at 25 °C in 100 mM phosphate buffer pH 7.2 + 150 mM NaCl (c[Protein] = 0.4 mg/mL) after sterile filtration. Three measurements were performed of each sample,

whereby three acquisitions were averaged per measurement. Results are reported as intensity value as shown in the Zetasizer software (version 7.13).

Differential scanning fluorimetry. Differential scanning fluorimetry (DSF) was performed as described previously[98] using a final concentration of 8 µM of protein equivalents and a final 5-fold SYPRO Orange concentration. Samples were heated in 1 °C/min increments using a temperature gradient from 25 to 95 °C. Gathered data were normalized as described previously without smoothing.[199]

HEK Blue IFNα/β cell culture assay. The cell culture assay was performed in HEK-Blue™ IFN-α/β cells according to the manufacturer's instructions. The absorbance was measured after 120 min of incubation at 37 °C. The potency of the WT, mutant, and 8 kDa PEtOx bioconjugate was reported previously.[98] It was measured again on the same plates together with the other molecular weight bioconjugates to increase comparability.

***In vivo* pharmacokinetic study in mice**. Animal experiments were carried out as previously described,[324] in compliance with the regulations of the German animal protection laws and authorized by the responsible state authority (Regierungspräsidium Darmstadt, Dezernat V54 - Veterinärwesen und Verbraucherschutz). Male and female transgenic C57BL/6 B6.Tg(ISRE-eGFP)Tovey mice [298] between 8 and 18 weeks of age were divided into groups of 15 animals for each bioconjugate (mean group age 10 to 13 weeks). Mice were weighed, bioconjugates were diluted with sterile PBS and 3 µg/kg bodyweight of IFN-α2a-WT equivalents (therefore the protein amount was always the same) of the respective dilution were administered intravenously in the tail vein. The 15 mice were separated into 3 groups of 5 animals, whereby each group donated blood at two time points (**Table S4**). On the first time point, mice donated 100 µL of blood after anesthetization with isoflurane by the retro-orbital vein plexus. At the second time point, Ketamine/Xylazine (100 mg/10 mg per kg body weight) was injected intraperitoneally, and mice were exsanguinated *via* cardiac heart puncture. Serum was obtained by blood centrifugation at 14.000 × g at 4 °C for 10 min, snap-frozen in liquid nitrogen and stored at -80 °C until further analysis. After thawing on ice, the collected serum samples were diluted appropriately and analyzed by ELISA (see below for details) according to the manufacturer's instructions. The primary data set was fitted using non-linear least-squares fits using RStudio (version 4.0.5).[299]

Plasma stability of Interferon-α2a and bioconjugates. Plasma stability was analyzed by spiking of protein and bioconjugate samples into human plasma at a concentration of 3 ng/mL as previously described.[324] the spiked plasma samples were then incubated at 37 °C at 300 rpm over 48 h, whereby samples were taken at indicated time points and snap-frozen in liquid nitrogen. Collected samples were then analyzed by ELISA. The averaged concentration of each tested sample at 0h was used as a relative 100 % reference.

Enzyme-linked immunosorbent assay. Serum samples from the *in vivo* P.K. study and plasma samples from the stability study were analyzed according to the manufacturer's instructions and as described before.[324]. Plasma samples were diluted 1:1 with dilution buffer before analysis. Samples from the *in*

vivo mouse study were diluted 5 to 20-fold depending on the expected sample concentration. For calibration, a calibration curve of the pure bioconjugate was used to account for polymer specific decreased IFN binding of the ELISA-Kit, using the same concentrations as the ones provided by the manufacturer.

Ferret studies. To test the efficacy of the bioconjugates against IAV infection, a previously established protocol was adapted.[325] Groups of 4 male or female ferrets (*Mustela putorius furo*) aged 16 weeks or older were injected intraperitoneally (i.p.) with one of the respective interferon conjugates (3 µg/kg body weight), and one group was treated with i.p. injection of PBS as a negative control. One group of 4 ferrets was treated every 12 hours throughout the study with oral oseltamivir suspension (3 mg/kg body weight in water; "Tamiflu", Roche) as a positive control, prepared according to the package instructions. Twelve hours after bioconjugate treatment, the animals were infected intranasally with 2×10^5 $TCID_{50}$ of influenza A virus H1N1 A/INDRE/Mexico/4487/2009 (MX10).[326] Nasal washes were performed once daily, and a clinical examination was performed twice daily for 3 days after infection. Nasal washes were kept on ice and centrifuged for 15 mins at 3,000 rpm at 4 °C to pellet debris. Nasal wash supernatants were transferred to fresh Eppendorf tubes on ice, titrated by 10-fold dilution in 96-well plates, and then incubated for 48 hours at 37°C. The medium was then removed from the plates, and influenza-infected cell monolayers were washed once with PBS diluted one-third in water and air-dried at room temperature for 15 min. The plates were heat-fixed at 65°C for 8 hours. Influenza-infected cells were stained with a polyclonal ferret anti-H1N1pdm09 immune serum[327] at a dilution of 1:500 and a goat anti-ferret horseradish peroxidase (HRP)–conjugated secondary antibody (A140-108P, Bethyl Laboratories) at a dilution of 1:750. Infected cells were visualized by the development of a red precipitate after incubation with 3-amino-9-ethylcarbazole at room temperature. Viral titers were expressed as tissue-culture infectious dose 50 ($TCID_{50}$).

Determination of clinical score of disease severity after influenza virus challenge. Clinical signs were scored using a 0-1-2-3 scale (**Table S8**), with 0 representing the baseline physiological state. The scores were added together for each animal at each observation time point to give the clinical score.

Titration of virus in ferret tissues. On day 3 after infection, infected ferrets were anesthetized by injection of ketamine and medetomidine, exsanguinated, and the nasal turbinates, lung, and trachea were harvested. Tissue samples were weighed and homogenized in a total volume of 500 µL serum-free DMEM containing penicillin/streptomycin and were then titrated by $TCID_{50}$ assay and stained as described above. Briefly, samples were homogenized for two cycles of 5500 rpm for 20 seconds and were incubated on ice between cycles. Homogenized tissues were briefly centrifuged to pellet debris and the supernatants were transferred to fresh tubes for titration.

Results and Discussion

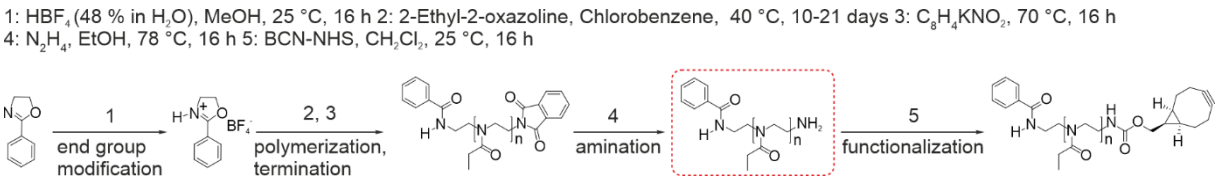

Scheme 1: Synthesis of BCN functionalized 15 and 25 kDa PEtOx polymers. Red circled intermediates were used for AUC (Figure 1) and SEC-MALLS (Figure S3).

PEtOx was polymerized *via* cationic ring-opening polymerization (CROP) of 2-ethyl-2-oxazoline with 2-phenyl-2-oxazolinum tetrafluoroborate as an initiator (**Scheme 1**).[328] The polymerization was quenched by addition of potassium phthalimide, which was deprotected by hydrolysis, yielding PEtOx-NH_2. Subsequently, the ω-amino PEtOx was modified with a BCN-NHS ester. Synthesis of 8 kDa PEtOx was performed as reported previously.[98] A change in polymerization synthesis was necessary as the previously described synthesis, using non-modified end group,[98] led to less defined, longer polymers, which we noticed later during conjugation (*vide infra*). We were unable to identify the reason and mechanism of the occurring side reaction in the initial polymers. The adaption of the initiator and reduction of the reaction temperature, as previously described by Hoogenboom and coworkers,[323] led to distinct, higher molecular weights, terminally end-functionalized PEtOx polymers with acceptable dispersities. The polymers were characterized by ^{1}H NMR spectroscopy (**Figure S1 and S2**), AUC (**Figure 1, Table 1 and Table S1**), standard calibrated SEC respectively (**Figure S1, S2 and Table 1**) and SEC-MALLS (**Figure S3 and Table 1**).

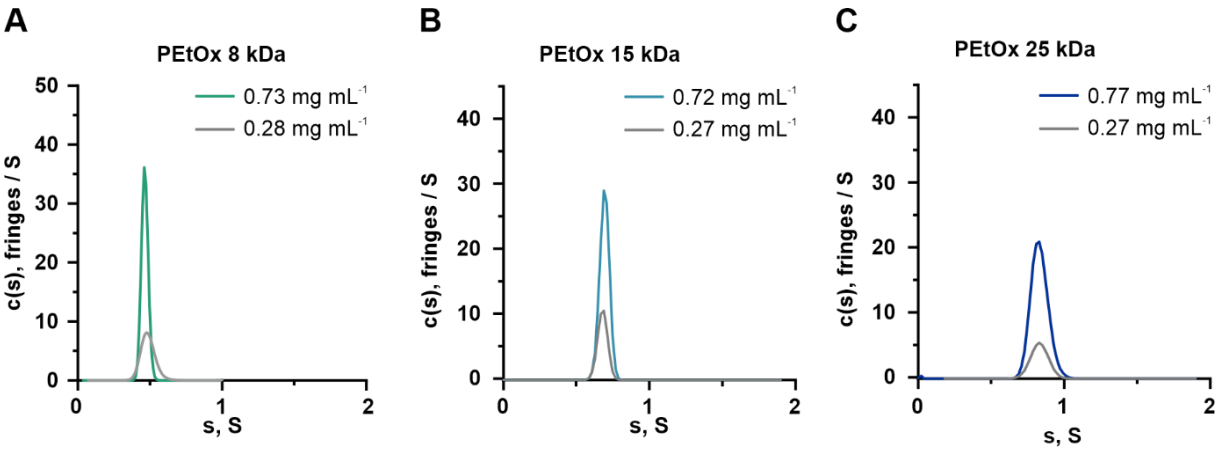

Figure 1: Differential distributions of sedimentation coefficients, c(s), by using the RI detection of (A) 8 kDa PEtOx, (B) 15 kDa PEtOx, and (C) 25 kDa PEtOx. The analyzed intermediates, which were used for AUC, are depicted in scheme 1.

Table 1: Molecular weights by standard calibrated SEC, AUC, and SEC-MALLS of the used PEtOx polymers. For AUC and SEC-MALLS the amino intermediate was used (Scheme 1). For standard calibrated SEC the table displays the results of the final BCN-PEtOx polymer though all intermediates were tested (Figure S1 and S2).

Sample	SEC (kDa; Đ)	AUC (kDa)	SEC-MALLS (kDa)
PEtOx 8*	8.2; 1.10	5.7	-
PEtOx 15	20.6; 1.26	14.6	17.9
PEtOx 25	36.7; 1.34	24.3	25.4

*The exact molecular weight of PEtOx 8 was already determined in a previous study by MALDI-TOF to be 8.4 kDa, using the same polymer batch.[98]

AUC of polymers in water was performed using the amino intermediate (**Scheme 1**). Signal (weight) average sedimentation coefficients, *s*, for the lowest polymer solution concentration increased from *s* = 0.49 S for PEtOx 8 kDa, over *s* = 0.68 S for PEtOx 15 kDa to *s* = 0.83 S for PEtOx 25 kDa (**Figure 1 and Table S1**). Standard calibrated SEC resulted in higher apparent molecular weights as AUC and SEC-MALLS (**Table 1**), as also observed in a previous study.[178]

Conjugation of polymers to IFNK31N$_3$

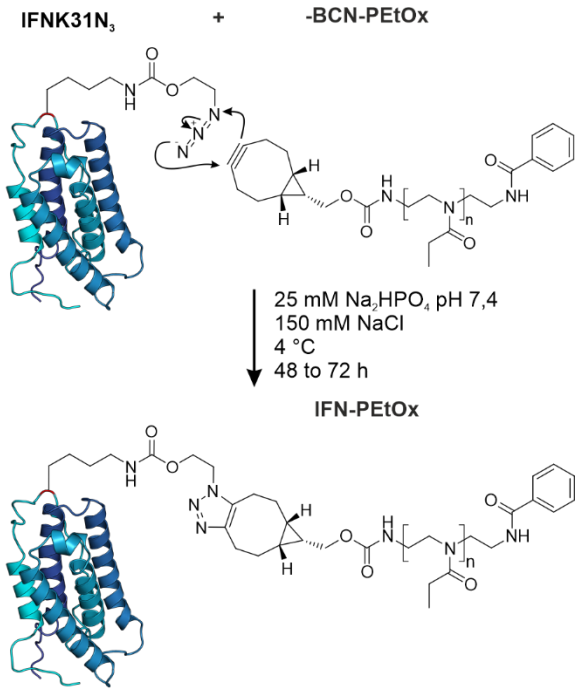

Scheme 2: Polymer conjugation of BCN-PEtOx to IFNK31N$_3$.

The expression, purification, and functionalization of the IFN-α2a mutant IFNK31N$_3$ with BCN-PEtOx carrying an azide functionalized IFN-α2a was reported before (**Scheme 2**).[92, 93, 97, 98, 184, 233, 252, 268, 270, 283, 285, 329] Purification was by fast protein liquid chromatography (FPLC) (**Figure S4**) with significantly lower product yields for the 15 kDa compared to the 8 kDa and 25 kDa bioconjugate, respectively (**Table S2**). Initial 15 and 25 kDa BCN-PEtOx appeared to be more challenging in terms of control of polymer properties (**Figure S4A**). Additional bands in the SDS-PAGE analysis suggested the presence of IFN-polymer multimers, hence incorporating additional BCN-groups in the polymer chain for 15 and 25 kDa BCN-PEtOx polymers. This challenge was met by adapting the route of PEtOx synthesis (*vide supra*) (**Scheme 1**).[323] The rigorous selection of fractions reduced the dispersity of the final tested bioconjugates (**Figure S4C, D**). Pure bioconjugates resulted from this improvement as confirmed by SDS-PAGE and RP-HPLC (**Figure 2A, 2B, and S5**). Both bioconjugates eluted at similar retention times, suggesting comparable hydrophilicity (**Figure 2B and S5**). The second smaller peak was likely the IFN-α2a bioconjugate dimer, extrapolating from previous observations in which the IFN-α2a WT main peak was

followed by the peak of the IFN-α2a dimer (data not shown). These were previously reported for IFN-α2a.[324, 330] All bioconjugates had an increased hydrodynamic diameter, which grew with polymer size with significant differences between each bioconjugate and the wild type (WT) (**Figure 2C and Table S3**). This is in line with previously reported results of similar bioconjugates.[178, 184, 268, 294, 306] When compared to hydrodynamic diameters of similar IFN-α-PEG bioconjugates the 15 kDa bioconjugate ranges between hydrodynamic diameters reported for 10 and 20 kDa IFN-α2a-PEG bioconjugates and the 25 kDa PEtOx bioconjugate slightly above diameters reported for 20 kDa IFN-α2a-PEG bioconjugates.[324] In the literature, PEtOx is described to have a smaller hydrodynamic size compared to PEG of same molecular weight.[178, 294] Although comparable stability was measured among the bioconjugates by differential scanning fluorimetry (**Figure 2D and Table S3**), it was reduced compared to the azido-mutant and the WT. Similar observations had been reported before for IFN-α2a bioconjugates.[98] These differences of less than 3 °C are minor and in the same range of changes seen for different concentrations or buffer compositions of the WT.[313]

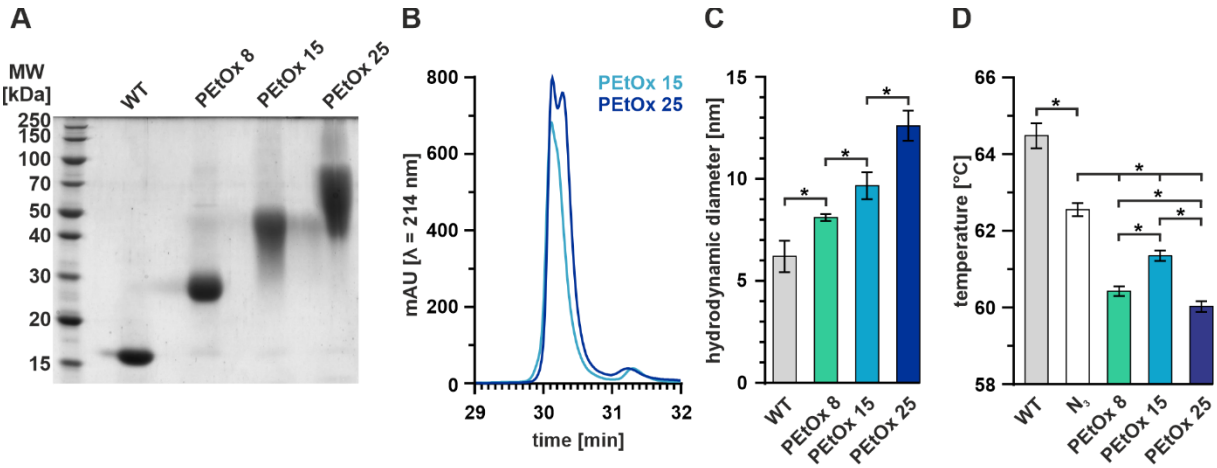

Figure 2: SDS-PAGE of (A) IFN-α2a WT (WT), IFNK31N$_3$-PEtOx 8 kDa (PEtOx 8), IFNK31N$_3$-PEtOx 20 kDa (PEtOx 20) and IFNK31N$_3$-PEtOx 35 kDa (PEtOx 35). (B) Magnification of RP-HPLC chromatograms of PEtOx-bioconjugates (for entire chromatograms, please see Figure S5). RP-HPLC of IFN-PEtOx 8 was already reported.[98] (C) Hydrodynamic diameter of IFN-α2a WT and PEtOx bioconjugates. (n = 3; mean ± standard deviation; analysis for differences by one-sided ANOVA test followed by Tukey *post hoc* test for pair-wise comparison; $p < 0.05$ was considered statistically significant and differences were marked by asterisks). The hydrodynamic diameter of IFN-α2a WT was reprinted from ref 324, Copyright (2022), with permission from Elsevier. (D) Melting points of IFN-α2a WT its mutant and PEtOx bioconjugates determined by differential scanning fluorimetry (n ≥ 4; mean ± standard deviation; one-sided ANOVA test followed by Tukey *post hoc* test for pair-wise comparison; $p < 0.05$ was considered statistically significant and selected differences relevant for this study were marked by asterisks) Melting point of IFN-α2a WT and mutant was reprinted from ref 324, Copyright (2022), with permission from Elsevier.

Potency and *in vivo* pharmacokinetics of PEtOx bioconjugates

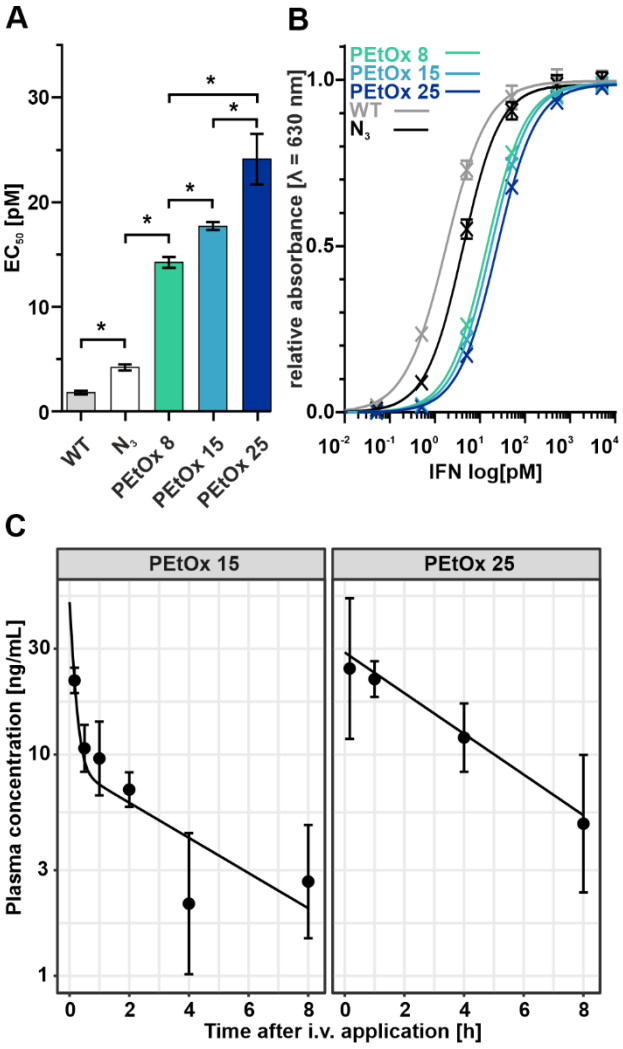

Figure 3: EC_{50} values of IFN-α2a WT its mutant and PEtOx bioconjugates (n ≥ 3; mean ± standard deviation; analysis for differences by one-sided ANOVA test followed by Tukey *post hoc* test for pair-wise comparison; $p < 0.05$ was considered statistically significant and differences were marked by asterisks. (B) Stimulation curve of HEKBlue 293 IFN-α/β cells after 20 h of IFN-α stimulation with PEtOx bioconjugates (mean ± standard deviation, n ≥ 3). (C) Pharmacokinetics of PEtOx bioconjugates (mean ± standard deviation, n ≥ 4).

The potency of PEtOx bioconjugates was tested using an *in vitro* reporter cell line assay (**Figure 3A and B, Table S3**). All bioconjugates had a significantly reduced potency compared to the WT and unconjugated mutant. Among the bioconjugates, polymer lengths negatively correlated with potency. The measured reduction in potency matched previous results of similar PEG and PEtOx bioconjugates concerning potency in correlation to the hydrodynamic diameter of the bioconjugate.[268, 270, 324] This confirmed earlier statements on the similarities of PEtOx and PEG bioconjugates.[98, 166, 184, 268, 270] The 15 and 25 kDa bioconjugates were selected for the *in vivo* studies, and plasma stability was demonstrated in mice for at least two days (**Figure S6**). The pharmacokinetic (PK) profile of the 15 kDa conjugates had a rapid absorption phase of about 6.7 h^{-1} ($t_{1/2}$ ~ 6 min; **Figure 3C, Table S5-7**), followed by a terminal distribution phase of about 0.2 h^{-1} ($t_{1/2}$ > 3.5 h). Likely, this reflected rapid glomerular filtration, hence the renal loss. In contrast, the PEtOx 25 kDa bioconjugate profile was monoexponential, with an overall slope of about 0.2 h^{-1} ($t_{1/2}$ > 3.25 h; **Figure 3C, Table S5-7**). Therefore, the 25 kDa bioconjugate was selected for further efficacy studies as it suggested improved plasma retention compared to its 15 kDa counterpart.

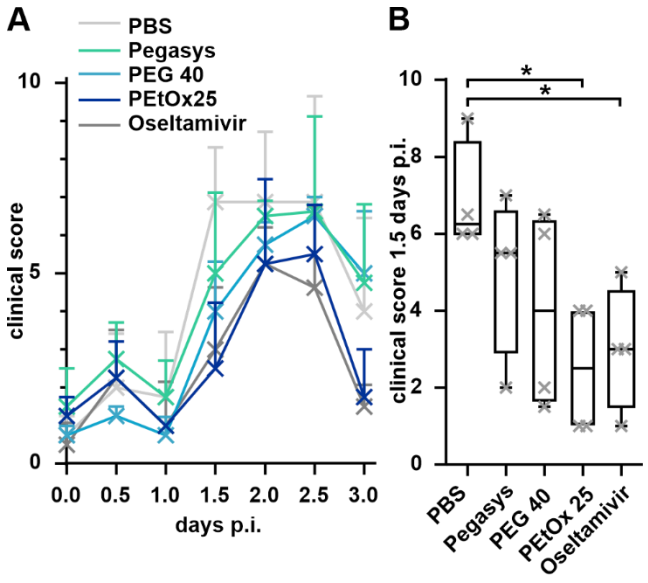

Figure 4: (A) clinical score of tested ferret groups over 3 days post-infection. (B) Box plots of the clinical score of tested ferret groups displayed in A at 1.5 days post-infection. Individual animals are indicated with crosses (n = 4). analysis for the difference by two-tailed t-test comparisons, using Welch's correction between groups; $p < 0.05$ was considered statistically significant and marked by asterisks.

Efficacy study in ferrets with influenza

Groups of four ferrets were treated with either IFN-PEtOx 25, phosphate buffered saline (PBS) (negative control), the neuraminidase inhibitor oseltamivir (positive control), Pegasys (IFN-α2a conjugated non-specifically to one branched 2x20 kDa PEG), or IFNK31N_3-BCN-PEG 40 kDa (IFN-PEG 40).[324] IFN-PEG 40 was previously introduced and had similar attributes as Pegasys regarding the pharmacokinetics and hydrodynamic diameter.[324] In this study the potency was 2-fold higher than the potency of Pegasys and 1.5-fold lower than IFN-PEtOx 25.[324] Twelve hours later, the ferrets were intranasally infected with 2×10^5 $TCID_{50}$ H1N1pdm09. A single treatment of the ferrets with IFN-PEtOx 25, but not with Pegasys or IFN-PEG 40 significantly reduced the course of clinical disease, similar to twice-daily treatment with oseltamivir (**Figure 4**), with significant differences on day 1.5 post infection. Viral titers in nasal washes, trachea titers and viral titers of nasal turbinate washes on day three did not differ between groups except for the oseltamivir-treated animals on day two after injection (**Figure S7**). These differences on titers may reflect the treatment courses and mode of action, with a single dose IFN treatment and resulting immune stimulation being different from twice daily administered oseltamivir and its immediate impact on viral replication through neuraminidase blockade.

Conclusions

In conclusion, hydrodynamic radii-balanced, PEtOxylated IFN-α2a bioconjugates yield lasting exposure in mice and disease-modifying effects in IAV-infected ferrets. Single, intraperitoneally injected doses of the bioconjugate reduced the disease burden following H1N1 influenza infections, similar to twice daily, orally given suspensions of neuraminidase inhibitors. Differences in efficacy seen between Pegasys and IFN-PEtOx 25 could have been attributed to either Pegasys' lower potency or longer polymer chain. However, the IFN-PEG 40 group – sharing potency with the IFN-PEtOx 25 and size with Pegasys – points evidence toward the pivotal importance of polymer choice for successful therapy. Future efforts, e.g., introducing further targeting ligands, might potentially turn into marginal improvement.[233] The affinity of IFN-α2a is already so high that only very few targeting ligands will be discovered, improving homing of such potent bioconjugates. Particularly in light of mounting first-line

antiviral drug resistance in influenza strains, PEtOxylated IFN-α2a bioconjugates may critically expand our arsenal, particularly for future pandemic threats.

Supporting Information

Supporting Information includes characterization of poly(2-ethyl-2-oxazoline)s by SEC, NMR, SEC-MALLS and AUC, purification of bioconjugates, important biological parameters of tested compounds, full RP-HPLC chromatograms of bioconjugates, data of the *in vivo* pharmacokinetic study in mice and *in vivo* pharmacodynamic study in ferrets and bioconjugate plasma stability data.

Acknowledgments

We acknowledge Prof. Dr. Edward A. Lemke from the Johannes Gutenberg University of Mainz / EMBL Heidelberg for donating the pEVOL-pylRS vector. We acknowledge the support of Paria Pouyan from the Free University of Berlin for helping with dynamic light scattering measurements. Lisa Jäpel is acknowledged for support with the SEC-MALLS measurements. The project was funded within the framework 'Next-PEG' by the Federal Ministry of Education and Research (BMBF) of Germany (# 13XP5049), the "Thüringer Aufbaubank (TAB)", and the "Europäischer Fonds für regionale Entwicklung (EFRE)" (2018 FGI 0025). G.C. acknowledges support from the Free State of Thuringia and the European Social Fund (2019SD0129).

Supporting Information to Chapter 4

Materials and Methods

Polymer characterization

Size exclusion chromatography and NMR

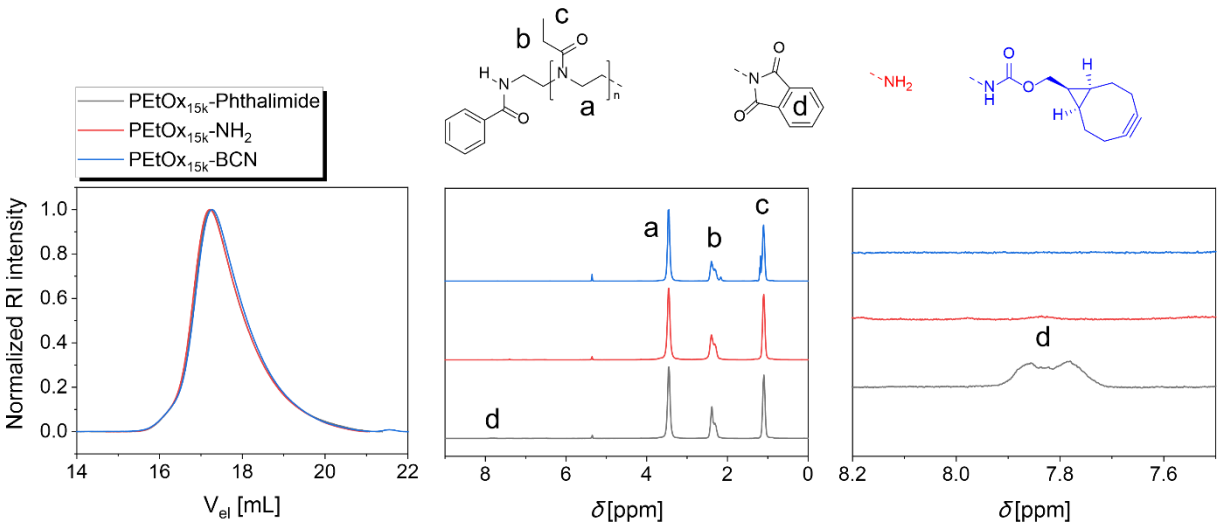

Figure S1. Characterization data of the BCN-PEtOx 15kDa polymer including all intermediate steps. **Left**: Overlay of the SEC elugrams (DMAc, 0.21 wt% LiCl, RI-det.). **Middle**: Overlay of the full ^{1}H NMR spectra (CD_2Cl_2, 300 MHz). **Right**: Zoom into the overlaid ^{1}H NMR spectra into a region depicting the phthalimide signal (labelled as "d").

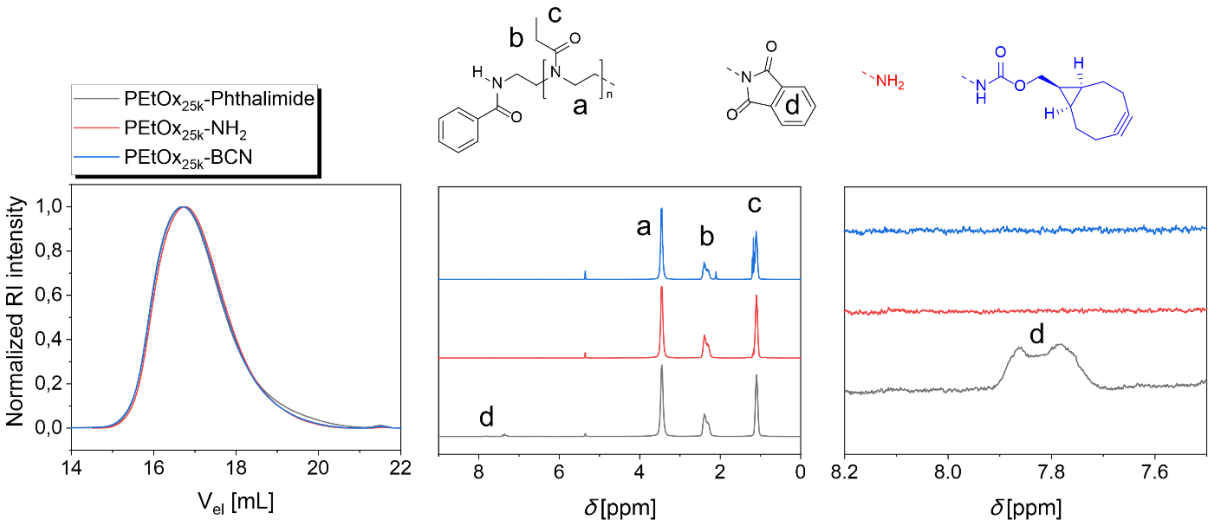

Figure S2. Characterization data of the BCN-PEtOx 25 kDa polymer including all intermediate steps. **Left**: Overlay of the SEC elugrams (DMAc, 0.21 wt% LiCl, RI-det.). **Middle**: Overlay of the full ^{1}H NMR spectra (CD_2Cl_2, 300 MHz). **Right**: Zoom into the overlaid ^{1}H NMR spectra into a region depicting the phthalimide signal (labelled as "d").

SEC-MALLS

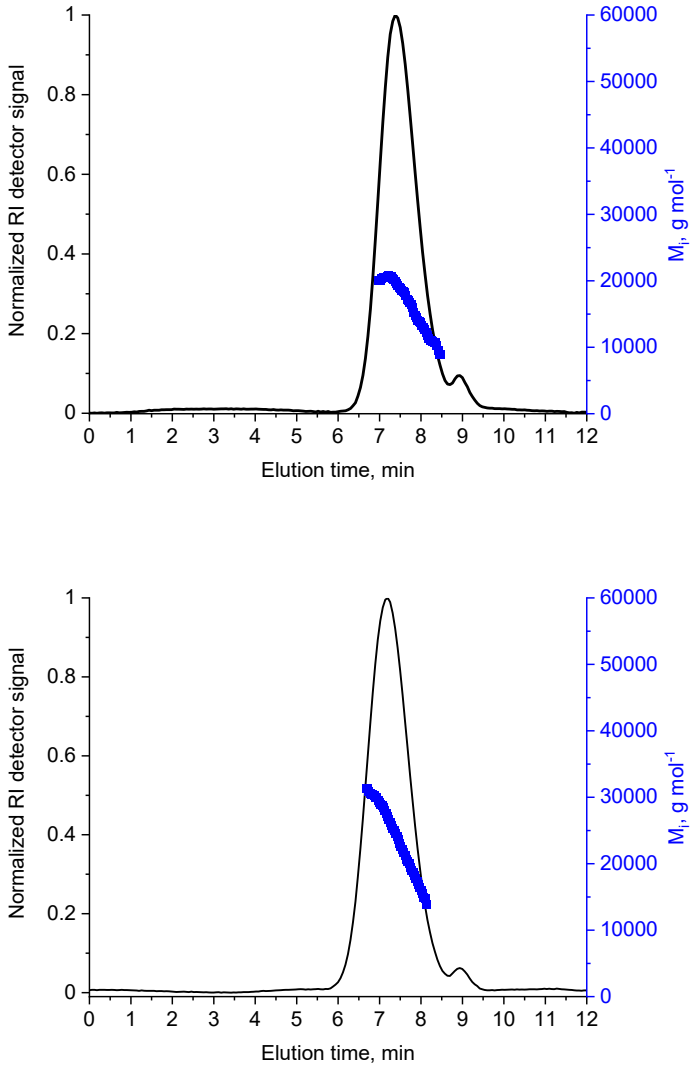

Figure S3. SEC-MALLS elugrams of the PEtOx-NH_2 polymers with the normalized RI detector trace and the molecular weight trace M_i. **Top:** PEtOx-NH_2 15 kDa. **Bottom:** PEtOx-NH_2 25 kDa.

Analytical Ultracentrifugation

Table S1: Hydrodynamic properties determined from sedimentation-diffusion analysis of sedimentation velocity AUC experiments. Signal (weight) average sedimentation coefficients, *s,* and translational frictional ratios, *f/fsph*, were determined by RI detection. Utilized sample concentrations were approx. 0.25 mg mL^{-1}.

Sample	*s, S*	f/f_{sph}
PEtOx 8 kDa	0.49	1.37
PEtOx 15 kDa	0.68	1.80
PEtOx 25 kDa	0.83	2.07

Table S2: Conjugation efficiencies of used polymers displayed in figure S6 in relation to the used protein educt and the total yield of selected fractions in relation to the used protein educt.

compound	total product yield [%]	yield of selected fractions [%]
PEtOx 8 kDa	37	21
PEtOx 15 kDa	15	7
PEtOx 25 kDa	37	14

Bioconjugation

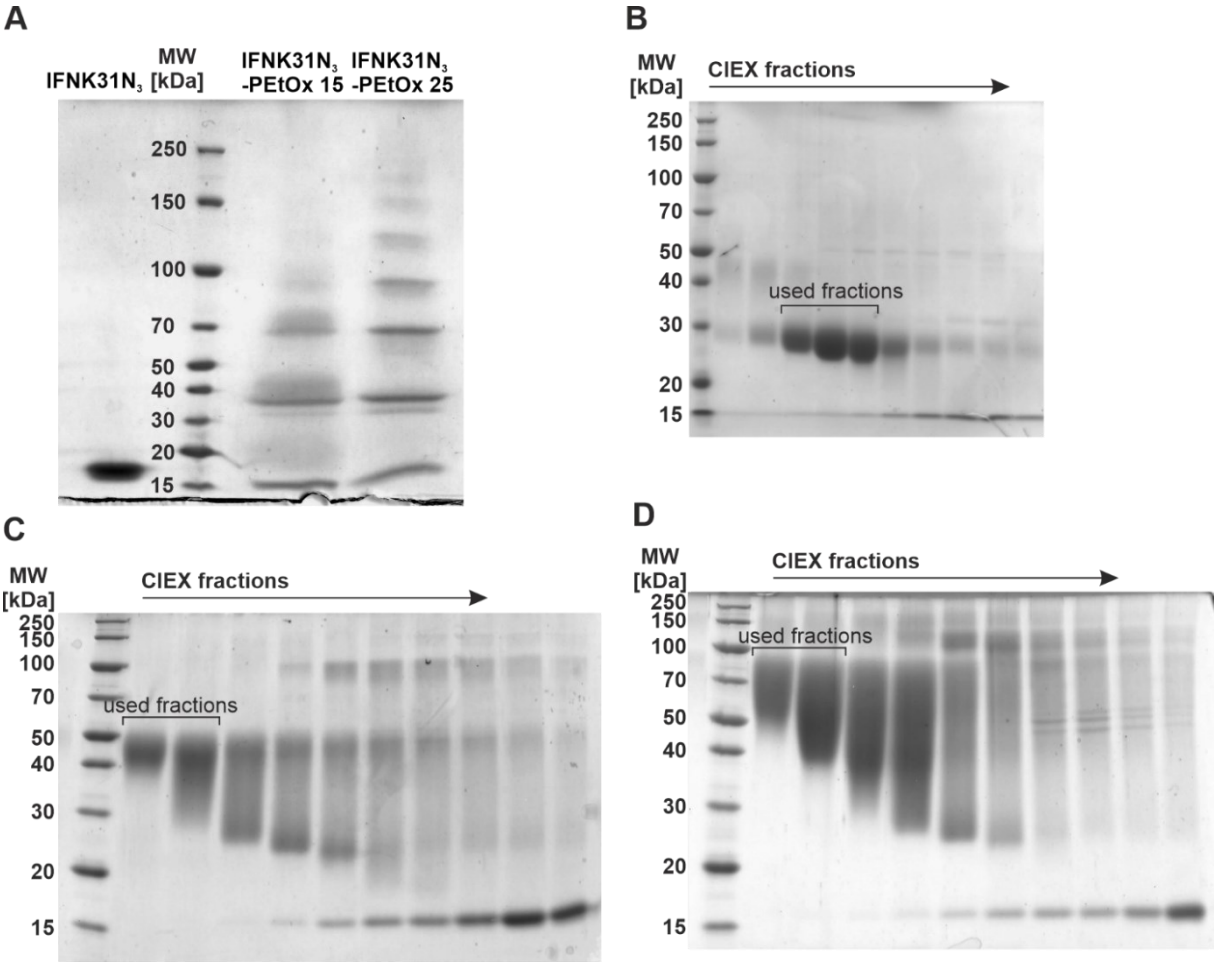

Figure S4: (A) Occurring conjugation "ladders" of 15 and 25 kDa IFN-PEtOx conjugates using the polymerization route of the 8 kDa PEtOx. As shown a regular band pattern is observed. As the differences between bands are about 25 to 30 kDa this occurrence must be caused by the formation of additional reactive groups on the polymer as a polymerization of the sole protein (MW= 19.5 kDa) would lead to a band pattern with smaller steps. Exemplary SDS-PAGE of fractions from CIEX purification of (B) IFNK31N_3-PEtOx 8 kDa, (C) IFNK31N_3-PEtOx 15 kDa, (D) IFNK31N_3-PEtOx 25 kDa. Used and pooled fractions for the presented experiments are indicated.

Important biological and physical parameters of tested compounds

Table S3: Important biological and chemical parameters of IFN-α2a and its bioconjugates. Mean values are indicated with standard deviations.

Compound	Hydrodynamic diameter [nm] [a]	T_M[°C]	EC_{50} [pM]
IFN-WT	6.2 ± 0.8*	64.5 ± 0.3*	1.8 ± 0.2
N_3	n.d.	62.6 ± 0.2*	4.2 ± 0.3
PEtOx 8 kDa**	8.1 ± 0.2	60.4 ± 0.1	14.3 ± 0.5
PEtOx 15 kDa	9.7 ± 0.7	61.4 ± 0.1	17.7 ± 0.4
PEtOx 25 kDa	12.6 ± 0.7	60.0 ± 0.1	24.1 ± 2.4

n.d. = not determined. *Marked values were reported in a previous study and are redisplayed for comparison.[324] **The approximately 10 kDa molecular weight bioconjugates were presented in a previous contribution,[98] however, the data reported here is either novel (hydrodynamic diameter), or was measured again to obtain comparable data among all polymers (EC_{50} [pM]).

RP-HPLC

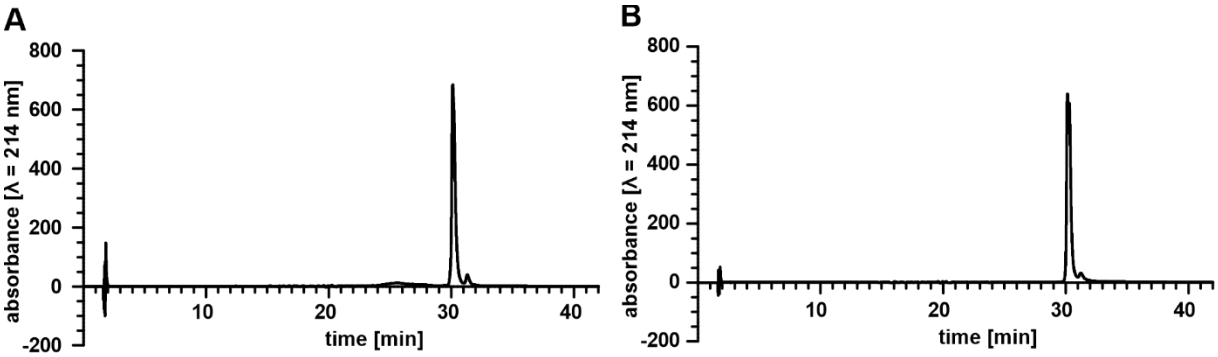

Figure S5: RP-HPLC analysis of (A) IFN-PEtOx 15 kDa and (B) IFN-PEtOx 25 kDa.

In vivo pharmacokinetic study

Table S4: *In vivo* experimental setting of PEtOx bioconjugates after IFN-bioconjugate application

	used group (5 mice each)			medical intervention	
Time [h]	Group 1	Group 2	Group 3	blood collection	sacrifice
0.16	x			x	
1		x		x	
4			x	x	
8	x			x	x
24		x		x	x
48			x	x	x

Biphasic PK: $Conc(t) = CP_a \cdot e^{-\alpha \cdot t} + CP_b \cdot e^{-\beta \cdot t}$

Mono-exponential PK $Conc(t) = CP_a \cdot e^{-\alpha \cdot t}$

Table S5: Calculated *in vivo* elimination constants and calculated initial concentrations of bioconjugates

Compound	α [h^{-1}]	β [h^{-1}]	CP_a [ng/mL]	CP_b [ng/mL]
PEtOx 15	6.744	0.183	40.10	8.73
PEtOx 25*	0.212	-	28.88	-

* no distribution phase, mono-exponential PK

Non-Compartmental Analysis

Table S6: Calculated *in vivo* apparent total body clearance, apparent volume of distribution and area under the curve values till last time point/infinity of bioconjugates

Compound	CL [L/h · kg^{-1}]	V_Z [L · kg^{-1}]	V_{ss} [L · kg^{-1}]	$AUC_{0\text{-tlast}}$ [h · ng/mL]	$AUC_{0\text{-}\infty}$ [h · ng/mL]
PEtOx 15	0.0477	0.295	0.284	44.23	62.85
PEtOx 25	0.0206	0.108	0.102	114.96	145.69

Table S7: Terminal disposition rate constant, serum half-life, area under the first moment curve till last time point/infinity and mean residence time

Compound	λ_Z [h^{-1}]	$t_{1/2}$ [h]*	$AUMC_{0\text{-tlast}}$ [h^2 · ng/mL]	$AUMC_{0\text{-}\infty}$ [h^2 · ng/mL]	MRT_{Last} [h]	MRT_∞ [h]
PEtOx 15	0.162	4.3	110.24	374.12	2.49	5.95
PEtOx 25	0.190	3.6	313.38	720.72	2.72	4.95

* based on λ_Z

Plasma stability

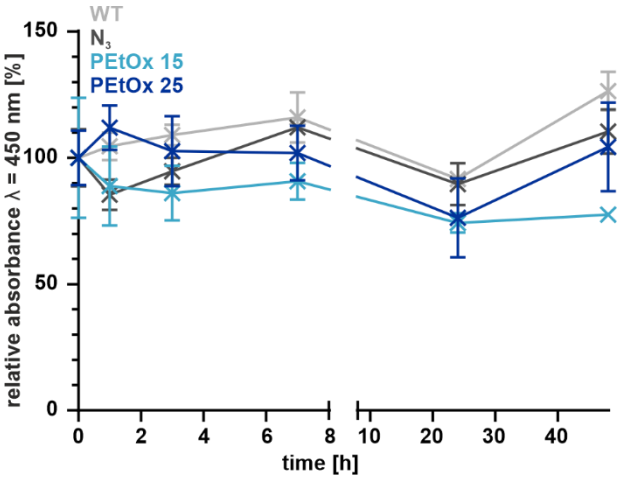

Figure S6: plasma stability of IFN-α2a its azide mutant and PEtOx bioconjugates, tested over 48 h (mean ± standard deviation, n = 3).

In vivo pharmacodynamic study

Table S8: Score sheet used for clinical score determination

symptoms	severity of symptoms			
	0	1	2	3
Temperature	< 38.5 °C	38.5° to 39.0°C	39.0° to 39.5°C	>39.5°C
initial weight loss	none	0 to 5%/	5 to 10%	>10%
activity	normal	calm	depressed	inactive
nasal exudate	none	serous	sero-mucous	muco-purulent
congestion	none	mild	intermediate	severe
sneezing	none	rarely	occasionally	frequently
assessment of labored breathing	none	occasional wheezing	continuous wheezing	labored breathing

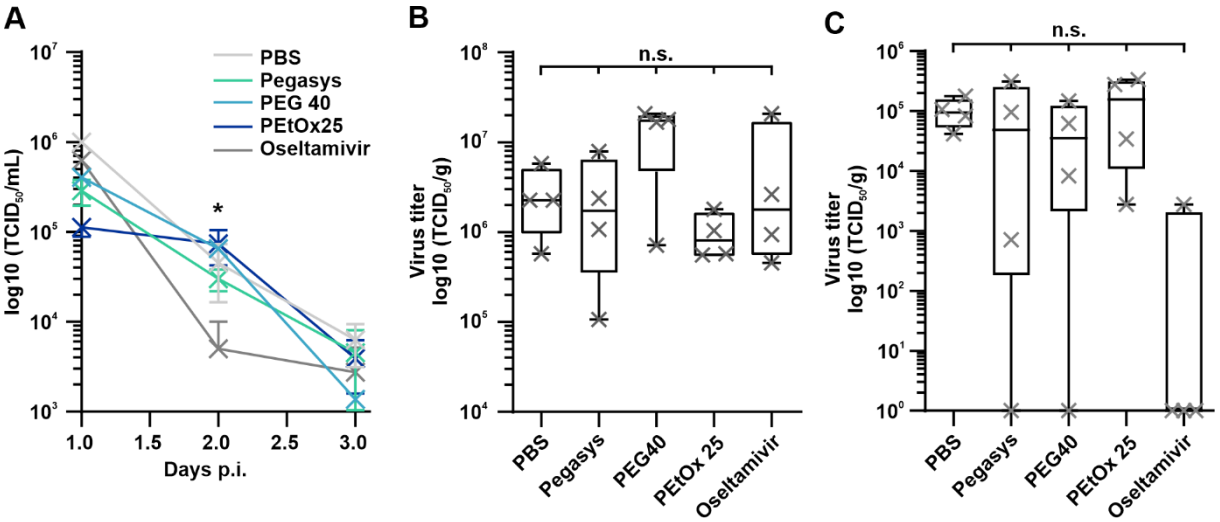

Figure S7: (A) Nasal titers of ferrets. (B) Nasal turbinate titers on day 3 p.i.. (C) Trachea titers on day 3 p.i..

Chapter 5 – Linear Polyglycerol for N-terminal-selective Modification of Interleukin-4

Michael Tully,‡ Niklas Hauptstein,‡ Kai Licha, Lorenz Meinel,

Tessa Lühmann, Rainer Haag

‡ These authors contributed equally to this work.

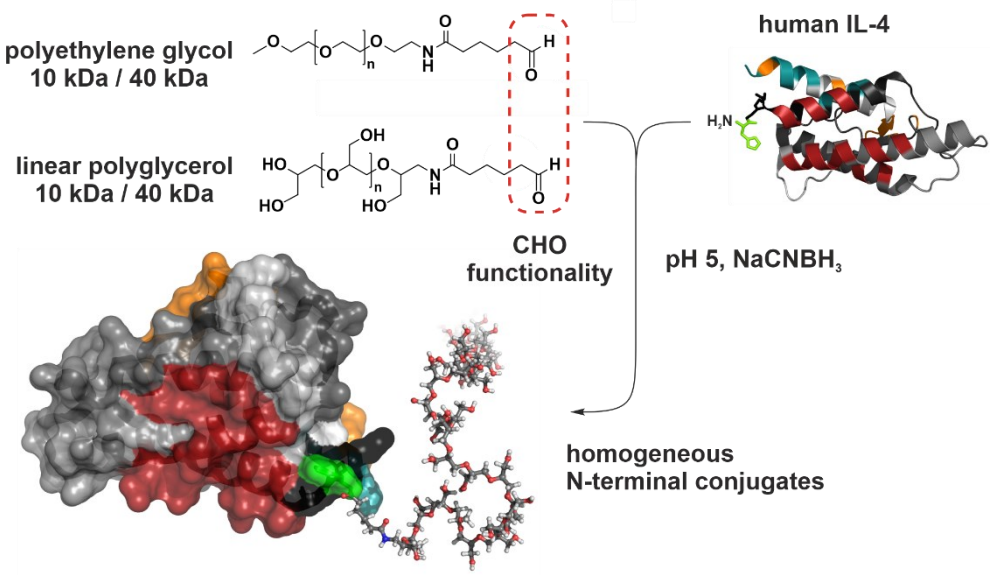

Keywords: protein delivery, polymeric drug delivery systems, Pegylation, polyethylene glycol (PEG), conjugates, polymers, biopharmaceutical characterization,

Reprinted (adapted) with permission from: Tully, M.; Hauptstein, N.; Licha, K.; Meinel, L.; Lühmann, T.; Haag, R., Linear Polyglycerol for N-terminal-selective Modification of Interleukin-4. J. Pharm. Sci. 2022, 111 (6), 1642-1651. DOI: 10.1016/j.xphs.2021.10.032.

Abstract

Polymer conjugation to biologics is of key interest to the pharmaceutical industry for the development of potent and long acting biotherapeutics, with poly(ethylene glycol) (PEG) being the gold standard. Within the last years, unwanted PEG-related side effects (immunological reactions, antibody formation) arose, therefore creating several attempts to establish alternative polymers with similar potential to PEG. In this article, we synthesized *N*-terminal bioconjugates of the potential therapeutic human interleukin-4 (hIL-4 WT) with linear polyglycerol (LPG) of 10 and 40 kDa and compared it with its PEG analogs of same nominal weights. Polyglycerol is a highly hydrophilic polymer with good biocompatibility and therefore represents an alternative polymer to PEG.

Both polymer types resulted in similar conjugation yields, comparable hydrodynamic sizes and an unaltered secondary structure of the protein after modification. LPG- and PEG-bioconjugates remained stable in human plasma, whereas binding to human serum albumin (HSA) decreased after polymer modification. Furthermore, only minor differences in bioactivity were observed between LPG- and PEG-bioconjugates of same nominal weights. The presented findings are promising for future pharmacokinetic evaluation of hIL-4-polymer bioconjugates.

Introduction

The clinical use of small, but potent biologics with molecular masses up to 50 kDa is still vastly expandable. Due to their small size, most of these drugs display a limited blood circulation time, therefore leading to fast elimination, which makes high frequent dosing necessary [331, 332]. To eliminate this problem, several techniques are available ranging from encapsulation of proteins into micelles[333], or nanogels[334] to covalent modification, with poly(ethylene glycol) (PEG) representing the most prominent polymer in that field[335]. PEG is an amphiphilic polymer that equips biologics with desirable properties including a diminished renal excretion through size expansion as well as a stealth behavior, that leads to reduced opsonization and clearance through the immune system[58]. Drawbacks of PEG include a reduced bioactivity after conjugation[57] and its tendency to accumulate in the body, due to its non-degradability[58]. Within recent years the formation of anti-PEG antibodies was reported [256] which led to an accelerated blood clearance (ABC) in some cases thereby impairing PEG's initial benefits [151, 257, 336, 337]. Rare anaphylactic reactions observed for the new SARS-CoV-2 mRNA vaccine by BioNTech-Pfizer might be attributed to the PEG-moiety located on the lipid nanoparticle for vaccine delivery[338]. However, it is not clear yet how serious these PEG-related issues really are, especially in the clinical field. PEG is still regarded as a safe excipient and is the preferred macromolecule for half-life extension and drug delivery, with other polymers being studied as well [281, 339].

Polyglycerol (PG) is a highly hydrophilic polymer showing excellent biocompatibility [162, 165, 340, 341] and further displays stealth properties, that are similar to PEG [342-344]. Its half-life is longer than PEG of similar molecular weight,[162] which led us to the idea of employing linear polyglycerol (LPG) as a

polymer for bioconjugation to extend the blood circulation time of biopharmaceuticals. We chose human Interleukin-4 (hIL-4 WT) as a model protein, a potent cytokine bearing highly anti-inflammatory attributes through polarization of macrophages into the beneficial M2 type [184, 345]. hIL-4 has several potential applications to target chronic inflammations in wounds, arthritic joints and similar affected tissues [233, 345]. For site-selective conjugation, we decorated hIL-4's *N*-terminus with LPG-variants of 10 or 40 kDa *via* a reductive alkylation approach, which has already been used previously for other proteins [346]. The LPG-conjugates were then systematically compared to PEG-analogs of same nominal weights and characterized mainly regarding their hydrodynamic size and structural changes followed by evaluation of their bioactivity and behavior towards human plasma components *in vitro*.

Materials and Methods

Materials

10 kDa methoxy-PEG-hexylaldehyde (mPEG-aldehyde), and -azide (mPEG-N_3) were from Rapp Polymers (Tübingen, Germany). 40 kDa mPEG-amine-HCl was from JenKem Technology (Texas, USA). Highly purified water from a MilliQ®-system was used for all biological experiments. Buffers were degassed and filtered through 0.22 µm regenerated cellulose (RC) filter (Sartorius, Göttingen, Germany) before use. All other chemicals and solvents were obtained from Sigma Aldrich (Steinheim, Germany) and used without further purification, unless otherwise noted.

Synthesis of LPG-10-, LPG-40- and mPEG-40-aldehyde

A detailed description of the synthesis part can be found in the Supporting Information.

Expression, purification and characterization of wild-type Interleukin-4

Human Interleukin-4 (hIL-4 WT) was expressed as described before[184, 198, 346]. In brief hIL-4 WT was cloned into the pET21a-vector between the NdeI and BamHI restriction site, bearing an ampicillin resistance. Expression took place in *E. coli* BL21(DE3) Star bacteria (Thermo Fisher scientific) in Terrific Broth Medium at 37 °C. The bacteria were induced at an OD_{600} of 0.6 with 1 mM IPTG and incubated for 5–6 h. Afterwards, bacteria were harvested by centrifugation at 4 °C and 5000 x g for 20 min, resuspended in lysis buffer (50 mM Tris-HCl pH 8.0, 50 mM NaCl, 1 mM EDTA) and sonicated. The pellet was then washed twice with lysis buffer containing 1 % Triton X-100, followed by a lysis buffer wash, centrifuged and subsequently unfolded in lysis buffer containing 5 M guanidinium hydrochloride, 2 mM reduced glutathione and 0.2 mM oxidized glutathione. Refolding was performed as described in literature[347]. The refolded protein was dialyzed against PBS overnight. On the next day its pH was adjusted to 5 with AcOH, followed by purification on an ÄKTA pure 25 FPLC system (GE Healthcare, Freiburg, Germany) employing ion exchange chromatography (IEX) using a HiTrap Q XL 5 mL column (Cytiva Europe GmbH, Freiburg, Germany) (Buffer A: 25 mM NaOAc, pH 5.0, Buffer B: 25 mM NaOAc pH 5.0 + 2 M NaCl) with a linear gradient from 0–40 % B in 12 CV, with hIL-4 WT

eluting at 30 % B. hIL-4 WT containing fractions were pooled, dialyzed against buffer A and applied to an additional IEX purification step (same buffers as above) using a YMC Biopro IEX smart sep S20 1 mL column (YMC Europe GmbH, Dinslaken, Germany) with a gradient from 12–60 % B. Collected hIL-4 WT fractions were evaluated on purity by SDS-PAGE and subsequently pooled followed by determination of hIL-4 WT concentration by standard BCA assay (Pierce BCA Assay Kit, Thermo Fisher scientific) following the manufacturer's instructions.

Synthesis and purification of PG- and PEG-Interleukin-4 bioconjugates

Linear polyglycerol or polyethylene glycol, all mono-functionalized with a single aldehyde group, were conjugated to hIL-4's *N*-terminus *via* reductive amination at pH 5, as described previously[348]. In short, 600 µg of protein were diluted into 1 mL pre-chilled 0.1 M NaOAc pH 5 in a 2 mL glass vial followed by addition of three-fold molar excess of activated polymer in the same buffer. After gentle mixing, the reaction was initiated by adding freshly prepared $NaCNBH_3$ solution (0.5 M) as reducing agent to a final concentration of 20 mM. The reaction mixture was shaken on a bioshaker (Quantifoil instruments, Jena, Germany) for 16 h at 4 °C. The batch was then diluted 10-fold in 25 mM NaOAc pH 5 and subsequently loaded on an ÄKTA pure 25 FPLC system equipped with two HiTrap SP FF 1 mL columns (both GE Healthcare, Freiburg, Germany) connected in series (flow rate 1 ml/min), where 25 mM NaOAc pH 5 served as eluent A. To isolate the monoconjugates from free polymer, unreacted protein and multi-PEGylated/PGylated species, first a washing step with 5 % eluent B (B = eluent A + 2 M NaCl) for five column volumes (CV) was conducted followed by a linear gradient from 10–50 % B for 16 CV to elute multi- and mono-PEGylated/PGylated proteins. The fractions with mono-conjugated product were collected, pooled and rebuffered against phosphate-buffered saline (PBS) pH 7.4 (137 mM NaCl, 2.7 mM KCl, 10 mM Na_2HPO_4, 1.8 mM KH_2PO_4) in Amicon Ultra 2 centrifugal filter units (MWCO 3 kDa, Sigma Aldrich, Steinheim, Germany). Concentration was determined by Nanodrop 2000c (Thermo Fisher, Dreieich, Germany) at 280 nm with an extinction coefficient of 8860 M^{-1} cm^{-1} [184]. Samples were then aliquoted, snap frozen in liquid N_2 and stored at -80 °C until further use.

Sodium dodecylsulfate-polyacrylamide gel electrophoresis (SDS-PAGE)

SDS-PAGE analysis was performed under standard denaturing Laemmli-conditions with acrylamide concentrations of 5-12 % in the separation gel. Purified fractions were analyzed on gradient gels with a concentration of 5–12 %. Gels were run at 200 V and analyzed *via* ImageLab software 5.2.1. Standard Coomassie staining was used to visualize the protein bands.

Size-exclusion multi-angle light scattering (SEC-MALS)

For molecular weight determination, size-exclusion chromatography coupled to multi-angle light-scattering (SEC-MALS) was performed on a Hitachi L-2130 HPLC system that was equipped with a UV-Vis absorption detector (Hitachi L-2400), a DAWN 8^+ MALS detector, and an Optilab refractive

index detector (both Wyatt Technology, Dernbach, Germany). For size exclusion, a Superdex 200 Increase 10/300 GL column (GE Healthcare, Uppsala, Sweden) was used with the mobile phase consisting of PBS pH 7.4 operated at a flow rate of 0.5 mL/min. 50 µg of bioconjugate (based on protein weight) were injected in each run. Data analysis was followed by the software Astra 6.0 (Wyatt Technology, Dernbach, Germany). Protein conjugate analysis was performed by the Wyatt protein-conjugate application, which was embedded in the Astra software. UV extinction coefficient for hIL-4 WT was 8860 M^{-1} cm^{-1}, for *dn/dc* (differential refractive index) of hIL-4 WT, a typical value of 0.185 mL/g was used. *dn/dc* for PEG and LPG were measured at 25 °C on a SEC-3010 RI detector (WGE Dr. Bures GmbH, Dallgow, Germany) which was calibrated against potassium chloride and determined as 0.143 mL/g (PEG) and 0.142 mL/g (LPG).

Reversed Phase (RP)-HPLC analysis

RP-HPLC analysis was performed on an Agilent 1260 Infinity II system, equipped with a VWD detector. The wavelength was set to 214 nm and column oven temperature to 30 °C. 5 µg of each sample were applied to a ZORBAX 300SB-CN column (4.6 x 150 mm, particle size = 5 µm) (Agilent, Santa Clara, CA, USA) with an autoinjector. For elution of hIL-4 WT or its bioconjugates, a linear gradient of 5–60 % was used over 30 min at a flow rate of 1 mL/min (eluent A: Water + 0.1 % TFA, eluent B: Acetonitrile + 0.1 % TFA).

Matrix-assisted laser desorption ionization time of flight mass spectrometry (MALDI-TOF-MS)

The samples were desalted using ZipTipC18-tips (Pierce C18 Tips, Thermo Fisher Scientific) following the manufacturer's instructions. Matrix-assisted laser desorption ionization (MALDI-MS) spectra were acquired in the linear positive mode using an ultrafleXtreme mass spectrometer (Bruker Daltonics, Bremen), equipped with a 355 nm smartbeam-II™ laser. Mass spectra were calibrated with bovine serum albumin. Sinapinic acid was used as a matrix.

Dynamic Light Scattering (DLS)

For determination of the hydrodynamic size of hIL-4 WT and its bioconjugates, dynamic light scattering was performed on a Malvern Zetasizer ZS (Malvern Panalytical, Herrenberg, Germany). All measurements were done at 25 °C in 0.1 M phosphate buffer pH 7.2 (c = 0.4 mg/mL) and samples were filtered (0.22 µm) prior to measurements. The hydrodynamic radius is expressed as volume value, as displayed in the Zetasizer software version 7.13.

Far-UV Circular Dichroism (CD)

CD spectra were recorded on a Jasco J810 (Bruker Instruments, Massachusetts, USA) from 190–250 nm at 20 °C to monitor changes in the far-UV region of hIL-4 WT after polymer modification. Measurements were done in 0.1 M phosphate buffer pH 7.2 at a concentration of 0.10–0.11 mg/mL

using a bandwidth of 2 nm and a 1 cm-path-length cuvette. Each spectrum was baseline corrected using a blank spectrum of buffer.

HEK Blue IL-4/IL-13 Cells *in vitro* secreting alkaline phosphatase (SEAP) assay

The cell culture assay was performed according to the manufacturer's instructions. The used cells (HEK-Blue™ IL-4/IL-13 Cells), colorimetric reagents and antibiotics were bought from Invivogen (Toulouse, France).

Plasma stability in human serum

For plasma stability, human AB+ plasma from healthy men was used (Sigma Aldrich, Germany, P9523). Plasma was thawed on ice only once for aliquotation and thawed once again on ice when used. The plasma was incubated in an Eppendorf thermoshaker at 37 °C, 600 rpm. hIL-4 WT or its bioconjugates were spiked into the plasma at a final concentration of 1 ng/mL, small aliquots were taken at predetermined time points and frozen in liquid nitrogen until further characterization. For quantification of hIL-4 WT or its bioconjugates an IL-4 Human ProQuantum Immunoassay Kit (Thermo fisher scientific, A35587) was used according to the manufacturer's instructions with an ABI Prism 7900 HT Real time PCR machine using the standard temperature ramp protocol and micro Amp^{tm} 96-well qPCR plates (Applied Biosystems, Germany, N8010560).

Microscale-thermophoresis (MST) for determination of HSA-binding

Microscale thermophoresis experiments were carried out on a Monolith NT.115 instrument (NanoTemper technologies GmbH, München, Germany) using red laser with LED settings of 40 % and low MST power. HSA was fluorescently labeled with Alexa Fluor™ 647 NHS dye (Thermo Fisher Scientific, Massachusetts, USA) prior to measurements using the standard protocol provided by the manufacturer. To minimize alterations in binding due to a high degree of labeling, we used a neutral pH for labeling to favor modification at the protein's *N*-terminus rather than its lysine-residues [349]. After purification, the degree of HSA-labeling was determined as 0.33 according to the manufacturer's instructions. Without the use of surfactant, HSA was sticking to the capillaries during measurement causing fluctuations in fluorescence, that was also present when using premium type capillaries (NanoTemper technologies GmbH). Therefore, we selected PBS pH 7.4 including 0.05 % Tween®20 as buffer system for our measurements. Concentration of HSA was set to 50 nM whereas the hIL-4 WT samples were added in a concentration range between 0.4–10,250 nM. Samples were centrifuged at 13,000 g for 5 min directly before measurements and subsequently loaded into normal Monolith NT.115 capillaries. All samples were prepared and measured in triplicates, with 2–6 runs per measurement.

Anti-PEG antibody ELISA of LPG, PEG and its hIL-4-bioconjugates

Binding of hIL-4 bioconjugates to anti-PEG antibodies was analyzed by a commercially available Poly(ethylene) glycol ELISA Kit (ab215546, Abcam, Berlin, Germany). The assay was performed in duplicates according to the manufacturer's instructions. Binding of the free polymers (mPEG-N_3 and LPG-N_3, both 10 kDa) to anti-PEG antibodies was determined by the Methoxy-PEG SPARCL™ Assay (Life Diagnostics, USA). The assay was performed in duplicates using a Tecan Infinite M Plex Plate reader (Tecan Group Ltd., Männedorf, Switzerland) according to the manufacturer's instructions with slight modifications. For luminescence measurement, 38 µL were injected and luminescence was acquired over 4000 ms, with an initial 100 ms settle time.

Surface plasmon resonance (SPR)

SPR was performed on a Biacore X100 (GE Healthcare, Freiburg, Germany) to study the binding of commercial anti-PEG antibodies to immobilized LPG and mPEG (both 10 kDa). Therefore, the polymers were functionalized with biotin, starting from LPG-NH_2 or mPEG-N_3, respectively. To a solution of LPG-NH_2 (1 mg/mL in PBS/DMSO (10/1)) a 20-fold molar excess of *N*-hydroxysuccinimidobiotin (Abcr, Germany) was added and stirred over night at room temperature followed by dialysis against water. mPEG-N_3 was modified by copper-catalyzed azide-alkyne click reaction in PBS/MeOH (1/1) in the presence of 5 mM sodium ascorbate, 0.5 mM $CuSO_4$ and 2.5 mM THPTA (Lumiprobe GmbH, Hannover, Germany), as previously described [350]. The polymer was dissolved in PBS/MeOH (33 mg/mL) and mixed with a 10-fold molar excess of propargyl-biotin (Lumiprobe GmbH, Hannover, Germany) followed by the addition of a pre-mix consisting of $CuSO_4$, THPTA and sodium ascorbate. The mixture was stirred for three days at room temperature followed by dialysis against water.

Each of the biotin-labeled polymers was subsequently immobilized on one cell of a streptavidin gold chip (GE Healthcare, Freiburg, Germany) in HBS-N buffer (100 mM HEPES pH 7.4, 150 mM NaCl) with a contact time of 1080 s to reach a final immobilization level of around 850–1000 RU. For SPR-experiments, anti-PEG antibodies directed against the PEG-backbone (mouse monoclonal, clone 09F02, Biovision Inc., USA) or the methoxy group of PEG (rabbit monoclonal, clone RM105, Invitrogen) were allowed to flow over the respective LPG- or PEG-modified surface at concentrations of 0, 10 or 100 nM (flow rate: 30 µL/min, association time: 150 s, dissociation time: 900 s). At the end of each cycle, the chip was regenerated by a solution of 10 mM Glycine pH 2 for 12 s. Blank runs with buffer were subtracted from the binding curves, which were measured in comparison to an uncoated reference cell on the same SA-chip.

Results and Discussion

Expression of hIL-4 WT and synthesis of its mono-PG and -PEG bioconjugates

LPG-mono-aldehyde as well as mPEG-40-aldehyde were synthesized as described previously (for polymer characteristics see table S1)[166]. To exclude a variety in linker structure, the same moiety consisting of a hexyl-spacer between polymer backbone and reactive group was used (**Scheme 1**).

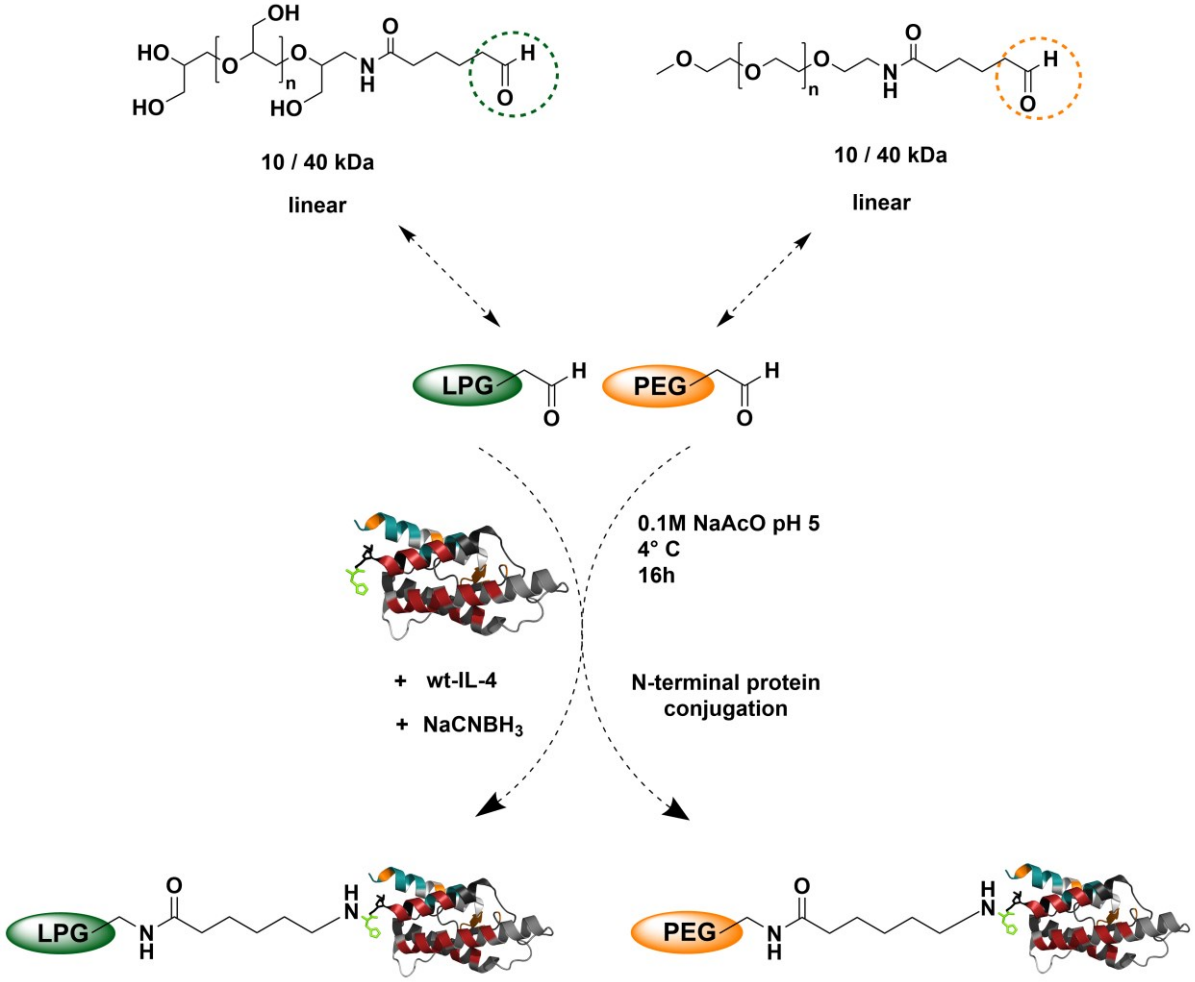

Scheme 1. Reaction scheme for the synthesis of *N*-terminal hIL-4 WT bioconjugates. (PDB of hIL-4 WT: 2b8u)

hIL-4 WT was expressed in *E. coli* using a simple expression protocol yielding sufficient amounts, as demonstrated in Figure 1 (Lane 2: appearance of protein band at 15 kDa). The *N*-terminus of hIL-4 WT is not engaged into

any molecular interactions regarding hIL-4 WT tertiary structure or during receptor binding with IL-4 receptor-α (IL-4Rα) in its Type I and II receptor binding complex (**Figure 2**) therefore representing a suitable attachment site for polymer modification. Targeting the *N*-terminus for selective bioconjugation bears some advantages, as it is usually solvent exposed thereby enabling direct use of the wild-type protein. Its *N*-terminal α-amino group shows a pk_a-value ≈ 6–9 and therefore displays higher reactivity at acidic pH than lysine ε-amino groups (pk_a ≈ 10.5) [349, 351].

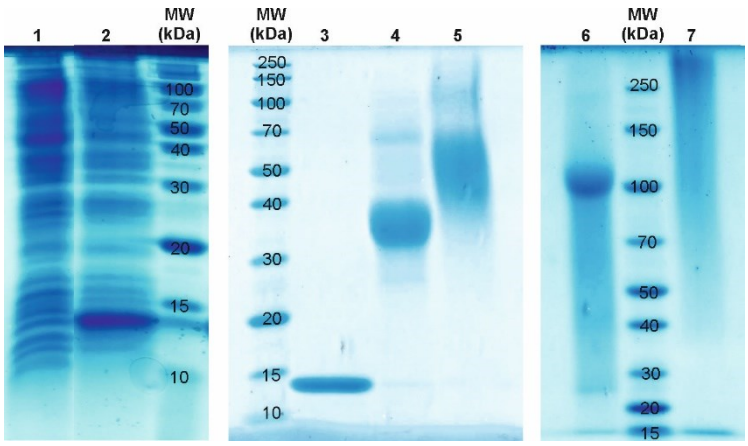

Figure 1. SDS-PAGE of hIL-4 WT and its purified bioconjugates. (1) hIL-4 WT uninduced (2) hIL-4 WT induced for 6 h (3) hIL-4 WT, (4) hIL-4-NH-10-PEG, (5) hIL-4-NH-10-LPG, (6) hIL-4-NH-40-PEG (7) hIL-4-NH-40-LPG.

On the SDS-gel, a shift to higher molecular weight can be observed after polymer conjugation, with the mono-conjugated product being the preferred one under acidic conditions (**Figure 1**). The diminished gel-migration of the bioconjugates (compared to M_w-marker) is possibly due to polymer specific interactions with SDS and has already been described for PEG [238, 352]. hIL-4-NH-LPG bioconjugates showed even shorter migration confirming earlier findings for *N*-terminally modified anakinra [166], and suggests a reduced interaction with SDS for LPG-bioconjugates. Due to reactions with hIL-4's side chain lysine-NH_2 groups, multiple bands occurred on the gel reflecting di- or multi-PEGylated/PGylated species (**Figure S1**), with the mono-product being the preferred one under acidic conditions. The mono-conjugated hIL-4 bioconjugate was isolated by ion exchange chromatography, where unmodified hIL-4 WT as well as multi-conjugated hIL-4 WT varied in their elution profile due to a different extent of charge shielding of the protein surfaces. (**Figure S2**). Overall yields of mono-hIL-4 bioconjugates after purification were around 32 % (LPG) and 42 % (PEG) in the case of the 10 kDa polymers and expectedly decreased for the larger 40 kDa chains (12 % and 32 %, respectively).

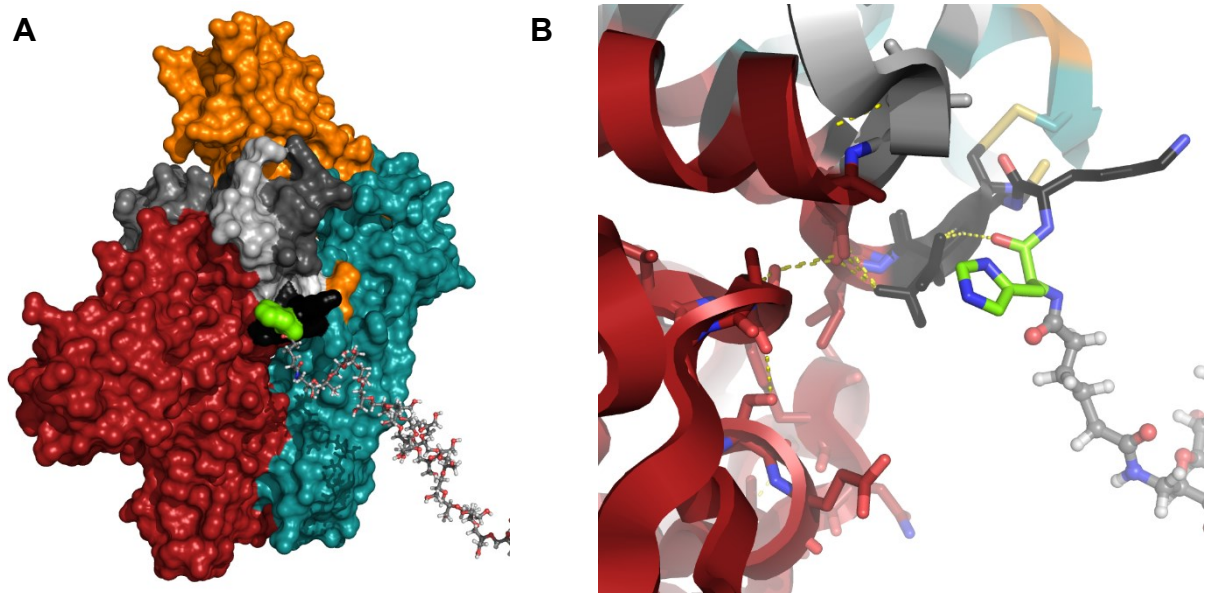

Figure 2. (A) hIL-4 WT engaged in its receptor binding complex(es) Type I and II (PDB: 2b8u, 3bpl and 3bpn are superimposed). hIL-4 WT is displayed in black to white (N to C terminus) with its *N*-terminal residue highlighted in green. Side chain residues engaged into receptor binding are displayed in the color of the receptor. IL-4Rα is displayed in red. IL-4Rγc is displayed in petrol (Type I). IL-13Rα1 is displayed in orange (Type II). LPG is displayed as a stick model and was attached artificially to the *N*-terminal histidine for demonstration purposes of its positioning. (B) Polar contacts in the *N*-terminal environment during Type I and II receptor binding.

Characterization of hIL-4 WT bioconjugates by MALDI-TOF MS, SEC-MALS and RP-HPLC

MALDI MS spectra of hIL-4 WT and its 10 kDa bioconjugates showed molecular weights close to their theoretical values (≈ 25 kDa, Figure 3B/C) and further confirmed good comparability between LPG- and PEG-variants of the protein. Enzymatic in-gel digestion of hIL-4 WT and hIL-4-NH-10-PEG was employed to proof the *N*-terminal conjugation of the polymers. The resulting peptide digests contained different fragments including one *N*-terminal peptide bearing the 10 kDa PEG-moiety that was only found in the bioconjugate. We therefore assumed the *N*-terminus being the main polymer attachment site on the protein (Figure S4).

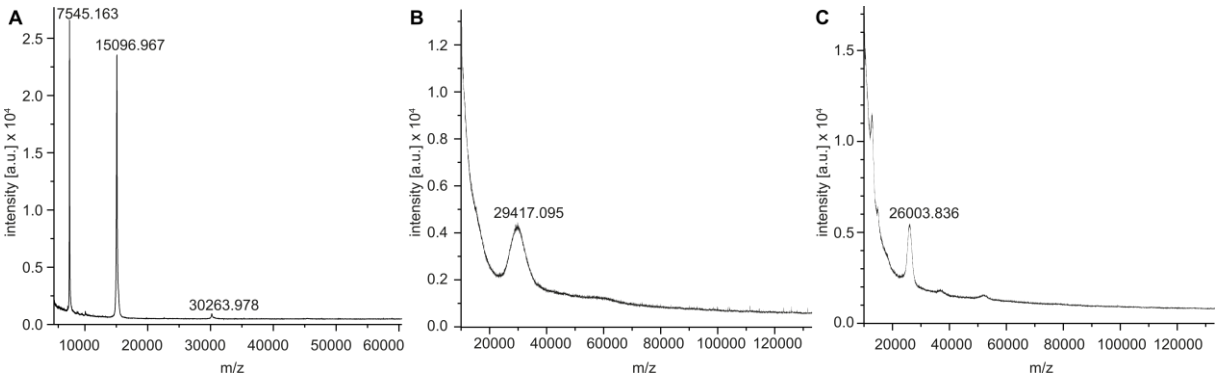

Figure 3. MALDI-TOF analysis of (A) hIL-4 WT (expected Mass $+1H^+$: 15095.40) (B) hIL-4-NH-10-LPG (C) hIL-4-NH-10-PEG.

Further analysis by SEC-MALS confirmed the good comparability between masses of hIL-4-NH-10-LPG and -PEG, respectively. For the 40 kDa-bioconjugates, a mass close to its theoretical value (≈ 55 kDa) was obtained for hIL-4-NH-40-PEG, whereas a slightly larger molecular weight was determined for the 40 kDa LPG-analog, most likely due to its larger dispersity being also observed in SDS-PAGE (**Table 1, Figure 1**).

In SEC, hIL-4 WT was retained longest on the column (retention time (r.t.) 35.80 min), as it displayed the smallest hydrodynamic size of all analyzed compounds (Figure 4A). Upon polymer conjugation, elution was shifted to earlier time points, where the hIL-4-NH-LPG bioconjugates eluted a bit later than their PEG-analogs being substantiated by LPG's slightly more compact structure[162] (r.t. 27.11 min (10-LPG) vs. 25.00 min (10-PEG) and 18.79 min (40-LPG) vs. 18.18 min (40-PEG)). We observed this phenomenon previously as well for another *N*-terminally modified protein, displaying a similar SEC-profile of LPG- and PEG-bioconjugates [166].

Table 1. Molecular weight of hIL-4 WT and its bioconjugates determined by SEC-MALS and MALDI-TOF-MS

	SEC-MALS [kDa]	Đ	MALDI-TOF-MS [kDa]
hIL-4 WT	15.6	1.00	15.1
hIL-4-NH-10-LPG	29.8	1.06	29.4
hIL-4-NH-10-PEG	30.9	1.01	26.0
hIL-4-NH-40-LPG	72.9	1.08	n.d.
hIL-4-NH-40-PEG	59.9	1.01	n.d.

n.d.: not determined, Đ: dispersity

The hydrophobic elution behavior of IL-4 WT and its bioconjugates was examined by RP-HPLC analysis using a CN column, which shows stronger separation according to protein hydrophobicity than common C18 columns. As demonstrated from the elution profile in reference to hIL-4 WT (r.t. 26.31 min), LPG and PEG significantly impact the protein's overall hydrophilicity (**Figure 4B**). Conjugation of PEG to hIL-4 WT decreased its hydrophilicity and led to stronger retention on the column, which was quite similar for 10 kDa (r.t. 27.13 min) and 40 kDa PEG (r.t. 26.95 min). The slightly earlier elution of the 40 kDa PEG bioconjugate might be attributed to its larger sterical shielding against interaction with the column matrix. Due to the combination of its hydrophilic oxygen atoms and hydrophobic ethylene units, PEG displays amphiphilic properties. The stronger retention on reversed-phase columns has been shown previously for other PEGylated biomolecules which confirms our findings from HPLC analysis [353-355]. In contrast, conjugation of 10 kDa LPG to hIL-4 WT (r.t. 25.23 min) distinctly increased the hydrophilicity, therefore displaying earlier elution. This effect was even more pronounced in the case of 40 kDa LPG (r.t. 23.66 min), confirming a chain-length dependent effect for LPG.

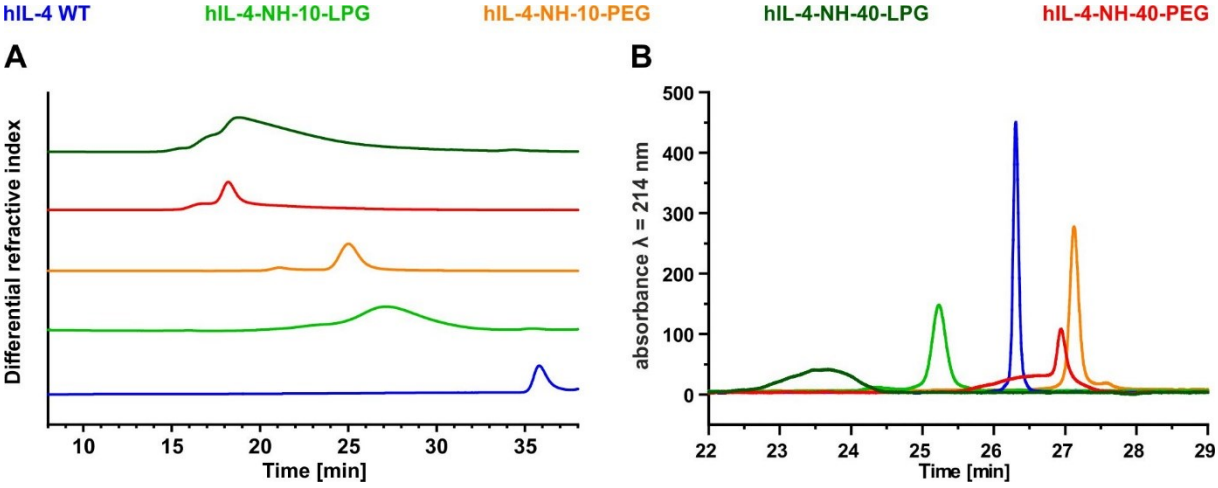

Figure 4. (A) SEC-traces and (B) RP-HPLC analysis of hIL-4 WT and its bioconjugates.

Determination of secondary structure and hydrodynamic size

To exclude perturbance of hIL-4's secondary structure after polymer modification, circular dichroism was employed for structural characterization. hIL-4 WT shows a strong alpha helical motif, displaying three extrema at 193, 208 and 222 nm [184]. After polymer conjugation, no significant changes in the overall alpha-helical structure of hIL-4 WT were observed. (**Figure 5A**). There was no evidence of random-coil or beta-sheet formation present therefore supporting structural retainment of the bioconjugates, independent of polymer type or length.

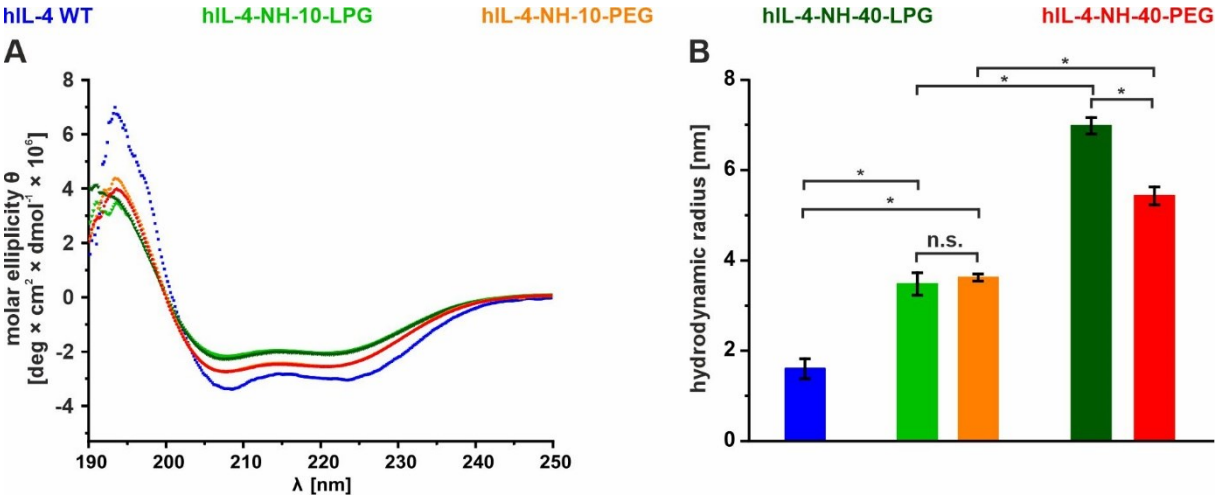

Figure 5. (A) CD-spectra of hIL-4 WT and its bioconjugates at 20 °C (n = 3). Data for hIL-4 WT adapted from Ref. [198], with permission from Wiley-VCH Verlag GmbH & Co. KGaA, Weinheim (License Number: 5154190195649). (B) Hydrodynamic radius of hIL-4 WT and its bioconjugates at 25 °C (n = 3, hIL-4-NH-10-LPG: n = 2). *p ≤ 0.05 (Data analyzed using one-way ANOVA).

Hydrodynamic size of hIL-4 bioconjugates

Dynamic light scattering was employed to determine the hydrodynamic size of the bioconjugates. hIL-4 WT showed a radius of 1.6 nm at pH 7.4, which was close to earlier reported values obtained from similar molecular weight proteins (**Figure 5B and Table 2**) [356]. Conjugation of a single polymer led to a distinct increase in size, that was even more pronounced in the case of the 40 kDa bioconjugates thereby confirming a chain-length dependent volume expansion. PEG's known ability to form stable hydration layers consisting of around three water molecules per monomer unit[357] impacts the overall hydrodynamic volume of protein conjugates, possibly attributed similar for LPG. Furthermore, the highly flexible PEG chain of a mono-bioconjugate usually shows random-coil structure adjacent to the protein (dumbbell-model)[245], leading to a larger overall size.

Despite its higher abundance of OH-groups in polymer backbone, differences between 10 kDa LPG- and PEG-conjugates were not significant, with IL-4-NH-LPG-10 kDa being slightly more compact, which confirms our findings from SEC. The hIL-4-NH-40-LPG bioconjugate was slightly larger than its PEG-analog, which is likely attributed to a salt effect in DLS, whereas SEC confirmed comparable hydrodynamic sizes between the LPG- and PEG-40-bioconjugate. Previous studies by various methods showed, that high molecular weight LPG alone (100 kDa) displayed a distinct smaller size than its PEG-analog of same nominal weight (7.4–7.6 nm difference in radius)[162]. However, in our case we did not observe such a clear difference between the LPG- and PEG-bioconjugates within the molecular weight range used in this study. We speculate this distinct compactness might only be pronounced for the free polymer bearing larger chain lengths and therefore higher molecular weights.

***In vitro* activity of hIL-4 bioconjugates**

To assess the impact of polymer conjugation on hIL-4's *in vitro* activity, we tested our bioconjugates in a HEK 293 cell line expressing IL-4-Rα and IL-13Rα1. Binding of hIL-4 WT to IL-4-Rα is recognized by IL-13Rα1 resulting in a dimerization of the receptor, which triggers a tyrosine kinase (Tyk2, JAK1)-mediated translocation of STAT6 into the nucleus[358]. The latter promotes expression of secreted embryonic alkaline phosphatase (SEAP), which can be finally determined in a colorimetric assay.

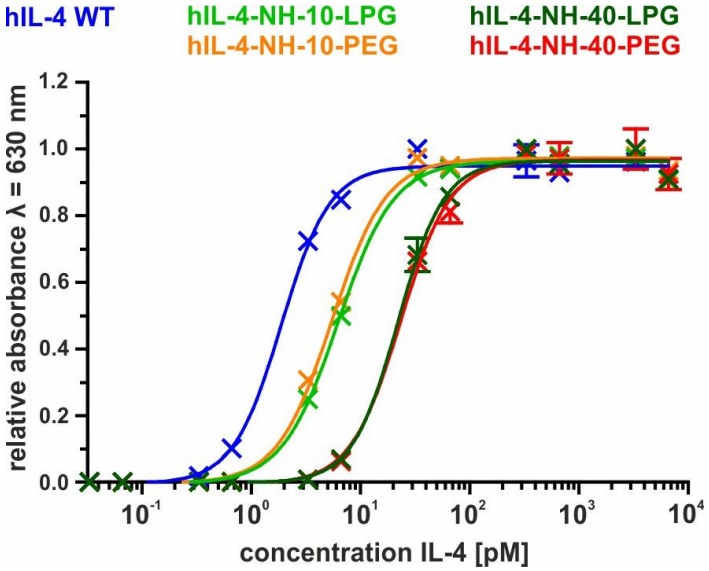

Figure 6. SEAP assay of HEK Blue IL-4/IL-13 cells after 20 h of stimulation with hIL-4 WT and its bioconjugates. Data points represent mean with SD (n = 3).

hIL-4 WT binds to its IL-4Rα-subunit in the pM range[359], which was confirmed by an EC50-range of 1.7 – 2.1 pM in our assay (**Figure 6, Table 2**). Upon polymer conjugation, the biological activity of hIL-4 WT diminished, with hIL-4-NH-10-LPG and hIL-4-NH-10-PEG displaying an approximately three-fold reduced bioactivity. Further extension of the polymer chain resulted in an almost twelve-fold decrease of receptor activation. (EC50: 20.0 – 24.2 pM and 20.8 – 25.9 pM for hIL-4-NH-40-LPG and -40-PEG, respectively). The loss in bioactivity thereby scaled proportionally to the increase in polymer molecular weight, as each additional 10 kDa polymer-unit resulted in an approximately three-fold reduction of *in vitro* activity of hIL-4 WT (Table 2). Despite their different hydrophilicity profile, LPG- and PEG-bioconjugates of same nominal weights displayed comparable biological activities, which is in line with other LPG- and PEG-bioconjugates reported [166, 288]. Therefore, we assume the rationale behind diminished biological potency originates from steric hindrance caused by larger hydrodynamic sizes rather than from variations in the bioconjugates hydrophilicity.

In another study by Lühmann *et al.*, 4 kDa poly(2-methyloxazoline) (PMeOx) was employed for the site-specific modification of hIL-4 followed by characterization of its *in vitro* activity with a similar SEAP-assay as applied here [184]. The SEAP-expression level of PMeOx-hIL-4 was close to unmodified hIL-4 WT but diminished about factor 1.2–1.4, which is proportionally in line with the results obtained for our hIL-4-NH-LPG and -PEG bioconjugates. PMeOx displays comparable hydrophilicity to PEG, but a slightly smaller hydrodynamic size, which might be beneficial in maintaining the biological activity of proteins [178, 360]. Coupling of PMeOx occurred at an alkyne-functionalized lysine at position #K42, which is in close proximity to hIL-4's *N*-terminus therefore allowing a certain comparability with the bioconjugates investigated here. However, the molecular weight of the polymers is different (4 kDa vs. 10 and 40 kDa, respectively) which impedes a direct contrasting of the *in vitro* activity of the respective bioconjugates.

Plasma stability and HSA-binding of hIL-4 WT and its bioconjugates

To reveal potential benefits through polymer conjugation impacting the plasma stability of hIL-4 WT, we incubated the free protein or its bioconjugates for 24 h in human plasma and collected samples at predetermined timepoints. No significant decrease in hIL-4 WT content in plasma was observed for up to 24 h therefore demonstrating good stability *in vitro* (**Figure 7A**). Conjugation of LPG or PEG of different molecular weights to hIL-4 WT had no significant impact on its plasma stability, as all bioconjugates remained stable for up to 24 h, which confirms previous data for PEGylated murine IL-4 [233].

Table 2. Important biological parameters of hIL-4 WT and its bioconjugates. Hydrodynamic radius is displayed as mean ± SD (n = 3, *n=2). EC50 and K_D values are displayed as 95% confidence intervals.

	Hydrodynamic radius	EC50 [pM]	K_D to HSA [nM]
hIL-4 WT	1.6 ± 0.2	1.7-2.1	19.5-65.3
hIL-4-NH-10-LPG*	3.5 ± 0.3	5.8-6.7	281.1-347.2
hIL-4-NH-10-PEG	3.6 ± 0.1	5.1-5.8	93.7-255.1
hIL-4-NH-40-LPG	7.0 ± 0.2	20.0-24.2	126.1-286.6
hIL-4-NH-40-PEG	5.4 ± 0.2	20.8-25.9	298.9-332.0

Besides stability, we further investigated binding of hIL-4 WT and its bioconjugates to the most abundant plasma protein human serum albumin (HSA). In pharmaceutical development, plasma protein binding is of high interest, as its extent usually impacts bioavailability and -distribution of drugs. HSA is often used as a target to increase blood circulation time by incorporating albumin-binding motifs on the target protein[361, 362], or direct fusion to an albumin molecule [363]. Figure 7B shows the binding curves for hIL-4 WT and its LPG- and PEG-bioconjugates, where free hIL-4 WT displayed relatively strong binding in the nM-range (k_D = 42.4 nM). Upon polymer conjugation, the affinity to HSA decreased with ascending polymer length in the case of hIL-4-PEG-conjugates (k_D = 159.4 nM and 315.5 nM for hIL-4-NH-10-PEG and -40-PEG, respectively), which we mostly attribute to steric hindrance and the stealth effect of PEG [364]. Furthermore, PEG might prevent hydrophobic interactions between hIL-4 WT and HSA due to its amphiphilic nature [365-367]. The LPG-variants of hIL-4 WT on the other hand showed an inverse behavior regarding HSA-affinity, with the larger hIL-4-NH-40-LPG displaying superior affinity to HSA (k_D = 206.3 nM) compared to its 10-kDa analog (k_D = 314.1 nM). We assume that the distinct higher hydrophilicity of the hIL-4-NH-40-LPG bioconjugate might promote HSA-binding to hIL-4 WT, even though differences are only modest. Even though the overall HSA binding diminished in comparison to hIL-4 WT, this minor effect will be likely negligible for the circulation half-life of hIL-4-LPG bioconjugates. hIL-4 WT alone shows a serum half-life of only 19 min in humans[368], which can already be extended six-fold in mice through the addition of a 10 kDa PEG moiety[233] showing as similar HSA binding properties as hIL-4-NH-40-LPG (**Figure 7B**). Therefore, an extended circulation time of

hIL-4-LPG bioconjugates will be mostly attributed to an increase in hydrodynamic size rather than to their binding to HSA.

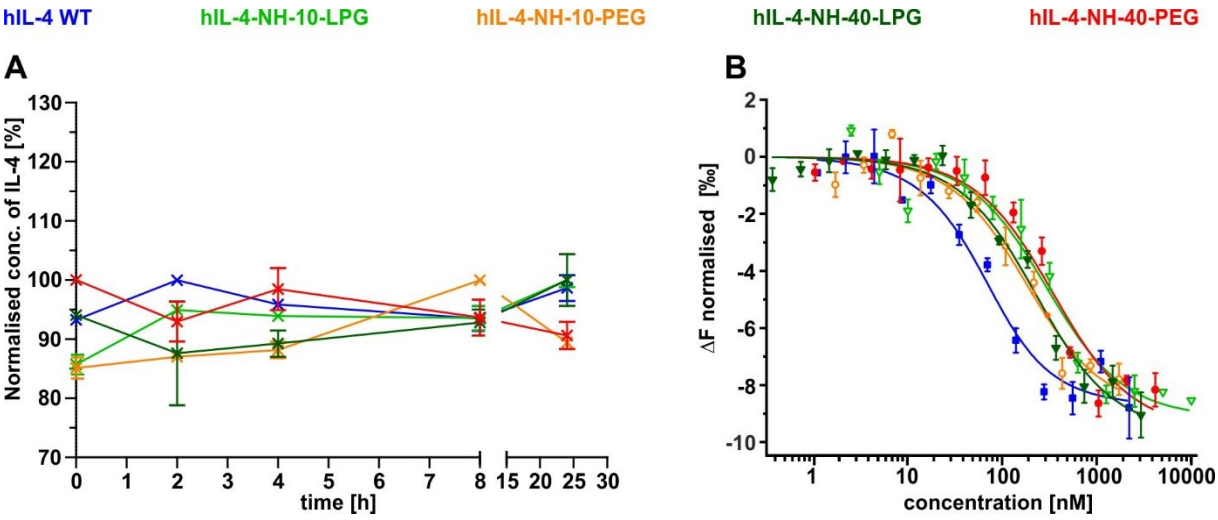

Figure 7. (A) ELISA quantification of hIL-4 WT and its bioconjugates after incubation in human plasma for 24 h. (B) Binding analysis of hIL-4 WT and its bioconjugates with fluorescently labeled HSA upon thermophoresis. Each data point represents mean with SD (n = 3).

Binding of LPG, PEG and its hIL-4-bioconjugates to anti-PEG antibodies

The immunogenicity of PEG is mostly elicited in combination with highly immunogenic, non-human proteins, rather than from the PEG-moiety itself. The extent of anti-PEG antibody formation *in vivo* thereby correlates with the immunogenicity of the conjugated protein.[369] To disclose differences between LPG and PEG in terms of anti-polymer antibody formation, we speculate that human IL-4 might not represent the best model protein for this purpose. Other proteins with higher immunogenicity from a different host might be better candidates for this type of study. Therefore, we rather focused on the antigenicity and cross-reactivity of LPG to anti-PEG antibodies by analyzing the free polymers and the respective hIL-4-bioconjugates *via* ELISA (**Figure S5**) and surface plasmon resonance (SPR) (**Figure 8**) techniques. To examine the cross-reactivity of LPG to anti-PEG antibodies, we analyzed the free polymers and the respective hIL-4-bioconjugates via ELISA (**Figure S5**) and surface plasmon resonance (SPR) (**Figure 8**). For binding of PEG to its antibodies, typically 3–6 oxyethylene units are necessary [154]. Previous studies on the cross-reactivity of other polymers towards commercial anti-PEG antibodies revealed the importance of the C-C-O motif in the polymer backbone which promotes specificity via hydrophobic interactions of the ethylene units with the respective antibody [370]. As an increase in the hydrophilicity of the C-C-O unit was speculated to mitigate this interaction,[370] we aimed to examine this on LPG and its hIL-4-bioconjugates.

The hIL-4-NH-PEG bioconjugates showed clear binding to the respective immobilized anti-PEG antibodies, which was diminished in the case of the hIL-4-LPG bioconjugates (**Figure S5A**). The latter thereby followed the curve of unmodified hIL-4 WT suggesting non-specific binding to anti-PEG antibodies with no significant contribution of the LPG-unit. The BSA-PEG standard used in this assay consisted of BSA modified with 10 PEG-moieties of 5 kDa therefore leading to a stronger signal at

lower concentrations. Furthermore, analysis of the free polymers unraveled significant binding of mPEG to anti-PEG antibodies directed against the terminal methoxy group and C-C-O backbone, whereas LPG of same molecular weight displayed negligible binding (**Figure S5B**). Similar results were found for the free polymers by employing SPR (**Figure 8**), where LPG displayed no substantial binding to commercial anti-PEG antibodies directed against the PEG-backbone or its terminal methoxy group (**Figure 8A**). In contrast, mPEG demonstrated clear binding to both tested antibodies (**Figure 8B**). Our results indicate that increasing the hydrophilicity of the C-C-O motif could lead to a diminished binding to anti-PEG antibodies. However, to fully confirm this, more anti-PEG antibodies of other subclasses (IgM, IgG) with varying specificity would need to be tested.

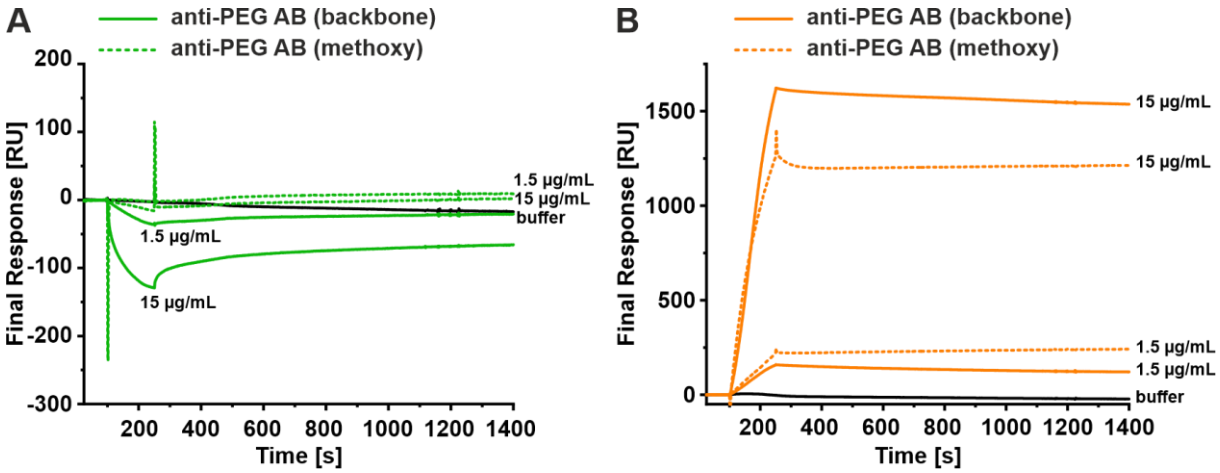

Figure 8. Binding of anti-PEG antibodies at indicated concentrations to (A) immobilized LPG and (B) immobilized mPEG.

Conclusion

In this article, we demonstrate site-selective *N*-terminal ligation of human interleukin-4 WT with the two distinct polymer types, linear polyglycerol and poly(ethylene glycol). *N*-terminal conjugation was achieved through a reductive alkylation approach at acidic pH yielding the respective mono-conjugates of hIL-4 WT, which were subsequently contrasted in terms of molecular size, *in vitro* stability, bioactivity and HSA-binding properties. hIL-4-PEG and -LPG bioconjugates of same nominal weights showed comparable molecular masses and hydrodynamic sizes. The alpha-helical structure of hIL-4 WT was retained after polymer modification, whereas the bioactivity decreased in a molecular weight dependent manner, where hIL-4-PEG and -LPG bioconjugates of same nominal weights behaved similar. All bioconjugates as well as the free protein showed no degradation for up to 24 h in human plasma therefore indicating good *in vitro* stability. The affinity of hIL-4 WT to the plasma protein HSA generally diminished after polymer conjugation. Furthermore, we found a reduced binding for free LPG and its hIL-4-LPG bioconjugates to anti-PEG antibodies, which was in contrast to free PEG and hIL-4-PEG bioconjugates.

To our knowledge, this is the first study describing the *N*-terminal polymer modification of hIL-4 WT. We believe the data presented here could serve as a fundamental to unravel differences in the pharmacokinetic and pharmacodynamic *in vivo* profile of PEGylated and PGylated forms of hIL-4 WT. From an *in vitro* perspective, *N*-terminal hIL-4-LPG bioconjugates showed equivalent biological performance to their PEG-analogs therefore highlighting the good potential of LPG as an alternative polymer platform to improve the pharmacokinetics of small biologics.

Associated Content

Supporting Information Available

The following files are available free of charge: Polymer synthesis and characterization, SDS-gels, chromatograms, mass spectra, anti-PEG antibody ELISAs.

Author Information

Corresponding author

*E-mail: haag@chemie.fu-berlin.de

Notes

M. Tully and N. Hauptstein have contributed equally to this work. The authors declare no competing financial interest.

Acknowledgements

Paria Pouyan and Daniel Kutifa (Freie Universität Berlin) are thanked for the supply of linear polyglycerols. For all NMR and MS measurements, we would like to acknowledge the assistance of the Core Facility BioSupraMol supported by the Deutsche Forschungsgemeinschaft (DFG) and the division of Mass spectrometry at the Institute of organic chemistry, University of Wuerzburg for their help in MALDI-TOF MS analysis of bioconjugates. This work was supported by the Bundesministerium für Bildung und Forschung (grant number 13XP5049A/B).

Supporting Information to Chapter 5

Experimental

Dialysis tubes, molecular weight cut-off (MWCO) 1 kDa, were from Carl Roth (Karlsruhe, Germany). 40 kDa LPG-N_3 was purified additionally by Tangential Flow Filtration (RC-membrane, MWCO 10 kDa). Gel-permeation chromatography (GPC) of the LPG-N_3 polymers was performed on an Agilent HPLC system containing an IsoPump (G1310A), a refractive index detector (G1362A) and a manual injection unit (G1328B) (Agilent 1100 Series, PSS, Mainz, Germany). 0.1 M $NaNO_3$ was used as mobile phase on three Suprema size exclusion columns (calibrated against pullulan (342–708,000 Da)) connected in series to determine molecular weight distribution of the LPGs (**Table S1**).

Synthesis of LPG-10, LPG-40 and PEG-40-aldehyde

The synthesis of LPG- and PEG-aldehyde follows a previous protocol[166] and is described here in short. LPG-Br was synthesized starting from the monomer ethoxy ethyl glycidyl ether (EEGE)[371] through anionic ring-opening polymerization according to Weinhart, *et al.*[372] In short, tetraoctylammonium bromide as initiator was added to a dried Schlenk flask under inert atmosphere, melted under vacuum and dissolved in dry toluene after cooling to room temperature. Subsequently, EEGE was added while cooling to 4 °C with an ice bath and the polymerization was initiated by fast addition of the catalyst triisobutylaluminium *via* syringe. After 16 h at room temperature, the reaction was quenched with ethanol and further purified by several cycles consisting of freezing and subsequent centrifugation, followed by final dialysis against acetone. The obtained product LPEEGE-Br was then deprotected over night in 3 % HCl (conc.), azidated and subsequently reduced with Tris(2-carboxyethyl)phosphine-hydrochloride (TCEP-HCl) to yield the respective LPG mono amine. In a final step, LPG-amine was modified with the short linker 6,6-dimethoxyhexanoic acid (synthesized from 2-Hydroxycyclohexanone dimer, as described previously[151, 373]) in DMF in the presence of N,N,N′,N′-Tetramethyl-O-(N-succinimidyl)uronium hexafluorophosphate (HSTU) and N,N-Diisopropylamine. After 72 h, the reaction mixture was dialyzed against water (three days) followed by acidic deprotection (3 % HCl conc.) and lyophilization to yield the aldehyde-bearing polymer as slightly yellow solid.

Synthesis of mPEG-40-aldehyde followed the same protocol as described above, starting from the amine-stage with the commercially available mPEG-40-NH_2-HCl.

Endoproteinase GluC in-gel digest

In gel digest of hIL-4-NH-10-PEG was performed as described before with GluC (Promega) in 100 mM ammonium bicarbonate buffer instead of Elastase[198]. After 5% TFA extraction following overnight digest MALDI-MS was performed as described in the experimental section. GluC was chosen over Trypsin to yield a longer amino acid chain rest, as Il-4 contains a lysine at position 2, leaving only a 2 AA residue.

Table S1. Molecular weight characteristics and level of aldehyde content of the different polymers used in this study. (adapted from ref [166])

polymer sample	M_n [g/mol]	M_w [g/mol]	Đ	end group conversion to protected aldehyde [%]
10-LPG-N_3	12222	14620	1.20	66
40-LPG-N_3	49377	64421	1.30	61
10-mPEG-CHO	-	11153[a]	1.05	>95
40-mPEG-NH_2-HCl	-	42266[b]	1.03	13
10-LPG-N_3	10518	13979	1.33	-
10-mPEG-N_3	-	11153[a]	1.05	-

The number in the polymer sample describes the nominal molecular weight in kDa. The properties of PEG were used as supplied by the manufacturer's data sheet. The calculation of the number of protected aldehyde-functionalized polymer chains is described previously.[166] Đ = dispersity. [a]M_p-value. [b]MALDI-TOF.

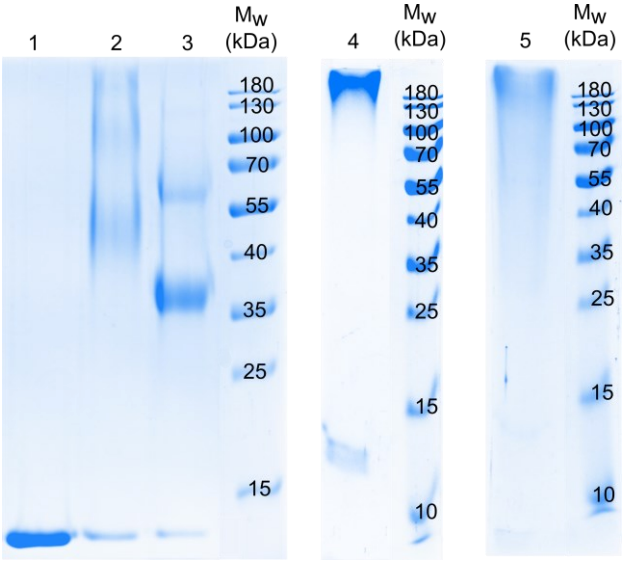

Figure S1. SDS-PAGE of coupling reactions of hIL-4 WT with its different polymers. (1) hIL-4 WT, (2) hIL-4-NH-10-LPG, (3) hIL-4-NH-10-PEG, (4) hIL-4-NH-40-LPG, (5) hIL-4-NH-40-PEG.

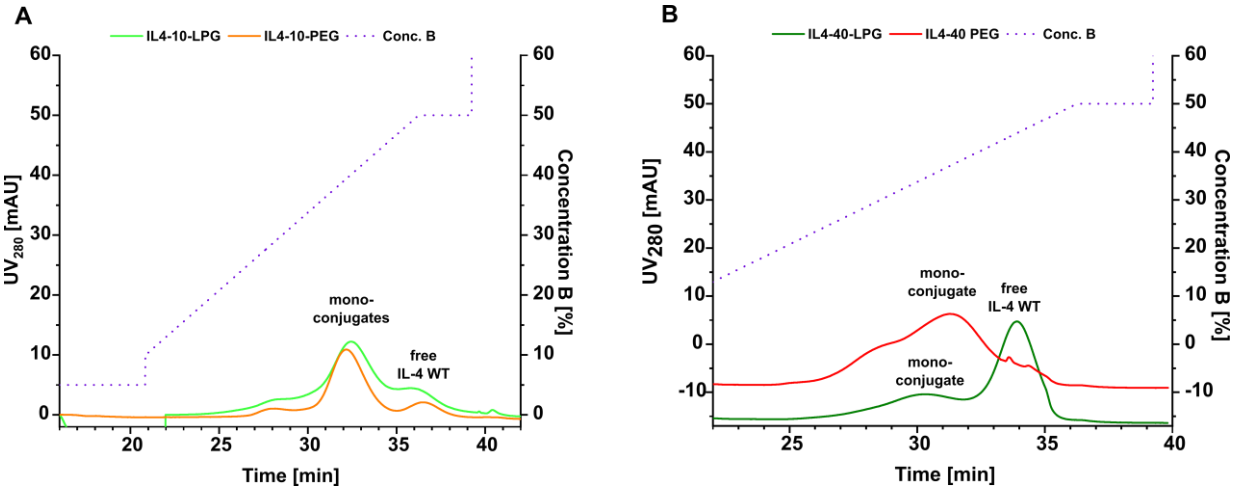

Figure S2. FPLC cation exchange chromatogram of purification of (A) hIL-4-NH-10 kDa and (B) hIL-4-NH-40 kDa conjugates.

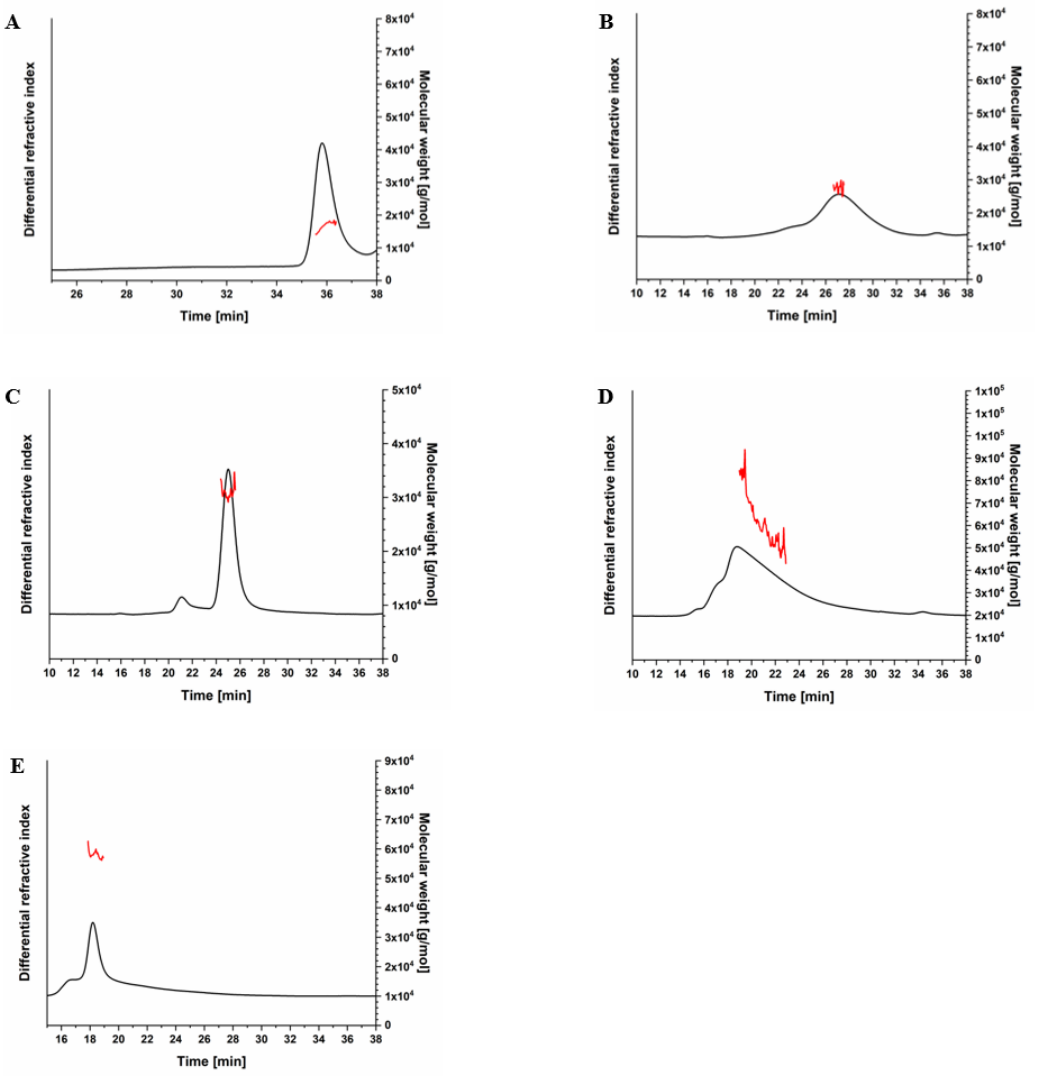

Figure S3. SEC-MALS data of hIL-4 WT and its LPG- and PEG-conjugates. (A) hIL-4 WT (B) hIL4-NH-10-LPG, (C) hIL-4-NH-10-PEG, (D) hIL-4-NH-40-LPG, (E) hIL-4-NH-40-PEG.

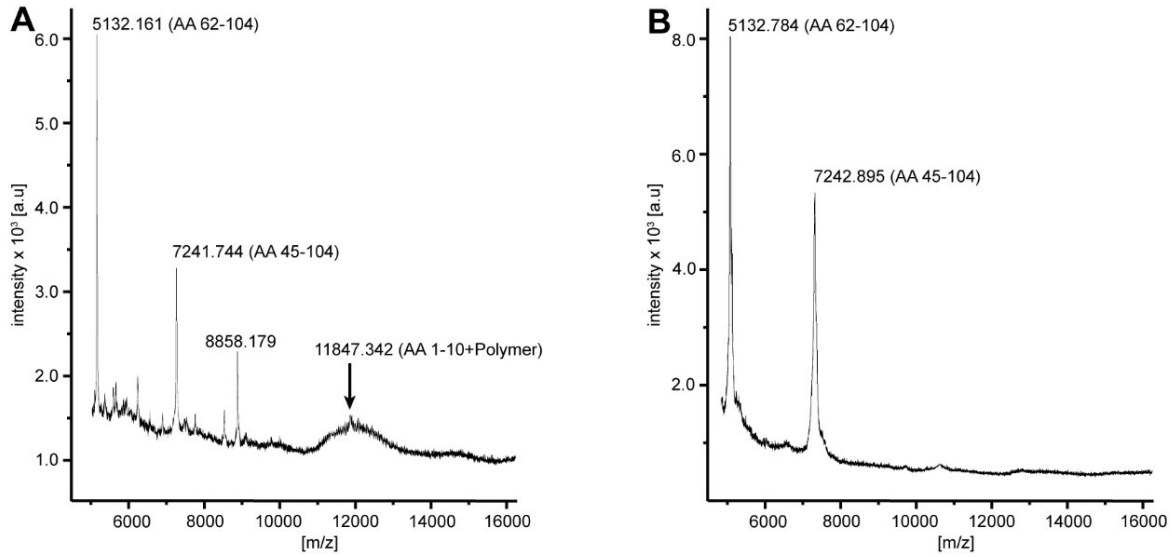

Figure S4. Mass spectra of peptide mixtures after GluC in-gel digestion. (A) GluC in-gel digest of hIL-4-NH-10-PEG. The arrow indicates the *N*-terminal fragment bearing the 10 kDa PEG, which was only found in the conjugate, with a peak mass of 11,847 Da (1-10: 1275.48 Da + 10572 Da PEG). (B) GluC in-gel digest of hIL-4 WT.

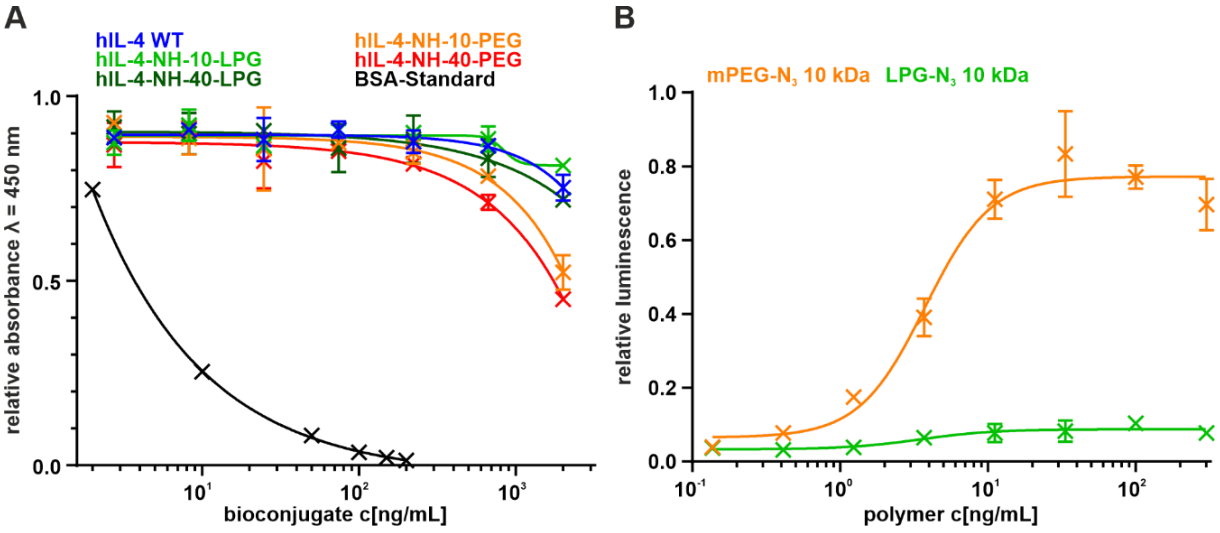

Figure S5. (A) Anti-PEG ELISA of hIL-4 WT and its bioconjugates using a recombinant monoclonal antibody directed against the PEG backbone structure. Each data point represents mean with SD (n = 2). (B) Anti-PEG ELISA of 10 kDa polymers using a combination of a monoclonal antibody directed against the terminal methoxy group of mPEG and a monoclonal antibody directed against the PEG backbone. Each data point represents mean with SD (n = 2).

Chapter 6 – Chemo-enzymatic PEGylation/POxylation of murine Interleukin-4

Dorothee Haas‡, Niklas Hauptstein‡, Michael Dirauf, Marc D. Driessen, Matthias Ruopp, Ulrich S. Schubert, Tessa Lühmann, Lorenz Meinel

‡ These authors contributed equally to this work.

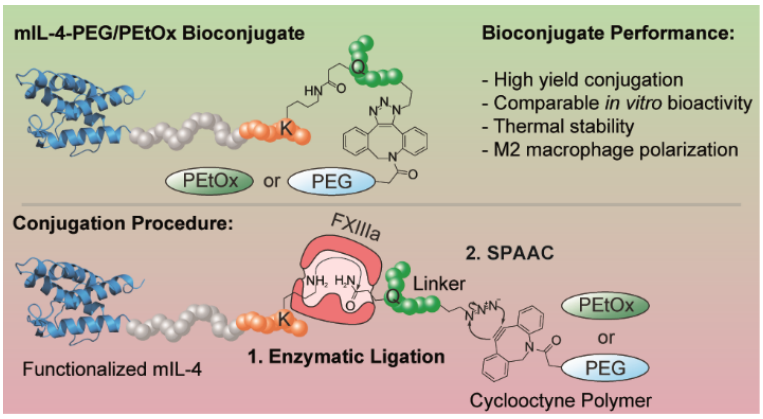

Keywords: codon expansion; polyethylene glycol; poly(2-ethyl-2-oxazoline); Interleukin-4; Factor XIIIa

Abstract

Interleukin-4 (IL-4) is a potentially interesting anti-inflammatory therapeutic, which is rapidly excreted. Therefore, serum half-life extension by polymer conjugation is desirable, which may be done by PEGylation. Here, we use PEtOx as an alternative to PEG for bioconjugate engineering. We genetically extended murine IL-4 (mIL-4) with the D-domain of insulin like growth factor I (IGF-I), a previously identified substrate of transglutaminase (TG) Factor XIIIa (FXIIIa). Thereby, engineered mIL-4 (mIL-4-TG) became an educt for TG catalyzed C-terminal, site-directed conjugation. This was deployed to enzymatically couple an azide group containing peptide sequence to mIL-4, allowing C-terminal bioconjugation of polyethylene glycol or poly(2-ethyl-2-oxazoline). Both bioconjugates had wild type potency and alternatively polarized macrophages.

Introduction

IL-4 polarizes macrophages to the alternative M2 phenotype with potential therapeutic value for inflammatory conditions including rheumatoid arthritis.[233, 374, 375] IL-4 activity is species specific for mouse (mIL-4)[233] and humans (hIL-4).[184] This study focuses on mIL-4. The human- as well as the murine IL-4 are small proteins with a molecular weight around 13.5 kDa. IL-4 is cleared rapidly by renal excretion after i.v. injection resulting in serum half-life times of around 20 min in humans, thereby limiting its therapeutical possibilities.[368] Previous studies presenting mIL-4 mutants with an unnatural amino acid (uAA) being introduced by means of genetic code expansion were successfully conjugated to polyethylene glycol (PEG) and resulted in bioactive and pharmacokinetically improved bioconjugates.[184, 233] The advantage of specific bioconjugation through uAA including product homogeneity comes at the expense of yield, costs of goods and complex production efforts.[376] Alternatives include bioinspired, enzymatic bioconjugation approaches.[377, 378] One approach is by using tansglutaminases (TGases), enzymes that catalyze the formation of an isopeptide bonds among proteins catalyzing a nucleophilic attack of lysine (K) at glutamine (Q).[379] TGases have been used for the immobilization of proteins to extracellular matrices,[380] covalent protein incorporation in fibrin hydrogels, [381-385] and site-specific modification of antibodies.[386] The circulating coagulation factor FXIII, which is activated in a thrombin-dependent manner to its active form FXIIIa is a therapeutically used TGase.[387] This activity of FXIIIa was successfully used for a variety of substrates, for example for short peptides derived from α_2-plasmin inhibitor[388] as well as the D-domain of IGF-I.[329]

PEG is a frequently used polymer for bioconjugation, reflecting its known safety profile, biocompatibility and ability for addressing pharmacokinetic challenges of biologics with improper disposition kinetics.[153, 335] However, recent studies reported rare cases of PEG accumulation in liver, bone, skin, and other tissues with potential safety concerns.[320, 339, 389] Further studies reported the formation of anti-PEG antibodies after repeated exposure with potential impact on the bioconjugates' terminal half-life. Although in another context than bioconjugation, PEG related safety aspects were discussed for mRNA vaccination.[157, 390] These findings elicited the search for alternative polymers. One

potential class are hydrophilic poly(2-oxazoline)s (POx) such as poly(2-ethyl-2-oxazoline)s (PEtOx)with ethyl moieties.[178, 179, 182, 391-394] For example, a site-specific POxylated form of the dopamine receptor antagonist rotigotine was already profiled in patients.[186] Several studies have shown, that PEtOx is comparable to PEG regarding its biocompatibility[177, 185] (red blood cell aggregation,[179] cytotoxicity,[179] potency,[98, 395] serum half-life extension[393]). Especially daily exposure to PEG promotes the formation of anti-PEG antibodies, thereby impairing PEGs initial benefits.[151, 155, 256, 257, 396]

Here, mIL-4 was used for biorthogonal chemo-enzymatic bioconjugation in a site-specific manner. The general strategy was to recombinantly integrate IGF-I's D-domain, a known substrate to FXIIIa, into the mIL-4 sequence (**Scheme 1A**). The resulting mIL-4 mutant was enzymatically decorated with an azide group containing peptide, thereby becoming an educt for copper-free click chemistry (**Scheme 1B**) with dibenzocyclooctyne (DBCO) end functionalized PEtOx, or PEG (**Scheme 1C**).

Results and Discussion

We genetically engineered mIL-4-wt and its mutant mIL-4-TG containing an additional hydrophilic peptide spacer and a recognition peptide sequence for FXIIIa at the C-terminus, referred to as mIL-4-TG. This TG recognition peptide sequence (PLKPAKSA) is derived from the D-domain of IGF-I by means of which IGF-I is enzymatically bound to the extracellular matrix (**Scheme 1A**).[93, 329, 377, 378] The use of microbial transglutaminases is an alternative. However, we selected FXIIIa, an FDA and EMA approved drug substance – as of previously demonstrated compatibility with the D-domain of IGF-I.[286, 378] IGF-I is also an FDA approved drug substance.

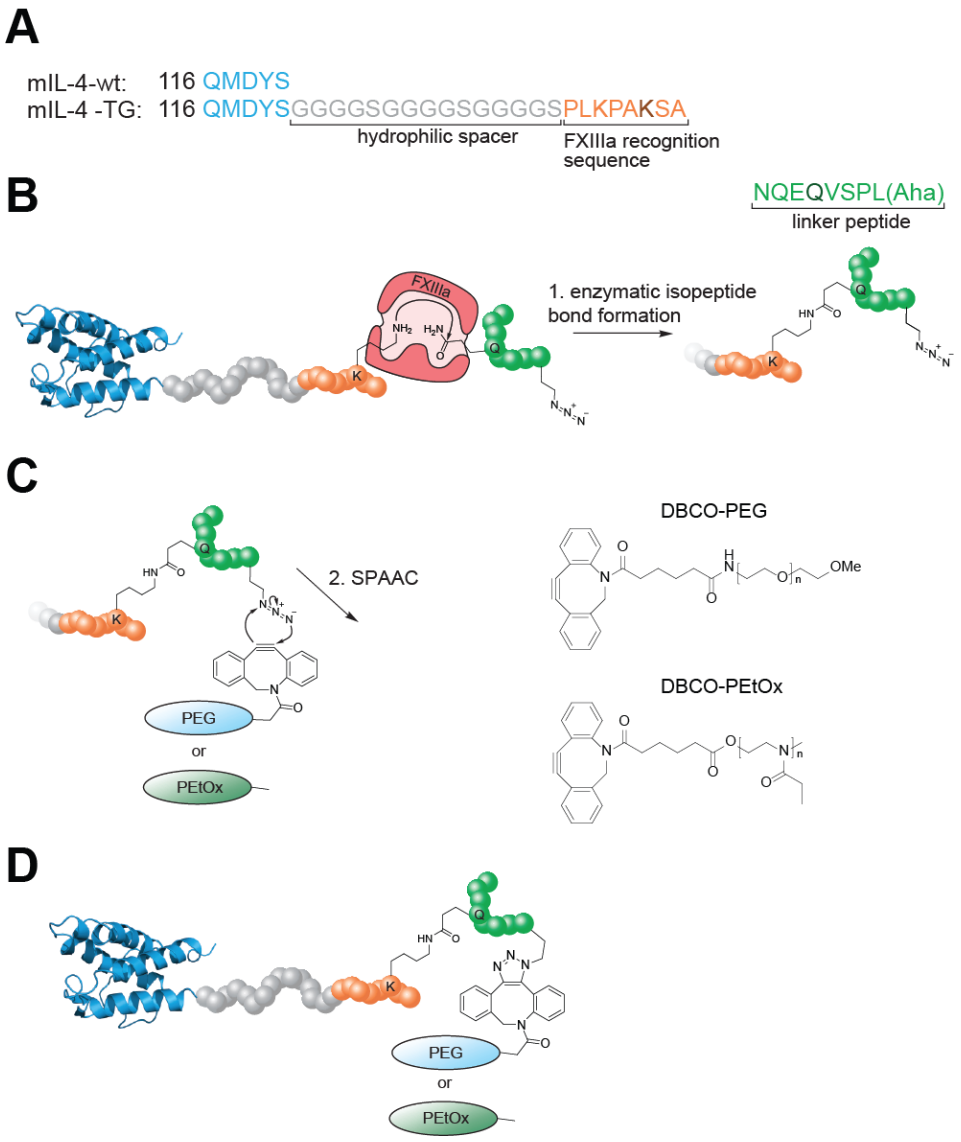

Scheme 1: Site-specific modification of murine IL-4. (A) Amino acid sequence alignment of mIL-4-wt and mIL-4-TG. The C-terminus of the mIL-4-TG mutant carries a hydrophilic $(GGGGS)_3$ spacer (grey) followed by a FXIIIa recognition sequence derived from the IGF-I D-domain PLKPAKSA (orange). (B) The mIL-4-TG mutant was enzymatically coupled by FXIIIa to a linker peptide with the sequence NQEQVSPL containing azidohomoalanine (Aha; green). (C) A DBCO-functionalized polymer (PEG or PEtOx) was 'clicked' to the azide group of the linker peptide resulting in (D), the final mIL-4 bioconjugates.

Factor XIIIa catalyzes a covalent isopeptide bond between the C-terminal lysine (K) of mIL-4-TG and a peptide containing glutamine (Q) and Aha featuring the product for SPAAC reactions (**Scheme 1B**). Subsequently, this product was reacted with either DBCO functionalized PEG or PEtOx (**Scheme 1C**), resulting in PEGylated or PEtOxylated mIL-4-TG, respectively (**Scheme 1D**).

Protein expression in *E. coli* for both cytokines (mIL-4-wt and mIL-4-TG) was optimized **(Figure S1)** starting off our previous studies.[233] To increase the initially low protein yield of recombinantly expressed mIL-4-wt, alanine (A) was introduced N-terminally.[397] As a consequence, the initiator methionine (M) was co-translationally cleaved after translation, which commonly appears, when the 2nd amino acid bears a small side chain.[398] RP-HPLC analysis of the purified cytokines resulted in one major and one small

peak for mIL-4-wt and an unknown impurity, respectively (purity was approximately 88% based on area under the curve comparison**; Figure 1A**). For mIL-4-TG, we identified one additional unknown impurity and an overall purity of about 87%. The purity of these intermediates was not further optimized but optimized for the final product (*vide infra*).

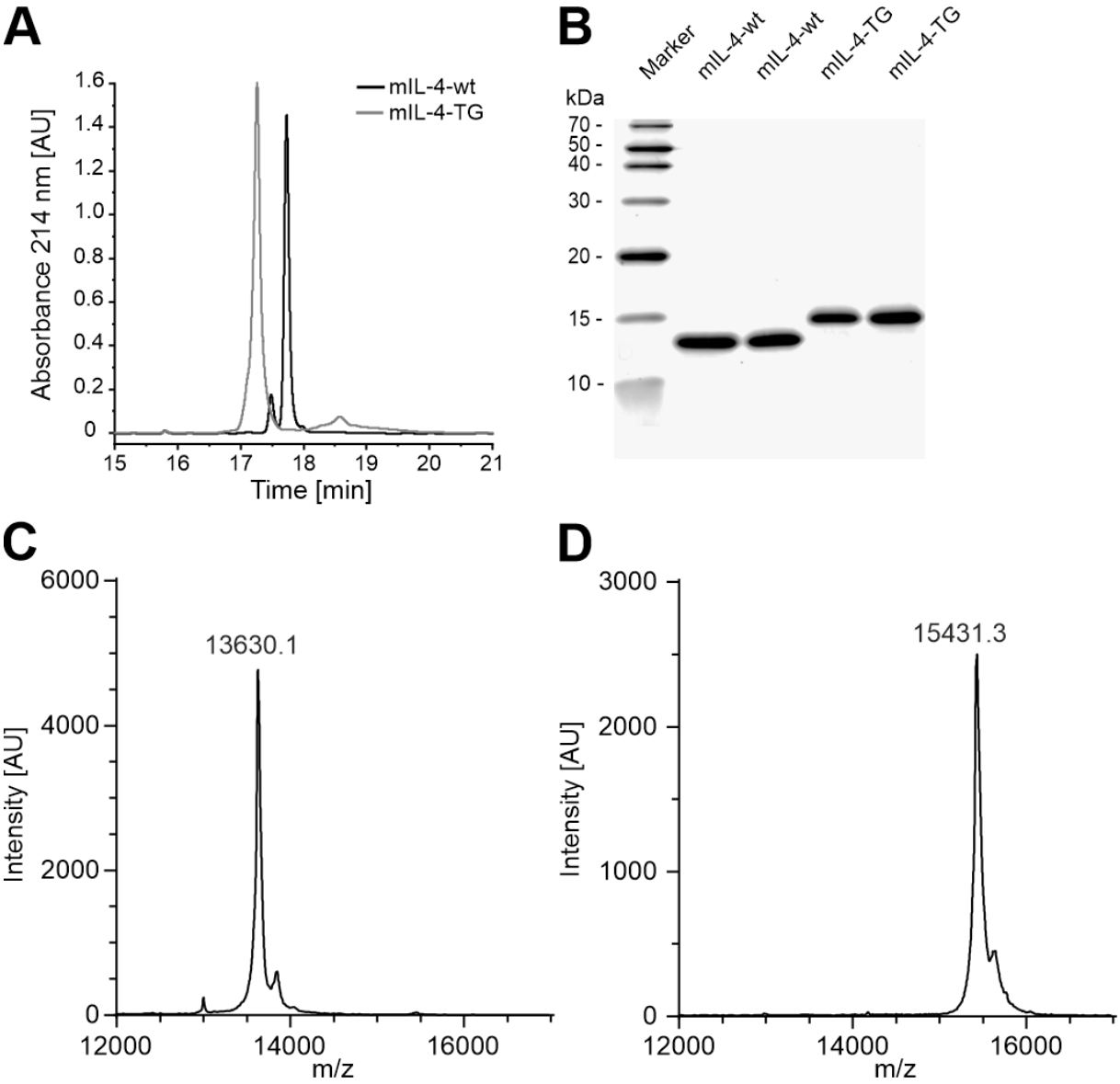

Figure 1. Analytical characterization of mIL-4-wt and mIL-4-TG. (A) RP-HPLC chromatograms of mIL-4-wt (black) and mIL-4-TG (grey). (B) Reducing SDS-PAGE of two batches of mIL-4-wt and mIL-4-TG. (C) MALDI-MS of mIL-4-wt (calculated mass mIL-4-wt + H^+: 13,761.00 Da, calculated mass mIL-4-wt - (M): 13,629.81 Da). (D) MALDI-MS of mIL-4-TG + H^+ (calculated mass: 15,428.76 Da).

Both cytokines migrated as of their expected mass with no additional bands being visible in SDS-PAGE with Coomassie staining (**Figure 1B**). Their identity was further detailed by MALDI-MS (**Figure 1C, D**). The mIL-4-TG was enzymatically reacted with the L-azidohomoalanine (Aha) containing TG peptide (**Figure S2+3**). The resulting products migrated at about 17 kDa (approximately expected mass of mIL-4-TG with one Aha containing linker peptide), one further band at about 18 kDa (approximately

expected mass of the mIL-4-TG with two Aha containing linker peptide), and a third band, possibly as of unreacted mIL-4-TG, were observed (**Figure 2A, B, S3A**).

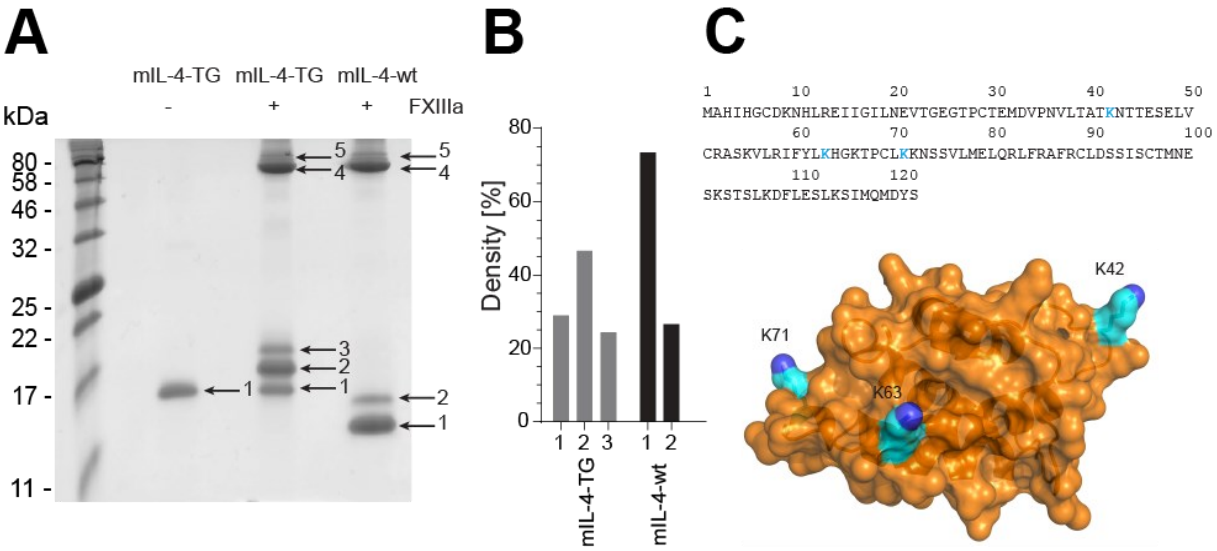

Figure 2: (A) Coupling of linker peptide to mIL-4-TG and to mIL-4-wt 1 = protein, 2 = protein + 1 conjugated peptide, 3 = protein + 2 conjugated peptides, 4 = human serum albumin (is contained in the formulation of FXIIIa for long term stabilization), 5 = FXIIIa. (B) densiometric quantification of bands displayed in A. Band density was measured with ImageJ.[399] (C) Sequence of murine IL-4 and a homology model of murine IL-4 displayed in orange. The model is based on human IL-4 (PDB: 1bbn) modelled with swiss model.[400] Likely TG modified residues K42, K63 and K71 are displayed in cyan in the sequence and on the protein surface.

This assignment was confirmed by MALDI-MS measurements (**Figure S3B**). An optimum reaction time of about 30 minutes (**Figure S3C**) and a stoichiometric ratio of 10:1 for the linker peptide and mIL-4-TG (**Figure S3D**) favored the formation of mIL-4 with one Aha containing linker peptide. A TG recognition peptide sequences within mIL-4-wt was also identified when using the Aha containing linker peptide in presence of Factor XIIIa (**Figure 2A, B**). This resulted in two bands, one band migrating at a molecular weight of mIL-4-wt and another one migrating at a higher molecular weight suggesting mIL-4-wt reacted with one Aha containing linker peptide. These SDS-PAGE findings were further detailed by in-gel trypsin digestion (band #2 mIL-4-wt lane in **Figure 2A**) followed by nano ESI-tandem-MS. Overall achieved sequence coverage was 95% (data not shown). An initial in-gel digest resulted in inconclusive results, possibly resulting from technical difficulties and reflecting challenges in annotation and identification of cross-linked (”branched”) peptides resulting from the isopeptide bonds. These isopeptide bonds are not foreseen in common software packages. Therefore, additional experiments were performed by coupling a hydrazine cleavable biotin-linker to the Aha carrying peptide through DBCO and reacting it in presence of Factor XIIIa with mIL-4-TG or mIL-4-wt. The resulting products were analyzed after tryptic in-solution digest by nano ESI-tandem-MS, but purified before MS by means of the biotin label to enrich protein fragments carrying the peptide. To further reduce possible false positive assignments by the algorithms, the search was subsequently narrowed down to a wildcard range for the peptide (1,338 to 1,342 Da) (**Figure S4**).

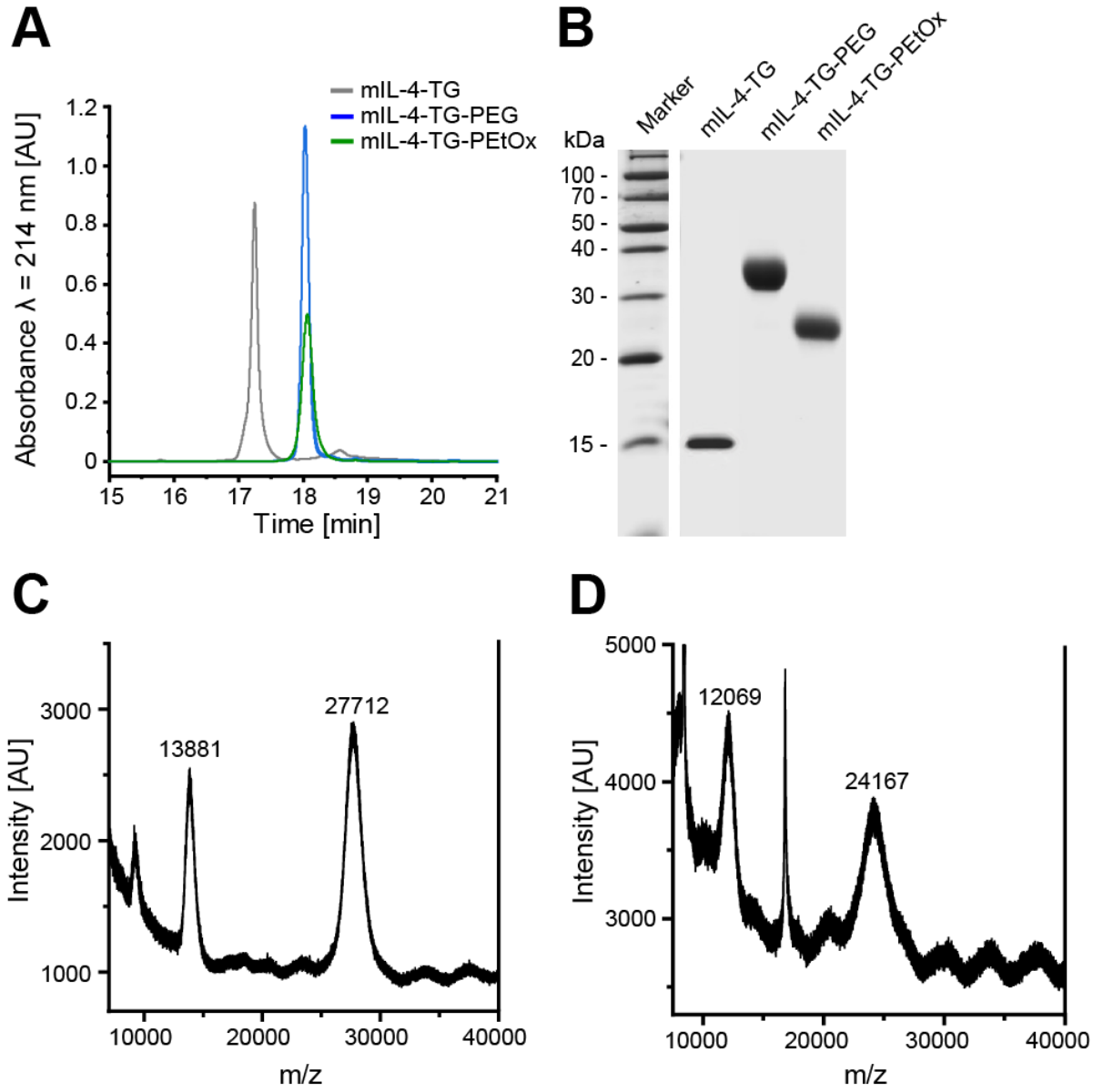

Figure 3: Characterization of mIL-4-TG-PEG and mIL-4-TG-PEtOx. (A) RP-HPLC chromatogram of mIL-4-TG (grey), mIL-4-TG-PEG (blue) and mIL-4-TG-PEtOx (green). (B) SDS-PAGE analysis of purified bioconjugates. (C) MALDI-MS of mIL-4-TG-PEG (calculated mass: 26,500 Da). (D) MALDI-MS of mIL-4-TG-PEtOx (calculated mass: 24,300 Da).

The exact peptide mass was calculated as 1,339.619 Da (Peptide + cleavable linker residue - ammonia loss after isopeptide bond formation). Hence, three TG recognition peptide sequences were identified within mIL-4-wt on top of the engineered additional binding site in mIL-4-TG and one off-target in the artificial linker at K141. The sites (referring to the mIL-4-wt sequence given in Figure S4C) are located at positions K42, K63 or K71, with K42 positioned in the unstructured region between the short β_A-sheet and α_B-helix , K63 positioned at the end of the α_B-helix and K71 positioned at the beginning of the α_C-helix (**Figure 2C**).[401] The three modifications were neither found in mIL-4-wt nor mIL-4-TG based on SDS-PAGE analysis, as only one additional band was found during SDS-PAGE (and not three), indicating that the binding preferences are different among the internal sites and the C-terminal TG-Tag.

It is likely, that only one of the three found sites is the preferred site of modification, with the other two being hardly modified, though we cannot distinctively identify the preferred one based on our gathered data. Although the crystal structure of mIL-4-wt has not been published as of yet, a sequence homology model from structure-elucidated human IL-4-wt was extrapolated and the three TG recognition peptide sequences highlighted, accordingly (**Figure S5**). In contrast to mIL-4-wt, hIL-4-wt had no internal TG recognition sequence for FXIIIa (**Figure S6**).[268]

Two reactions were conducted, thereby decorating the azido functionalized mIL-4-TG with the Aha containing peptide by the FXIIIa catalyzed reaction, and binding DBCO-PEG or DBCO-PEtOx to the Aha containing peptide, respectively (**Figure S7A**). The resulting product was successfully separated by cation exchange chromatography (**Figure S7B, C**) but not by size exclusion chromatography (data not shown) from unreacted educts. Both, mIL-4-TG-PEG and mIL-4-TG-PEtOx peaks had slightly increased retention times in RP-HPLC as compared to mIL-4-TG and purities exceeded 95% for each bioconjugate (**Figure 3A**) and as qualitatively confirmed by SDS-PAGE (**Figure 3B**) and MALDI-MS (**Figure 3C, D and Figure S8**). Additionally, successful conjugation was confirmed by western blot analysis (**Figure S9**).

The unfolding temperatures, determined by differential scanning fluorimetry, of mIL-4-wt and mIL-4-TG were neither impacted by PEtOxylation nor PEGylation (**Figure 4 and Figure S10**). This finding differs from previously published results in which PEtOxylation had a destabilizing effect on the protein, compared to PEG [98] and indicating that polymer effects in bioconjugates are not general, but specific to the respective biologic.

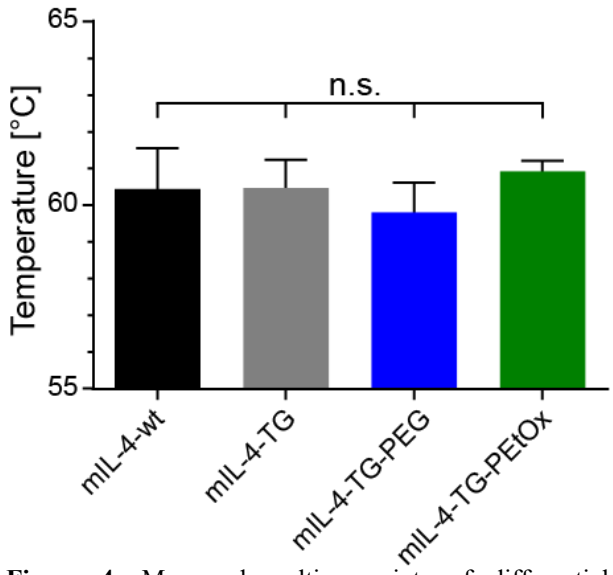

Figure 4: Measured melting points of differential scanning fluorimetry of bioconjugates (n = 4). Standard deviations are indicated with error bars. (mIL-4-wt = black, mIL-4-TG = grey, mIL-4-TG-PEG = blue, mIL-4-TG-PEtOx = green)

Furthermore, retained bioactivity was observed in potency assays using murine T-cell lines for mIL-4-wt, mIL-4-TG, and the PEtOxylated or PEGylated bioconjugates (**Figure 5A, B**). EC_{50} values were comparable among groups, with small but significant differences for the mIL-4-TG-PEtOx group as compared to mIL-4-wt and commercially obtained recombinant mIL-4-wt, respectively (**Figure 5C**).

Further, the impact of bioconjugation on gene expression of relevant immunomodulatory genes in a monocyte derived cell line was analyzed (**Figure 6 and S11**). All cytokines – bioconjugated or not – significantly reduced the expression of M1-polarized macrophage markers

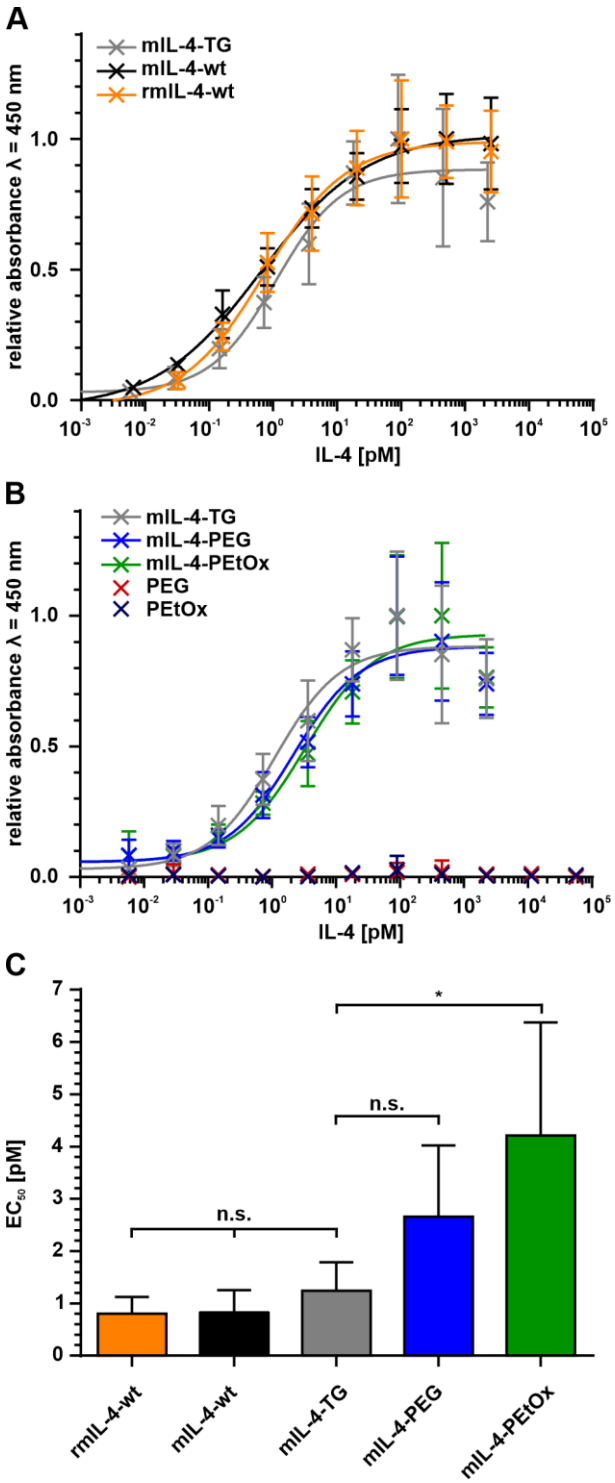

Figure 5: HT-2 clone 5AE cell proliferation in response to (A) mIL-4-wt compared to unconjugated mIL-4-TG. (B) mIL-4-TG and mIL-4-TG-bioconjugates (C) EC_{50} values of A and B. Mean ± SD, $n \geq 5$, one-way ANOVA followed by Tukey's Multiple Comparison Test; $p \leq 0.05$ was considered statistically significant and highlighted by asterisks.

as compared to LPS stimulated cells (positive control) and no differences were observed among groups other than the comparison to the LPS control **(Figure 6A, B)**. Similarly, M2-polarization markers were consistently upregulated by all cytokine groups with small or no differences for Arginase-1 (Arg-1) and no difference among groups for chitinase-like protein 3 (Chil3) (**Figure 6C, D**).

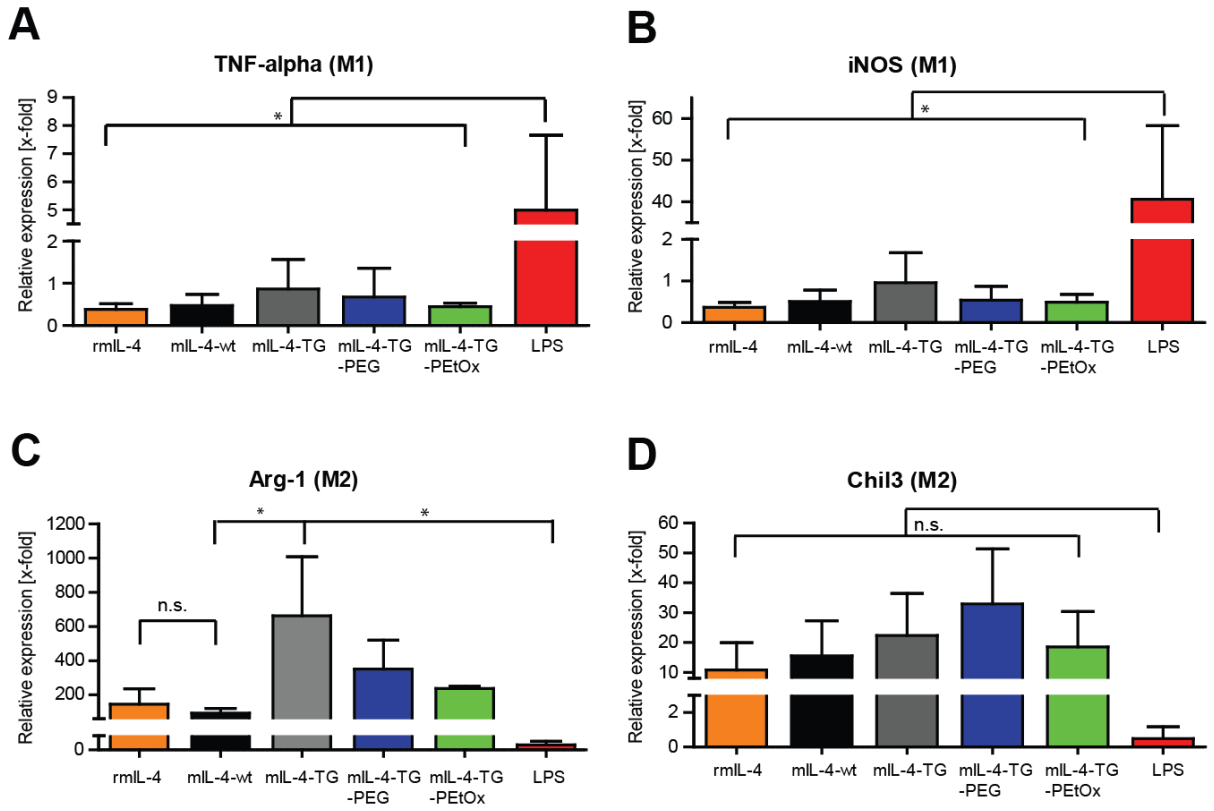

Figure 6: J774A.1 macrophage gene expression of (A) TNF alpha, (B) iNOS, (C), Arg-1 and (D) Chil3 following exposure to mIL-4 mutants, mIL-4 bioconjugates and LPS. ΔCt-values were normalized to untreated cells. Mean ± SD, n=3, one-way ANOVA followed by Tukey's Multiple Comparison Test; $p \leq 0.05$ was considered statistically significant and highlighted by asterisks.

Conclusion

A chemo-enzymatic strategy was developed to C-terminally decorate mIL-4 with two polymers – PEG and PEtOx - integrating an enzymatic conjugation step with a copper-free click chemistry reaction step. The enzymatic bioconjugation was largely restricted to a C-terminally introduced FXIIIa-recognized peptide sequence in the mIL-4 mutant. However, FXIIIa modified hitherto unknown additional sites within mIL-4 at #K42, #K63 and #K71. The enzymatically modified mIL-4 was further decorated with PEG or PEtOx resulting in comparable physical and biological properties of both bioconjugates. Future pharmacokinetic studies are required to assess the impact of bioconjugate disposition for PEtOxylated mIL-4. Available studies of PEGylated mIL 4[233] and comparing studies or radiolabeled PEG and PEtOx polymers[402] clearly indicate PEtOx's (and mIL-4-TG-PEtOx) possibilities, as a clinically relevant alternative to PEG for bioconjugation.

Supporting Information

Supporting information 1 includes: used materials and performed methods, polymer synthesis and characterization, peptide synthesis and purification, the expression optimization of mIL-4-wt and mIL-4-TG, LC-MS analysis of the linker peptide, optimization of the enzymatic TG reaction between mIL-4-TG and the linker peptide including product analysis, MS/MS spectra of identified off target FXIIIa reaction sites within the mIL-4-wt sequence, sequence homology model of mIL-4-wt to hIL-4, FXIIIa reaction with hIL-4, figures elucidating the reaction and purification of the full bioconjugates, MALDI-MS of mIL-4 bioconjugates, melting curves of the differential scanning fluorimetry assay and their first derivatives, additional qPCR data.

Supporting information 2 includes found wildcard peptides with theoretical and observed masses.

Acknowledgements

We acknowledge support by the group of Prof. F. Würthner (Institute of Organic Chemistry, University of Würzburg) and the assistance of the Core Facility BioSupraMol (Freie Universität Berlin) supported by the Deutsche Forschungsgemeinschaft (DFG) for MALDI-TOF MS analysis of proteins and bioconjugates. We gratefully acknowledge funding by the German Federal Ministry of Education and Research (BMBF) (Project “Next-PEG; 13XP5049B and 13XP5049C).

Supporting Information to Chapter 6

Experimental

Materials and Methods

Dichloromethane (DCM), *N*,*N*-dimethylformamide (DMF) and *N*,*N*-diisopropylethylamine (DIPEA) were purchased from Carl Roth GmbH (Karlsruhe, Germany). Coomassie® Brilliant Blue G250, D,L-dithiothreitol, ZipTip® C_{18}-tips and L-**a**zido**h**omo**a**lanine (**Aha**) hydrochloride were obtained from Merck KGaA (Darmstadt, Germany). 2,2‘-(Ethylenedioxy)diethanethiol (DODT), trifluoroacetic acid (TFA, HPLC grade), ammonium persulfate (APS), carbenicillin, isopropyl β-D-1-thiogalactoside (IPTG), kanamycin, L-glutathione oxidized, L-glutathione reduced, tetramethylethylenediamine (TEMED), tryptone, phenylmethanesulfonylfluoride (PMSF), RPMI 1640 with L-glutamine, HT-2 clone 5AE cells and yeast extract were from Sigma-Aldrich (St. Louis, Missouri). DMEM High Glucose with L-glutamine and sodium pyruvate, PageRuler™ Broad Range pre-stained, PageRuler™ Broad Range unstained, SYBR Green qPCR Master Mix and Trizol® Reagent were purchased from Thermo Fisher Scientific (Waltham, Massachusetts). Luna® C_{18} LC Column was from Phenomenex (Aschaffenburg, Germany). HiTrap SP HP 1 mL column and HiTrap SP XL 5 mL column were purchased from Cytiva Europe GmbH (Freiburg im Breisgau, Germany). YMC BioPro IEX SmartSep S20 column and YMC-Triart Bio C4 column were from YMC Europe (Dinslaken, Germany). Vivaspin centrifugal concentrators were from Sartorius AG (Göttingen, Germany). DBCO-mPEG (10 kDa) was purchased from Iris Biotech (Marktredewitz, Germany). Recombinant mouse IL-2, recombinant mouse IL-4 and 1st mouse IL-4 antibody (Mab404) were from R&D Systems (Minneapolis, Minnesota). The Goat Anti-Rat IgG H&L (HRP) (ab97057) 2nd antibody was received from abcam (Cambridge, United Kingdom) DNAse I was from AppliChem GmbH (Darmstadt, Germany). Fibrogammin® (FXIII) was purchased from CSL Behring (Darmstadt, Germany). WST-1 Cell Proliferation Reagent was purchased from Roche (Basel, Switzerland). PrestoBlue™ Cell Viability Reagent and BCA Protein Assay Kit were from Thermo Fisher Scientific (Darmstadt, Germany). J774A.1 cells were kindly donated by Prof. Kissel (Marburg, Germany). High-Capacity Reverse Transcriptase cDNA Kit was from Applied Biosciences (Waltham, Massachusetts). FXIII Assay substance was purchased from Zedira Gmbh (Darmstadt, Germany).

Polymer Synthesis and Characterization. DBCO-PEtOx was synthesized and characterized as described previously.[98] Briefly, methyl tosylate (1 eq.) was mixed with 2-ethyl-2-oxazoline (100 eq.) in an argon filled Schlenk flask with dry acetonitrile and heated under reflux conditions. The reaction was terminated by addition of DBCO-acid (1.1 eq.) and triethylamine (2.15 eq.) subsequent to cooling the reaction to room temperature and stirred overnight. The mixture was diluted with dichloromethane (DCM), washed with a saturated aqueous $NaHCO_3$ solution and saturated aqueous NaCl solution. The

organic layer was dried over Na_2SO_4, filtered and concentrated under reduced pressure. The residue was re-dissolved in a small amount of DCM and precipitated in cold diethyl ether.

Peptide Synthesis and Purification. The linker peptide with the sequence Ac-NQEQVSPL-(Aha)-OH was synthesized with Liberty Blue™ Automated Microwave Peptide Synthesizer (CEM Corporation, Matthews, North Carolina). Cleavage was performed for 1 h under constant shaking at RT from the resin using a mixture of 92.5% TFA, 2.5% triisopropylsilane, 2.5% 2,2′-(ethylendioxy)diethanthiol, 2.5% H_2O. Precipitation was performed using -20 °C cold diethyl ether. The peptide was purified using a reversed-phase FPLC system (ÄKTA Explorer, GE Healthcare, Freiburg im Breisgau, Germany). Separation was achieved on a Luna® 15 µm C18 LC column (250 × 21.2 mm). Prior, the peptide was dissolved in water containing 0.1% TFA (eluent A) and 30% acetonitrile containing 0.1% TFA (eluent B). The column was equilibrated with 33% eluent B and the peptide was eluted by a linear gradient over 50 min to 80% eluent B with a flow rate of 2 mL/min. Fractions were collected, analyzed with liquid chromatography mass spectrometry (LC-MS) and freeze-dried.

Expression of mIL-4-wt and mIL-4-TG. mIL-4-wt and mIL-4-TG were expressed as described previously.[403] As described in the main text, mIL-4-wt bears an artificially introduced alanine on position two to increase its yield during expression, which was not needed for mIL-4-TG expression.[397] Briefly, standard Terrific Broth (TB) medium supplemented with carbenicillin for mIL-4-wt (35 µg/mL, pET11a), or kanamycin for mIL-4-TG (100 µg/mL, pET28b) was inoculated with *E. coli* BL21 DE3 encoding for mIL-4-wt and mIL-4-TG and cultured in at 37 °C under gentle agitation until OD_{600} = 1.0, when protein expression was subsequently induced with 1 mM IPTG. After 3 h, the bacterial cells were harvested by centrifugation at 5,000 × g for 20 min at 4 °C and resuspended in resuspension buffer (50 mM Tris-HCl pH 8.0, 50 mM NaCl, 1 mM EDTA) supplemented with PMSF (final concentration 100 µM), lysozyme (final concentration 75 µg/mL) and DNAse (final concentration 75 µg/mL). The cells were lysed using a high-pressure homogenizer (Emulsiflex C5, Avestin, Ottawa, Canada) with the cell suspension cooled on ice. The sediment was resuspended once in resuspension buffer plus 1% Triton X-100 and washed twice with resuspension buffer. mIL-4 was extracted from the remaining pellet as described previously.[233] Briefly, the protein was unfolded using unfolding buffer (50 mM Tris-HCl pH 8.0, 50 mM NaCl, 1 mM EDTA, 5 M guanidine-HCl, 2 mM glutathione reduced, 0.2 mM glutathione oxidized), ultracentrifuged at 100,000 × g at 4 °C for 1 h and refolded by dialyzing the supernatant in dialysis tubes (MWCO 6-8 kDa) against refolding buffer (0.5 M L-arginine, 50 mM Tris-HCl pH 8.0, 50 mM NaCl, 1 mM EDTA, 2 mM glutathione reduced, 0.2 mM glutathione oxidized) for 4 h. The protein was purified with via cation exchange chromatography (CIEX) FPLC on an ÄKTA Explorer. Prior, the solution was dialyzed against 4 L 25 mM ammonium acetate pH = 5.0 overnight and clarified by centrifugation. The supernatant was filtered with syringe filter (0.22 µm) and loaded onto a HiTrap SP XL 5 mL column. The separation was achieved by an isocratic gradient of 12% 25 mM ammonium acetate containing 2 M NaCl pH = 5.0 over five column volumes (CV), followed by a linear gradient up to 40% ammonium acetate containing 2 M NaCl over 12 CV. The fractions eluting at a conductivity of

36 to 40 mS/cm were analyzed with SDS-PAGE, dialyzed against 25 mM ammonium acetate pH = 5.0 and loaded onto two consecutive HiTrap SP HP 1 mL Columns. The separation was achieved by an isocratic gradient of 12% 25 mM ammonium acetate containing 2 M NaCl pH = 5.0 over a ten CV period, followed by a linear gradient up to 60% ammonium acetate containing 2 M NaCl over 48 CV. The fractions eluting at 38 mS/cm conductivity were collected and analyzed with SDS-PAGE. FPLC fractions with natively folded protein were pooled and concentrated with Sartorius VivaSpin Centrifugal Units MWCO = 3500 Da, dialyzed against PBS pH = 7.4 with Slide-A-Lyzer Dialysis Tubes MWCO = 3000 Da, frozen in liquid nitrogen and stored at -80 °C until further use. Protein concentration was determined with BCA Assay Kit and measured according to manufacturer's instructions at λ = 562 nm using a Spectramax 250 microplate reader (Molecular Devices, Sunnyvale, California).

Sodium dodecyl sulfate–polyacrylamide gel electrophoresis analysis. Purified proteins and site-specifically modified protein conjugates were analyzed by **s**odium dodecyl sulfate–polyacrylamide gel electrophoresis (SDS-PAGE) as described earlier.[404] PageRuler™ Unstained Broad Range Protein Ladder or PageRuler™ Broad Range pre-stained was used for molar mass approximation. Bands were visualized using aqueous Coomassie Brilliant Blue G250 solution (4 mg/L) containing 35 mM HCl.

Reversed-phase high performance liquid chromatography analysis. Reversed-phase high performance liquid **c**hromatography (RP-HPLC) was performed on a YMC-Triart Bio C4 column (150 × 4.6 mm) at 25 °C at a flow rate of 0.5 mL/min. The column was equilibrated with water containing 0.1% TFA (v/v) (eluent A) and 5% acetonitrile containing 0.1% TFA (eluent B). Proteins were eluted by a linear gradient over 27 min to 100% eluent B. mIL-4 variants and mIL-4-TG-Linker-Polymer conjugates were detected at λ = 214 nm.

Conjugation of mIL-4-TG to the linker peptide in presence of activated factor XIII. FXIII (250 U/mL, Fibrogammin®) was activated in the presence of 2.5 mM $CaCl_2$ and 30 U/mL thrombin for 4 hours at 37 °C. Activity was checked using FXIII Assay substance. 250 U/mL aliquots of FXIIIa were snap frozen and stored at -80 °C until further use. Thawed FXIIIa was stored for up to 24 h at 4 °C and discarded afterwards. To retains its stability FXIIIa contains 10 mg/mL human serum albumin (HSA) as an excipient, which can be removed later on during ion exchange chromatography. mIL-4-TG with a final concentration of 1 mg/mL was incubated with 5 to 15-fold molar excess of linker peptide in the presence of 10 U/mL FXIIIa. The reaction was carried out in TBS buffer plus 2.5 mM $CaCl_2$ at 37 °C under gentle agitation for 5 to 60 min and stopped by adding EDTA to a final concentration of 20 mM. The reaction mixtures were transferred into Slide-A-Lyzer dialysis tubes (2 mL, MWCO 3.5 kDa) and dialyzed against PBS overnight. The reaction mixtures containing FXIIIa, mIL-4-TG and mIL-4-TG-Linker products were analyzed with SDS-PAGE, RP-HPLC and MALDI-MS as described below.

Site-specific conjugation of mIL-4-TG-Linker with polymer via strain promoted azide alkyne cycloaddition (SPAAC)

The FXIIIa reaction mixture was diluted 1:1 with PBS and incubated with 20-fold molar excess of DBCO-PEG 10 kDa or DBCO-PEtOx 8 kDa under gently agitation at 4 °C for 24 h The reaction was analyzed with SDS-PAGE, RP-HPLC and MALDI-MS as described earlier.

Identification of natural mIL-4-wt and mIL-4-TG FXIIIa conjugation sites. mIL-4-wt and mIL-4-TG (250 µg each) were conjugated with an excess of linker peptide as described above in two separate approaches. Briefly, before digestion, the sample (500 µL, 1 mg/mL) was dialyzed against 50 mM Tris-HCl pH 8.0 overnight using Slide-A-Lyzer MWCO 3.5 kDa to reduce the excess of linker peptide in the sample for the Dde-Biotin-DBCO-Linker Click reaction, which is performed after digestion (*vide infra*). Afterwards the protein (250 µg) was denaturized with 6 M guanidine HCl, 2 mM ß-mercaptoethanol (final volume = 500 µL) at 95 °C for 20 min. After denaturation, the sample was cooled to RT, diluted with 50 mM Tris-HCl to less than 1 M guanidine HCl and $CaCl_2$ was added to a final concentration of 1 mM. Afterwards trypsin was added in a 1:40 ratio (trypsin: protein (w/w)) and incubated for 3 h at 37 °C under constant light shaking. Then, the same amount of trypsin was added again and the sample was incubated overnight at 37 °C under constant light shaking. Afterwards, a 5-fold molar excess of Dde-Biotin-DBCO-Linker was added and the sample was incubated overnight at 4 °C. For pulldown of clicked peptides pierce-streptavidin beads (binding capacity 15 to 28 µg/mL beads) were used. 100 µL of streptavidin beads were washed three times with PBS and added to the sample afterwards. The mixture was incubated for 1 h at RT and subsequently washed thrice with PBS. Then the beads were incubated with a 2.5% hydrazine in PBS solution for 2 h at RT to cleave off the peptide. Following cleavage, the supernatant was separated form agarose beads using pierce spin columns. For reduction and alkylation, DTT was added to result in a final concentration of 50 mM and the sample was incubated for 10 min at 70 °C. After cooling to RT, iodoacetamide was added to result in a final concentration of 120 mM and the sample was incubated for 20 min in the dark. After alkylation, the samples were desalted using strata X33 columns (1mL). For all steps only gravitational flow was used. The columns were activated with 3 mL 100 % ACN and then washed with 3 mL 100% deionized water. Then the sample was added. Afterwards, the column was washed with 5 mL 0.4% formic acid in H_2O. Elution was performed with 0.5 mL 0.4% formic acid in 80% acetonitrile. The eluted samples were then snap frozen in liquid nitrogen and freeze dried. For analysis samples were resuspended in 30 µL 0.2% formic acid, 2% acetonitrile and used for LC MS/MS analysis immediately.

Mass spectrometry. For matrix-assisted laser-desorption ionisation mass spectrometry (**MALDI-MS**) analysis, samples were desalted using ZipTip® C_{18}-tips following the manufacturer's instructions. Proteins were analyzed as described previously.[288] MALDI mass spectra of bioconjugates were acquired in the linear positive mode using an Autoflex II LRF instrument (Bruker, Billerica, Massachusetts). The

mass spectra were calibrated externally with a protein standard I from Bruker Daltonics Inc. (Bruker, Billerica, Massachusetts) containing insulin, ubiquitin, myoglobin and cytochrome C.

For LC MS/MS analysis of crosslinked peptides, the analysis was performed as described previously, with small adaptions. Deviating parameters are described below.[98] In brief, NanoLC-MS/MS analyses were performed on a LTQ-Orbitrap Velos Pro (Thermo Fisher Scientific, Darmstadt, Germany) equipped with a PicoView Ion Source (New Objective, Littleton, USA) and coupled to an EASY-nLC 1000 (Thermo Fisher Scientific, Darmstadt, Germany). Peptides were loaded on a precolumn (trap column, 2 cm x 150 µM ID) packed with 3 µm C18 ReproSil and then eluted to capillary columns (30 cm x 150 µm ID) self-packed with ReproSil Pur 120 C18-AQ, 1.9 µm and separated with a 30-minute linear gradient from 3 to 30% acetonitrile and 0.1% formic acid and a flow rate of 500 nL/min.
A TOP5 data-dependent MS/MS method was used; dynamic exclusion was applied with a repeat window of 7 seconds and an exclusion duration of 7 seconds; singly charged precursors were excluded from selection.

The following modifications were allowed in the final search:
Fixed: carboxymethyl @ C,
Common: oxidation @ M, Acetyl @ N-terminus, Acetyl @ K
Rare: Gln to pyro-Glu @ peptide N-terminus Q, Glu to pyro-Glu @ peptide N-terminus E; Met-loss @ N-Terminus M, Met-loss+Acetyl @ N-Terminus
Custom (Wildcard): cleaved Dde-biotin-azidohomoalanine-Linker-peptide @ K (variable mass differences, see below)

With total common and rare max to 1 each. Data was searched with semi-specific (N-terminal ragged) cleavage at R/K (tryptic cleavage) against custom database containing the corresponding mIL-4-wt, or mIL-4-TG sequence, decoys were added. Results were filtered and only peptide matches with a scoring of >80 and a log prob > 1.05 were considered.
For analysis Byonic software by Protein metrics[405] was used. A set of searches was performed, starting with wildcard searches (i.e. enabling the software to identify potential sites of an unknown modification, where only a mass range is specified) allowing several (standard) modifications as well as a peptide adduct (linker peptide with cleaved Dde-biotin) at K between 1,100 Da and 1,500 Da, here an additional 25 modifications were enabled, as suggested by a preliminary search with the software "Preview" (ProteinMetrics). In an effort to reduce possible false positive assignments by the search algorithms, the search was subsequently narrowed down to a very narrow wildcard range) for the peptide (1,339 to 1,340 Da), and only limited modifications, as listed above. The exact peptide mass was calculated to be 1,339.619 Da (Peptide + cleavable linker residue - ammonia loss from coupling). Qualifying spectra (specifications were a log prob > 1.05 and a byonic score > 80) corresponded to an added mas of 1,339.619 Da. For Identification of potential sites, only spectra with wildcard modifications with an

added mass discrepancy of approximately 10 ppm or less (i.e. Wildcard modifications between 1,339.606 and 1,339.632 Da) were considered.

Purification of mIL-4-TG-Linker-Polymer conjugates. For separation of mIL-4-TG-Linker-Polymer conjugates, cation exchange chromatography on a FPLC system (GE Healthcare) was used. FXIIIa reaction mixture was dialyzed against 50 mM sodium acetate pH = 4.0 (eluent A) and loaded onto a 1 mL YMC BioPro IEX SmartSep S20 column. mIL-4-TG-Linker-Polymer conjugates were eluted by a linear gradient over 144 min to 50% 2 M NaCl, 50 mM sodium acetate buffer pH = 4.0 (eluent B) with a flow rate of 1 mL/min. The elution profile was monitored at λ = 214 nm. Fractions were collected, analyzed with SDS-PAGE, pooled and characterized with MALDI-MS and RP-HPLC as described above.

Cell proliferation assay using water soluble tetrazolium salt 1 (WST-1). For the measurement of bioactivity of mIL-4 conjugates compared to unmodified mIL-4, cell proliferation assay with HT-2 clone 5AE cells was performed. Shortly, 45.000 cells/well were plated in 96-well plates in assay medium (RPMI 1640 supplemented with and 10% FBS, 100 U/mL penicillin G and 100 µL/mL streptomycin) and incubated for 18 h at 37 °C and 5% CO_2. Concentrations of purchased recombinant mIL-4 (rmIL-4), mIL-4-wt, mIL-4-TG and mIL-4-TG-Linker-Polymer conjugates ranging from 0.0001 to 35 ng/mL were added to the cells. After incubation for 24 h under the same conditions, the cells were treated with WST-1 reagent for 4 h at 37 °C and 5% CO_2. The absorbance was measured on a plate reader (Tecan Infinite® 200 PRO, Tecan Group, Männedorf, Switzerland) according to manufacturer's instructions at λ = 450 and λ = 620 nm as reference wavelength. Measurements were performed in three technical replicates, which mean values were used for the evaluation of three biological replicates. Mean values were normalized to untreated cells.

Western blotting. 1 µg of protein was used for each lane. After finishing SDS PAGE, gels were removed carefully and the stacking gel was discarded. Afterwards, the gel was placed onto a nitrocellulose membrane, which was placed on a Whatman paper and covered with a Whatman paper. Air bubbles were removed afterwards to ensure an equal flow of electricity. All Whatman papers and nitrocellulose membranes were pre-wetted in transfer buffer. This sandwich was placed between two thin sponges and inserted into the blotting chamber. The chamber was filled with transfer buffer and was run for 90 min at 80 V.

After finishing the transfer of proteins onto the nitrocellulose membrane, the membrane was blocked with 5% skim milk powder in TBS-T (w/v) solution for 1h at 4°C. The membrane was washed afterwards once with 20 mL TBS-T for 5 min and probed with the 1st antibody overnight at 4°. For the 1st antibody a dilution of 1:1000 was used and the antibody was diluted in 5% skim milk powder in TBS-T (w/v) solution. At the following day, the 1st antibody was removed and the membrane washed again 3 times with 20 mL TBS-T for 15 min and probed with the 2nd antibody for 1 h at room

temperature. The 2nd antibody was diluted 1:2000 in 1x TBS-T solution. The membrane was washed again 3 times with 20 mL TBS-T for 15 min. Afterwards the membrane was detected for 1 minute using the SuperSignal™ West Pico PLUS Chemiluminescent Substrate on a chemiluminescent imaging unit (Odyssey FC, Leicor, Bad Homburg vor der Höhe, Germany). The marker was detected separately under normal light using a gene flash syngene bio imaging system (Syngene, Cambridge, United Kingdom). Afterwards, pictures were superimposed.

Macrophage polarization assay with quantitative polymerase chain reaction (qPCR). To measure the ability of mIL-4-wt, mIL-4-TG and mIL-4-TG-Linker-Polymer conjugates to drive macrophages polarization, macrophages polarization studies with J774A.1 cells was performed. Briefly, 200.000 cells/well were seeded in 6-well plates in assay medium (DMEM supplemented with 10 % FBS, 100 U/mL penicillin G and 100 µl/mL streptomycin) and incubated for 24 h at 37 °C and 5% CO_2. The media was changed to serum-free DMEM media and cells were incubated for 3 h. Cells were stimulated with lipopolysaccharide (LPS) (100 ng/mL) as M1 control, rmIL-4 as M2 control, mIL4-wt, mIL4-TG and mIL-4-Linker-Polymer conjugates (each 50 ng/mL) for 24 h at 37 °C and 5% CO_2. Cells were washed with sterile PBS twice, harvested by cell scraping and taken up in PBS. RNA was isolated with Trizol® Reagent as described by Simms.[406] RNA concentration was measured with spectrometer at $\lambda = 260$ nm and $\lambda = 280$ nm and purity was assessed by calculating the 260/280 ratio. RNA was transcribed into cDNA with High Capacity cDNA Reverse Transcription Kit. Gene-specific primers were designed, which sequences are listed in supplementary material (Table S1). qPCR was performed on a qPCR Machine ABI Prism 7900 (Applied Biosystems, Foster City, USA) using SYBR Green Master Mix.

Following temperature protocol was used:

Temperature	Time	
50° C	2 min	
95° C	2 min	
95° C	15 s	40x
65° C	15 s	
72° C	1 min	

Measurements were performed in four (TNF-alpha, iNOS, Arg-1) or three (Ym1) technical replicates, which mean values were included into the evaluation of three biological replicates. Ct-values of GAPDH expression level were subtracted and normalized to the expression level of untreated cells.

Differential scanning fluorimetry (DSF). DSF was performed according to a previously published protocol with small adaptions mentioned below.[98] The protein concentration was set to 6 µM in 25 µL buffer (100 mM Na_2HPO_4 pH 7.4, 150 mM NaCl). Normalisation was performed as described before, but no smoothing was performed.[199] For melting point determination the half maximal denaturation (HMD) method was used as mIL-4 and its conjugates have two maxima around 60 °C (**Figure S8**). The first derivative method was discarded as it did not represent the measured data as good as the HMD method.

Statistical analysis. Data were analyzed with GraphPad Prism 5 (GraphPad Software, La Jolla, CA) using one-way ANOVA followed by Tukey's multiple *post hoc* tests for pairwise comparisons. Results were considered statistically significant at $p \leq 0.05$ and highlighted by asterisks and results are shown as mean with standard deviation (SD) unless specified otherwise.

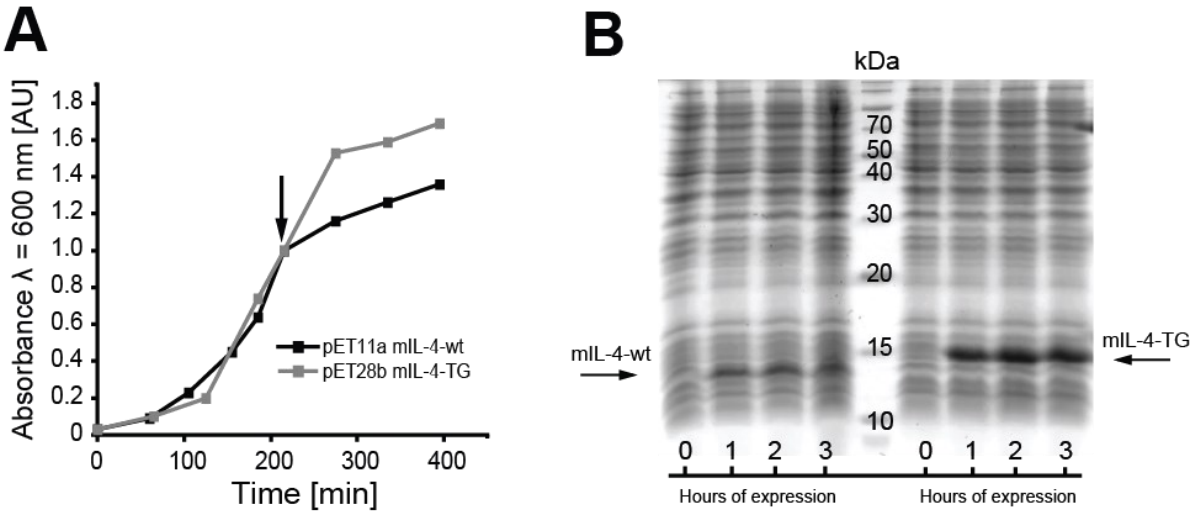

Supplementary Figure S1: Protein expression with *E. coli*. (A) Growth curves of *E. coli* during protein expression. Arrow indicates induction of protein expression with 1 mM IPTG at OD_{600} = 1.0. (B) SDS-PAGE analysis of *E. coli* lysates during protein expression of mIL-4 -wt and mIL-4-TG. Left side: Expression of mIL-4-wt 0-3 hours after induction with 1 mM IPTG. Middle: Molecular marker. Right side: Expression of mIL-4-TG 0-3 hours after induction with 1 mM IPTG. Arrows indicate the produced protein at 13.8 kDa (mIL-4-wt) and 15.5 kDa (mIL-4-TG).

A

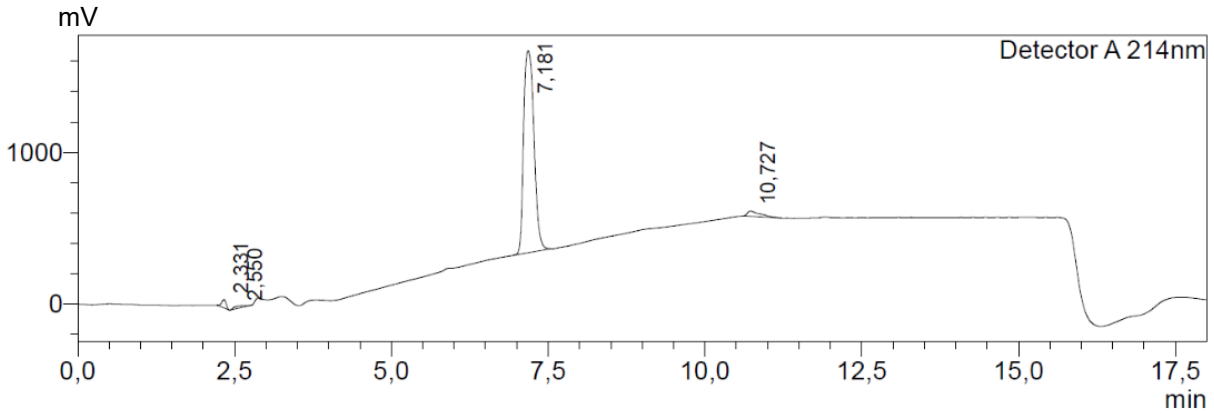

B

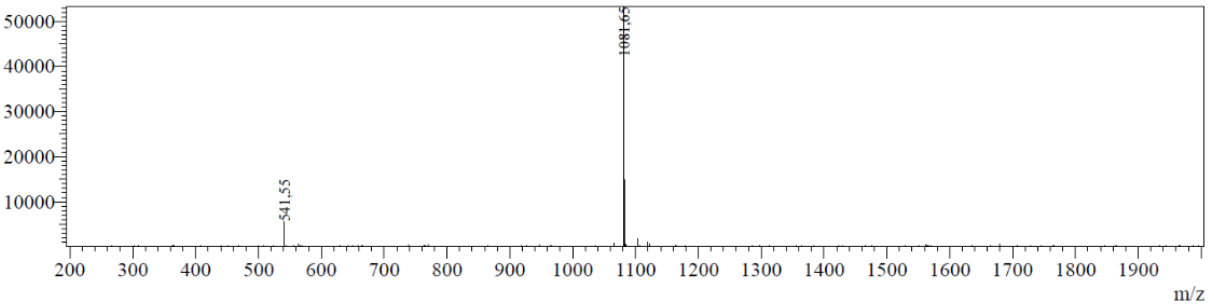

Supplementary Figure S2: LC-MS analysis of linker peptide with the amino acid sequence NQEQVSPL-Aha after FPLC purification. Calculated Mass: 1081.52 Da. Found mass: $[M+H]^{+1}$: 1081.65 Da, $[M+H]^{+2}$: 541.55 Da. (**A)** LC-Chromatogram and (B) mass spectrum of the peak at 7.45 min.

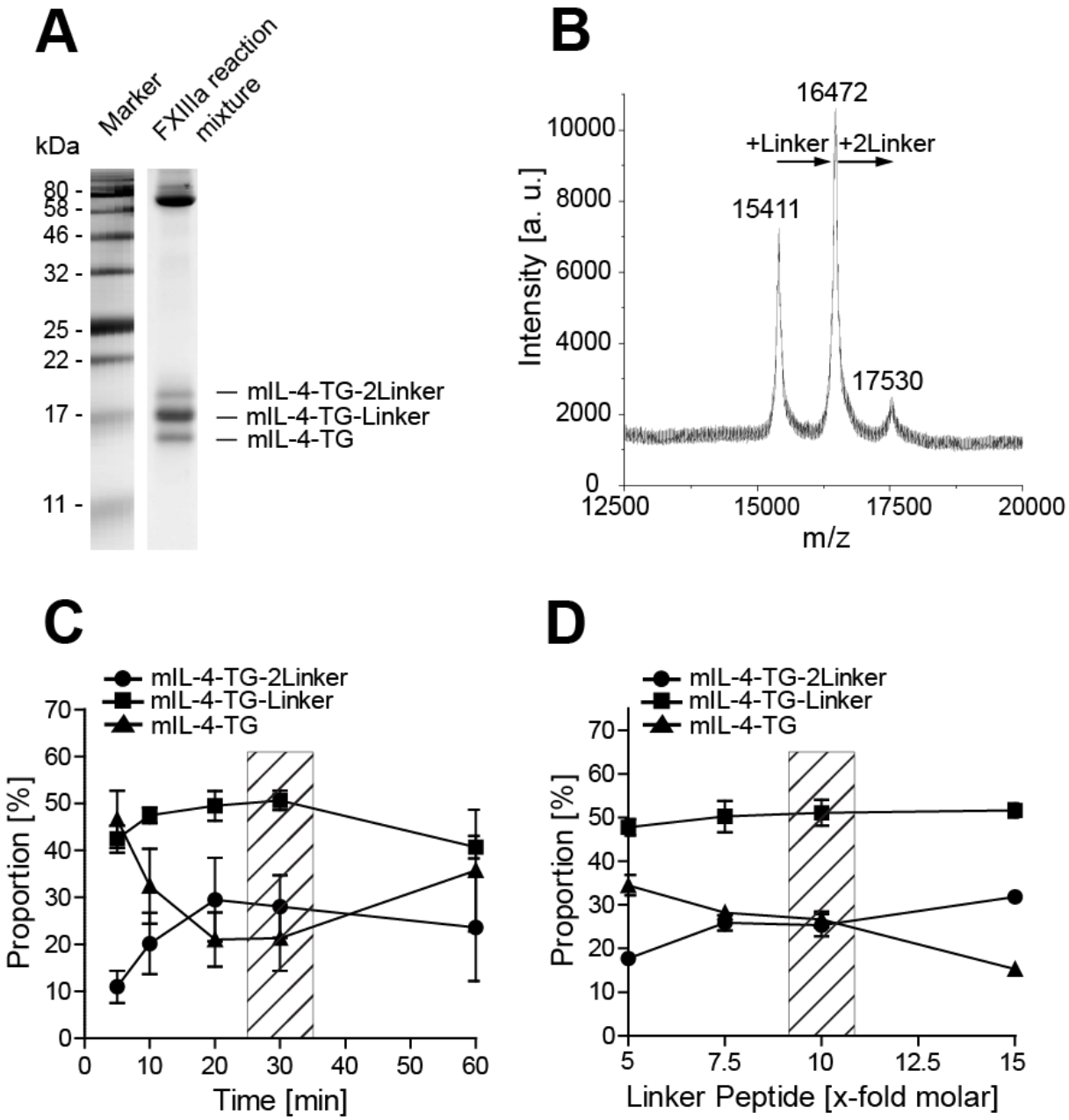

Supplementary Figure S3: FXIIIa catalyzed reaction of mIL4-TG with linker peptides. (A) Reducing SDS-PAGE analysis of FXIIIa reaction mixture (1, molar mass marker; 2, FXIIIa reaction mixture consisting of unmodified mIL-4-TG at 15.5 kDa, mIL-4-TG-Linker at 16.6 kDa, mIL-4-TG-2Linker at 17.7 kDa and FXIIIa (83 kDa) supplemented with HSA (66 kDa). (B) MALDI-MS of FXIIIa reaction mixture: Observed mass 15411, 16472 and 17530 Da, calculated mass 15499, 16580 and 17662 Da for mIL-4-TG, mIL-4-TG-Linker and mIL-4-TG-2Linker, respectively. (C) Proportion of mIL-4-TG, mIL-4-TG-Linker and mIL-4-TG-2Linker after 5, 10, 20, 30 and 60 minutes reaction time. The dashed box highlights the selected reaction condition for further modification. (D) Proportion of mIL-4-TG, mIL-4-TG-Linker and mIL-4-TG-2Linker at 5, 7.5, 10 and 15-fold molar excess of linker peptide after 30 minutes. The dashed box highlights the selected reaction condition for further modification. of reaction. Quantification in C and D was performed with ImageJ based on band intensities of the respective bands of the SDS-PAGE gels on which the reactions were analyzed (gels not shown).

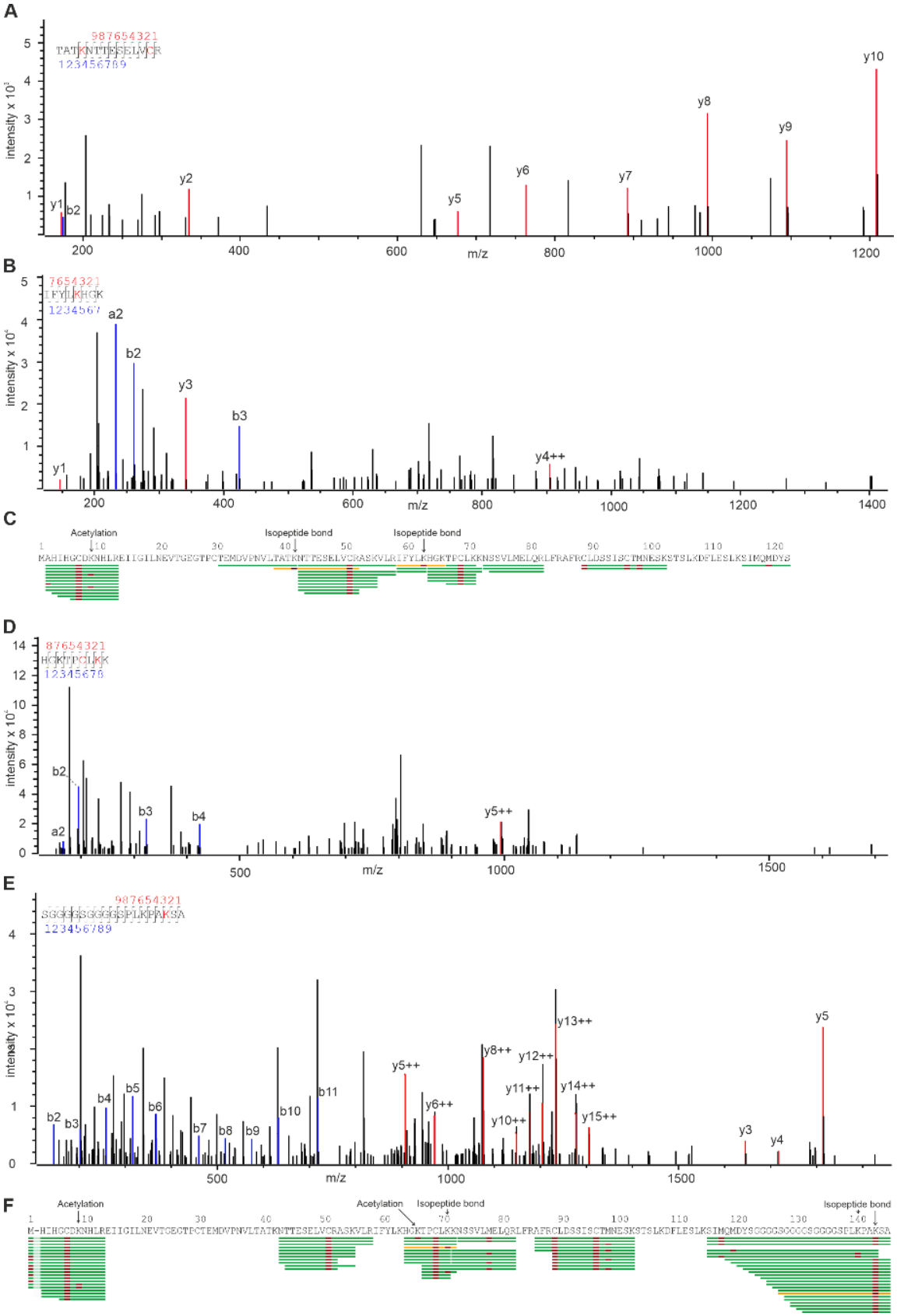

Supplementary Figure S4: Exemplary spectra of identified lysine residues that were targeted by FXIIIa. (A) MS/MS Spectrum of an identified peptide modified with the linker peptide at K42 found in mIL-4-wt. (B) MS/MS spectrum of an identified peptide modified with the linker peptide at K63 found in mIL-4-wt. (C) Peptide coverage on mIL-4-wt using the wildcard range for the linker peptide (1338 -1342 Da). Peptides which spectra are displayed in A and B are highlighted in yellow. (D) MS/MS Spectrum of an identified peptide modified with the linker peptide at K71 found in mIL-4-TG. (E) MS/MS Spectrum of an identified peptide modified with the linker peptide at K144 found in mIL-4-TG. (F) Peptide coverage on mIL-4-TG using the narrow wildcard range for the peptide (1338 - 1342 Da). Peptides, which spectra are displayed in D and E are highlighted in yellow.

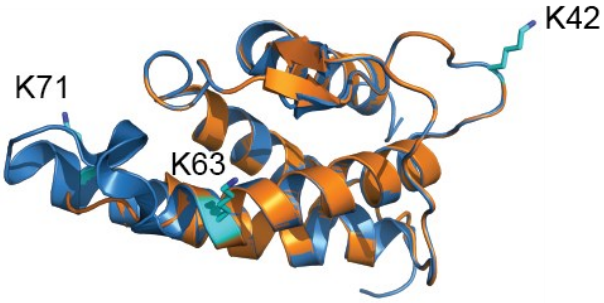

Figure S5: Sequence homology model of human IL-4 (PBD: 1bbn and murine IL-4 as shown in blue and in orange, respectively. K42, K63 and K71 are displayed as sticks in cyan. Homology modelling was performed with swiss model.[400]

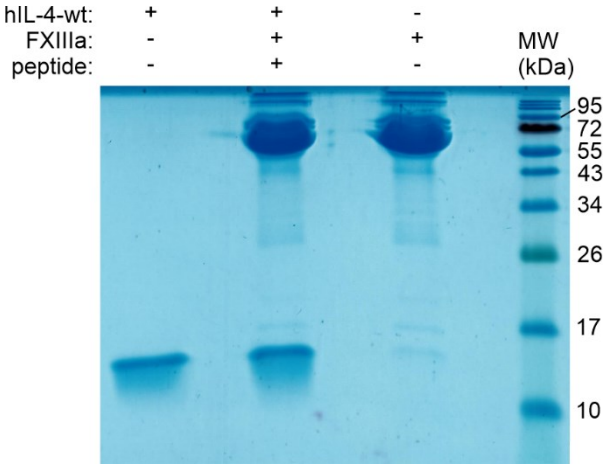

Supplementary Figure S6: FXIIIa reaction with hIL-4 with a 10-fold molar excess of peptide over 30 minutes (including negative controls). hIL-4 was recombinantly produced as described previously.[268]

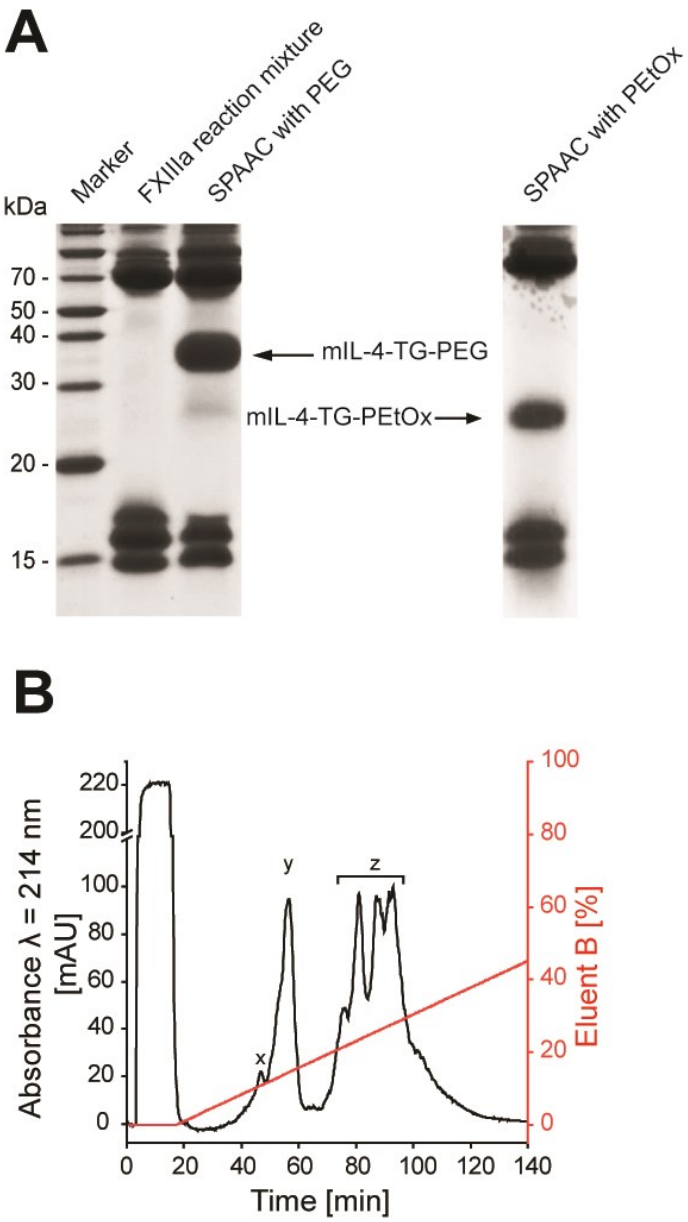

Supplementary Figure S7: Site-specific PEGylation/POxylation of mIL-4-TG *via* SPAAC. (A) SDS-PAGE analysis of SPAAC reaction mixture (1, molar mass; 2, FXIIIa reaction mixture; 3, SPAAC reaction mixture with DBCO-PEG, 4, SPAAC reaction mixture with DBCO-PEtOx). (B) CIEX-FPLC chromatogram of mIL-4-TG-PEG separation on a YMC column. (C) SDS-PAGE analysis of CIEX-FPLC peaks.

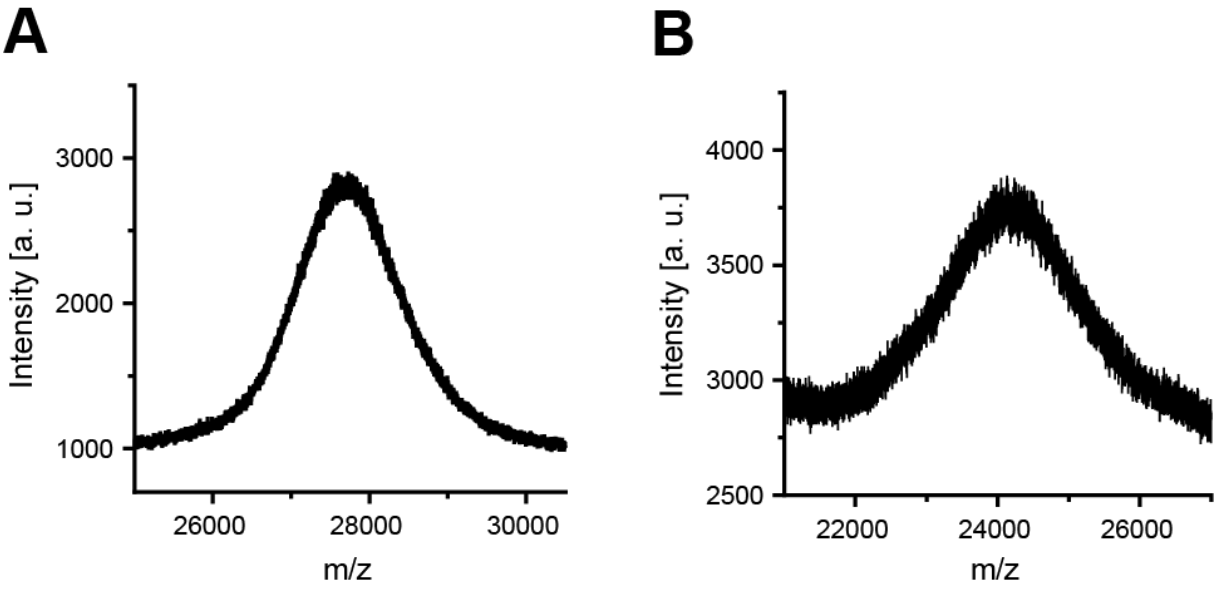

Figure S8: MALDI-MS of mIL-4 bioconjugates. (A) MALDI-MS of mIL-4-TG-PEG. (B) MALDI-MS of mIL-4-TG-PEtOx.

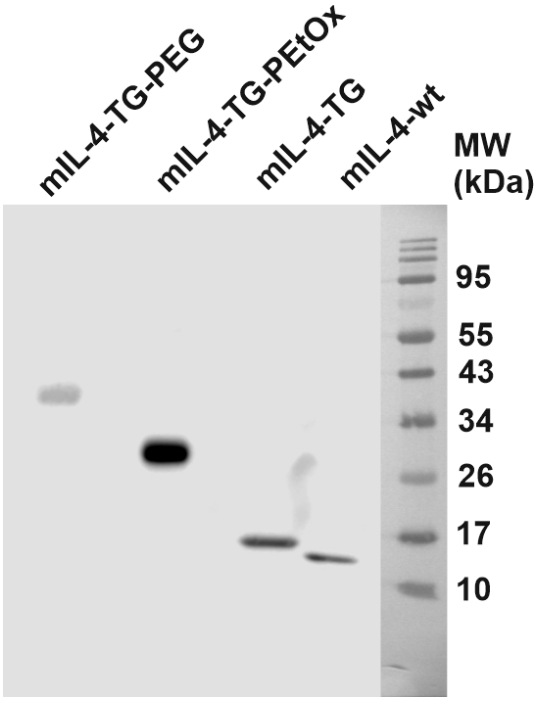

Figure S9: Western blot analysis of mIL-4-wt, mIL-4-TG and its bioconjugates.

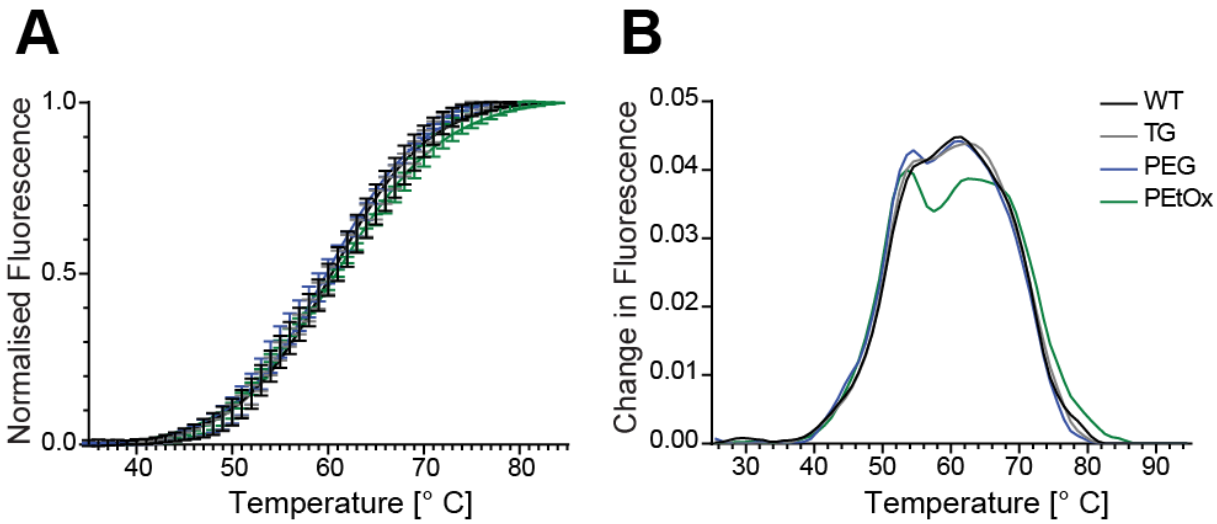

Figure S10: (A) Normalised, averaged fluorescence of the differential scanning fluorimetry assay with mIL-4 WT mIL-4-TG and its bioconjugates (n = 4). The lowest value of each measurement was set to 0 as well as all values below this temperature. The highest value of each measurement was set to 1 as well as all values above this temperature. The normalized values were averaged, and adjacent points connected. Standard deviations are indicated with error bars (mIL-4-wt = black, mIL-4-TG = grey, mIL-4-TG-PEG = blue, mIL-4-TG-PEtOx = green). (B) Averaged first derivate plot of figure A.

Table S1: Primers used for quantitative PCR.

Function	Gene	Sequence	
M1	mTNF-α	Forward	5‘-CACGCTCTTCTGTCTACTGAAC-3’
		Reverse	5‘-TGGGCCATAGAACTGATGAGAG-3’
	miNOS	Forward	5‘-GAGGTCTTTGAAATCCCTCCTG-3’
		Reverse	5‘-ATACCACTTCAACCCGAGCTC-3’
M2	mArg-1	Forward	5‘-AGCACTGAGGAAAGCTGGTC-3‘
		Reverse	5‘-GAGCTGTCATTAGGGACATCAAC-3‘
	mChil3	Forward	5‘-TTTCTCCAGTGTAGCCATCCTT-3‘
		Reverse	5‘-TCTGGGTACAAGATCCCTGAA-3‘
House-keeping	mGAPDH	Forward	5‘-TGCTGAGTATGTCGTGGAGTC-3’
		Reverse	5‘-GCGGAGATGATGACCCTTTTG-3’

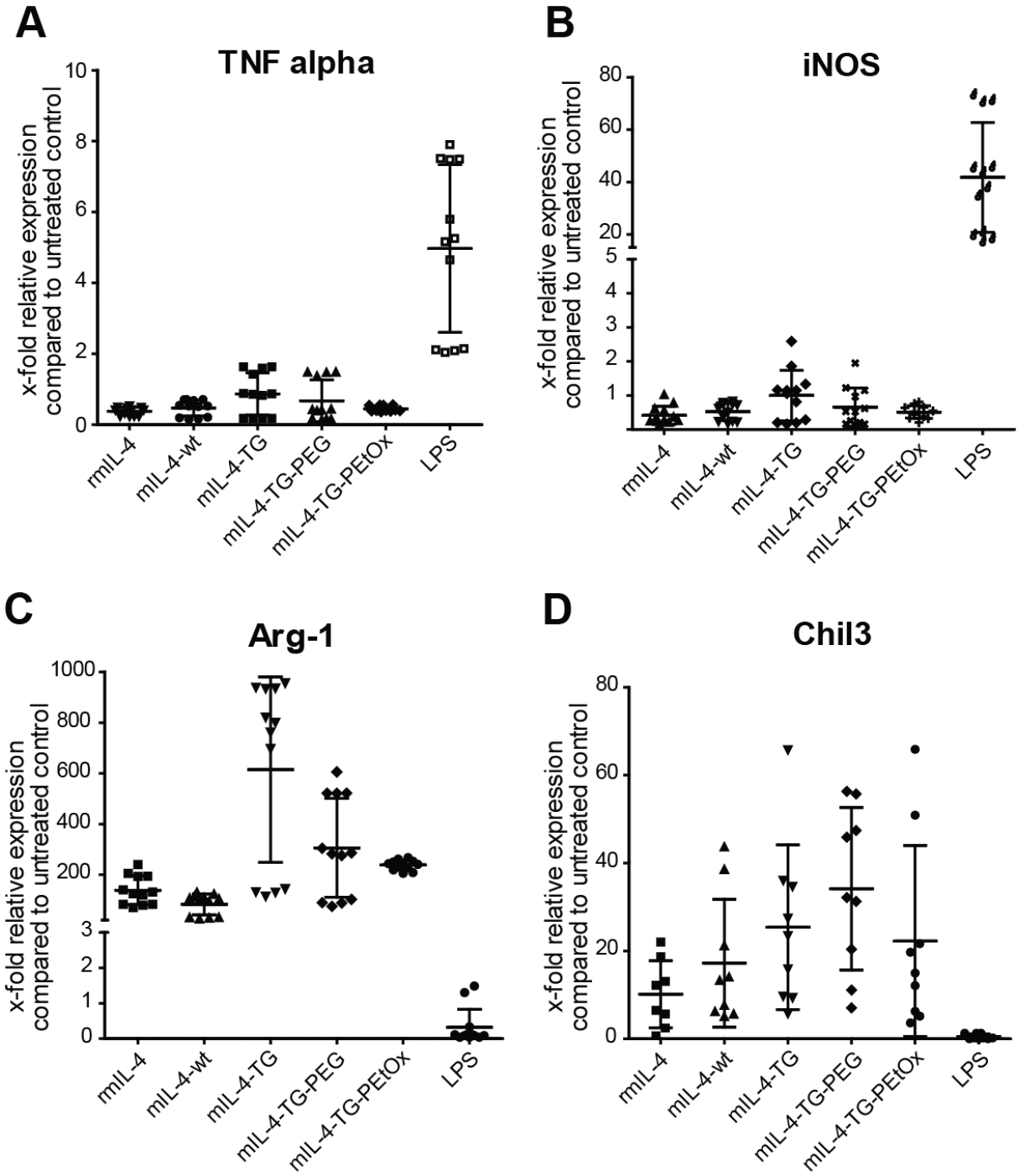

Figure S11: Individual outcome from qPCR and resulting mean ± SD of (A) TNF alpha, (B) iNOS, (C) Arg-1 and (D) Chil3.

Chapter 7 – Bioresponsive release of Interferon-α2a by Matrix Metallopeptidase 9 from Extracellular Matrix after Transglutaminase enabled immobilization

Niklas Hauptstein, Benedikt Gantert, Tessa Lühmann, Lorenz Meinel

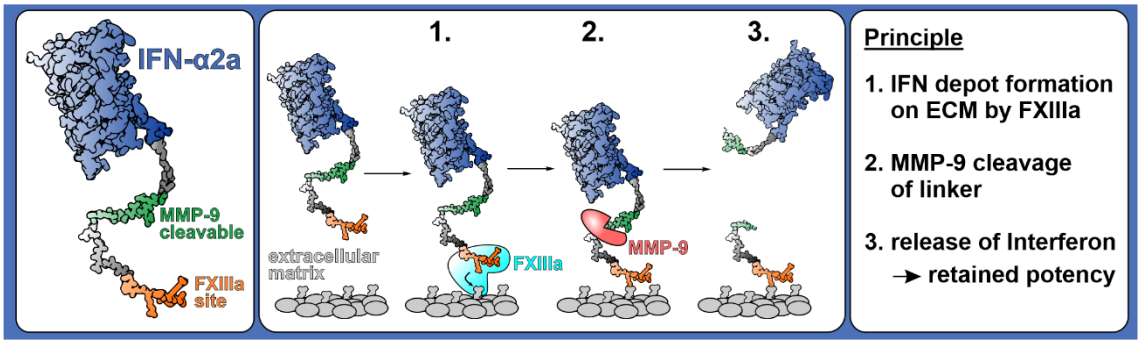

Unpublished manuscript

Abstract

Interferons (IFN) are potent immune modulating cytokines, with antiviral and antiproliferative properties. After their discovery in 1957, they are used since 1986 for the treatment of viral diseases like hepatitis B and C. Especially Interferon-α2a (IFN-α2a), which belongs to the type-I IFNs is known for its antiviral properties. These type-I IFNs were currently investigated in a pulmonic nebulized application study during the SARS-CoV-2 pandemic crisis as a first line treatment to inhibit virus replication in the respiratory tract to minimize severe progress. In this study, IFN-α2a was C-terminally elongated with a matrix metallopeptidase-9 (MMP-9) sensitive linker (PSL) and a transglutaminase (TG) recognition sequence, which is recognized by the active human blood coagulation factor XIIIa (FXIIIa), called IFN-PSL-TG. Additionally, a mutant not-cleavable by MMP-9 was designed (IFN-SCR-TG). Both mutants were bioactive, and it was shown, that the TG sequence is successfully recognized by FXIIIa. As a result, both mutants were immobilized *in vitro* to fibronectin, an essential building block of the extracellular matrix (ECM), in contrast to IFN-α2a WT, which was not bound to the fibronectin. The MMP-9 sensitive linker was also investigated, but it was shown, that IFN-α2a WT has an internal MMP-9 cleavage sequence, that is closely located to the C-terminus of the protein, therefore making the PSL linker gratuitous. Finally, IFN-SCR-TG was successfully bound to extra cellular matrix in an *in vitro* experiment and released by MMP-9 through cleavage of the IFN internal MMP-9 sequence.

Introduction

Interferons (IFNs) are important immune modulating proteins that belong to the class II cytokine family.[5] IFNs contain three classes, whereby IFN-α2a belongs to the type-I IFNs.[5, 6, 188, 252] IFN-α2a is already approved since 1986 by the FDA for the treatment of virus infections like Hepatitis B and C,[407] though several artificial modifications have led to more modern IFNs, which have replaced the wild type (WT) protein in the clinical application.[62, 252, 253, 408] At the beginning of the SARS-CoV-2 pandemic crisis it became evident that no general first line treatment has been developed so far, that can be quickly and locally applied against viruses, which affect the respiratory tract. Such a medication would help to reduce severity of SARS-CoV-2 infections. Type-I IFNs can stimulate the innate immune system, independently of the virus.[118, 122, 125, 188] Therefore, IFN-α and IFN-β, which are both approved in the clinic, were quickly considered for a localized pulmonic application to milden the symptoms, and reduce the viral burden as well as chronic outcomes.[119] Additionally, Corona viruses can delay the initial IFN Type-I/III response, resulting in undampened virus replication.[122, 124, 126, 409] Furthermore, an early application is necessary as recent findings have pointed out, that a late but strong IFN type-I activation often leads to hyper inflammation, causing a severe disease progress.[122, 125, 126] Contrastingly, an early IFN response can help to control viral replication.[122, 125, 126]

Initial clinical trials with a formulated nebulized application of IFN-β to the respiratory tract have shown, that type-I IFNs can help to reduce the severity of the disease and shorten the recovery time.[119]

In this study, two IFN-α2a mutants, called IFN-PSL-TG and IFN-SCR-TG were designed, which can be immobilized on extracellular matrix e.g., of the respiratory tract and IFN-PSL-TG was designed to be released upon pathogen recognition, leading to a faster innate immune response. This was achieved by modifying IFN-α2a by C-terminal mutational elongation containing two features (**Scheme 1**): (i) A sequence, that is recognized by the human transglutaminase (TG) FXIIIa as a lysine donor, leading to an immobilization on extracellular matrix (ECM) of the respiratory tract, whereby fibronectin acts as the glutamine donor. (ii) An MMP-9 sensitive linker (PSL), which releases the functional IFN-α2a protein upon viral exposure (**Scheme 1B**). MMP-9 is secreted by infiltrating neutrophils and macrophages upon viral detection. As a control, another mutant was designed (IFN-SCR-TG), which also contains the TG sequence, but a linker, that contains the same amino acids as IFN-PSL-TG in a scrambled (SCR) arrangement, which prevents MMP-9 cleavage.

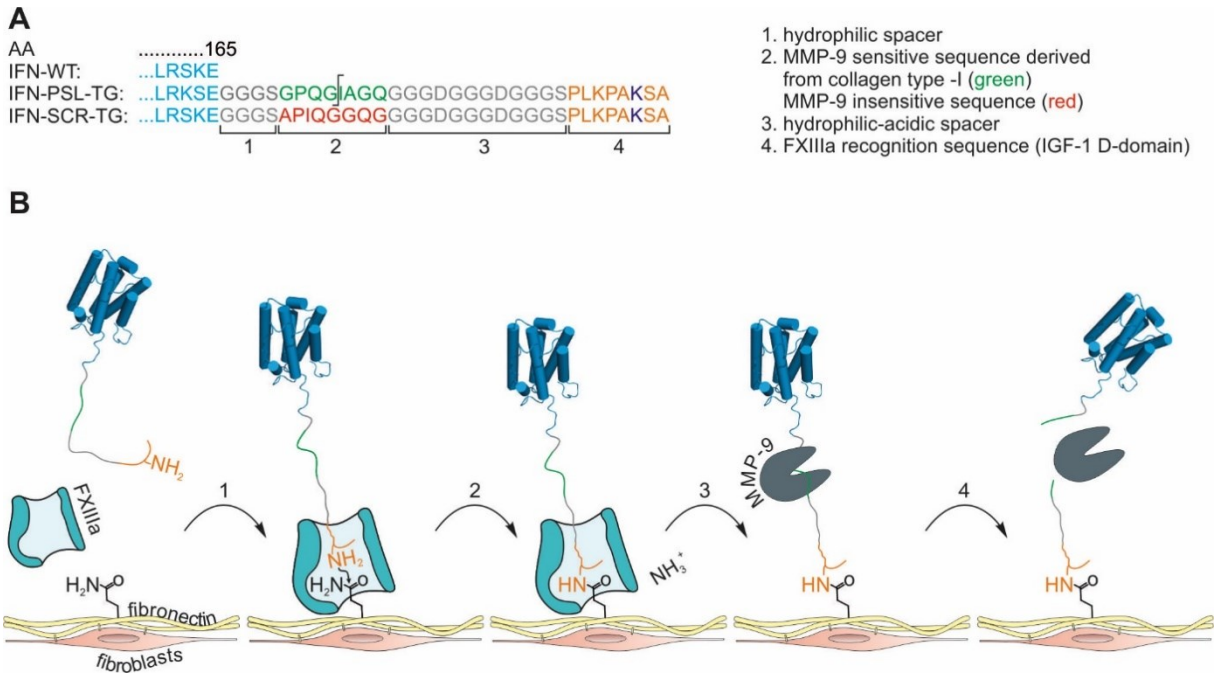

Scheme 1: (A) Partial amino acid sequence of IFN-α2a WT and produced mutants, explaining the C-terminal added features and their origin. (B) Binding and release concept of IFN functionalized for pulmonic application (pIFN). 1: pIFN and FXIIIa are co-inhaled using a nebulizer, reaching the alveolar lung system 2: pIFN is covalently bound by FXIIIa to the extracellular matrix 3: upon pathogen recognition MMP-9 is expressed by immigrating macrophages and neutrophils, which recognizes the cleavable sequence. 4: pIFN is released and stimulates the innate immune system for a faster response.

Materials and Methods

Materials

1,4-dithiothreitol (DTT), carbenicillin, isopropyl-β-D-thiogalactopyranosid (IPTG), penicillin-streptomycin, phenylmethylsulfonyl fluoride (PMSF), guanidine hydrochloride, Primer, NDSB-201, lysozyme, DNAse-I, Triton X-100, acetonitrile HPLC grade, goat anti-mouse IgG horseradish peroxidase (HRP) secondary antibody and trifluoracetic acid were purchased from Sigma Aldrich (Schnelldorf, Germany). PageRuler™ Prestained Protein Ladder, PageRuler™ broad range protein ladder, coomassie brilliant blue G250, NuPAGE LDS Sample Buffer (4X), slide-a-lyzer, Dulbeco's Modified Eagle's Medium (DMEM), Gibco-FBS-HI (Origin Brasil) BCA assay, synthesized IFN-α2a genes, *E.coli* BL21(DE3)Star bacteria, Pierce C18 Tips, iodacetamide (IAA), 1-Step™ Ultra TMB-ELISA substrate solution and formic acid MS grade were ordered from Thermo Fisher Scientific Germany (Darmstadt, Germany). BioPro IEX SmartSep S20 1 mL and 5 mL were ordered from YMC Europe (Dinslaken, Germany). XK16/600 Superdex 75 pg column was ordered from Cytiva Life Sciences (Freiburg, Germany). Zorbax 300SB-CN column was ordered from Agilent (Waldbronn, Germany). Vivaspin centrifugal concentrators were ordered from Sartorius AG (Göttingen, Germany). Spectra/Por 1 Dialysis Membrane Standard RC tubing was ordered from Repligen (Ravensburg, Germany). ROTIPHORESE® NF-Acrylamide/Bis-Solution 30 (29:1) and 10x RotiBlock solution was ordered from Carl Roth GmbH (Karlsruhe, Germany). HEK-Blue™ IFN-α/β Cells, blasticidin and zeocin were ordered from Invivogen (Toulouse, France). Trypsin MS grade was ordered from Promega (Walldorf, Germany). Monoclonal IFN-α (6B18) Mouse mAb #3110 was ordered from cell signaling technologies (Frankfurt am Main, Germany). Strata™-X 33 µm Polymeric Reversed Phase syringe columns were ordered from Phenomenex (Aschaffenburg, Germany). Pre columns and columns for LC-MS/MS analysis were ordered from PepSep (Marslev, Denmark). ReproSil-Pur 120 C18-AQ, 1.9 µm was ordered from Dr. Maisch (Ammerbuch-Entringen, Germany). Bovine Serum Albumin standard for MALDI-TOF MS calibration were purchased from Bruker (Bremen, Germany).

Methods

Expression, refolding and purification of Interferon-α2a WT, and mutants. Expression, refolding and purification of mentioned proteins (IFN-α2a WT, IFN-PSL-TG and IFN-SCR-TG) was performed as described before for IFN-α2a WT.[98] In brief, genes were cloned into a pET21a(+) plasmid between NdeI and BamHI. The plasmid was transformed into *E. coli* BL21(DE3) bacteria and expression took place by 1 mM IPTG induction at an OD600 of 0.7 for 8 h. Afterwards, cells were harvested by centrifugation and the washed remaining pellet, containing the inclusion bodies unfolded in 7 M guanidinium. The unfolded protein was refolded overnight, followed by centrifugation and dialysis. In the following days, purification was performed by FPLC (1x AIEX, 1x CIEX, 1x SEC). Purified fractions were set to 1 mg/mL, snap frozen in liquid N_2 and stored at -80 °C until further usage.

Matrix-assisted laser-desorption ionization time of flight mass spectrometry. Matrix-assisted laser-desorption ionization time of flight mass spectrometry (MALDI-TOF MS) analysis was performed as described before.[98]

Reversed phase high pressure liquid chromatography analysis. Reversed phase high pressure liquid chromatography (RP-HPLC) analysis was performed as described before.[98] In brief, analysis took place using an Agilent Zorbax 300SB-CN column (4.6 x 150 mm, 5 µm). A gradient from 5-70 % B over 35 min was used. Eluent A = H_20 + 0.1 % TFA, Eluent B = Acetonitrile + 0.1 % TFA, used wavelength = 214 nm.

HEK Blue IFNα/β cell culture assay. The *in vitro* cell culture assay was performed according to the manufacturer's instruction. In brief, cells were seeded in a 96 well plate on day 1 and stimulated with IFNs in a 10-fold dilution series starting at a concentration of 1 µg/mL. On day 2, 20 µL of the supernatant was mixed with 180 µL of Quanti-Blue™ and detected at a wavelength of 630 nm after 120 min using a plate reader (Tecan Infinite 200 pro, Tecan Deutschland GmbH, Crailsheim, Germany).

sodium dodecyl sulfate polyacrylamide gel electrophoresis. Sodium dodecyl sulfate polyacrylamide gel electrophoresis **(**SDS-PAGE) was performed as described before.[98] In brief, standard Tris-glycine buffer systems were used with a final Tris-HCl concentration of 37.5 mM and 1 g/L SDS. Acrylamide concentrations were adapted between 5 and 15 % depending on the needed separation.

Immobilization of Interferons to fibronectin. For each time point 2 µg of IFN were mixed with a 2-fold molar excess of fibronectin in 20 µL FXIIIa reaction buffer (50 mM Tris pH 7.6, 150 mM NaCl, 2,5 mM $CaCl_2$) and incubated at 37°C for 5 minutes. Afterwards FXIIIa was added to a final concentration of 10 U/mL. At each time point 20 µL were removed and mixed with 3µL 6x SDS reducing buffer, additionally containing 200 mM EDTA and immediately incubated at 80°C for 10 min. Afterwards, SDS-PAGE was performed as described before using 5-20 % gradient gels.

Western blotting. Western blotting was described as performed before.[270] In brief, after finishing SDS PAGE, gels were removed carefully, and the stacking gel was discarded. Afterwards, the gel was blotted on nitrocellulose membrane for 90 min at 80 V.

After finishing the transfer, the membrane was blocked with 5% skim milk powder in TBS-T (w/v) solution for 1h at 4°C. The membrane was washed with TBS-T for 5 min and probed with the 1st antibody overnight at 4°C. For the 1st antibody a dilution of 1:2000 was used and the antibody was diluted in 5% skim milk powder in TBS-T (w/v) solution. At the following day, the 1st antibody was removed and the membrane washed again 3 times with TBS-T for 10 min and probed with the 2nd antibody for 1 h at room temperature. The 2nd antibody was diluted 1:4000 in 1x Rotiblock solution. The membrane was washed again 3 times with 10 mL TBS-T for 10 min. Afterwards the membrane was

detected for 1 minute using the SuperSignal™ West Pico PLUS Chemiluminescent Substrate on a chemiluminescent imaging unit (Odyssey FC, Leicor, Bad Homburg vor der Höhe, Germany).

Matrix metallopeptidase 9 digest of Interferon proteins. For each time point 2 µg of protein were incubated with matrix metallopeptidase 9 (MMP-9), which had a final concentration of 8 nM, in 10 µL MMP-9 cleavage buffer (50 mM Tris, pH 6.9, 200 mM NaCl, 5mM CaCl2, 1 µM ZnCl2, 0.05% Brij® 35). The samples were incubated at 37°C at 400 rpm. At indicated time points 10 µL were removed and mixed with 3 µL SDS reducing buffer, containing 200 mM EDTA and heated at 80°C for 10 min.

Trypsin in solution digest. 8M Guanidinium hydrochloride (GdHCl) dissolved in 100 mM ammonium bicarbonate (ABC) buffer was added to the protein solution to a final concentration of 6M GdHCl. Additionally, DTT was added to a final concentration of 2 mM. The solution was heated at 70 °C for 20 min. The solution was diluted with ABC buffer to a final GdHCl concentration of 0.8 M. At this point 1:40 (w/w) of trypsin was added and the sample was incubated for 2h at 37°C 400 rpm. Afterwards another 1:40 trypsin was added and the sample was incubated overnight. At the next day DTT was added to a final concentration of 40 mM and the sample was heated for 10 min at 70 °C. Afterwards Iodacetamide was added to a final concentration of 120 mM and the sample was incubated for 20 min in the dark. The pH was checked regularly to be between 7 and 8 by using pH universal indicator paper. If the sample was too acidic. Small amounts of 1M Tris-HCl pH 8 were added. The samples were then desalted using Strata™-X 33 µm Polymeric Reversed Phase syringe columns columns 1cc according to a previously published protocol [98]. After desalting, the samples were snap frozen in liquid nitrogen and lyophilised and handled for ESI-MS/MS as previously described [98].

***In vitro* production of extracellular matrix (ECM).** ECM was produced as described before in 96-well plates. [410] In brief, Nih3T3 fibroblasts were seeded on day 1 at high confluency and supplemented with FBS and ascorbic acid containing DMEM medium. The medium was exchanged each day and cells were cultivated for 6 days. At day 6, cells were detached by osmotic pressure using distilled water and the ECM was washed. Afterwards, the ECM was stored in PBS + 2% P/S at 4 °C for up to 3 months.

ECM FXIIIa binding assay. IFN was added to final concentrations in 80 µL FXIIIa buffer (50 mM Tris pH 7.6, 150 mM NaCl, 2.5 mM $CaCl_2$) as indicated. The samples were added to 96-well ECM plates which were washed previously twice with FXIIIa buffer. The plate was heated in a cell culture incubator for 15 min to reach a temperature of 37 °C. At this time point FXIIIa was added to a final concentration of 10 U/mL and a final volume of 100 µL. At the indicated time points the samples were aspirated and PBS, containing 50 mM EDTA was added into the wells to stop the FXIIIa reaction. After the last reaction was completed, the ECM was washed with TBS-T (20 mM tris, 150 mM NaCl, 0.1 % Tween 20, pH 7.4) for 10 min and subsequently blocked with 1x RotiBlock in TBS-T for 1 h at RT. After blocking the ECM was washed three times with TBS-T for 10 min and the first antibody (dilution 1:1000 in TBS-T) was applied at 4 °C overnight. The next day the ECM was washed three times with

TBS-T for 15 min. Afterwards the second antibody (dilution 1:2000 in TBS-T) was applied for 1 h at RT. Next, the ECM was washed three times with TBS-T for 15 min. To detect the horseradish peroxidase (HRP) of the second antibody the 1-Step™ Ultra TMB-ELISA Substrate Solution was used according to instructions.

Release of Interferon from extracellular matrix by Matrix Metallopeptidase 9. IFN was bound to ECM as described above for 90 min. The total concentration of FXIIIa was 10 U/mL and 2 µM (44 µg/mL) for IFN-SCR-TG. After 90 minutes, the supernatant was removed from ECM by aspiration and the ECM was washed twice with MMP-9 cleavage buffer. Afterwards 100 µL of MMP-9 cleavage buffer containing 8 nM of MMP-) was added to the wells. The "no FXIIIa" control, the 0 h time point as well as the antibody control were not treated with MMP-9. Instead, only buffer was added. The cleavage was stopped at the indicated time points by aspiration and washing with PBS + 50 mM EDTA, which was done twice. All control wells were aspirated and washed at 0.5 h. All washed wells remained in PBS + 50 mM EDTA until the reaction was terminated in all wells. Afterwards, ECM was treated as described above. The ECM was washed with TBS-T, blocked and incubated with the mouse anti IFN-α antibody overnight at 4 °C. On the next day, The ECM was washed again, incubated with the goat anti mouse HRP-antibody and the signal was detected with 1-Step™ Ultra TMB-ELISA Substrate.

Peptide synthesis. Peptide synthesized in a Liberty Blue™ Automated Microwave Peptide Synthesizer was performed as described before (CEM Corporation Matthews, North Carolina) using the suggested standard coupling protocols by the manufacturer.[270] In brief, amino acids were coupled by standard SPPS chemistry on a Wang Harz resin using Fmoc-amino acids (0.2 M in DMF), Oxyma base (1 M in DMF) and *N,N′*-diisopropylcarbodiimid (DIC) (0.5 M in DMF) for coupling. Coupling of all amino acids was performed for 125 seconds at 90 °C. 20 % piperidine in DMF was used for Fmoc deprotection. Acetylation was performed with 20 % acetic anhydride in DMF for 20 min. Cleavage was performed with 92.5% TFA, 2.5% triisopropylsilane, 2.5% 2,2′-(ethylendioxy)diethanthiol, 2.5% H_2O. Precipitation was performed using 10-fold excess of -20 °C cold diethyl ether thrice. Purification was performed with RP-FPLC on an Äkta Explorer (Cytiva, Freiburg im Breisgau, Germany) using a Luna® 15 µm C18 LC column (250 × 21.2 mm) using a linear gradient of 33 % to 80 % B (Eluent A = H_2O + 0.1 % TFA , Eluent B = Acetonitrile + 0.1 % TFA), flow = 2 mL/min. Fractions were analysed by liquid chromatography and clean fractions freeze dried.

Results

Production and purification of IFN proteins was performed as described before.[98] In brief, IFNs were expressed in *E.coli* BL21(DE3)Star bacteria. As the IFNs precipitated as insoluble inclusion bodies, the proteins were extracted by high pressure homogenisation, washed and subsequently refolded. This process was followed by Ion exchange and size exclusion chromatography, yielding IFNs with more than 90% purity, as shown by SDS-PAGE and MALDI-TOF MS (**Figure 1**).

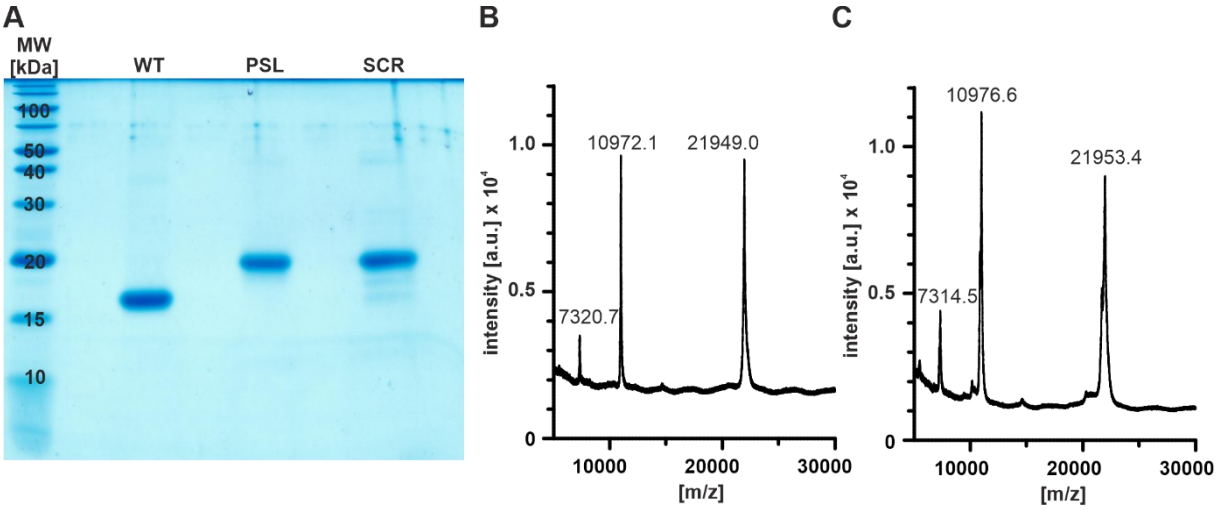

Figure 1: (A) SDS-Gel of purified IFNs: IFN-α2a WT (WT), IFN-PSL-TG (PSL) and IFN-SCR-TG (SCR). (B) MALDI-TOF MS of IFN-PSL-TG expected mass= 21963.0 (C) MALDI-TOF MS of IFN-SCR-TG expected mass = 21963.0.

Initially the pulmonic mutants contained two serine residues in the linker instead of the two aspartates, which are shown in scheme 1 (**Scheme 1A**; linker part 3). Due to the isoelectric shift caused by the TG recognition sequence, which contains two lysine residues, the isoelectric point of both mutants was shifted to close to physiological pH (theoretical pI of mutants with serine residues = 6.83). This led to protein aggregation overnight (even at 4°C) if incubated in buffers close to physiological pH (data not shown). Therefore, two serine residues were replaced in the linker by aspartate to counter the isoelectric shift an keep the natural isoelectric point of 5.96. These mutants were stable at physiological pH.

Afterwards, the mutants were characterized by RP-HPLC analysis, showing similar elution patterns for the pulmonic IFN (pIFN) mutants. Both mutants eluted slightly earlier than IFN-α2a WT (**Figure 2A** and **Table 1**).

Table 1: Potency of tested IFNs given as 95 % confidence intervals and the retention time [r.t.] during RP-HPLC analysis.

sample	EC_{50} [pM]	r.t. [min]
IFN-WT	1.7-2.4	28.9
IFN-PSL-TG	2.5-3.8	28.5
IFN-SCR-TG	3.4-4.3	28.5

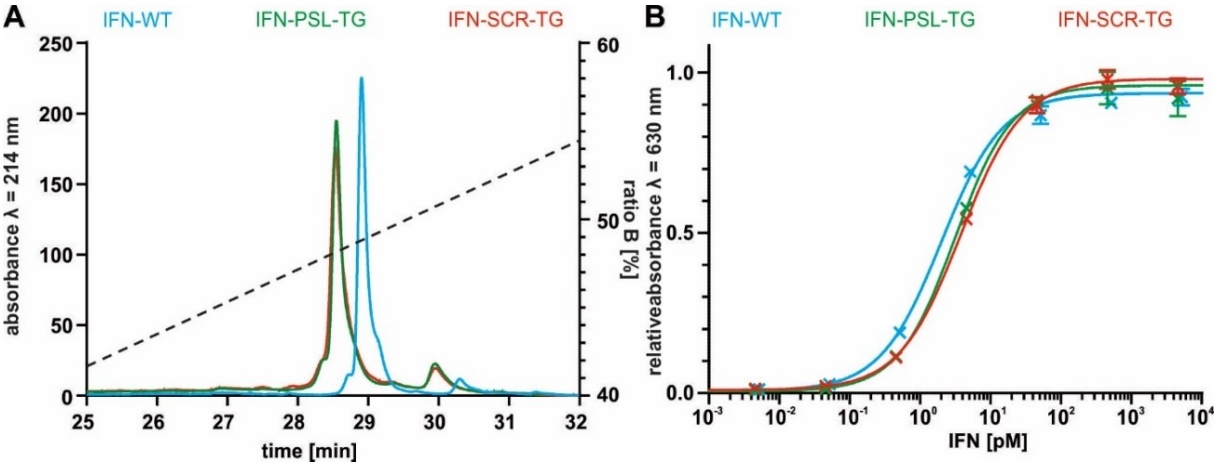

Figure 2: (A) RP-HPLC analysis of IFN-α2a WT, IFN-PSL-TG and IFN-SCR-TG. (B) Secreting alkaline phosphatase assay of HEKBlue™ 293 IFN-α/β cells after 20 h of stimulation with IFN-α2a WT, IFN-PSL-TG and IFN-SCR-TG (mean ± standard deviation, n=3). (WT=blue, IFN-PSL-TG=green, IFN-SCR-TG= red)

The mutants were then tested in an *in vitro* bioactivity assay to test if the C-terminal elongation had an impact on their biological potency using a IFN sensitive HEK cell line (**Figure 2B** and **Table 1**).[98] As shown, the C-terminal elongation has no impact on the protein's biological potency and both mutants retain a biological activity that is similar to IFN-α2a WT.

Afterwards, the TG recognition site was evaluated using a model peptide with the sequence Ac-NQEQVSPL(Aha)-NH_2, which has also been used for a previously published study,[270] whereby the model peptide acts as the glutamine donor in the enzymatic reaction (**Figure 3**).

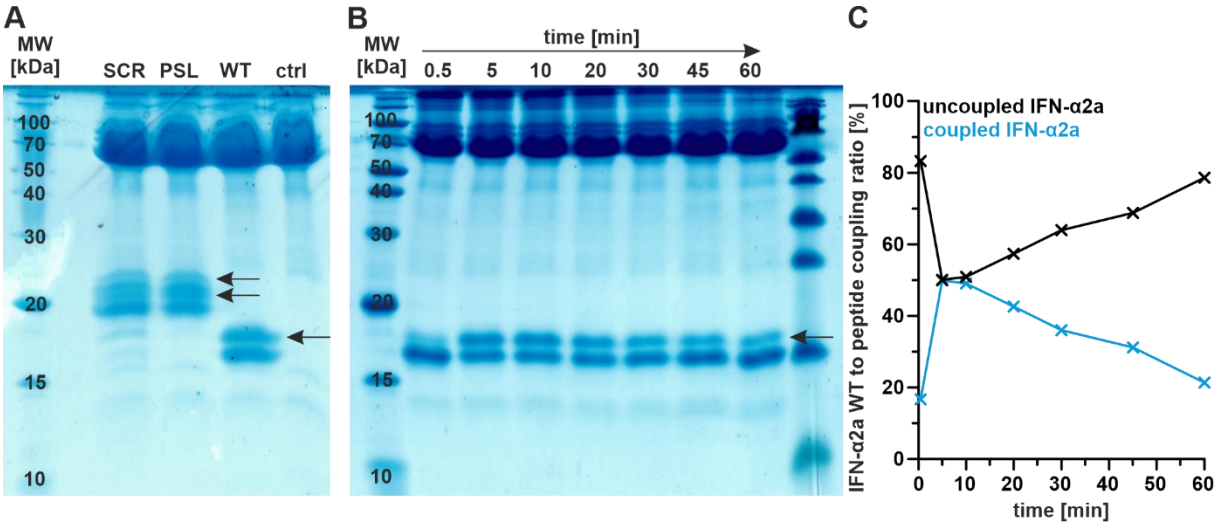

Figure 3: Incubation of IFNs with a 20-fold molar excess of the model peptide and FXIIIa. Coupled products are indicated with black arrows in A and B. (A) Incubation of IFNs for 20 min with the model peptide; IFN-SCR-TG, (SCR), IFN-PSL-TG (PSL), IFN-α2a WT (WT) and FXIIIa only (ctrl). (B) Timeline of IFN-α2a WT incubation with the model peptide and FXIIIa. (C) Coupling efficiency analysis of B, analyzed with imageJ by SDS-PAGE band intensity quantification.

Unexpectedly IFN-α2a WT appears to have an internal TG recognition sequence as analyzed by SDS-PAGE (**Figure 3A**). Consequently, the mutants showed a triple band as the peptide was coupled to the internal TG site, as well as to the artificially attached C-terminal TG site. This phenomenon was further evaluated in a time course experiment (**Figure 3B and 3C**), showing that the peptide is quickly attached to 50 % of the available IFN-α2a WT, but is then slowly lysed afterwards.

To evaluate if the internal TG recognition sequence is also targetable for the coupling of IFN-α2a WT to the extracellular matrix, all IFNs were used in a similar time course experiment. In this case fibronectin was added as a glutamine donor instead of the model peptide (**Figure 4**).

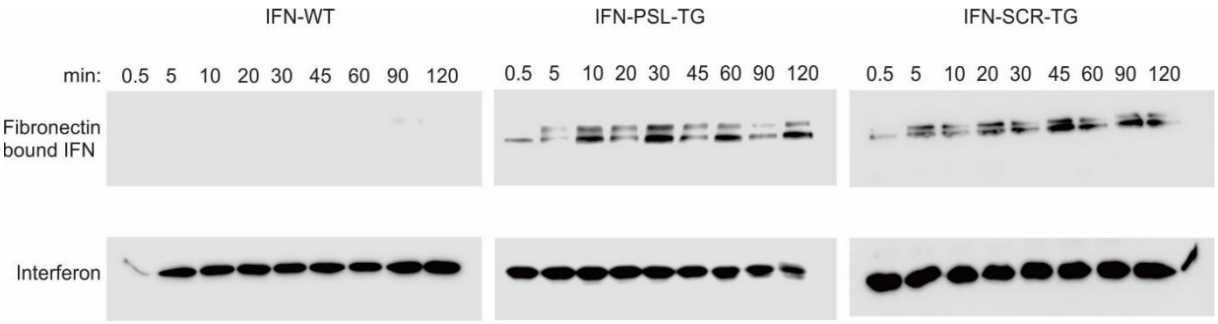

Figure 4: Timeline of IFN-α2a WT, IFN-PSL-TG and IFN-SCR-TG covalent attachment to fibronectin, catalyzed by FXIIIa.

As shown in figure 4, IFN-α2a WT is not coupled to fibronectin by FXIIIa, in contrast to the engineered pIFNs, for which coupled products are already detectable by immunoblotting after 30 seconds, though the overall coupling efficiency appears to be low. On the other hand, no lysis effect, as shown in figure 3, appears to happen. Therefore, the products are stably covalently bonded to fibronectin. As observed for IFN-PSL-TG and IFN-SCR-TG, an additional band appears after 5 min slightly over the fibronectin band, which may be a fibronectin dimer.

After proving the functionality of the TG recognition sequence the MMP-9 cleavable linker was evaluated (**Figure 5**).

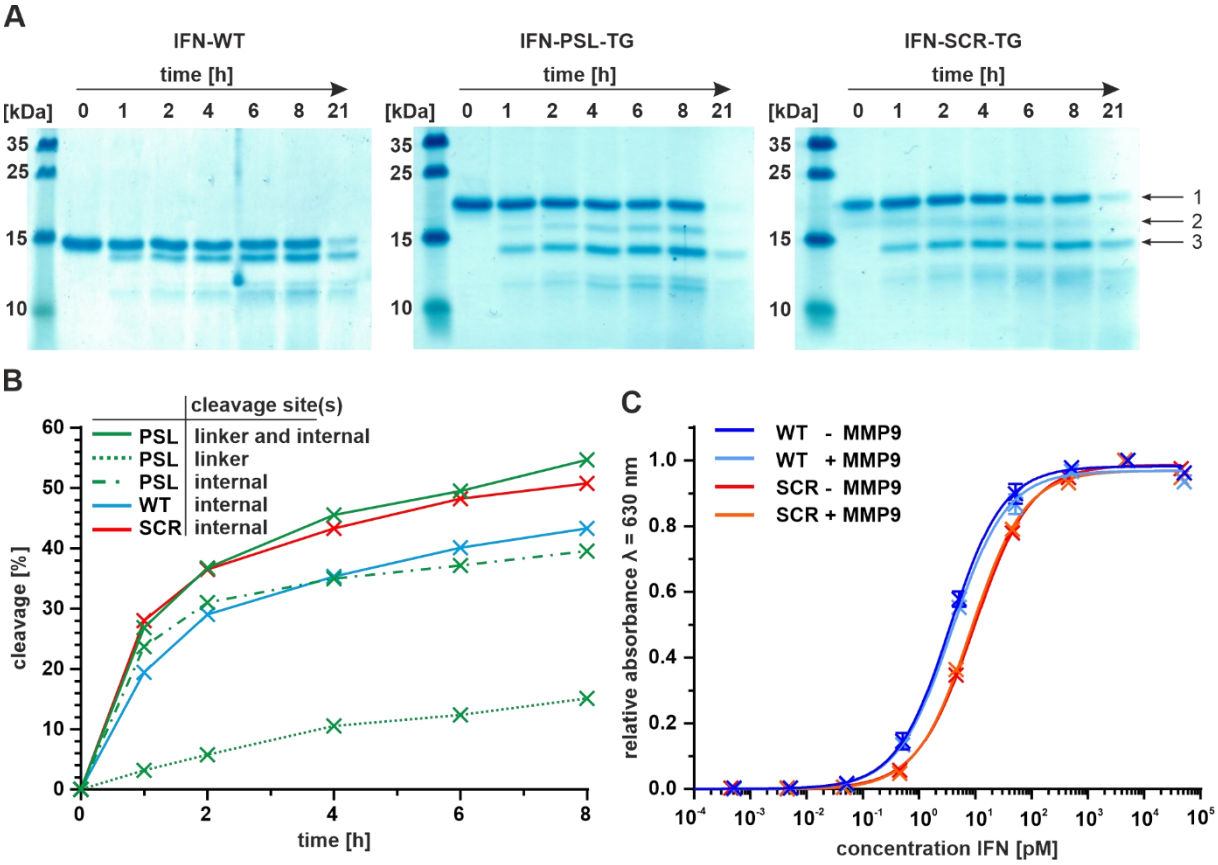

Figure 5: (A) Timeline of IFN-α2a WT (left), IFN-PSL-TG (middle) and IFN-SCR-TG (right) cleavage by MMP-9 over 21 h. Arrows on the right indicate the main products (1) non-cleaved protein (except for IFN-α2a WT), (2) cleaved MMP-9 linker in case of IFN-PSL-TG, (3) internally cleaved IFN. (B) Cleavage efficiency evaluation of A based on SDS-PAGE band intensity quantification performed with ImageJ. For IFN-PSL-TG the total cleavage rate (linker and internal), the cleavage rate of the internal linker (internal) and the cleavage rate of the artificial C-terminal TG linker (linker) is shown for IFN- α2a WT and IFN-SCR-TG the cleavage rate of the internal linker is shown. (C) potency curves of IFN-α2a WT and IFN-SCR-TG before (-) and after (+) MMP-9 digest.

Unexpectedly, IFN-α2a WT appears to have an internal MMP-9 cleavage sequence, which is much better recognized than the artificially introduced MMP-9 cleavable sequence, resulting in a cleavage efficiency of up to 55 % after 8 h (**Figure 5B**). If combined with the cleavage pattern of IFN-SCR-TG, the internal MMP-9 cleavage site must be close to the proteins C-terminus, as the retention distance on the SDS-PAGE between the non-cleaved and cleaved product differs between IFN-α2a WT and the mutant. To test, if the internal cleavage sequence affects the potency of IFN-α2a WT and IFN-SCR-TG, an additional potency assay was performed after 8h of incubation with MMP-9 (**Figure 5C**). As shown, the internal cleavage of a C-terminal portion of IFN does not affect its potency.

To locate the internal MMP-9 cleavage sequence, IFN-α2a WT was digested with MMP-9 and afterwards analyzed by trypsin in solution digest, followed by ESI MS/MS analysis (**Figure 6**).

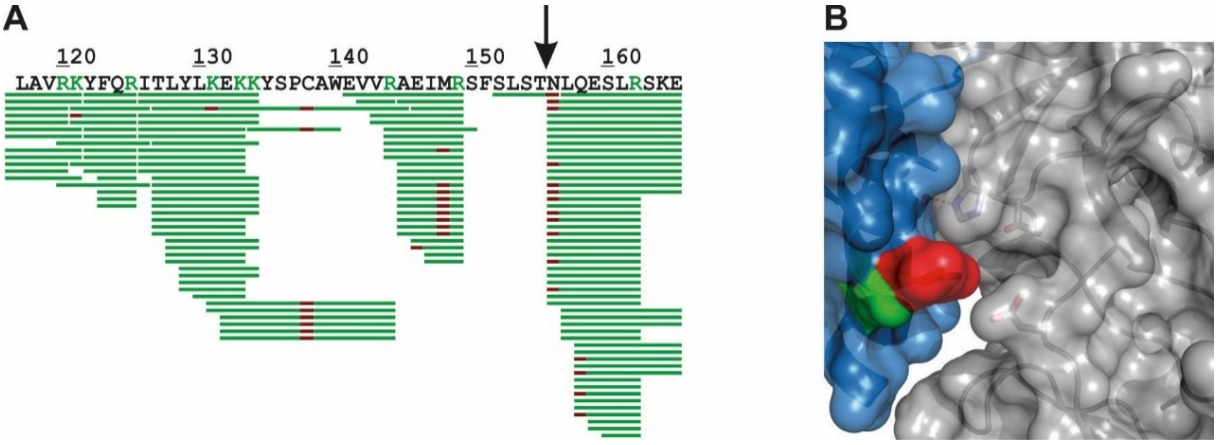

Figure 6: (A) MMP-9 tryptic digest of IFN-α2a WT displaying the found peptides for the last 68 amino acids. R and K are highlighted in green, indicating, that these cleavage sites are caused by trypsin. Modifications (see methods) are highlighted in red. The most likely cleavage site is marked with an arrow. (B) Cleavage site of IFN-α2a in its ternary receptor binding complex (pdb:3SE3). IFN is highlighted in blue, IFNAR2 is highlighted in grey. The side chain residues S152, L153, T155 and N156 of IFN-α2a WT as well as T75, H76 and D138 of IFNAR2 are displayed. T155 is highlighted in green, T156 is highlighted in red. Hydrogen bonds are displayed as yellow dashed lines.

As shown in figure 6A, the most likely cleavage site is between T155 and N156. The respective cleavage site is indicated on a molecular level in figure 6B. T155 does not interact with Interferon-α/β receptor 2 (IFNAR2) and N156 interacts only by hydrophobic interactions and van der waals (vdw) forces with H76 of IFNAR2.[8]

To test the binding concept in a more realistic *in vitro* setting, extracellular matrix (ECM) was produced as described before[410] and IFN-SCR-TG was incubated at concentrations of 5, 10, 20 and 40 µg/mL for up to 90 minutes with, or without FXIIIa (**Figure 7A and B**). IFN-PSL-TG was discarded for further analysis due to the additional detected cleavage site at IFN-α2a´s C-terminus. As shown in figure 7, a concentration and time dependent increase in immobilization can be observed, which was highest for the highest used concentration and time. Values were 3-5-fold higher compared to IFN-SCR-TG incubated on ECM without FXIIIa. As observed, a constant amount of IFN-SCR-TG absorbs unspecifically to the ECM, which amount is independent of the used IFN-SCR-TG concentration, FXIIIa addition and time (indicated by the grey bars in figure 7B). An IFN-SCR-TG concentration increase also increased the amount of detected IFN-SCR-TG, which is therefore covalently bound by FXIIIa to the ECM. Therefore, the usage of FXIIIa can immobilize significantly more amounts of IFN compared to the control, where no FXIIIa was added. For all used concentrations significant differences were measurable after 30 minutes of incubation. To further evaluate the suitability of the model, IFN-SCR-TGs cleavage from ECM was evaluated (**Figure 7C**). Before starting MMP-9 cleavage the relative difference between unspecifically absorbed IFN and covalently bound IFN was analyzed (**Figure 7C; left**). As shown a 5-fold higher amount of IFN-SCR-TG was immobilized with FXIIIa, compared to no FXIIIa. The cleavage efficiency of MMP-9 was best within the first hour of incubation, but drastically reduced afterwards. Nevertheless, 20 % of bound IFN-SCR-TG was released from ECM.

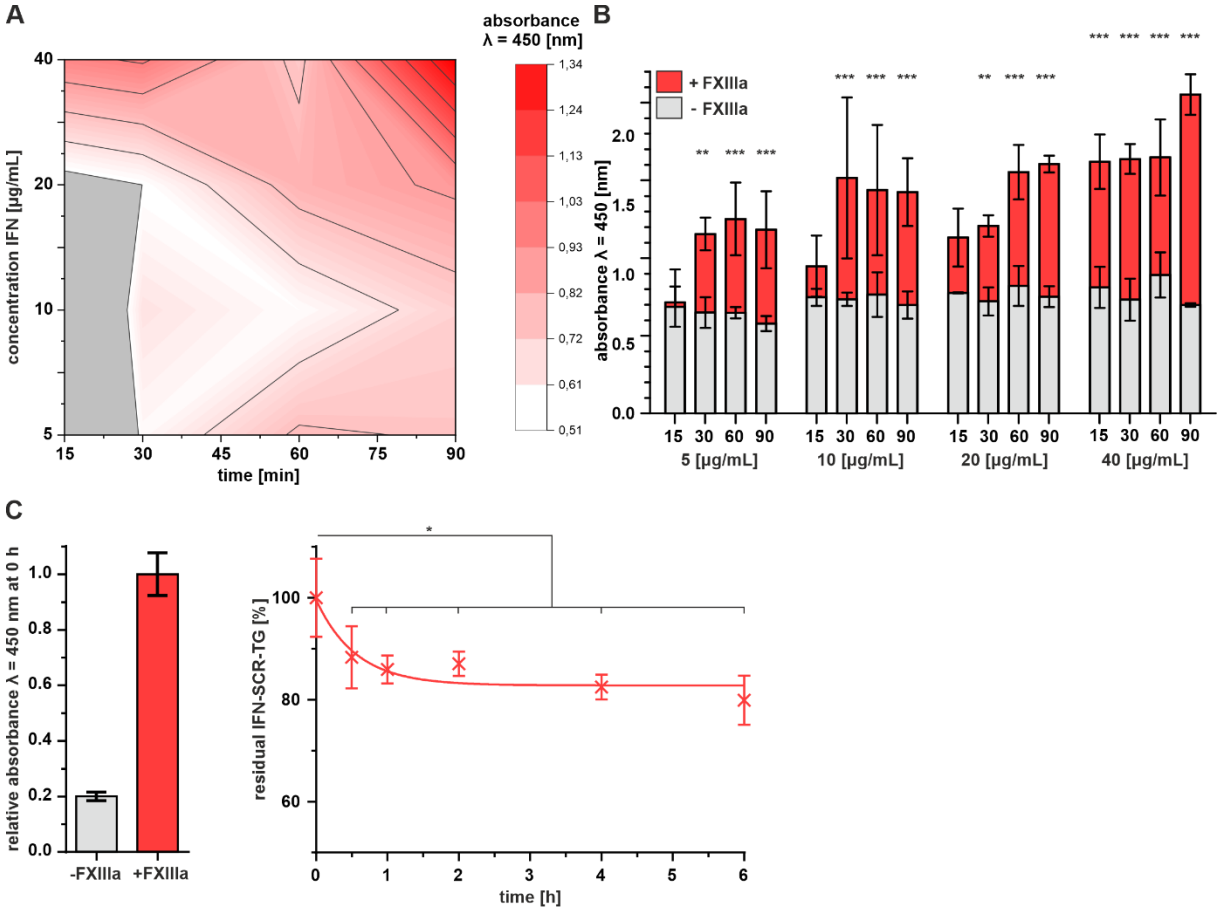

Figure 7: Qualitative analysis of immobilized IFN-SCR-TG on the surface of artificial ECM by enzymatic FXIIIa immobilization. (A) 2D Diagram of B with subtracted background. Increased binding is indicated with intensifying red. Grey areas are below the indicated threshold of 0.51. (B) Measured absorbance of IFN-SCR-TG bound to the ECM by HRP-ELISA (n=3). IFN-SCR-TG incubated with 10 U/mL FXIIIa is marked in red. IFN-SCR-TG without FXIIIa is marked in grey. Standard deviations are indicated. Significances were analyzed by two-way ANOVA between the control samples and the FXIIIa containing samples. (C) Cleavage of IFN-SCR-TG by MMP-9 from ECM after immobilization with FXIIIa (left). A control without FXIIIa is indicated (right).

Discussion

In this study, two IFN-α2a WT mutants, containing a TG recognition sequence at the proteins C-terminus were successfully purified and characterized by MALDI-TOF MS and RP-HPLC analysis. The pulmonic IFN mutants were analyzed for their purity and potency (**Figure 2**), which showed wildtype like activity. Additionally, the added features, which are the TG recognition sequence, and an MMP-9 protease sensitive linker were analyzed for their functionality by SDS-PAGE (**Figure 3 and 5**), Western blot analysis (**Figure 4**), as well as in an *in vitro* ECM binding assay (**Figure 7**). During investigation, two unknown features of IFN-α2a WT were discovered, which are an internal TG recognition sequence, though this is only valid for peptides (**Figure 3 and 4**), and an internal MMP-9 protease sensitive sequence, that is close to the proteins C-terminus (**Figure 5 and 6**). The exact location was determined to be likely between T155 and N156. A cleavage on this position is in accordance with the proteins retained potency after cleavage (**Figure 5C**). It was demonstrated, that significantly higher amounts of IFN can be covalently immobilized on ECM by FXIIIa and that the amount of bound IFN is

dependent on its concentration and incubation time (**Figure 7**). Furthermore, it was shown, that the bound IFN can be released by MMP-9 and that this cleavage is more efficient in solution (**Figure 5**), than from ECM itself (**Figure 7B**). It is likely, that MMP-9 does not only cleave IFN during incubation, but also other ECM proteins, resulting in an enzyme saturation, which inhibits further IFN-SCR-TG release. As a constant release of MMP-9 by macrophages can be expected in an *in vivo* setting, this should not impair the feasibility of the concept, though must be proven in future experiments. Additionally, an absolute quantification of deposited IFN on the ECM might be necessary for precise dose determination, as well as possible side effect reduction and must be performed in an *in vivo* experiment. Furthermore, side effects caused by IFN, which is not bound by FXIIIa during the initial application must be evaluated to assess the products benefit for patients.

Conclusion

In conclusion, the presented results demonstrate that the engineered mutant IFN-SCR-TG is a promising candidate for creating MMP-9 sensitive IFN depots, using FDA approved FXIIIa for immobilization. These depots are likely useful in preemptive pulmonic applications to dampen the viral load in the case of a respiratory infection[252] and decrease the time between pathogen infiltration and the innate immune response.

Conclusions and Outlook of the Thesis

In this thesis, poly(ethylene glycols) (PEG), linear polyglycerols (LPG) and poly-(2-ethyl-2-oxazolines) (PEtOx) with molecular weights from 10-40 kDa were synthesized and terminally functionalized with cyclooctyne groups (**Chapter 2,3,4 and 6**), or aldehyde groups (**Chapter 5**) to enable conjugation to azide functionalized proteins, or wildtype proteins. Conjugation was performed to either site specific azide functionalized Interferon-α2a (IFN-α2a) (**Chapter 2-4**) by strain promoted azide alkyne cycloaddition (SPAAC), human Interleukin-4 (hIL-4) by reductive alkylation (**Chapter 5**), or chemoenzymatic functionalized murine Interleukin-4 (mIL-4) by enzymatic functionalization of the C-terminus followed by SPAAC (**Chapter 6**). Additionally, IFNs pharmaceutical potential for its clinical future use was evaluated (**Chapter 1**), as well as its potential usability in a pulmonic application by enzymatic depot formation on extracellular matrix using the human coagulation factor XIIIa (FXIIIa) (**Chapter 7**).

Before the polymers were used for conjugation they were characterized for their molecular weight and dispersity (**Chapter 2-5**). The resulting, purified bioconjugates were characterized for their physico-chemical properties, including their molecular weight (**Chapter 2-6**), relative hydrophilicity (**Chapter 2-6)**, secondary structure (**Chapter 2 and 5**), hydrodynamic diameter (**Chapter 3-5**), thermal stability (**Chapter 2,3,4 and 6**), and their interaction with the proteins surface (**Chapter 2**). The latter two points were also investigated in an *in silico* study (**Chapter 2**). Furthermore, important biological parameters were investigated. This includes the bioconjugates potency compared to the wildtype protein(s) (**Chapter 2-6**), the binding affinity of anti-PEG IgG antibodies to PEG and LPG polymers and PEG and LPG bioconjugates (**Chapter 5**), induction of gene expression in macrophages in comparison to the wildtype proteins (**Chapter 6**), *in vivo* pharmacokinetics of higher molecular weight bioconjugates (**Chapter 3 and 4**) and an *in vivo* pharmacodynamic study using an influenza ferret model (**Chapter 4**), which highlighted that polymer type and size has an impact on the bioconjugates efficacy under *in vivo* conditions. Based on the presented results in these chapters, several trends and relations of parameters to each other were found.

As shown by thermal stability tests at physiological pH on IFN-α2a (**Chapter 2-4**) and mIL-4 bioconjugates (**Chapter 6**), the polymers length and hydrophilicity has an influence on the protein's thermal stability. Tough these differences are partially significant they are still rather small (± < 3 °C) and further aggregation and stability studies of each bioconjugate are needed to judge if these differences are pharmaceutically relevant. Noteworthy, as shown in chapter 2-4, a longer polymer chain does not necessarily lead to a more stable, or unstable bioconjugate based on its pure Tm value, but long term stability studies of IFN bioconjugates have shown that a longer polymer can positively influence its long term stability,[411] which may also be investigated in the future for LPG and PEtOx bioconjugates. Additionally, the influence of the polymer on the biological component varies and likely depends on the conjugation site and its influence on the surrounding accessible surface, by altering its interaction with

surrounding solvent and formation of new bonds between the polymer and the protein surface. It can therefore stabilize or destabilize the protein, or have no measurable influence on the proteins melting point. These findings are likely true for all three polymers as it was described before for PEG[412-415], is demonstrated in chapter 2,4 and 6 for PEtOx, as well as for LPG in chapter 2 and 3 with comparison to literature.[166] As a general trend (based on the three investigated polymers), a more hydrophilic polymer can better stabilize the protein than a hydrophobic polymer (**Chapter 2-4**)[166, 288], though differences are small.

Hydrophilicity of the bioconjugates was determined by HPLC analysis. The hydrophilicity of the conjugated polymer significantly impacted the hydrophilicity of the corresponding bioconjugate. LPG conjugation always led to an earlier retention time (**Chapter 2, 3 and 5**)[166] and PEtOx conjugation always led to later retention times (**Chapter 2, 4 and 6**)[360], when compared to the sole protein part. Interestingly, PEG conjugation altered IFN-α2a bioconjugates to be more hydrophilic (**Chapter 2 and 3**) and IL-4 bioconjugates to be more hydrophobic (**Chapter 5 and 6**), when compared to their unconjugated counterparts. In all cases, longer polymers led to an increase of the shown trends, but the effect was clearly stronger for LPG bioconjugates, than for PEG and PEtOx bioconjugates.

Hydrodynamic diameter analysis of bioconjugates agreed with findings described in literature, whereby LPG polymers lead to a similar growth rate in hydrodynamic size, as their PEG equivalents (**Chapter 3 and 5**).[166, 288] For PEtOx bioconjugates (**Chapter 4**), a slightly smaller growth rate in hydrodynamic diameter was measured which agrees with findings of unconjugated polymers.[178, 360]

The hydrodynamic diameters of found bioconjugates correlated well with their *in vitro* and *in vivo* parameters. As shown by multiple *in vitro* potency assays (**Chapter 2-6**), in which the IFN and IL-4 bioconjugates were compared to each other over a range of 10-40 kDa, using different linkers and conjugation strategies, as well as different potency assays, no significant difference was measured among them, when compared to bioconjugates of the same hydrodynamic size. This agrees with previously described studies.[166, 184] These findings are also in line with the conducted polymer surface interaction study (**Chapter 2**; LIP Assay), which qualitatively revealed no significant interaction of all three polymers with IFNs protein surface on a minute timescale, therefore attributing the loss in potency of investigated bioconjugates to a mostly steric effect of the bioconjugates polymer with regard to protein receptor interaction[245], as protein polymer surface interactions are likely weak and only cover the protein surface transiently.

Polymer related differences were detected during the executed pharmacokinetic study, which is presented in chapter 3. In comparison to PEG bioconjugates, LPG bioconjugates of similar hydrodynamic size had similar terminal excretion rates, but LPG showed an initial more rapid distribution phase within the first 8 hours, which lead to overall slightly lower plasma levels and affected their overall serum half-life's. Another *in vivo* study indicated similar differences between PEG and LPG bioconjugates in their initial phase, tough not explicitly stated by the authors.[166] As written in

chapter 3, the reason for this effect remains elusive and needs further *in vivo* studies, which may be performed in a bioimaging study using radiolabeled LPGs to accurately determine LPGs biodistribution. An uptake effect, or faster distribution into body compartments is likely the reason for this phenomenon, which saturates over time as the difference in disposition kinetics between LPG and PEG bioconjugates align in the terminal phase. Tested PEtOx bioconjugates behaved like similar sized PEG bioconjugates (**Chapter 4**), which agrees with recently described findings of tested radiolabeled polymers.[402] Additionally, radii balanced IFN-PEtOx bioconjugates were tested in an *in vivo* ferret influenza model (**Chapter 4**), against marketed Pegasys and IFN-PEG 40 kDa (which was characterized in chapter 3) and showed an improvement of clinical symptoms similar to the marketed influenza drug Oseltamivir, but further studies are needed to evaluate its potency conclusively.

In conclusion, the three used conjugation techniques, (i) site specific azide functionalization of the protein by amber codon expansion, followed by SPAAC, (ii) N-terminal reductive alkylation using aldehyde functionalized polymers at slightly acidic pH and (iii) enzymatic azide functionalization of C-terminally modified proteins, followed by SPAAC, are all viable options for polymer conjugation and all have their advantages, as well as disadvantages. Therefore, it is advisable to consider each of the presented techniques for bioconjugation and balance reasons for a final choice when engineering bioconjugates.

The two investigated PEG alternative polymers LPG and PEtOx are both viable options as PEG replacements, when a narrow dispersity, sufficiently high molecular weight and a high degree of functionalization is achieved during synthesis. This will likely be a key challenge to transfer their potential from the herein demonstrated lab applications to industrial relevant scales. LPG and PEtOx did show slightly different attributes than PEG, which can be exploited to boost the efficacy of LPG and PEtOx bioconjugates, but this must be evaluated for each application scenario.

The usage of FXIIIa to functionalize wildtype proteins for site selective bioconjugation and for tissue immobilization has likely a high potential but shows its limitations in the presented work. Tough the conjugation site is kind of specific to the artificially engineered peptide sequence, off targets were identified in both tested applications (**Chapter 6 and 7**). The steric complexity of both substrates seems to be important for the off targeting, as off targets were only detected for protein-peptide substrate pairs (**Chapter 6 and 7**), but not for the tested protein-protein substrate pair (**Chapter 7**). Additionally, an absolute quantification of immobilized substrate on the ECM is challenging and future work needs to be performed to evaluate this aspect and clarify specifically, if the immobilized protein amount is sufficient to trigger disease modifying effects. In contrast to the slow catalysis of isopeptide bonds between proteins and tissues (or other proteins), catalysis of protein-peptide bonds showed high yields (**Chapter 6 and 7**) demonstrating its potential for medicine and industry, though the reaction time must be optimized for every substrate.

References

1. Gasteiger, E.; Hoogland, C.; Gattiker, A.; Duvaud, S. e.; Wilkins, M. R.; Appel, R. D.; Bairoch, A., Protein Identification and Analysis Tools on the ExPASy Server. In *The Proteomics Protocols Handbook*, Walker, J. M., Ed. Humana Press: Totowa, NJ, 2005; pp 571-607.
2. Langer, J. A.; Cutrone, E. C.; Kotenko, S., The Class II cytokine receptor (CRF2) family: overview and patterns of receptor–ligand interactions. *Cytokine Growth Factor Rev.* **2004,** *15* (1), 33-48.
3. Lee, A. J.; Ashkar, A. A., The Dual Nature of Type I and Type II Interferons. *Front. Immunol.* **2018,** *9* (2061).
4. Stanifer, M. L.; Pervolaraki, K.; Boulant, S., Differential Regulation of Type I and Type III Interferon Signaling. *Int. J. Mol. Sci.* **2019,** *20* (6).
5. Mesev, E. V.; LeDesma, R. A.; Ploss, A., Decoding type I and III interferon signalling during viral infection. *Nat. Microbiol.* **2019,** *4* (6), 914-924.
6. Schroder, K.; Hertzog, P. J.; Ravasi, T.; Hume, D. A., Interferon-γ: an overview of signals, mechanisms and functions. *J. Leukocyte Biol.* **2004,** *75* (2), 163-189.
7. Mendoza, J. L.; Schneider, W. M.; Hoffmann, H.-H.; Vercauteren, K.; Jude, K. M.; Xiong, A.; Moraga, I.; Horton, T. M.; Glenn, J. S.; de Jong, Y. P.; Rice, C. M.; Garcia, K. C., The IFN-λ-IFN-λR1-IL-10Rβ Complex Reveals Structural Features Underlying Type III IFN Functional Plasticity. *Immunity* **2017,** *46* (3), 379-392.
8. Thomas, C.; Moraga, I.; Levin, D.; Krutzik, P. O.; Podoplelova, Y.; Trejo, A.; Lee, C.; Yarden, G.; Vleck, S. E.; Glenn, J. S.; Nolan, G. P.; Piehler, J.; Schreiber, G.; Garcia, K. C., Structural linkage between ligand discrimination and receptor activation by type I interferons. *Cell* **2011,** *146* (4), 621-32.
9. Mendoza, J. L.; Escalante, N. K.; Jude, K. M.; Sotolongo Bellon, J.; Su, L.; Horton, T. M.; Tsutsumi, N.; Berardinelli, S. J.; Haltiwanger, R. S.; Piehler, J.; Engleman, E. G.; Garcia, K. C., Structure of the IFNγ receptor complex guides design of biased agonists. *Nature* **2019,** *567* (7746), 56-60.
10. Snell, L. M.; McGaha, T. L.; Brooks, D. G., Type I Interferon in Chronic Virus Infection and Cancer. *Trends Immunol.* **2017,** *38* (8), 542-557.
11. EMA, Plegridy 125 micrograms solution for injection in pre-filled syringe, https://www.ema.europa.eu/en/documents/product-information/plegridy-epar-product-information_en.pdf, accessed january 2022.
12. Salvetti, M.; Yun, J.; Appiah-Badu, D.; Sabatella, G.; Naylor, M. L., 070 Baseline characteristics and safety profile of patients with relapsing-remitting multiple sclerosis (RRMS) in the first interim analysis of the peginterferon BETA-1A treatment in the phase 4 plegridy observational program (POP). *J. Neurol. Neurosurg. Psychiatry* **2018,** *89* (6), A29-A29.
13. Reder, A. T.; Feng, X., How type I interferons work in multiple sclerosis and other diseases: some unexpected mechanisms. *J. Interferon Cytokine Res.* **2014,** *34* (8), 589-599.
14. Feng, X.; Bao, R.; Li, L.; Deisenhammer, F.; Arnason, B. G. W.; Reder, A. T., Interferon-β corrects massive gene dysregulation in multiple sclerosis: Short-term and long-term effects on immune regulation and neuroprotection. *EBioMedicine* **2019,** *49*, 269-283.
15. Passegué, E.; Ernst, P., IFN-alpha wakes up sleeping hematopoietic stem cells. *Nat. Med.* **2009,** *15* (6), 612-613.
16. Essers, M. A. G.; Offner, S.; Blanco-Bose, W. E.; Waibler, Z.; Kalinke, U.; Duchosal, M. A.; Trumpp, A., IFNα activates dormant haematopoietic stem cells in vivo. *Nature* **2009,** *458* (7240), 904-908.
17. EMA, Besremi 250 micrograms/0.5 mL solution for injection in pre-filled pen, https://www.ema.europa.eu/en/documents/product-information/besremi-epar-product-information_en.pdf, (accessed 2022-06-05).
18. de Bruin, A. M.; Voermans, C.; Nolte, M. A., Impact of interferon-γ on hematopoiesis. *Blood* **2014,** *124* (16), 2479-2486.
19. Baldridge, M. T.; King, K. Y.; Boles, N. C.; Weksberg, D. C.; Goodell, M. A., Quiescent haematopoietic stem cells are activated by IFN-gamma in response to chronic infection. *Nature* **2010,** *465* (7299), 793-797.

20. Hervas-Stubbs, S.; Perez-Gracia, J. L.; Rouzaut, A.; Sanmamed, M. F.; Le Bon, A.; Melero, I., Direct effects of type I interferons on cells of the immune system. *Clin. Cancer Res.* **2011,** *17* (9), 2619-27.
21. Castro, F.; Cardoso, A. P.; Gonçalves, R. M.; Serre, K.; Oliveira, M. J., Interferon-Gamma at the Crossroads of Tumor Immune Surveillance or Evasion. *Front. Immunol.* **2018,** *9*, 847-847.
22. Jorgovanovic, D.; Song, M.; Wang, L.; Zhang, Y., Roles of IFN-γ in tumor progression and regression: a review. *Biomark Res.* **2020,** *8* (1), 49.
23. Ni, L.; Lu, J., Interferon gamma in cancer immunotherapy. *Cancer Med* **2018,** *7* (9), 4509-4516.
24. Frazão, J. B.; Colombo, M.; Simillion, C.; Bilican, A.; Keller, I.; Wüthrich, D.; Zhu, Z.; Okoniewski, M. J.; Bruggmann, R.; Condino-Neto, A.; Newburger, P. E., Gene expression in chronic granulomatous disease and interferon-γ receptor-deficient cells treated in vitro with interferon-γ. *J. Cell. Biochem.* **2019,** *120* (3), 4321-4332.
25. Sommereyns, C.; Paul, S.; Staeheli, P.; Michiels, T., IFN-lambda (IFN-lambda) is expressed in a tissue-dependent fashion and primarily acts on epithelial cells in vivo. *PLoS Pathog.* **2008,** *4* (3), e1000017.
26. Mahlakõiv, T.; Hernandez, P.; Gronke, K.; Diefenbach, A.; Staeheli, P., Leukocyte-Derived IFN-α/β and Epithelial IFN-λ Constitute a Compartmentalized Mucosal Defense System that Restricts Enteric Virus Infections. *PLoS Pathog.* **2015,** *11* (4), e1004782.
27. Sato, S.; Li, K.; Kameyama, T.; Hayashi, T.; Ishida, Y.; Murakami, S.; Watanabe, T.; Iijima, S.; Sakurai, Y.; Watashi, K.; Tsutsumi, S.; Sato, Y.; Akita, H.; Wakita, T.; Rice, C. M.; Harashima, H.; Kohara, M.; Tanaka, Y.; Takaoka, A., The RNA sensor RIG-I dually functions as an innate sensor and direct antiviral factor for hepatitis B virus. *Immunity* **2015,** *42* (1), 123-32.
28. Espinosa, V.; Dutta, O.; McElrath, C.; Du, P.; Chang, Y. J.; Cicciarelli, B.; Pitler, A.; Whitehead, I.; Obar, J. J.; Durbin, J. E.; Kotenko, S. V.; Rivera, A., Type III interferon is a critical regulator of innate antifungal immunity. *Sci. Immunol.* **2017,** *2* (16).
29. Galani, I. E.; Triantafyllia, V.; Eleminiadou, E. E.; Koltsida, O.; Stavropoulos, A.; Manioudaki, M.; Thanos, D.; Doyle, S. E.; Kotenko, S. V.; Thanopoulou, K.; Andreakos, E., Interferon-λ Mediates Non-redundant Front-Line Antiviral Protection against Influenza Virus Infection without Compromising Host Fitness. *Immunity* **2017,** *46* (5), 875-890.e6.
30. Zanoni, I.; Granucci, F.; Broggi, A., Interferon (IFN)-λ Takes the Helm: Immunomodulatory Roles of Type III IFNs. *Front. Immunol.* **2017,** *8*, 1661-1661.
31. Broggi, A.; Tan, Y.; Granucci, F.; Zanoni, I., IFN-λ suppresses intestinal inflammation by non-translational regulation of neutrophil function. *Nat. Immunol.* **2017,** *18* (10), 1084-1093.
32. Szabo, S. J.; Kim, S. T.; Costa, G. L.; Zhang, X.; Fathman, C. G.; Glimcher, L. H., A novel transcription factor, T-bet, directs Th1 lineage commitment. *Cell* **2000,** *100* (6), 655-69.
33. Markowitz, C. E., Interferon-beta: mechanism of action and dosing issues. *Neurology* **2007,** *68* (24 Suppl 4), S8-11.
34. Muir, A. J.; Arora, S.; Everson, G.; Flisiak, R.; George, J.; Ghalib, R.; Gordon, S. C.; Gray, T.; Greenbloom, S.; Hassanein, T.; Hillson, J.; Horga, M. A.; Jacobson, I. M.; Jeffers, L.; Kowdley, K. V.; Lawitz, E.; Lueth, S.; Rodriguez-Torres, M.; Rustgi, V.; Shemanski, L.; Shiffman, M. L.; Srinivasan, S.; Vargas, H. E.; Vierling, J. M.; Xu, D.; Lopez-Talavera, J. C.; Zeuzem, S., A randomized phase 2b study of peginterferon lambda-1a for the treatment of chronic HCV infection. *Journal of Hepatology* **2014,** *61* (6), 1238-1246.
35. Biopharmaceuticals, E., Phase 3 Study to Evaluate the Efficacy and Safety of Peginterferon Lambda for 48 Weeks in Patients With Chronic HDV (LIMT-2), https://clinicaltrials.gov/ct2/show/NCT05070364, (accessed January 2022). **2021**.
36. Phillips, S.; Mistry, S.; Riva, A.; Cooksley, H.; Hadzhiolova-Lebeau, T.; Plavova, S.; Katzarov, K.; Simonova, M.; Zeuzem, S.; Woffendin, C.; Chen, P.-J.; Peng, C.-Y.; Chang, T.-T.; Lueth, S.; De Knegt, R.; Choi, M.-S.; Wedemeyer, H.; Dao, M.; Kim, C.-W.; Chu, H.-C.; Wind-Rotolo, M.; Williams, R.; Cooney, E.; Chokshi, S., Peg-Interferon Lambda Treatment Induces Robust Innate and Adaptive Immunity in Chronic Hepatitis B Patients. *Front. Immunol.* **2017,** *8* (621).
37. Muir, A. J.; Shiffman, M. L.; Zaman, A.; Yoffe, B.; de la Torre, A.; Flamm, S.; Gordon, S. C.; Marotta, P.; Vierling, J. M.; Lopez-Talavera, J. C.; Byrnes-Blake, K.; Fontana, D.; Freeman, J.; Gray, T.; Hausman, D.; Hunder, N. N.; Lawitz, E., Phase 1b study of pegylated interferon lambda 1 with or without ribavirin in patients with chronic genotype 1 hepatitis C virus infection. *Hepatology* **2010,** *52* (3), 822-32.

38. Ingelheim, B., Fachinformation Imukin, https://s3.eu-central-1.amazonaws.com/prod-cerebro-ifap/media_all/60809.pdf, accessed january 2022. **2013**.
39. EMA, Betaferon 250 microgram/ml, powder and solvent for solution for injection, https://www.ema.europa.eu/en/documents/product-information/betaferon-epar-product-information_en.pdf, accessed january 2022.
40. EMA, Extavia 250 microgram/ml powder and solvent for solution for injection., https://www.ema.europa.eu/en/documents/product-information/extavia-epar-product-information_en.pdf, accessed january 2022.
41. Biogen, AVONEX® 30 Mikrogramm/0,5 ml Injektionslösung, https://s3.eu-central-1.amazonaws.com/prod-cerebro-ifap/media_all/81480.pdf, accessed january 2022. **2017**.
42. Merck, Fachinformation Rebif 44 Mikrogramm/0,5 ml Injektionslösung in einer Patrone, https://www.fachinfo.de/pdf/011740, accessed january 2022. **2020**.
43. Huang, Y.-W.; Hsu, C.-W.; Lu, S.-N.; Yu, M.-L.; Su, C.-W.; Su, W.-W.; Chien, R.-N.; Hsu, C.-S.; Hsu, S.-J.; Lai, H.-C.; Qin, A.; Tseng, K.-C.; Chen, P.-J., Ropeginterferon alfa-2b every 2 weeks as a novel pegylated interferon for patients with chronic hepatitis B. *Hepatol. Int.* **2020,** *14* (6), 997-1008.
44. Hsu, S.-J.; Yu, M.-L.; Su, C.-W.; Peng, C.-Y.; Chien, R.-N.; Lin, H.-H.; Lo, G.-H.; Su, W.-W.; Kuo, H.-T.; Hsu, C.-W.; Yang, S.-S.; Yang, S.-S.; Tseng, K.-C.; Qin, A.; Huang, Y.-W.; Chuang, W.-L., Ropeginterferon Alfa-2b administered every two weeks for patients with genotype 2 chronic hepatitis C. *J. Formosan Med. Assoc.* **2020**.
45. Gisslinger, H.; Zagrijtschuk, O.; Buxhofer-Ausch, V.; Thaler, J.; Schloegl, E.; Gastl, G. A.; Wolf, D.; Kralovics, R.; Gisslinger, B.; Strecker, K.; Egle, A.; Melchardt, T.; Burgstaller, S.; Willenbacher, E.; Schalling, M.; Them, N. C.; Kadlecova, P.; Klade, C.; Greil, R., Ropeginterferon alfa-2b, a novel IFNα-2b, induces high response rates with low toxicity in patients with polycythemia vera. *Blood* **2015,** *126* (15), 1762-9.
46. Corp, P., US Patent US8143214B2, https://patentimages.storage.googleapis.com/c9/85/98/6cbc39aa94a8a6/US8143214.pdf, accessed january 2022. **2008**.
47. Dohme, M. S., Fachinformation PegIntron® Clearclick® Fertigpen, https://www.msd.de/fileadmin/files/fachinformationen/pegintron.pdf, accessed january 2022. **2015**.
48. Wang, Y.-S.; Youngster, S.; Grace, M.; Bausch, J.; Bordens, R.; Wyss, D. F., Structural and biological characterization of pegylated recombinant interferon alpha-2b and its therapeutic implications. *Adv. Drug Delivery Rev.* **2002,** *54* (4), 547-570.
49. Wang, Y. S.; Youngster, S.; Bausch, J.; Zhang, R.; McNemar, C.; Wyss, D. F., Identification of the major positional isomer of pegylated interferon alpha-2b. *Biochemistry* **2000,** *39* (35), 10634-40.
50. Dohme, M. S., Fachinformation IntronA® 18 Mio. I.E./3 ml, – 25 Mio. I.E./2,5 ml, https://www.msd.de/fileadmin/files/fachinformationen/introna_loesung.pdf, accessed january 2022. **2018**.
51. Ratiopharm, Fachinformation Ribavirin-ratiopharm 200 mg/ 400 mg Filmtabletten, https://www.ratiopharm.de/assets/products/de/label/Ribavirin-ratiopharm%20200%20mg%20Filmtabletten.pdf?pzn=9487452, accessed january 2022. **2016**.
52. EMA, Pegasys INN-Peginterferon alpha 2a, https://www.ema.europa.eu/en/documents/product-information/pegasys-epar-product-information_en.pdf, (accessed 2022-06-05).
53. Foser, S.; Schacher, A.; Weyer, K. A.; Brugger, D.; Dietel, E.; Marti, S.; Schreitmüller, T., Isolation, structural characterization, and antiviral activity of positional isomers of monopegylated interferon alpha-2a (PEGASYS). *Protein Expr Purif* **2003,** *30* (1), 78-87.
54. Roche, Fachinformation Roferon A®, https://www.roche.de/dok/Roferon-reg-A-Fertigspritze-fachinfo-0-na-attach.pdf, accessed january 2022. **2018**.
55. Wills, R. J., Clinical Pharmacokinetics of Interferons. *Clin. Pharmacokinet.* **1990,** *19* (5), 390-399.
56. Wills, R. J.; Dennis, S.; Spiegel, H. E.; Gibson, D. M.; Nadler, P. I., Interferon kinetics and adverse reactions after intravenous, intramuscular, and subcutaneous injection. *Clin. Pharmacol. Ther.* **1984,** *35* (5), 722-7.
57. Harris, J. M.; Chess, R. B., Effect of pegylation on pharmaceuticals. *Nat. Rev. Drug Discov.* **2003,** *2* (3), 214-221.

58. Knop, K.; Hoogenboom, R.; Fischer, D.; Schubert, U. S., Poly(ethylene glycol) in Drug Delivery: Pros and Cons as Well as Potential Alternatives. *Angew. Chem. Int. Ed.* **2010,** *49* (36), 6288-6308.
59. Renal Filtration, Absorption and Catabolism of Human Alpha Interferon. *J. Interferon Res.* **1981,** *1* (3), 347-352.
60. Gupta, S. K.; Swan, S. K.; Marbury, T.; Smith, W.; Schwartz, S.; Kolz, K.; Cutler, D. L., Multiple-dose pharmacokinetics of peginterferon alfa-2b in patients with renal insufficiency. *Br. J. Clin. Pharmacol.* **2007,** *64* (6), 726-732.
61. Bino, T.; Edery, H.; Gertler, A.; Rosenberg, H., Involvement of the Kidney in Catabolism of Human Leukocyte Interferon. *J. Gen. Virol.* **1982,** *59* (1), 39-45.
62. Rajender Reddy, K.; Modi, M. W.; Pedder, S., Use of peginterferon alfa-2a (40 KD) (Pegasys®) for the treatment of hepatitis C. *Adv. Drug Delivery Rev.* **2002,** *54* (4), 571-586.
63. Glue, P.; Fang, J. W.; Rouzier-Panis, R.; Raffanel, C.; Sabo, R.; Gupta, S. K.; Salfi, M.; Jacobs, S., Pegylated interferon-alpha2b: pharmacokinetics, pharmacodynamics, safety, and preliminary efficacy data. Hepatitis C Intervention Therapy Group. *Clin. Pharmacol. Ther.* **2000,** *68* (5), 556-67.
64. Zeuzem, S.; Welsch, C.; Herrmann, E., Pharmacokinetics of peginterferons. *Semin. Liver Dis.* **2003,** *23 Suppl 1*, 23-8.
65. Salmon, P.; Le Cotonnec, J. Y.; Galazka, A.; Abdul-Ahad, A.; Darragh, A., Pharmacokinetics and pharmacodynamics of recombinant human interferon-beta in healthy male volunteers. *J Interferon Cytokine Res* **1996,** *16* (10), 759-64.
66. Isaacs, A.; Lindenmann, J.; Andrewes, C. H., Virus interference. I. The interferon. *Proc. R. Soc. Lond. B. Biol. Sci.* **1957,** *147* (927), 258-267.
67. Wheelock, E. F., Interferon-Like Virus-Inhibitor Induced in Human Leukocytes by Phytohemagglutinin. *Science* **1965,** *149* (3681), 310-1.
68. Rubinstein, M.; Rubinstein, S.; Familletti, P. C.; Gross, M. S.; Miller, R. S.; Waldman, A. A.; Pestka, S., Human leukocyte interferon purified to homogeneity. *Science* **1978,** *202* (4374), 1289-90.
69. Abuchowski, A.; van Es, T.; Palczuk, N. C.; Davis, F. F., Alteration of immunological properties of bovine serum albumin by covalent attachment of polyethylene glycol. *J. Biol. Chem.* **1977,** *252* (11), 3578-3581.
70. Abuchowski, A.; McCoy, J. R.; Palczuk, N. C.; van Es, T.; Davis, F. F., Effect of covalent attachment of polyethylene glycol on immunogenicity and circulating life of bovine liver catalase. *J. Biol. Chem.* **1977,** *252* (11), 3582-3586.
71. Nagata, S.; Taira, H.; Hall, A.; Johnsrud, L.; Streuli, M.; Ecsödi, J.; Boll, W.; Cantell, K.; Weissmann, C., Synthesis in E. coli of a polypeptide with human leukocyte interferon activity. *Nature* **1980,** *284* (5754), 316-320.
72. Wang, L.; Magliery, T. J.; Liu, D. R.; Schultz, P. G., A New Functional Suppressor tRNA/Aminoacyl−tRNA Synthetase Pair for the in Vivo Incorporation of Unnatural Amino Acids into Proteins. *J. Am. Chem. Soc.* **2000,** *122* (20), 5010-5011.
73. Kinstler, O.; Molineux, G.; Treuheit, M.; Ladd, D.; Gegg, C., Mono-N-terminal poly(ethylene glycol)-protein conjugates. *Adv Drug Deliv Rev* **2002,** *54* (4), 477-85.
74. Sheppard, P.; Kindsvogel, W.; Xu, W.; Henderson, K.; Schlutsmeyer, S.; Whitmore, T. E.; Kuestner, R.; Garrigues, U.; Birks, C.; Roraback, J.; Ostrander, C.; Dong, D.; Shin, J.; Presnell, S.; Fox, B.; Haldeman, B.; Cooper, E.; Taft, D.; Gilbert, T.; Grant, F. J.; Tackett, M.; Krivan, W.; McKnight, G.; Clegg, C.; Foster, D.; Klucher, K. M., IL-28, IL-29 and their class II cytokine receptor IL-28R. *Nat. Immunol.* **2003,** *4* (1), 63-8.
75. Kotenko, S. V.; Gallagher, G.; Baurin, V. V.; Lewis-Antes, A.; Shen, M.; Shah, N. K.; Langer, J. A.; Sheikh, F.; Dickensheets, H.; Donnelly, R. P., IFN-lambdas mediate antiviral protection through a distinct class II cytokine receptor complex. *Nat. Immunol.* **2003,** *4* (1), 69-77.
76. Deiters, A.; Cropp, T. A.; Summerer, D.; Mukherji, M.; Schultz, P. G., Site-specific PEGylation of proteins containing unnatural amino acids. *Bioorg. Med. Chem. Lett.* **2004,** *14* (23), 5743-5.
77. Bailon, P.; Palleroni, A.; Schaffer, C. A.; Spence, C. L.; Fung, W. J.; Porter, J. E.; Ehrlich, G. K.; Pan, W.; Xu, Z. X.; Modi, M. W.; Farid, A.; Berthold, W.; Graves, M., Rational design of a potent, long-lasting form of interferon: a 40 kDa branched polyethylene glycol-conjugated interferon alpha-2a for the treatment of hepatitis C. *Bioconjugate Chem.* **2001,** *12* (2), 195-202.

78. Perry, J. L.; Reuter, K. G.; Kai, M. P.; Herlihy, K. P.; Jones, S. W.; Luft, J. C.; Napier, M.; Bear, J. E.; DeSimone, J. M., PEGylated PRINT nanoparticles: the impact of PEG density on protein binding, macrophage association, biodistribution, and pharmacokinetics. *Nano letters* **2012,** *12* (10), 5304-5310.
79. Chin, J. W., Expanding and reprogramming the genetic code. *Nature* **2017,** *550* (7674), 53-60.
80. Liu, C. C.; Schultz, P. G., Adding New Chemistries to the Genetic Code. *Annu. Rev. Biochem.* **2010,** *79* (1), 413-444.
81. Chin, J. W., Expanding and Reprogramming the Genetic Code of Cells and Animals. *Annu. Rev. Biochem.* **2014,** *83* (1), 379-408.
82. Kularatne, S. A.; Deshmukh, V.; Gymnopoulos, M.; Biroc, S. L.; Xia, J.; Srinagesh, S.; Sun, Y.; Zou, N.; Shimazu, M.; Pinkstaff, J.; Ensari, S.; Knudsen, N.; Manibusan, A.; Axup, J.; Kim, C.; Smider, V.; Javahishvili, T.; Schultz, P. G., Recruiting cytotoxic T cells to folate-receptor-positive cancer cells. *Angew. Chem. Int. Ed. Engl.* **2013,** *52* (46), 12101-12104.
83. VanBrunt, M. P.; Shanebeck, K.; Caldwell, Z.; Johnson, J.; Thompson, P.; Martin, T.; Dong, H.; Li, G.; Xu, H.; D'Hooge, F.; Masterson, L.; Bariola, P.; Tiberghien, A.; Ezeadi, E.; Williams, D. G.; Hartley, J. A.; Howard, P. W.; Grabstein, K. H.; Bowen, M. A.; Marelli, M., Genetically Encoded Azide Containing Amino Acid in Mammalian Cells Enables Site-Specific Antibody–Drug Conjugates Using Click Cycloaddition Chemistry. *Bioconjugate Chem.* **2015,** *26* (11), 2249-2260.
84. Si, L.; Xu, H.; Zhou, X.; Zhang, Z.; Tian, Z.; Wang, Y.; Wu, Y.; Zhang, B.; Niu, Z.; Zhang, C.; Fu, G.; Xiao, S.; Xia, Q.; Zhang, L.; Zhou, D., Generation of influenza A viruses as live but replication-incompetent virus vaccines. *Science* **2016,** *354* (6316), 1170-1173.
85. Mills, J. H.; Khare, S. D.; Bolduc, J. M.; Forouhar, F.; Mulligan, V. K.; Lew, S.; Seetharaman, J.; Tong, L.; Stoddard, B. L.; Baker, D., Computational Design of an Unnatural Amino Acid Dependent Metalloprotein with Atomic Level Accuracy. *J. Am. Chem. Soc.* **2013,** *135* (36), 13393-13399.
86. Doherty, D. H.; Rosendahl, M. S.; Smith, D. J.; Hughes, J. M.; Chlipala, E. A.; Cox, G. N., Site-specific PEGylation of engineered cysteine analogues of recombinant human granulocyte-macrophage colony-stimulating factor. *Bioconjugate Chem.* **2005,** *16* (5), 1291-1298.
87. Rosendahl, M. S.; Doherty, D. H.; Smith, D. J.; Carlson, S. J.; Chlipala, E. A.; Cox, G. N., A Long-Acting, Highly Potent Interferon α-2 Conjugate Created Using Site-Specific PEGylation. *Bioconjugate Chem.* **2005,** *16* (1), 200-207.
88. Zhang, Y.; Zang, C.; An, G.; Shang, M.; Cui, Z.; Chen, G.; Xi, Z.; Zhou, C., Cysteine-specific protein multi-functionalization and disulfide bridging using 3-bromo-5-methylene pyrrolones. *Nat. Commun.* **2020,** *11* (1), 1015.
89. Peciak, K.; Laurine, E.; Tommasi, R.; Choi, J.-w.; Brocchini, S., Site-selective protein conjugation at histidine. *Chem. Sci.* **2019,** *10* (2), 427-439.
90. Kato, Y., Translational Control using an Expanded Genetic Code. *Int. J. Mol. Sci.* **2019,** *20* (4), 887.
91. Hancock, S. M.; Uprety, R.; Deiters, A.; Chin, J. W., Expanding the Genetic Code of Yeast for Incorporation of Diverse Unnatural Amino Acids via a Pyrrolysyl-tRNA Synthetase/tRNA Pair. *J. Am. Chem. Soc.* **2010,** *132* (42), 14819-14824.
92. Lühmann, T.; Gutmann, M.; Moscaroli, A.; Raschig, M.; Béhé, M.; Meinel, L., Biodistribution of Site-Specific PEGylated Fibroblast Growth Factor-2. *ACS Biomater. Sci. Eng.* **2020,** *6* (1), 425-432.
93. Wu, F.; Braun, A.; Lühmann, T.; Meinel, L., Site-Specific Conjugated Insulin-like Growth Factor-I for Anabolic Therapy. *ACS Biomater. Sci. Eng.* **2018,** *4* (3), 819-825.
94. Tabisz, B.; Schmitz, W.; Schmitz, M.; Luehmann, T.; Heusler, E.; Rybak, J. C.; Meinel, L.; Fiebig, J. E.; Mueller, T. D.; Nickel, J., Site-Directed Immobilization of BMP-2: Two Approaches for the Production of Innovative Osteoinductive Scaffolds. *Biomacromolecules* **2017,** *18* (3), 695-708.
95. Wandrey, G.; Wurzel, J.; Hoffmann, K.; Ladner, T.; Büchs, J.; Meinel, L.; Lühmann, T., Probing unnatural amino acid integration into enhanced green fluorescent protein by genetic code expansion with a high-throughput screening platform. *J. Biol. Eng.* **2016,** *10* (1), 11.
96. Luhmann, T.; Spieler, V.; Werner, V.; Ludwig, M. G.; Fiebig, J.; Mueller, T. D.; Meinel, L., Interleukin-4-Clicked Surfaces Drive M2 Macrophage Polarization. *Chembiochem* **2016,** *17* (22), 2123-2128.

97. Lühmann, T.; Jones, G.; Gutmann, M.; Rybak, J.-C.; Nickel, J.; Rubini, M.; Meinel, L., Bio-orthogonal Immobilization of Fibroblast Growth Factor 2 for Spatial Controlled Cell Proliferation. *ACS Biomater. Sci. Eng.* **2015,** *1* (9), 740-746.
98. Hauptstein, N.; Pouyan, P.; Kehrein, J.; Dirauf, M.; Driessen, M. D.; Raschig, M.; Licha, K.; Gottschaldt, M.; Schubert, U. S.; Haag, R.; Meinel, L.; Sotriffer, C.; Lühmann, T., Molecular Insights into Site-Specific Interferon-α2a Bioconjugates Originated from PEG, LPG, and PEtOx. *Biomacromolecules* **2021,** *22* (11), 4521-4534.
99. Skidmore, L.; Sakamuri, S.; Knudsen, N. A.; Hewet, A. G.; Milutinovic, S.; Barkho, W.; Biroc, S. L.; Kirtley, J.; Marsden, R.; Storey, K.; Lopez, I.; Yu, W.; Fang, S. Y.; Yao, S.; Gu, Y.; Tian, F., ARX788, a Site-specific Anti-HER2 Antibody-Drug Conjugate, Demonstrates Potent and Selective Activity in HER2-low and T-DM1-resistant Breast and Gastric Cancers. *Mol. Cancer Ther.* **2020,** *19* (9), 1833-1843.
100. Tian, F.; Lu, Y.; Manibusan, A.; Sellers, A.; Tran, H.; Sun, Y.; Phuong, T.; Barnett, R.; Hehli, B.; Song, F.; DeGuzman, M. J.; Ensari, S.; Pinkstaff, J. K.; Sullivan, L. M.; Biroc, S. L.; Cho, H.; Schultz, P. G.; DiJoseph, J.; Dougher, M.; Ma, D.; Dushin, R.; Leal, M.; Tchistiakova, L.; Feyfant, E.; Gerber, H.-P.; Sapra, P., A general approach to site-specific antibody drug conjugates. *Proc. Natl. Acad. Sci. U. S. A.* **2014,** *111* (5), 1766-1771.
101. Subramanian, G. M.; Fiscella, M.; Lamousé-Smith, A.; Zeuzem, S.; McHutchison, J. G., Albinterferon α-2b: a genetic fusion protein for the treatment of chronic hepatitis C. *Nat. Biotechnol.* **2007,** *25* (12), 1411-1419.
102. Zeuzem, S.; Sulkowski, M. S.; Lawitz, E. J.; Rustgi, V. K.; Rodriguez-Torres, M.; Bacon, B. R.; Grigorescu, M.; Tice, A. D.; Lurie, Y.; Cianciara, J.; Muir, A. J.; Cronin, P. W.; Pulkstenis, E.; Subramanian, G. M.; McHutchison, J. G., Albinterferon Alfa-2b was not inferior to pegylated interferon-α in a randomized trial of patients with chronic hepatitis C virus genotype 1. *Gastroenterology* **2010,** *139* (4), 1257-66.
103. Foster, G. R.; Zeuzem, S.; Pianko, S.; Sarin, S. K.; Piratvisuth, T.; Shah, S.; Andreone, P.; Sood, A.; Chuang, W. L.; Lee, C. M.; George, J.; Gould, M.; Flisiak, R.; Jacobson, I. M.; Komolmit, P.; Thongsawat, S.; Tanwandee, T.; Rasenack, J.; Sola, R.; Messina, I.; Yin, Y.; Cammarata, S.; Feutren, G.; Brown, K. K., Decline in pulmonary function during chronic hepatitis C virus therapy with modified interferon alfa and ribavirin. *J. Viral Hepat.* **2013,** *20* (4), e115-23.
104. Jones, T. D.; Hanlon, M.; Smith, B. J.; Heise, C. T.; Nayee, P. D.; Sanders, D. A.; Hamilton, A.; Sweet, C.; Unitt, E.; Alexander, G.; Lo, K. M.; Gillies, S. D.; Carr, F. J.; Baker, M. P., The development of a modified human IFN-alpha2b linked to the Fc portion of human IgG1 as a novel potential therapeutic for the treatment of hepatitis C virus infection. *J Interferon Cytokine Res* **2004,** *24* (9), 560-72.
105. Ji, S.-I.; Park, J.-H.; You, H.-g.; Chi, H.-j.; Bang, Y.-w.; Cha, S.-H., Intact bioactivities and improved pharmacokinetic of the SL335-IFN-β-1a fusion protein that created by genetic fusion of SL335, a human anti-serum albumin fab, and human interferon-β. *Immunol. Lett.* **2019,** *207*, 46-55.
106. Cho, S. Y.; Han, J.; Cha, S.-H.; Yoon, S.-i., Structural basis of serum albumin recognition by SL335, an antibody Fab extending the serum half-life of protein therapeutics. *Biochem. Biophys. Res. Commun.* **2020,** *526* (4), 941-946.
107. Barnard, J. G.; Babcock, K.; Carpenter, J. F., Characterization and Quantitation of Aggregates and Particles in Interferon-β Products: Potential Links Between Product Quality Attributes and Immunogenicity. *J. Pharm. Sci.* **2013,** *102* (3), 915-928.
108. Pepinsky, R. B.; LePage, D. J.; Gill, A.; Chakraborty, A.; Vaidyanathan, S.; Green, M.; Baker, D. P.; Whalley, E.; Hochman, P. S.; Martin, P., Improved pharmacokinetic properties of a polyethylene glycol-modified form of interferon-beta-1a with preserved in vitro bioactivity. *J Pharmacol Exp Ther* **2001,** *297* (3), 1059-66.
109. Frey, K.; Zivanovic, A.; Schwager, K.; Neri, D., Antibody-based targeting of interferon-alpha to the tumor neovasculature: a critical evaluation. *Integr Biol (Camb)* **2011,** *3* (4), 468-78.
110. Trinh, K. R.; Vasuthasawat, A.; Steward, K. K.; Yamada, R. E.; Timmerman, J. M.; Morrison, S. L., Anti-CD20-interferon-β fusion protein therapy of murine B-cell lymphomas. *J Immunother* **2013,** *36* (5), 305-318.
111. Ebbinghaus, C.; Ronca, R.; Kaspar, M.; Grabulovski, D.; Berndt, A.; Kosmehl, H.; Zardi, L.; Neri, D., Engineered vascular-targeting antibody-interferon-gamma fusion protein for cancer therapy. *Int. J. Cancer* **2005,** *116* (2), 304-13.

112. Han, Z.; Lu, Z.-R., Targeting Fibronectin for Cancer Imaging and Therapy. *J Mater Chem B* **2017,** *5* (4), 639-654.
113. Li, M.; Rao, C.; Pei, D.; Wang, L.; Li, Y.; Gao, K.; Wang, M.; Wang, J., Novaferon, a novel recombinant protein produced by DNA-shuffling of IFN-α, shows antitumor effect in vitro and in vivo. *Cancer cell international* **2014,** *14* (1), 8.
114. Lavoie, T. B.; Kalie, E.; Crisafulli-Cabatu, S.; Abramovich, R.; DiGioia, G.; Moolchan, K.; Pestka, S.; Schreiber, G., Binding and activity of all human alpha interferon subtypes. *Cytokine* **2011,** *56* (2), 282-9.
115. Piehler, J.; Thomas, C.; Garcia, K. C.; Schreiber, G., Structural and dynamic determinants of type I interferon receptor assembly and their functional interpretation. *Immunol. Rev.* **2012,** *250* (1), 317-334.
116. Bastard, P.; Rosen, L. B.; Zhang, Q.; Michailidis, E.; Hoffmann, H.-H.; Zhang, Y.; Dorgham, K.; Philippot, Q.; Rosain, J.; Béziat, V.; Manry, J.; Shaw, E.; Haljasmägi, L.; Peterson, P.; Lorenzo, L.; Bizien, L.; Trouillet-Assant, S.; Dobbs, K.; de Jesus, A. A.; Belot, A.; Kallaste, A.; Catherinot, E.; Tandjaoui-Lambiotte, Y.; Le Pen, J.; Kerner, G.; Bigio, B.; Seeleuthner, Y.; Yang, R.; Bolze, A.; Spaan, A. N.; Delmonte, O. M.; Abers, M. S.; Aiuti, A.; Casari, G.; Lampasona, V.; Piemonti, L.; Ciceri, F.; Bilguvar, K.; Lifton, R. P.; Vasse, M.; Smadja, D. M.; Migaud, M.; Hadjadj, J.; Terrier, B.; Duffy, D.; Quintana-Murci, L.; van de Beek, D.; Roussel, L.; Vinh, D. C.; Tangye, S. G.; Haerynck, F.; Dalmau, D.; Martinez-Picado, J.; Brodin, P.; Nussenzweig, M. C.; Boisson-Dupuis, S.; Rodríguez-Gallego, C.; Vogt, G.; Mogensen, T. H.; Oler, A. J.; Gu, J.; Burbelo, P. D.; Cohen, J. I.; Biondi, A.; Bettini, L. R.; D'Angio, M.; Bonfanti, P.; Rossignol, P.; Mayaux, J.; Rieux-Laucat, F.; Husebye, E. S.; Fusco, F.; Ursini, M. V.; Imberti, L.; Sottini, A.; Paghera, S.; Quiros-Roldan, E.; Rossi, C.; Castagnoli, R.; Montagna, D.; Licari, A.; Marseglia, G. L.; Duval, X.; Ghosn, J.; Tsang, J. S.; Goldbach-Mansky, R.; Kisand, K.; Lionakis, M. S.; Puel, A.; Zhang, S.-Y.; Holland, S. M.; Gorochov, G.; Jouanguy, E.; Rice, C. M.; Cobat, A.; Notarangelo, L. D.; Abel, L.; Su, H. C.; Casanova, J.-L., Autoantibodies against type I IFNs in patients with life-threatening COVID-19. *Science* **2020,** *370* (6515), eabd4585.
117. Zhang, Q.; Bastard, P.; Liu, Z.; Le Pen, J.; Moncada-Velez, M.; Chen, J.; Ogishi, M.; Sabli, I. K. D.; Hodeib, S.; Korol, C.; Rosain, J.; Bilguvar, K.; Ye, J.; Bolze, A.; Bigio, B.; Yang, R.; Arias, A. A.; Zhou, Q.; Zhang, Y.; Onodi, F.; Korniotis, S.; Karpf, L.; Philippot, Q.; Chbihi, M.; Bonnet-Madin, L.; Dorgham, K.; Smith, N.; Schneider, W. M.; Razooky, B. S.; Hoffmann, H.-H.; Michailidis, E.; Moens, L.; Han, J. E.; Lorenzo, L.; Bizien, L.; Meade, P.; Neehus, A.-L.; Ugurbil, A. C.; Corneau, A.; Kerner, G.; Zhang, P.; Rapaport, F.; Seeleuthner, Y.; Manry, J.; Masson, C.; Schmitt, Y.; Schlüter, A.; Le Voyer, T.; Khan, T.; Li, J.; Fellay, J.; Roussel, L.; Shahrooei, M.; Alosaimi, M. F.; Mansouri, D.; Al-Saud, H.; Al-Mulla, F.; Almourfi, F.; Al-Muhsen, S. Z.; Alsohime, F.; Al Turki, S.; Hasanato, R.; van de Beek, D.; Biondi, A.; Bettini, L. R.; D'Angio', M.; Bonfanti, P.; Imberti, L.; Sottini, A.; Paghera, S.; Quiros-Roldan, E.; Rossi, C.; Oler, A. J.; Tompkins, M. F.; Alba, C.; Vandernoot, I.; Goffard, J.-C.; Smits, G.; Migeotte, I.; Haerynck, F.; Soler-Palacin, P.; Martin-Nalda, A.; Colobran, R.; Morange, P.-E.; Keles, S.; Çölkesen, F.; Ozcelik, T.; Yasar, K. K.; Senoglu, S.; Karabela, Ş. N.; Rodríguez-Gallego, C.; Novelli, G.; Hraiech, S.; Tandjaoui-Lambiotte, Y.; Duval, X.; Laouénan, C.; Snow, A. L.; Dalgard, C. L.; Milner, J. D.; Vinh, D. C.; Mogensen, T. H.; Marr, N.; Spaan, A. N.; Boisson, B.; Boisson-Dupuis, S.; Bustamante, J.; Puel, A.; Ciancanelli, M. J.; Meyts, I.; Maniatis, T.; Soumelis, V.; Amara, A.; Nussenzweig, M.; García-Sastre, A.; Krammer, F.; Pujol, A.; Duffy, D.; Lifton, R. P.; Zhang, S.-Y.; Gorochov, G.; Béziat, V.; Jouanguy, E.; Sancho-Shimizu, V.; Rice, C. M.; Abel, L.; Notarangelo, L. D.; Cobat, A.; Su, H. C.; Casanova, J.-L., Inborn errors of type I IFN immunity in patients with life-threatening COVID-19. *Science* **2020,** *370* (6515), eabd4570.
118. Makris, S.; Paulsen, M.; Johansson, C., Type I Interferons as Regulators of Lung Inflammation. *Front. Immunol.* **2017,** *8*, 259-259.
119. Monk, P. D.; Marsden, R. J.; Tear, V. J.; Brookes, J.; Batten, T. N.; Mankowski, M.; Gabbay, F. J.; Davies, D. E.; Holgate, S. T.; Ho, L. P.; Clark, T.; Djukanovic, R.; Wilkinson, T. M. A., Safety and efficacy of inhaled nebulised interferon beta-1a (SNG001) for treatment of SARS-CoV-2 infection: a randomised, double-blind, placebo-controlled, phase 2 trial. *The Lancet. Respiratory medicine* **2021,** *9* (2), 196-206.
120. Mordstein, M.; Neugebauer, E.; Ditt, V.; Jessen, B.; Rieger, T.; Falcone, V.; Sorgeloos, F.; Ehl, S.; Mayer, D.; Kochs, G.; Schwemmle, M.; Günther, S.; Drosten, C.; Michiels, T.; Staeheli, P.,

Lambda interferon renders epithelial cells of the respiratory and gastrointestinal tracts resistant to viral infections. *J. Virol.* **2010,** *84* (11), 5670-7.
121. Andreakos, E.; Salagianni, M.; Galani, I. E.; Koltsida, O., Interferon-λs: Front-Line Guardians of Immunity and Homeostasis in the Respiratory Tract. *Front. Immunol.* **2017,** *8*, 1232-1232.
122. Channappanavar, R.; Fehr, A. R.; Vijay, R.; Mack, M.; Zhao, J.; Meyerholz, D. K.; Perlman, S., Dysregulated Type I Interferon and Inflammatory Monocyte-Macrophage Responses Cause Lethal Pneumonia in SARS-CoV-Infected Mice. *Cell host & microbe* **2016,** *19* (2), 181-93.
123. Schulz, K. S.; Mossman, K. L., Viral Evasion Strategies in Type I IFN Signaling - A Summary of Recent Developments. *Front. Immunol.* **2016,** *7*, 498.
124. Comar, C. E.; Goldstein, S. A.; Li, Y.; Yount, B.; Baric, R. S.; Weiss, S. R., Antagonism of dsRNA-Induced Innate Immune Pathways by NS4a and NS4b Accessory Proteins during MERS Coronavirus Infection. *mBio* **2019,** *10* (2).
125. Lee, J. S.; Park, S.; Jeong, H. W.; Ahn, J. Y.; Choi, S. J.; Lee, H.; Choi, B.; Nam, S. K.; Sa, M.; Kwon, J.-S.; Jeong, S. J.; Lee, H. K.; Park, S. H.; Park, S.-H.; Choi, J. Y.; Kim, S.-H.; Jung, I.; Shin, E.-C., Immunophenotyping of COVID-19 and influenza highlights the role of type I interferons in development of severe COVID-19. *Sci. Immunol.* **2020,** *5* (49), eabd1554.
126. Channappanavar, R.; Perlman, S., Pathogenic human coronavirus infections: causes and consequences of cytokine storm and immunopathology. *Semin. Immunopathol.* **2017,** *39* (5), 529-539.
127. Davidson, S.; McCabe, T. M.; Crotta, S.; Gad, H. H.; Hessel, E. M.; Beinke, S.; Hartmann, R.; Wack, A., IFNλ is a potent anti-influenza therapeutic without the inflammatory side effects of IFNα treatment. *EMBO Mol. Med.* **2016,** *8* (9), 1099-1112.
128. Andreakos, E.; Tsiodras, S., COVID-19: lambda interferon against viral load and hyperinflammation. *EMBO Mol. Med.* **2020,** *12* (6), e12465.
129. Davidson, S.; McCabe, T. M.; Crotta, S.; Gad, H. H.; Hessel, E. M.; Beinke, S.; Hartmann, R.; Wack, A., IFNλ is a potent anti-influenza therapeutic without the inflammatory side effects of IFNα treatment. *EMBO Mol. Med.* **2016,** *8* (9), 1099-112.
130. McLeod, V. M.; Chan, L. J.; Ryan, G. M.; Porter, C. J.; Kaminskas, L. M., Optimal PEGylation can improve the exposure of interferon in the lungs following pulmonary administration. *J. Pharm. Sci.* **2015,** *104* (4), 1421-30.
131. Colthorpe, P.; Farr, S. J.; Taylor, G.; Smith, I. J.; Wyatt, D., The pharmacokinetics of pulmonary-delivered insulin: a comparison of intratracheal and aerosol administration to the rabbit. *Pharm. Res.* **1992,** *9* (6), 764-8.
132. Colthorpe, P.; Fair, S. J.; Smith, I. J.; Wyatt, D.; Taylor, G., The Influence of Regional Deposition on the Pharmacokinetics of Pulmonary-Delivered Human Growth Hormone in Rabbits. *Pharm. Res.* **1995,** *12* (3), 356-359.
133. Niven, R. W.; Whitcomb, K. L.; Shaner, L.; Ip, A. Y.; Kinstler, O. B., The pulmonary absorption of aerosolized and intratracheally instilled rhG-CSF and monoPEGylated rhG-CSF. *Pharm. Res.* **1995,** *12* (9), 1343-9.
134. Megeed, Z.; Cappello, J.; Ghandehari, H., Genetically engineered silk-elastinlike protein polymers for controlled drug delivery. *Adv Drug Deliv Rev* **2002,** *54* (8), 1075-91.
135. Despanie, J.; Dhandhukia, J. P.; Hamm-Alvarez, S. F.; MacKay, J. A., Elastin-like polypeptides: Therapeutic applications for an emerging class of nanomedicines. *J. Controlled Release* **2016,** *240*, 93-108.
136. Hu, J.; Wang, G.; Liu, X.; Gao, W., Enhancing Pharmacokinetics, Tumor Accumulation, and Antitumor Efficacy by Elastin-Like Polypeptide Fusion of Interferon Alpha. *Adv. Mater.* **2015,** *27* (45), 7320-4.
137. Wang, Z.; Guo, J.; Sun, J.; Liang, P.; Wei, Y.; Deng, X.; Gao, W., Thermoresponsive and Protease-Cleavable Interferon-Polypeptide Conjugates with Spatiotemporally Programmed Two-Step Release Kinetics for Tumor Therapy. *Adv Sci (Weinh)* **2019,** *6* (16), 1900586.
138. Wang, Z.; Guo, J.; Ning, J.; Feng, X.; Liu, X.; Sun, J.; Chen, X.; Lu, F.; Gao, W., One-month zero-order sustained release and tumor eradication after a single subcutaneous injection of interferon alpha fused with a body-temperature-responsive polypeptide. *Biomater Sci* **2018,** *7* (1), 104-112.
139. Hu, X.; Seddighzadeh, A.; Stecher, S.; Zhu, Y.; Goyal, J.; Matson, M.; Marbury, T.; Smith, W.; Nestorov, I.; Hung, S., Pharmacokinetics, pharmacodynamics, and safety of peginterferon beta-1a in subjects with normal or impaired renal function. *J. Clin. Pharmacol.* **2015,** *55* (2), 179-188.

140. Gupta, S. K.; Pittenger, A. L.; Swan, S. K.; Marbury, T. C.; Tobillo, E.; Batra, V.; Sack, M.; Glue, P.; Jacobs, S.; Affrime, M., Single-dose pharmacokinetics and safety of pegylated interferon-alpha2b in patients with chronic renal dysfunction. *J. Clin. Pharmacol.* **2002,** *42* (10), 1109-15.
141. Uchihara, M.; Izumi, N.; Sakai, Y.; Yauchi, T.; Miyake, S.; Sakai, T.; Akiba, T.; Marumo, F.; Sato, C., Interferon Therapy for Chronic Hepatitis C in Hemodialysis Patients: Increased Serum Levels of Interferon. *Nephron* **1998,** *80* (1), 51-56.
142. Hu, X.; Seddighzadeh, A.; Stecher, S.; Zhu, Y.; Goyal, J.; Matson, M.; Marbury, T.; Smith, W.; Nestorov, I.; Hung, S., Pharmacokinetics, pharmacodynamics, and safety of peginterferon beta-1a in subjects with normal or impaired renal function. *J Clin Pharmacol.* **2015,** *55* (2), 179-188.
143. Brody, J. R.; Costantino, C. L.; Berger, A. C.; Sato, T.; Lisanti, M. P.; Yeo, C. J.; Emmons, R. V.; Witkiewicz, A. K., Expression of indoleamine 2,3-dioxygenase in metastatic malignant melanoma recruits regulatory T cells to avoid immune detection and affects survival. *Cell Cycle* **2009,** *8* (12), 1930-4.
144. Abiko, K.; Matsumura, N.; Hamanishi, J.; Horikawa, N.; Murakami, R.; Yamaguchi, K.; Yoshioka, Y.; Baba, T.; Konishi, I.; Mandai, M., IFN-γ from lymphocytes induces PD-L1 expression and promotes progression of ovarian cancer. *Br. J. Cancer* **2015,** *112* (9), 1501-9.
145. Briesemeister, D.; Sommermeyer, D.; Loddenkemper, C.; Loew, R.; Uckert, W.; Blankenstein, T.; Kammertoens, T., Tumor rejection by local interferon gamma induction in established tumors is associated with blood vessel destruction and necrosis. *Int. J. Cancer* **2011,** *128* (2), 371-8.
146. Ni, L.; Lu, J., Interferon gamma in cancer immunotherapy. *Cancer Med.* **2018,** *7* (9), 4509-4516.
147. Mejías, R.; Pérez-Yagüe, S.; Gutiérrez, L.; Cabrera, L. I.; Spada, R.; Acedo, P.; Serna, C. J.; Lázaro, F. J.; Villanueva, Á.; Morales, M. d. P.; Barber, D. F., Dimercaptosuccinic acid-coated magnetite nanoparticles for magnetically guided in vivo delivery of interferon gamma for cancer immunotherapy. *Biomaterials* **2011,** *32* (11), 2938-2952.
148. Ando, M.; Takahashi, Y.; Yamashita, T.; Fujimoto, M.; Nishikawa, M.; Watanabe, Y.; Takakura, Y., Prevention of adverse events of interferon γ gene therapy by gene delivery of interferon γ-heparin-binding domain fusion protein in mice. *Mol Ther Methods Clin Dev* **2014,** *1*, 14023-14023.
149. Lozhkov, A. A.; Klotchenko, S. A.; Ramsay, E. S.; Moshkoff, H. D.; Moshkoff, D. A.; Vasin, A. V.; Salvato, M. S., The Key Roles of Interferon Lambda in Human Molecular Defense against Respiratory Viral Infections. *Pathogens* **2020,** *9* (12), 989.
150. Stanifer, M. L.; Kee, C.; Cortese, M.; Zumaran, C. M.; Triana, S.; Mukenhirn, M.; Kraeusslich, H. G.; Alexandrov, T.; Bartenschlager, R.; Boulant, S., Critical Role of Type III Interferon in Controlling SARS-CoV-2 Infection in Human Intestinal Epithelial Cells. *Cell Rep.* **2020,** *32* (1), 107863.
151. Zhang, P.; Sun, F.; Liu, S.; Jiang, S., Anti-PEG antibodies in the clinic: Current issues and beyond PEGylation. *J. Controlled Release* **2016,** *244*, 184-193.
152. Alconcel, S. N. S.; Baas, A. S.; Maynard, H. D., FDA-approved poly(ethylene glycol)–protein conjugate drugs. *Polym. Chem.* **2011,** *2* (7), 1442-1448.
153. Ivens, I. A.; Achanzar, W.; Baumann, A.; Brändli-Baiocco, A.; Cavagnaro, J.; Dempster, M.; Depelchin, B. O.; Rovira, A. R.; Dill-Morton, L.; Lane, J. H.; Reipert, B. M.; Salcedo, T.; Schweighardt, B.; Tsuruda, L. S.; Turecek, P. L.; Sims, J., PEGylated Biopharmaceuticals : Current Experience and Considerations for Nonclinical Development. *Toxicol. Pathol.* **2015,** *43* (7), 959-983.
154. Huckaby, J. T.; Jacobs, T. M.; Li, Z.; Perna, R. J.; Wang, A.; Nicely, N. I.; Lai, S. K., Structure of an anti-PEG antibody reveals an open ring that captures highly flexible PEG polymers. *Commun. Chem.* **2020,** *3* (1), 124.
155. Yang, Q.; Lai, S. K., Anti-PEG immunity: emergence, characteristics, and unaddressed questions. *WIREs Nanomed Nanobiotechnol* **2015,** *7* (5), 655-677.
156. Rudmann, D. G.; Alston, J. T.; Hanson, J. C.; Heidel, S., High molecular weight polyethylene glycol cellular distribution and PEG-associated cytoplasmic vacuolation is molecular weight dependent and does not require conjugation to proteins. *Toxicol. Pathol.* **2013,** *41* (7), 970-83.
157. Chanan-Khan, A.; Szebeni, J.; Savay, S.; Liebes, L.; Rafique, N. M.; Alving, C. R.; Muggia, F. M., Complement activation following first exposure to pegylated liposomal doxorubicin (Doxil): possible role in hypersensitivity reactions. *Ann. Oncol.* **2003,** *14* (9), 1430-1437.
158. Sroda, K.; Rydlewski, J.; Langner, M.; Kozubek, A.; Grzybek, M.; Sikorski, A. F., Repeated injections of PEG-PE liposomes generate anti-PEG antibodies. *Cell. Mol. Biol. Lett.* **2005,** *10* (1), 37-47.

159. Dams, E. T. M.; Laverman, P.; Oyen, W. J. G.; Storm, G.; Scherphof, G. L.; Van der Meer, J. W. M.; Corstens, F. H. M.; Boerman, O. C., Accelerated blood clearance and altered biodistribution of repeated injections of sterically stabilized liposomes. *Journal of Pharmacology and Experimental Therapeutics* **2000,** *292* (3), 1071-1079.
160. Tagami, T.; Nakamura, K.; Shimizu, T.; Ishida, T.; Kiwada, H., The relationship between PEGylated siRNA-lipoplex and anti-PEG IgM on the induction of accelerated blood clearance (ABC) phenomenon. *Yakugaku Zasshi-Journal of the Pharmaceutical Society of Japan* **2008,** *128*, 109-110.
161. Ishida, T.; Kiwada, H., Accelerated blood clearance (ABC) phenomenon upon repeated injection of PEGylated liposomes. *Int. J. Pharm.* **2008,** *354* (1-2), 56-62.
162. Imran ul-haq, M.; Lai, B. F. L.; Chapanian, R.; Kizhakkedathu, J. N., Influence of architecture of high molecular weight linear and branched polyglycerols on their biocompatibility and biodistribution. *Biomaterials* **2012,** *33* (35), 9135-9147.
163. Thomas, A.; Müller, S. S.; Frey, H., Beyond Poly(ethylene glycol): Linear Polyglycerol as a Multifunctional Polyether for Biomedical and Pharmaceutical Applications. *Biomacromolecules* **2014,** *15* (6), 1935-1954.
164. Kainthan, R. K.; Brooks, D. E., In vivo biological evaluation of high molecular weight hyperbranched polyglycerols. *Biomaterials* **2007,** *28* (32), 4779-4787.
165. Kainthan, R. K.; Janzen, J.; Levin, E.; Devine, D. V.; Brooks, D. E., Biocompatibility Testing of Branched and Linear Polyglycidol. *Biomacromolecules* **2006,** *7* (3), 703-709.
166. Tully, M.; Dimde, M.; Weise, C.; Pouyan, P.; Licha, K.; Schirner, M.; Haag, R., Polyglycerol for Half-Life Extension of Proteins—Alternative to PEGylation? *Biomacromolecules* **2021,** *22* (4), 1406-1416.
167. Luxenhofer, R.; Sahay, G.; Schulz, A.; Alakhova, D.; Bronich, T. K.; Jordan, R.; Kabanov, A. V., Structure-property relationship in cytotoxicity and cell uptake of poly(2-oxazoline) amphiphiles. *J. Controlled Release* **2011,** *153* (1), 73-82.
168. Hoang Thi, T. T.; Pilkington, E. H.; Nguyen, D. H.; Lee, J. S.; Park, K. D.; Truong, N. P., The Importance of Poly(ethylene glycol) Alternatives for Overcoming PEG Immunogenicity in Drug Delivery and Bioconjugation. *Polymers* **2020,** *12* (2), 298.
169. Sedlacek, O.; Hruby, M.; Studenovsky, M.; Vetvicka, D.; Svoboda, J.; Kankova, D.; Kovar, J.; Ulbrich, K., Polymer conjugates of acridine-type anticancer drugs with pH-controlled activation. *Biorg. Med. Chem.* **2012,** *20* (13), 4056-63.
170. von Erlach, T.; Zwicker, S.; Pidhatika, B.; Konradi, R.; Textor, M.; Hall, H.; Luhmann, T., Formation and characterization of DNA-polymer-condensates based on poly(2-methyl-2-oxazoline) grafted poly(L-lysine) for non-viral delivery of therapeutic DNA. *Biomaterials* **2011,** *32* (22), 5291-303.
171. Rinkenauer, A. C.; Tauhardt, L.; Wendler, F.; Kempe, K.; Gottschaldt, M.; Traeger, A.; Schubert, U. S., A cationic poly(2-oxazoline) with high in vitro transfection efficiency identified by a library approach. *Macromol. Biosci.* **2015,** *15* (3), 414-25.
172. Tong, J.; Luxenhofer, R.; Yi, X.; Jordan, R.; Kabanov, A. V., Protein modification with amphiphilic block copoly(2-oxazoline)s as a new platform for enhanced cellular delivery. *Mol. Pharmaceutics* **2010,** *7* (4), 984-92.
173. Mero, A.; Fang, Z. H.; Pasut, G.; Veronese, F. M.; Viegas, T. X., Selective conjugation of poly(2-ethyl 2-oxazoline) to granulocyte colony stimulating factor. *J. Controlled Release* **2012,** *159* (3), 353-361.
174. He, Z. J.; Wan, X. M.; Schulz, A.; Bludau, H.; Dobrovolskaia, M. A.; Stern, S. T.; Montgomery, S. A.; Yuan, H.; Li, Z. B.; Alakhova, D.; Sokolsky, M.; Darr, D. B.; Perou, C. M.; Jordan, R.; Luxenhofer, R.; Kabanov, A. V., A high capacity polymeric micelle of paclitaxel: Implication of high dose drug therapy to safety and in vivo anti-cancer activity. *Biomaterials* **2016,** *101*, 296-309.
175. Pidhatika, B.; Moller, J.; Benetti, E. M.; Konradi, R.; Rakhmatullina, E.; Muhlebach, A.; Zimmermann, R.; Werner, C.; Vogel, V.; Textor, M., The role of the interplay between polymer architecture and bacterial surface properties on the microbial adhesion to polyoxazoline-based ultrathin films. *Biomaterials* **2010,** *31* (36), 9462-9472.
176. Chen, Y.; Pidhatika, B.; von Erlach, T.; Konradi, R.; Textor, M.; Hall, H.; Luhmann, T., Comparative assessment of the stability of nonfouling poly(2-methyl-2-oxazoline) and poly(ethylene glycol) surface films: an in vitro cell culture study. *Biointerphases* **2014,** *9* (3), 031003.

177. Mero, A.; Pasut, G.; Dalla Via, L.; Fijten, M. W.; Schubert, U. S.; Hoogenboom, R.; Veronese, F. M., Synthesis and characterization of poly(2-ethyl 2-oxazoline)-conjugates with proteins and drugs: suitable alternatives to PEG-conjugates? *J. Controlled Release* **2008,** *125* (2), 87-95.
178. Grube, M.; Leiske, M. N.; Schubert, U. S.; Nischang, I., POx as an Alternative to PEG? A Hydrodynamic and Light Scattering Study. *Macromolecules* **2018,** *51* (5), 1905-1916.
179. Bauer, M.; Lautenschlaeger, C.; Kempe, K.; Tauhardt, L.; Schubert, U. S.; Fischer, D., Poly(2-ethyl-2-oxazoline) as Alternative for the Stealth Polymer Poly(ethylene glycol): Comparison of in vitro Cytotoxicity and Hemocompatibility. *Macromol. Biosci.* **2012,** *12* (7), 986-998.
180. Farrugia, B. L.; Kempe, K.; Schubert, U. S.; Hoogenboom, R.; Dargaville, T. R., Poly(2-oxazoline) Hydrogels for Controlled Fibroblast Attachment. *Biomacromolecules* **2013,** *14* (8), 2724-2732.
181. Kempe, K.; Vollrath, A.; Schaefer, H. W.; Poehlmann, T. G.; Biskup, C.; Hoogenboom, R.; Hornig, S.; Schubert, U. S., Multifunctional Poly(2-oxazoline) Nanoparticles for Biological Applications. *Macromolecular Rapid Communications* **2010,** *31* (21), 1869-1873.
182. Bauer, M.; Schroeder, S.; Tauhardt, L.; Kempe, K.; Schubert, U. S.; Fischer, D., In vitro hemocompatibility and cytotoxicity study of poly(2-methyl-2-oxazoline) for biomedical applications. *Journal of Polymer Science Part A: Polymer Chemistry* **2013,** *51* (8), 1816-1821.
183. Tauhardt, L.; Frant, M.; Pretzel, D.; Hartlieb, M.; Bücher, C.; Hildebrand, G.; Schröter, B.; Weber, C.; Kempe, K.; Gottschaldt, M.; Liefeith, K.; Schubert, U. S., Amine end-functionalized poly(2-ethyl-2-oxazoline) as promising coating material for antifouling applications. *Journal of Materials Chemistry B* **2014,** *2* (30), 4883-4893.
184. Lühmann, T.; Schmidt, M.; Leiske, M. N.; Spieler, V.; Majdanski, T. C.; Grube, M.; Hartlieb, M.; Nischang, I.; Schubert, S.; Schubert, U. S.; Meinel, L., Site-Specific POxylation of Interleukin-4. *ACS Biomater. Sci. Eng.* **2017,** *3* (3), 304-312.
185. Sedlacek, O.; de la Rosa, V. R.; Hoogenboom, R., Poly(2-oxazoline)-protein conjugates. *Eur. Polym. J.* **2019,** *120*, 109246.
186. Moreadith, R.; Viegas, T.; Bentley, M.; Harris, J. M.; Fang, Z.; Yoon, K.; Dizman, B.; Weimer, R.; Rae, B.; Li, X.; Rader, C.; Standaert, D.; Olanow, W., Clinical development of a poly(2-oxazoline) (POZ) polymer therapeutic for the treatment of ParkinsoŽ s disease@ Proof of concept of POZ as a versatile polymer platform for drug development in multiple therapeutic indications. *Eur. Polym. J.* **2017,** *88*, 524-552.
187. McNab, F.; Mayer-Barber, K.; Sher, A.; Wack, A.; O'Garra, A., Type I interferons in infectious disease. *Nat. Rev. Immunol.* **2015,** *15* (2), 87-103.
188. Muller, U.; Steinhoff, U.; Reis, L. F.; Hemmi, S.; Pavlovic, J.; Zinkernagel, R. M.; Aguet, M., Functional role of type I and type II interferons in antiviral defense. *Science* **1994,** *264* (5167), 1918-21.
189. Perrillo, R., Benefits and risks of interferon therapy for hepatitis B. *Hepatology* **2009,** *49* (5 Suppl), S103-11.
190. Rijckborst, V.; Janssen, H. L. A., The Role of Interferon in Hepatitis B Therapy. *Current Hepatitis Reports* **2010,** *9* (4), 231-238.
191. Glue, P.; Fang, J. W. S.; Rouzier-Panis, R.; Raffanel, C.; Sabo, R.; Gupta, S. K.; Salfi, M.; Jacobs, S.; Group, t. H. C. I. T., Pegylated interferon-α2b: Pharmacokinetics, pharmacodynamics, safety, and preliminary efficacy data. *Clin. Pharmacol. Ther.* **2000,** *68* (5), 556-567.
192. Franco, E. J.; Hofstetter, H.; Hofstetter, O., A comparative evaluation of random and site-specific immobilization techniques for the preparation of antibody-based chiral stationary phases. *J. Sep. Sci.* **2006,** *29* (10), 1458-1469.
193. Wang, Q.; Wang, L., Genetic incorporation of unnatural amino acids into proteins in yeast. *Methods in molecular biology (Clifton, N.J.)* **2012,** *794*, 199-213.
194. Nödling, A. R.; Spear, L. A.; Williams, T. L.; Luk, L. Y. P.; Tsai, Y.-H., Using genetically incorporated unnatural amino acids to control protein functions in mammalian cells. *Essays in Biochemistry* **2019,** *63* (2), 237-266.
195. Reinkemeier, C. D.; Lemke, E. A., Raising the ribosomal repertoire. *Nat. Chem.* **2020,** *12* (6), 503-504.
196. Borrmann, A.; Milles, S.; Plass, T.; Dommerholt, J.; Verkade, J. M.; Wiessler, M.; Schultz, C.; van Hest, J. C.; van Delft, F. L.; Lemke, E. A., Genetic encoding of a bicyclo[6.1.0]nonyne-charged

amino acid enables fast cellular protein imaging by metal-free ligation. *Chembiochem* **2012,** *13* (14), 2094-9.
197. Platis, D.; Foster, G. R., High yield expression, refolding, and characterization of recombinant interferon α2/α8 hybrids in Escherichia coli. *Protein Expression Purif.* **2003,** *31* (2), 222-230.
198. Lühmann, T.; Spieler, V.; Werner, V.; Ludwig, M.-G.; Fiebig, J.; Mueller, T. D.; Meinel, L., Interleukin-4-Clicked Surfaces Drive M2 Macrophage Polarization. *ChemBioChem* **2016,** *17* (22), 2123-2128.
199. Sun, C.; Li, Y.; Yates, E. A.; Fernig, D. G., SimpleDSFviewer: A tool to analyze and view differential scanning fluorimetry data for characterizing protein thermal stability and interactions. *Protein Sci.* **2020,** *29* (1), 19-27.
200. Maier, J. A.; Martinez, C.; Kasavajhala, K.; Wickstrom, L.; Hauser, K. E.; Simmerling, C., ff14SB: Improving the Accuracy of Protein Side Chain and Backbone Parameters from ff99SB. *Journal of Chemical Theory and Computation* **2015,** *11* (8), 3696-3713.
201. Wang, J.; Wolf, R. M.; Caldwell, J. W.; Kollman, P. A.; Case, D. A., Development and testing of a general amber force field. *J. Comput. Chem.* **2004,** *25* (9), 1157-74.
202. D.A. Case, H. M. A., K. Belfon, I.Y. Ben-Shalom, S.R. Brozell, D.S. Cerutti, T.E. Cheatham, III, V.W.D. Cruzeiro, T.A. Darden, R.E. Duke, G. Giambasu, M.K. Gilson, H. Gohlke, A.W. Goetz, R. Harris, S. Izadi, S.A. Izmailov, C. Jin, K. Kasavajhala, M.C. Kaymak, E. King, A. Kovalenko, T. Kurtzman, T.S. Lee, S. LeGrand, P. Li, C. Lin, J. Liu, T. Luchko, R. Luo, M. Machado, V. Man, M. Manathunga, K.M. Merz, Y. Miao, O. Mikhailovskii, G. Monard, H. Nguyen, K.A. O'Hearn, A. Onufriev, F. Pan, S. Pantano, R. Qi, A. Rahnamoun, D.R. Roe, A. Roitberg, C. Sagui, S. Schott-Verdugo, J. Shen, C.L. Simmerling, N.R. Skrynnikov, J. Smith, J. Swails, R.C. Walker, J. Wang, H. Wei, R.M. Wolf, X. Wu, Y. Xue, D.M. York, S. Zhao, and P.A. Kollman, Amber 2021. *University of California* **2021**.
203. M. J. Frisch, G. W. T., H. B. Schlegel, G. E. Scuseria, M. A. Robb, J. R. Cheeseman, G. Scalmani, V. Barone, G. A. Petersson, H. Nakatsuji, X. Li, M. Caricato, A. Marenich, J. Bloino, B. G. Janesko, R. Gomperts, B. Mennucci, H. P. Hratchian, J. V. Ortiz, A. F. Izmaylov, J. L. Sonnenberg, D. Williams-Young, F. Ding, F. Lipparini, F. Egidi, J. Goings, B. Peng, A. Petrone, T. Henderson, D. Ranasinghe, V. G. Zakrzewski, J. Gao, N. Rega, G. Zheng, W. Liang, M. Hada, M. Ehara, K. Toyota, R. Fukuda, J. Hasegawa, M. Ishida, T. Nakajima, Y. Honda, O. Kitao, H. Nakai, T. Vreven, K. Throssell, J. A. Montgomery, Jr., J. E. Peralta, F. Ogliaro, M. Bearpark, J. J. Heyd, E. Brothers, K. N. Kudin, V. N. Staroverov, T. Keith, R. Kobayashi, J. Normand, K. Raghavachari, A. Rendell, J. C. Burant, S. S. Iyengar, J. Tomasi, M. Cossi, J. M. Millam, M. Klene, C. Adamo, R. Cammi, J. W. Ochterski, R. L. Martin, K. Morokuma, O. Farkas, J. B. Foresman, and D. J. Fox, Gaussian, Inc. Wallingford CT, Gaussian 09, Revision C.01. **2016**.
204. Klaus, W.; Gsell, B.; Labhardt, A. M.; Wipf, B.; Senn, H., The three-dimensional high resolution structure of human interferon alpha-2a determined by heteronuclear NMR spectroscopy in solution. *J. Mol. Biol.* **1997,** *274* (4), 661-75.
205. MOE, Molecular Operating Environment 2019.01. *Chemical Computing Group ULC, 1010 Sherbrooke St. West, Suite #910, Montreal, QC, Canada, H3A 2R7* **2019**.
206. Shelley, J. C.; Cholleti, A.; Frye, L. L.; Greenwood, J. R.; Timlin, M. R.; Uchimaya, M., Epik: a software program for pK(a) prediction and protonation state generation for drug-like molecules. *J. Comput. Aided Mol. Des.* **2007,** *21* (12), 681-91.
207. Greenwood, J. R.; Calkins, D.; Sullivan, A. P.; Shelley, J. C., Towards the comprehensive, rapid, and accurate prediction of the favorable tautomeric states of drug-like molecules in aqueous solution. *J. Comput. Aided Mol. Des.* **2010,** *24* (6-7), 591-604.
208. Bond, S. D.; Leimkuhler, B. J.; Laird, B. B., The Nosé–Poincaré Method for Constant Temperature Molecular Dynamics. *Journal of Computational Physics* **1999,** *151* (1), 114-134.
209. Sturgeon, J. B.; Laird, B. B., Symplectic algorithm for constant-pressure molecular dynamics using a Nosé–Poincaré thermostat. *J. Chem. Phys.* **2000,** *112* (8), 3474-3482.
210. Still, W. C.; Tempczyk, A.; Hawley, R. C.; Hendrickson, T., Semianalytical treatment of solvation for molecular mechanics and dynamics. *J. Am. Chem. Soc.* **1990,** *112* (16), 6127-6129.
211. Gerber, P. R.; Müller, K., MAB, a generally applicable molecular force field for structure modelling in medicinal chemistry. *J. Comput. Aided Mol. Des.* **1995,** *9* (3), 251-68.
212. Jorgensen, W. L.; Chandrasekhar, J.; Madura, J. D.; Impey, R. W.; Klein, M. L., Comparison of simple potential functions for simulating liquid water. *J. Chem. Phys.* **1983,** *79* (2), 926-935.

213. Miao, Y.; Feher, V. A.; McCammon, J. A., Gaussian Accelerated Molecular Dynamics: Unconstrained Enhanced Sampling and Free Energy Calculation. *Journal of Chemical Theory and Computation* **2015,** *11* (8), 3584-3595.
214. Pang, Y. T.; Miao, Y.; Wang, Y.; McCammon, J. A., Gaussian Accelerated Molecular Dynamics in NAMD. *J. Chem. Theory Comput.* **2017,** *13* (1), 9-19.
215. Phillips, J. C.; Braun, R.; Wang, W.; Gumbart, J.; Tajkhorshid, E.; Villa, E.; Chipot, C.; Skeel, R. D.; Kalé, L.; Schulten, K., Scalable molecular dynamics with NAMD. *J. Comput. Chem.* **2005,** *26* (16), 1781-802.
216. Darden, T.; York, D.; Pedersen, L., Particle mesh Ewald: An N·log(N) method for Ewald sums in large systems. *J. Chem. Phys.* **1993,** *98* (12), 10089-10092.
217. Roe, D. R.; Cheatham, T. E., PTRAJ and CPPTRAJ: Software for Processing and Analysis of Molecular Dynamics Trajectory Data. *Journal of Chemical Theory and Computation* **2013,** *9* (7), 3084-3095.
218. Schrödinger, L., The PyMOL Molecular Graphics System, Version 2.0
219. Radestock, S.; Gohlke, H., Exploiting the Link between Protein Rigidity and Thermostability for Data-Driven Protein Engineering. *Engineering in Life Sciences* **2008,** *8* (5), 507-522.
220. Fulle, S.; Gohlke, H., Analyzing the Flexibility of RNA Structures by Constraint Counting. *Biophys. J.* **2008,** *94* (11), 4202-4219.
221. Pfleger, C.; Rathi, P. C.; Klein, D. L.; Radestock, S.; Gohlke, H., Constraint Network Analysis (CNA): A Python Software Package for Efficiently Linking Biomacromolecular Structure, Flexibility, (Thermo-)Stability, and Function. *Journal of Chemical Information and Modeling* **2013,** *53* (4), 1007-1015.
222. Pfleger, C.; Radestock, S.; Schmidt, E.; Gohlke, H., Global and local indices for characterizing biomolecular flexibility and rigidity. *J. Comput. Chem.* **2013,** *34* (3), 220-233.
223. Jacobs, D. J.; Rader, A. J.; Kuhn, L. A.; Thorpe, M. F., Protein flexibility predictions using graph theory. *Proteins* **2001,** *44* (2), 150-65.
224. Gohlke, H.; Kuhn, L. A.; Case, D. A., Change in protein flexibility upon complex formation: Analysis of Ras-Raf using molecular dynamics and a molecular framework approach. *Proteins: Structure, Function, and Bioinformatics* **2004,** *56* (2), 322-337.
225. Rathi, P. C.; Radestock, S.; Gohlke, H., Thermostabilizing mutations preferentially occur at structural weak spots with a high mutation ratio. *Journal of biotechnology* **2012,** *159* (3), 135-144.
226. Gervais, M.; Brocas, A.-L.; Cendejas, G.; Deffieux, A.; Carlotti, S., Synthesis of Linear High Molar Mass Glycidol-Based Polymers by Monomer-Activated Anionic Polymerization. *Macromolecules* **2010,** *43* (4), 1778-1784.
227. Pouyan, P.; Nie, C.; Bhatia, S.; Wedepohl, S.; Achazi, K.; Osterrieder, N.; Haag, R., Inhibition of Herpes Simplex Virus Type 1 Attachment and Infection by Sulfated Polyglycerols with Different Architectures. *Biomacromolecules* **2021,** *22* (4), 1545-1554.
228. Kapourani, E.; Neumann, F.; Achazi, K.; Dernedde, J.; Haag, R., Droplet-Based Microfluidic Templating of Polyglycerol-Based Microgels for the Encapsulation of Cells: A Comparative Study. *Macromol. Biosci.* **2018,** *18* (10), 1800116.
229. Guillerm, B.; Monge, S.; Lapinte, V.; Robin, J.-J., How to Modulate the Chemical Structure of Polyoxazolines by Appropriate Functionalization. *Macromolecular Rapid Communications* **2012,** *33* (19), 1600-1612.
230. Dirauf, M.; Fritz, N.; Gottschaldt, M.; Weber, C.; Schubert, U. S., Poly(2-ethyl-2-oxazoline) Featuring a Central Amino Moiety. *Macromolecular Rapid Communications* **2021,** *42* (13), 2100132.
231. Wan, W.; Tharp, J. M.; Liu, W. R., Pyrrolysyl-tRNA synthetase: an ordinary enzyme but an outstanding genetic code expansion tool. *Biochimica et biophysica acta* **2014,** *1844* (6), 1059-70.
232. Normanly, J.; Kleina, L. G.; Masson, J.-M.; Abelson, J.; Miller, J. H., Construction of Escherichia coli amber suppressor tRNA genes: III. Determination of tRNA specificity. *J. Mol. Biol.* **1990,** *213* (4), 719-726.
233. Spieler, V.; Ludwig, M.-G.; Dawson, J.; Tigani, B.; Littlewood-Evans, A.; Safina, C.; Ebersbach, H.; Seuwen, K.; Raschig, M.; ter Mors, B.; Müller, T. D.; Meinel, L.; Lühmann, T., Targeting interleukin-4 to the arthritic joint. *J. Controlled Release* **2020,** *326*, 172-180.
234. Foser, S.; Schacher, A.; Weyer, K. A.; Brugger, D.; Dietel, E.; Marti, S.; Schreitmüller, T., Isolation, structural characterization, and antiviral activity of positional isomers of monopegylated interferon α-2a (PEGASYS). *Protein Expression Purif.* **2003,** *30* (1), 78-87.

235. Kofoed, C.; Riesenberg, S.; Šmolíková, J.; Meldal, M.; Schoffelen, S., Semisynthesis of an Active Enzyme by Quantitative Click Ligation. *Bioconjugate Chem.* **2019,** *30* (4), 1169-1174.
236. Miyajima, A.; Kitamura, T.; Harada, N.; Yokota, T.; Arai, K.-i., Cytokine Receptors and Signal Transduction. *Annual Review of Immunology* **1992,** *10* (1), 295-331.
237. Lipiäinen, T.; Peltoniemi, M.; Sarkhel, S.; Yrjönen, T.; Vuorela, H.; Urtti, A.; Juppo, A., Formulation and Stability of Cytokine Therapeutics. *J. Pharm. Sci.* **2015,** *104* (2), 307-326.
238. Zheng, C. Y.; Ma, G.; Su, Z., Native PAGE eliminates the problem of PEG–SDS interaction in SDS-PAGE and provides an alternative to HPLC in characterization of protein PEGylation. *Electrophoresis* **2007,** *28* (16), 2801-2807.
239. Greenfield, N. J., Using circular dichroism spectra to estimate protein secondary structure. *Nat. Protoc.* **2006,** *1* (6), 2876-90.
240. Munasinghe, A.; Mathavan, A.; Mathavan, A.; Lin, P.; Colina, C. M., Molecular Insight into the Protein–Polymer Interactions in N-Terminal PEGylated Bovine Serum Albumin. *J. Phys. Chem. B* **2019,** *123* (25), 5196-5205.
241. Radestock, S.; Gohlke, H., Protein rigidity and thermophilic adaptation. *Proteins: Structure, Function, and Bioinformatics* **2011,** *79* (4), 1089-1108.
242. Rodríguez-Martínez, J. A.; Solá, R. J.; Castillo, B.; Cintrón-Colón, H. R.; Rivera-Rivera, I.; Barletta, G.; Griebenow, K., Stabilization of alpha-chymotrypsin upon PEGylation correlates with reduced structural dynamics. *Biotechnology and bioengineering* **2008,** *101* (6), 1142-1149.
243. DeBenedictis, E. P.; Hamed, E.; Keten, S., Mechanical Reinforcement of Proteins with Polymer Conjugation. *ACS nano* **2016,** *10* (2), 2259-67.
244. Chao, S.-H.; Matthews, S. S.; Paxman, R.; Aksimentiev, A.; Gruebele, M.; Price, J. L., Two Structural Scenarios for Protein Stabilization by PEG. *J. Phys. Chem. B* **2014,** *118* (28), 8388-8395.
245. Pai, S. S.; Hammouda, B.; Hong, K.; Pozzo, D. C.; Przybycien, T. M.; Tilton, R. D., The Conformation of the Poly(ethylene glycol) Chain in Mono-PEGylated Lysozyme and Mono-PEGylated Human Growth Hormone. *Bioconjugate Chem.* **2011,** *22* (11), 2317-2323.
246. Feng, Y.; De Franceschi, G.; Kahraman, A.; Soste, M.; Melnik, A.; Boersema, P. J.; de Laureto, P. P.; Nikolaev, Y.; Oliveira, A. P.; Picotti, P., Global analysis of protein structural changes in complex proteomes. *Nat. Biotechnol.* **2014,** *32* (10), 1036-1044.
247. Piazza, I.; Kochanowski, K.; Cappelletti, V.; Fuhrer, T.; Noor, E.; Sauer, U.; Picotti, P., A Map of Protein-Metabolite Interactions Reveals Principles of Chemical Communication. *Cell* **2018,** *172* (1), 358-372.e23.
248. Dirauf, M.; Fritz, N.; Gottschaldt, M.; Weber, C.; Schubert, U. S., Poly(2-ethyl-2-oxazoline) Featuring a Central Amino Moiety. *Macromolecular Rapid Communications n/a* (n/a), 2100132.
249. Glue, P.; Fang, J. W.; Rouzier-Panis, R.; Raffanel, C.; Sabo, R.; Gupta, S. K.; Salfi, M.; Jacobs, S., Pegylated interferon-alpha2b: pharmacokinetics, pharmacodynamics, safety, and preliminary efficacy data. Hepatitis C Intervention Therapy Group. *Clin. Pharmacol. Ther.* **2000,** *68* (5), 556-67.
250. Zeuzem, S.; Welsch, C.; Herrmann, E., Pharmacokinetics of peginterferons. *Semin. Liver Dis.* **2003,** *23 Suppl 1*, 23-8.
251. Borden, E. C.; Sen, G. C.; Uze, G.; Silverman, R. H.; Ransohoff, R. M.; Foster, G. R.; Stark, G. R., Interferons at age 50: past, current and future impact on biomedicine. *Nat. Rev. Drug Discov.* **2007,** *6* (12), 975-990.
252. Hauptstein, N.; Meinel, L.; Lühmann, T., Bioconjugation strategies and clinical implications of Interferon-bioconjugates. *Eur. J. Pharm. Biopharm.* **2022,** *172*, 157-167.
253. EMA, Pegasys 180 micrograms solution for injection https://www.ema.europa.eu/en/documents/product-information/pegasys-epar-product-information_en.pdf, accessed November 2021.
254. EMA, PegIntron 50 micrograms powder and solvent for solution for injection https://ec.europa.eu/health/documents/community-register/2016/20160629135304/anx_135304_en.pdf, (accessed 2022-06-05).
255. EMA, Besremi 250 micrograms/0.5 mL solution for injection in pre-filled pen https://www.ema.europa.eu/en/documents/product-information/besremi-epar-product-information_en.pdf, accessed November 2021.
256. Kozma, G. T.; Shimizu, T.; Ishida, T.; Szebeni, J., Anti-PEG antibodies: Properties, formation, testing and role in adverse immune reactions to PEGylated nano-biopharmaceuticals. *Adv. Drug Delivery Rev.* **2020,** *154-155*, 163-175.

257. Elsadek, N. E.; Abu Lila, A. S.; Ishida, T., 5 - Immunological responses to PEGylated proteins: anti-PEG antibodies. In *Polymer-Protein Conjugates*, Pasut, G.; Zalipsky, S., Eds. Elsevier: 2020; pp 103-123.
258. Shadish, J. A.; DeForest, C. A., Site-Selective Protein Modification: From Functionalized Proteins to Functional Biomaterials. *Matter* **2020,** *2* (1), 50-77.
259. EMA Palynziq, INN-pegvaliase, https://www.ema.europa.eu/en/documents/product-information/palynziq-epar-product-information_en.pdf, accessed march 2022.
260. Murguia-Favela, L.; Min, W.; Loves, R.; Leon-Ponte, M.; Grunebaum, E., Comparison of elapegademase and pegademase in ADA-deficient patients and mice. *Clin Exp Immunol* **2020,** *200* (2), 176-184.
261. Graham, M. L., Pegaspargase: a review of clinical studies. *Adv. Drug Delivery Rev.* **2003,** *55* (10), 1293-1302.
262. Murguia-Favela, L.; Min, W.; Loves, R.; Leon-Ponte, M.; Grunebaum, E., Comparison of elapegademase and pegademase in ADA-deficient patients and mice. *Clinical and experimental immunology* **2020,** *200* (2), 176-184.
263. Moreno-Pérez, S.; Orrego, A. H.; Romero-Fernández, M.; Trobo-Maseda, L.; Martins-DeOliveira, S.; Munilla, R.; Fernández-Lorente, G.; Guisan, J. M., Chapter Three - Intense PEGylation of Enzyme Surfaces: Relevant Stabilizing Effects. In *Methods Enzymol.*, Kumar, C. V., Ed. Academic Press: 2016; Vol. 571, pp 55-72.
264. Arvedson, T.; O'Kelly, J.; Yang, B.-B., Design Rationale and Development Approach for Pegfilgrastim as a Long-Acting Granulocyte Colony-Stimulating Factor. *BioDrugs : clinical immunotherapeutics, biopharmaceuticals and gene therapy* **2015,** *29* (3), 185-198.
265. Veronese, F. M.; Mero, A., The Impact of PEGylation on Biological Therapies. *Biodrugs* **2008,** *22* (5), 315-329.
266. Alvarez Dorta, D.; Deniaud, D.; Mével, M.; Gouin, S. G., Tyrosine Conjugation Methods for Protein Labelling. *Chemistry* **2020,** *26* (63), 14257-14269.
267. Gauthier, M. A.; Klok, H.-A., Arginine-Specific Modification of Proteins with Polyethylene Glycol. *Biomacromolecules* **2011,** *12* (2), 482-493.
268. Tully, M.; Hauptstein, N.; Licha, K.; Meinel, L.; Lühmann, T.; Haag, R., Linear Polyglycerol for N-terminal-selective Modification of Interleukin-4. *J. Pharm. Sci.* **2022,** *111* (6), 1642-1651.
269. Popp, M. W.; Dougan, S. K.; Chuang, T.-Y.; Spooner, E.; Ploegh, H. L., Sortase-catalyzed transformations that improve the properties of cytokines. *Proceedings of the National Academy of Sciences* **2011,** *108* (8), 3169-3174.
270. Haas, D.; Hauptstein, N.; Dirauf, M.; Driessen, M. D.; Ruopp, M.; Schubert, U. S.; Lühmann, T.; Meinel, L., Chemo-Enzymatic PEGylation/POxylation of Murine Interleukin-4. *Bioconjugate Chem.* **2022,** *33* (1), 97-104.
271. Popp, M. W.; Antos, J. M.; Grotenbreg, G. M.; Spooner, E.; Ploegh, H. L., Sortagging: a versatile method for protein labeling. *Nat. Chem. Biol.* **2007,** *3* (11), 707-708.
272. Anami, Y.; Tsuchikama, K., Transglutaminase-Mediated Conjugations. In *Antibody-Drug Conjugates: Methods and Protocols*, Tumey, L. N., Ed. Springer US: New York, NY, 2020; pp 71-82.
273. Dickgiesser, S.; Deweid, L.; Kellner, R.; Kolmar, H.; Rasche, N., Site-Specific Antibody–Drug Conjugation Using Microbial Transglutaminase. In *Enzyme-Mediated Ligation Methods*, Nuijens, T.; Schmidt, M., Eds. Springer New York: New York, NY, 2019; pp 135-149.
274. Dennler, P.; Chiotellis, A.; Fischer, E.; Brégeon, D.; Belmant, C.; Gauthier, L.; Lhospice, F.; Romagne, F.; Schibli, R., Transglutaminase-Based Chemo-Enzymatic Conjugation Approach Yields Homogeneous Antibody–Drug Conjugates. *Bioconjugate Chem.* **2014,** *25* (3), 569-578.
275. Fontana, A.; Spolaore, B.; Mero, A.; Veronese, F. M., Site-specific modification and PEGylation of pharmaceutical proteins mediated by transglutaminase. *Adv. Drug Delivery Rev.* **2008,** *60* (1), 13-28.
276. DeFrees, S.; Wang, Z.-G.; Xing, R.; Scott, A. E.; Wang, J.; Zopf, D.; Gouty, D. L.; Sjoberg, E. R.; Panneerselvam, K.; Brinkman-Van der Linden, E. C. M.; Bayer, R. J.; Tarp, M. A.; Clausen, H., GlycoPEGylation of recombinant therapeutic proteins produced in Escherichia coli. *Glycobiology* **2006,** *16* (9), 833-843.
277. Østergaard, H.; Bjelke, J. R.; Hansen, L.; Petersen, L. C.; Pedersen, A. A.; Elm, T.; Møller, F.; Hermit, M. B.; Holm, P. K.; Krogh, T. N.; Petersen, J. M.; Ezban, M.; Sørensen, B. B.; Andersen, M. D.; Agersø, H.; Ahmadian, H.; Balling, K. W.; Christiansen, M. L. S.; Knobe, K.; Nichols, T.

C.; Bjørn, S. E.; Tranholm, M., Prolonged half-life and preserved enzymatic properties of factor IX selectively PEGylated on native N-glycans in the activation peptide. *Blood* **2011,** *118* (8), 2333-2341.
278. Ekladious, I.; Colson, Y. L.; Grinstaff, M. W., Polymer–drug conjugate therapeutics: advances, insights and prospects. *Nat. Rev. Drug Discov.* **2019,** *18* (4), 273-294.
279. Dozier, J. K.; Distefano, M. D., Site-Specific PEGylation of Therapeutic Proteins. *Int. J. Mol. Sci.* **2015,** *16* (10), 25831-25864.
280. Turecek, P. L.; Bossard, M. J.; Schoetens, F.; Ivens, I. A., PEGylation of Biopharmaceuticals: A Review of Chemistry and Nonclinical Safety Information of Approved Drugs. *J. Pharm. Sci.* **2016,** *105* (2), 460-475.
281. Qi, Y.; Chilkoti, A., Protein–polymer conjugation—moving beyond PEGylation. *Current Opinion in Chemical Biology* **2015,** *28*, 181-193.
282. Zhao, H.; Heusler, E.; Jones, G.; Li, L.; Werner, V.; Germershaus, O.; Ritzer, J.; Luehmann, T.; Meinel, L., Decoration of silk fibroin by click chemistry for biomedical application. *J. Struct. Biol.* **2014,** *186* (3), 420-430.
283. Gutmann, M.; Memmel, E.; Braun, A. C.; Seibel, J.; Meinel, L.; Lühmann, T., Biocompatible Azide–Alkyne "Click" Reactions for Surface Decoration of Glyco-Engineered Cells. *ChemBioChem* **2016,** *17* (9), 866-875.
284. Siverino, C.; Tabisz, B.; Lühmann, T.; Meinel, L.; Müller, T.; Walles, H.; Nickel, J., Site-Directed Immobilization of Bone Morphogenetic Protein 2 to Solid Surfaces by Click Chemistry. *J. Visualized Exp.* **2018,** (133), 56616.
285. Braun, A. C.; Gutmann, M.; Lühmann, T.; Meinel, L., Bioorthogonal strategies for site-directed decoration of biomaterials with therapeutic proteins. *J. Controlled Release* **2018,** *273*, 68-85.
286. Braun, A. C.; Gutmann, M.; Mueller, T. D.; Lühmann, T.; Meinel, L., Bioresponsive release of insulin-like growth factor-I from its PEGylated conjugate. *J. Controlled Release* **2018,** *279*, 17–28.
287. Gutmann, M.; Bechold, J.; Seibel, J.; Meinel, L.; Lühmann, T., Metabolic Glycoengineering of Cell-Derived Matrices and Cell Surfaces: A Combination of Key Principles and Step-by-Step Procedures. *ACS Biomater. Sci. Eng.* **2019,** *5* (1), 215-233.
288. Tully, M.; Wedepohl, S.; Kutifa, D.; Weise, C.; Licha, K.; Schirner, M.; Haag, R., Prolonged activity of exenatide: Detailed comparison of Site-specific linear polyglycerol- and poly(ethylene glycol)-conjugates. *Eur. J. Pharm. Biopharm.* **2021,** *164*, 105-113.
289. Wenande, E.; Garvey, L. H., Immediate-type hypersensitivity to polyethylene glycols: a review. *Clin Exp Allergy* **2016,** *46* (7), 907-22.
290. Pickert, J.; Hennighausen, I.; Mühlenbein, S.; Möbs, C.; Pfützner, W., Immediate-Type Hypersensitivity to Polyethylene Glycol (PEG) Including a PEG-containing COVID-19 Vaccine Revealed by Intradermal Testing. *J. Investig. Allergol. Clin. Immunol.* **2021**, 0.
291. Hoang Thi, T. T.; Pilkington, E. H.; Nguyen, D. H.; Lee, J. S.; Park, K. D.; Truong, N. P., The Importance of Poly(ethylene glycol) Alternatives for Overcoming PEG Immunogenicity in Drug Delivery and Bioconjugation. *Polymers* **2020,** *12* (2).
292. Schuck, P., Size-Distribution Analysis of Macromolecules by Sedimentation Velocity Ultracentrifugation and Lamm Equation Modeling. *Biophys. J.* **2000,** *78* (3), 1606-1619.
293. Schuck, P.; Perugini, M. A.; Gonzales, N. R.; Howlett, G. J.; Schubert, D., Size-distribution analysis of proteins by analytical ultracentrifugation: strategies and application to model systems. *Biophys. J.* **2002,** *82* (2), 1096-111.
294. Nischang, I.; Perevyazko, I.; Majdanski, T.; Vitz, J.; Festag, G.; Schubert, U. S., Hydrodynamic Analysis Resolves the Pharmaceutically-Relevant Absolute Molar Mass and Solution Properties of Synthetic Poly(ethylene glycol)s Created by Varying Initiation Sites. *Anal. Chem.* **2017,** *89* (2), 1185-1193.
295. Brown, P. H.; Balbo, A.; Zhao, H.; Ebel, C.; Schuck, P., Density Contrast Sedimentation Velocity for the Determination of Protein Partial-Specific Volumes. *PLoS One* **2011,** *6* (10), e26221.
296. Durchschlag, H., Determination of the partial specific volume of conjugated proteins. *Colloid. Polym. Sci.* **1989,** *267* (12), 1139-1150.
297. Dhalluin, C.; Ross, A.; Leuthold, L.-A.; Foser, S.; Gsell, B.; Müller, F.; Senn, H., Structural and Biophysical Characterization of the 40 kDa PEG−Interferon-α2a and Its Individual Positional Isomers. *Bioconjugate Chem.* **2005,** *16* (3), 504-517.
298. Tovey, M. G.; Lallemand, C.; Meritet, J.-F.; Maury, C., Adjuvant activity of interferon alpha: mechanism(s) of action. *Vaccine* **2006,** *24*, S46-S47.

299. Müller, K., here: A Simpler Way to Find Your Files. https://CRAN.R-project.org/package=here, (accessed 2022-06-05). **2020**.
300. Herzberger, J.; Niederer, K.; Pohlit, H.; Seiwert, J.; Worm, M.; Wurm, F. R.; Frey, H., Polymerization of Ethylene Oxide, Propylene Oxide, and Other Alkylene Oxides: Synthesis, Novel Polymer Architectures, and Bioconjugation. *Chem. Rev.* **2016,** *116* (4), 2170-2243.
301. Bis, R. L.; Stauffer, T. M.; Singh, S. M.; Lavoie, T. B.; Mallela, K. M. G., High yield soluble bacterial expression and streamlined purification of recombinant human interferon α-2a. *Protein Expression Purif.* **2014,** *99*, 138-146.
302. Shire, S. J., pH-dependent polymerization of a human leukocyte interferon produced by recombinant deoxyribonucleic acid technology. *Biochemistry* **1983,** *22* (11), 2664-2671.
303. Pohl, C.; Polimeni, M.; Indrakumar, S.; Streicher, W.; Peters, G. H. J.; Nørgaard, A.; Lund, M.; Harris, P., Electrostatics Drive Oligomerization and Aggregation of Human Interferon Alpha-2a. *J. Phys. Chem. B* **2021,** *125* (50), 13657-13669.
304. Li, Y.; Stafford, W. F.; Hesselberg, M.; Hayes, D.; Wu, Z.; Byrne, M., Characterization of the Self-Association of Human Interferon-α2b, Albinterferon-α2b, and Pegasys. *J. Pharm. Sci.* **2012,** *101* (1), 68-80.
305. Lu, Y.; Harding, S. E.; Turner, A.; Smith, B.; Athwal, D. S.; Grossmann, J. G.; Davis, K. G.; Rowe, A. J., Effect of PEGylation on the Solution Conformation of Antibody Fragments. *J. Pharm. Sci.* **2008,** *97* (6), 2062-2079.
306. Gokarn, Y. R.; McLean, M.; Laue, T. M., Effect of PEGylation on Protein Hydrodynamics. *Mol. Pharmaceutics* **2012,** *9* (4), 762-773.
307. Valderrama, O. J.; Nischang, I., Reincarnation of the Analytical Ultracentrifuge: Emerging Opportunities for Nanomedicine. *Anal. Chem.* **2021,** *93* (48), 15805-15815.
308. Zhang, K.-J.; Yin, X.-F.; Yang, Y.-Q.; Li, H.-L.; Xu, Y.-N.; Chen, L.-Y.; Liu, X.-J.; Yuan, S.-J.; Fang, X.-L.; Xiao, J.; Wu, S.; Xu, H.-N.; Chu, L.; Katlinski, K. V.; Katlinskaya, Y. V.; Guo, R.-B.; Wei, G.-W.; Wang, D.-C.; Liu, X.-Y.; Fuchs, S. Y., A Potent *In Vivo* Antitumor Efficacy of Novel Recombinant Type I Interferon. *Clin. Cancer Res.* **2017,** *23* (8), 2038-2049.
309. Kaminskas, L. M.; Ascher, D. B.; McLeod, V. M.; Herold, M. J.; Le, C. P.; Sloan, E. K.; Porter, C. J., PEGylation of interferon α2 improves lymphatic exposure after subcutaneous and intravenous administration and improves antitumour efficacy against lymphatic breast cancer metastases. *J Control Release* **2013,** *168* (2), 200-8.
310. Guo, L.; Geng, X.; Chen, Y.; Qi, F.; Liu, L.; Miao, Y.; Lin, Z.; Yu, M.; Li, Z.; Fu, Y.; Li, B.; Luo, Y., Pre-clinical toxicokinetics and safety study of M2ES, a PEGylated recombinant human endostatin, in rhesus monkeys. *Regulatory Toxicology and Pharmacology* **2014,** *69* (3), 512-523.
311. Baker, D. P.; Lin, E. Y.; Lin, K.; Pellegrini, M.; Petter, R. C.; Chen, L. L.; Arduini, R. M.; Brickelmaier, M.; Wen, D.; Hess, D. M.; Chen, L.; Grant, D.; Whitty, A.; Gill, A.; Lindner, D. J.; Pepinsky, R. B., N-Terminally PEGylated Human Interferon-β-1a with Improved Pharmacokinetic Properties and in Vivo Efficacy in a Melanoma Angiogenesis Model. *Bioconjugate Chem.* **2006,** *17* (1), 179-188.
312. Arduini, R. M.; Li, Z.; Rapoza, A.; Gronke, R.; Hess, D. M.; Wen, D.; Miatkowski, K.; Coots, C.; Kaffashan, A.; Viseux, N.; Delaney, J.; Domon, B.; Young, C. N.; Boynton, R.; Chen, L. L.; Chen, L.; Betzenhauser, M.; Miller, S.; Gill, A.; Pepinsky, R. B.; Hochman, P. S.; Baker, D. P., Expression, purification, and characterization of rat interferon-β, and preparation of an N-terminally PEGylated form with improved pharmacokinetic parameters. *Protein Expression Purif.* **2004,** *34* (2), 229-242.
313. Beldarraín, A.; Cruz, Y.; Cruz, O.; Navarro, M.; Gil, M., Purification and conformational properties of a human interferon alpha2b produced in Escherichia coli. *Biotechnol. Appl. Biochem.* **2001,** *33* (3), 173-82.
314. Beilharz, M. W.; Cummins, J. M.; Bennett, A. L., Protection from lethal influenza virus challenge by oral type 1 interferon. *Biochem. Biophys. Res. Commun.* **2007,** *355* (3), 740-744.
315. García-Sastre, A., Induction and evasion of type I interferon responses by influenza viruses. *Virus Res.* **2011,** *162* (1), 12-18.
316. Harris, J. M.; Chess, R. B., Effect of pegylation on pharmaceuticals. *Nat. Rev. Drug Discovery* **2003,** *2* (3), 214-221.
317. Huang, Y. W.; Hsu, C. W.; Lu, S. N.; Yu, M. L.; Su, C. W.; Su, W. W.; Chien, R. N.; Hsu, C. S.; Hsu, S. J.; Lai, H. C.; Qin, A.; Tseng, K. C.; Chen, P. J., Ropeginterferon alfa-2b every 2 weeks

as a novel pegylated interferon for patients with chronic hepatitis B. *Hepatol. Int.* **2020,** *14* (6), 997-1008.
318. Ryan, G. M.; Kaminskas, L. M.; Kelly, B. D.; Owen, D. J.; McIntosh, M. P.; Porter, C. J. H., Pulmonary Administration of PEGylated Polylysine Dendrimers: Absorption from the Lung versus Retention within the Lung Is Highly Size-Dependent. *Mol. Pharmaceutics* **2013,** *10* (8), 2986-2995.
319. Gursahani, H.; Riggs-Sauthier, J.; Pfeiffer, J.; Lechuga-Ballesteros, D.; Fishburn, C. S., Absorption of polyethylene glycol (PEG) polymers: the effect of PEG size on permeability. *J. Pharm. Sci.* **2009,** *98* (8), 2847-56.
320. Yamaoka, T.; Tabata, Y.; Ikada, Y., Distribution and tissue uptake of poly(ethylene glycol) with different molecular weights after intravenous administration to mice. *J. Pharm. Sci.* **1994,** *83* (4), 601-6.
321. Longley, C. B.; Zhao, H.; Lozanguiez, Y. L.; Conover, C. D., Biodistribution and excretion of radiolabeled 40 kDa polyethylene glycol following intravenous administration in mice. *J. Pharm. Sci.* **2013,** *102* (7), 2362-70.
322. Jilani, T. N.; Jamil, R. T.; Siddiqui, A. H. H1N1 Influenza. https://www.ncbi.nlm.nih.gov/books/NBK513241 (accessed 2022-06-05).
323. Monnery, B. D.; Jerca, V. V.; Sedlacek, O.; Verbraeken, B.; Cavill, R.; Hoogenboom, R., Defined High Molar Mass Poly(2-Oxazoline)s. *Angew. Chem. Int. Ed.* **2018,** *57* (47), 15400-15404.
324. Hauptstein, N.; Pouyan, P.; Wittwer, K.; Cinar, G.; Scherf-Clavel, O.; Raschig, M.; Licha, K.; Lühmann, T.; Nischang, I.; Schubert, U. S.; Pfaller, C. K.; Haag, R.; Meinel, L., Polymer selection impacts the pharmaceutical profile of site-specifically conjugated Interferon-α2a. *J. Controlled Release* **2022,** *348*, 881-892.
325. Kugel, D.; Kochs, G.; Obojes, K.; Roth, J.; Kobinger, G. P.; Kobasa, D.; Haller, O.; Staeheli, P.; Messling, V. v., Intranasal Administration of Alpha Interferon Reduces Seasonal Influenza A Virus Morbidity in Ferrets. *J. Virol.* **2009,** *83* (8), 3843-3851.
326. Meunier, I.; Embury-Hyatt, C.; Stebner, S.; Gray, M.; Bastien, N.; Li, Y.; Plummer, F.; Kobinger, G. P.; von Messling, V., Virulence differences of closely related pandemic 2009 H1N1 isolates correlate with increased inflammatory responses in ferrets. *Virology* **2012,** *422* (1), 125-131.
327. Walz, L.; Kays, S. K.; Zimmer, G.; von Messling, V., Neuraminidase-Inhibiting Antibody Titers Correlate with Protection from Heterologous Influenza Virus Strains of the Same Neuraminidase Subtype. *J. Virol.* **2018,** *92* (17), 1-15.
328. Monnery, B. D.; Jerca, V. V.; Sedlacek, O.; Verbraeken, B.; Cavill, R.; Hoogenboom, R., Defined High Molar Mass Poly(2-Oxazoline)s. *Angew. Chem., Int. Ed.* **2018,** *57* (47), 15400-15404.
329. Braun, A. C.; Gutmann, M.; Mueller, T. D.; Lühmann, T.; Meinel, L., Bioresponsive release of insulin-like growth factor-I from its PEGylated conjugate. *J. Controlled Release* **2018,** *279*, 17-28.
330. Lipiäinen, T.; Peltoniemi, M.; Sarkhel, S.; Yrjönen, T.; Vuorela, H.; Urtti, A.; Juppo, A., Formulation and stability of cytokine therapeutics. *J. Pharm. Sci.* **2015,** *104* (2), 307-26.
331. Alconcel, S. N. S.; Baas, A. S.; Maynard, H. D., FDA-approved poly(ethylene glycol)–protein conjugate drugs. *Polym. Chem.* **2011,** *2* (7), 1442-1448.
332. Zaman, R.; Islam, R. A.; Ibnat, N.; Othman, I.; Zaini, A.; Lee, C. Y.; Chowdhury, E. H., Current strategies in extending half-lives of therapeutic proteins. *J. Controlled Release* **2019,** *301*, 176-189.
333. Cheng, L.; Yang, L.; Meng, F.; Zhong, Z., Protein Nanotherapeutics as an Emerging Modality for Cancer Therapy. *Adv. Healthcare Mater.* **2018,** *7* (20), 1800685.
334. Steinhilber, D.; Witting, M.; Zhang, X.; Staegemann, M.; Paulus, F.; Friess, W.; Küchler, S.; Haag, R., Surfactant free preparation of biodegradable dendritic polyglycerol nanogels by inverse nanoprecipitation for encapsulation and release of pharmaceutical biomacromolecules. *J. Controlled Release* **2013,** *169* (3), 289-295.
335. Turecek, P. L.; Bossard, M. J.; Schoetens, F.; Ivens, I. A., PEGylation of Biopharmaceuticals: A Review of Chemistry and Nonclinical Safety Information of Approved Drugs. *J. Pharm. Sci.* **2016,** *105* (2), 460-475.
336. Kozma, G. T.; Mészáros, T.; Vashegyi, I.; Fülöp, T.; Örfi, E.; Dézsi, L.; Rosivall, L.; Bavli, Y.; Urbanics, R.; Mollnes, T. E.; Barenholz, Y.; Szebeni, J., Pseudo-anaphylaxis to Polyethylene Glycol (PEG)-Coated Liposomes: Roles of Anti-PEG IgM and Complement Activation in a Porcine Model of Human Infusion Reactions. *ACS nano* **2019,** *13* (8), 9315-9324.

337. Mohamed, M.; Abu Lila, A. S.; Shimizu, T.; Alaaeldin, E.; Hussein, A.; Sarhan, H. A.; Szebeni, J.; Ishida, T., PEGylated liposomes: immunological responses. *Sci. Technol. Adv. Mater.* **2019,** *20* (1), 710-724.
338. Castells, M. C.; Phillips, E. J., Maintaining Safety with SARS-CoV-2 Vaccines. *New England Journal of Medicine* **2020,** *384* (7), 643-649.
339. Hoang Thi, T. T.; Pilkington, E. H.; Nguyen, D. H.; Lee, J. S.; Park, K. D.; Truong, N. P., The Importance of Poly(ethylene glycol) Alternatives for Overcoming PEG Immunogenicity in Drug Delivery and Bioconjugation. *Polymers (Basel, Switz.)* **2020,** *12* (2).
340. Kainthan, R. K.; Hester, S. R.; Levin, E.; Devine, D. V.; Brooks, D. E., In vitro biological evaluation of high molecular weight hyperbranched polyglycerols. *Biomaterials* **2007,** *28* (31), 4581-4590.
341. Khandare, J.; Calderón, M.; Dagia, N. M.; Haag, R., Multifunctional dendritic polymers in nanomedicine: opportunities and challenges. *Chem. Soc. Rev.* **2012,** *41* (7), 2824-2848.
342. Deng, Y.; Saucier-Sawyer, J. K.; Hoimes, C. J.; Zhang, J.; Seo, Y.-E.; Andrejecsk, J. W.; Saltzman, W. M., The effect of hyperbranched polyglycerol coatings on drug delivery using degradable polymer nanoparticles. *Biomaterials* **2014,** *35* (24), 6595-6602.
343. Siegers, C.; Biesalski, M.; Haag, R., Self-Assembled Monolayers of Dendritic Polyglycerol Derivatives on Gold That Resist the Adsorption of Proteins. *Chemistry* **2004,** *10* (11), 2831-2838.
344. Zhao, L.; Xu, Y.-H.; Qin, H.; Abe, S.; Akasaka, T.; Chano, T.; Watari, F.; Kimura, T.; Komatsu, N.; Chen, X., Platinum on Nanodiamond: A Promising Prodrug Conjugated with Stealth Polyglycerol, Targeting Peptide and Acid-Responsive Antitumor Drug. *Adv. Funct. Mater.* **2014,** *24* (34), 5348-5357.
345. Luzina, I. G.; Keegan, A. D.; Heller, N. M.; Rook, G. A. W.; Shea-Donohue, T.; Atamas, S. P., Regulation of inflammation by interleukin-4: a review of "alternatives". *J. Leukocyte Biol.* **2012,** *92* (4), 753-764.
346. Molineux, G., The Design and Development of Pegfilgrastim (PEG-rmetHuG-CSF, Neulasta®). *Curr. Pharm. Des.* **2004,** *10* (11), 1235-1244.
347. Lundell, D.; Greenberg, R.; Alroy, Y.; Condon, R.; Fossetta, J. D.; Gewain, K.; Kastelein, R.; Lunn, C. A.; Reim, R.; Shah, C.; van Kimmenade, A.; Narula, S. K., Cytoplasmic and periplasmic expression of a highly basic protein, human interleukin 4, in Escherichia coli. *J. Ind. Microbiol.* **1990,** *5* (4), 215-227.
348. Liebner, R.; Meyer, M.; Hey, T.; Winter, G.; Besheer, A., Head to Head Comparison of the Formulation and Stability of Concentrated Solutions of HESylated versus PEGylated Anakinra. *J. Pharm. Sci.* **2015,** *104* (2), 515-526.
349. Rosen, C. B.; Francis, M. B., Targeting the N terminus for site-selective protein modification. *Nat. Chem. Biol.* **2017,** *13* (7), 697-705.
350. Presolski, S. I.; Hong, V. P.; Finn, M. G., Copper-Catalyzed Azide–Alkyne Click Chemistry for Bioconjugation. *Curr. Protoc. Chem. Biol.* **2011,** *3* (4), 153-162.
351. Grimsley, G. R.; Scholtz, J. M.; Pace, C. N., A summary of the measured pK values of the ionizable groups in folded proteins. *Protein Sci.* **2009,** *18* (1), 247-251.
352. Odom, O. W.; Kudlicki, W.; Kramer, G.; Hardesty, B., An Effect of Polyethylene Glycol 8000 on Protein Mobility in Sodium Dodecyl Sulfate–Polyacrylamide Gel Electrophoresis and a Method for Eliminating This Effect. *Anal. Biochem.* **1997,** *245* (2), 249-252.
353. Hu, J.; Duppatla, V.; Harth, S.; Schmitz, W.; Sebald, W., Site-Specific PEGylation of Bone Morphogenetic Protein-2 Cysteine Analogues. *Bioconjugate Chem.* **2010,** *21* (10), 1762-1772.
354. Park, E. J.; Na, D. H., Optimization of octreotide PEGylation by monitoring with fast reversed-phase high-performance liquid chromatography. *Anal. Biochem.* **2008,** *380* (1), 140-142.
355. Veronese, F. M.; Mero, A.; Caboi, F.; Sergi, M.; Marongiu, C.; Pasut, G., Site-Specific Pegylation of G-CSF by Reversible Denaturation. *Bioconjugate Chem.* **2007,** *18* (6), 1824-1830.
356. Nemzer, L.; Flanders, B.; Schmit, J.; Sorensen, C., Lysozyme Aggregation and Fibrillation Monitored by Dynamic Light Scattering. 2012; Vol. 2012, p H40.004.
357. Daley, K. R.; Kubarych, K. J., An "Iceberg" Coating Preserves Bulk Hydration Dynamics in Aqueous PEG Solutions. *J. Phys. Chem. B* **2017,** *121* (46), 10574-10582.
358. Heeb, L. E. M.; Egholm, C.; Boyman, O., Evolution and function of interleukin-4 receptor signaling in adaptive immunity and neutrophils. *Genes Immun.* **2020,** *21* (3), 143-149.

359. Duppatla, V.; Gjorgjevikj, M.; Schmitz, W.; Hermanns, H. M.; Schäfer, C. M.; Kottmair, M.; Müller, T.; Sebald, W., IL-4 Analogues with Site-Specific Chemical Modification at Position 121 Inhibit IL-4 and IL-13 Biological Activities. *Bioconjugate Chem.* **2014,** *25* (1), 52-62.
360. Viegas, T. X.; Bentley, M. D.; Harris, J. M.; Fang, Z.; Yoon, K.; Dizman, B.; Weimer, R.; Mero, A.; Pasut, G.; Veronese, F. M., Polyoxazoline: Chemistry, Properties, and Applications in Drug Delivery. *Bioconjugate Chem.* **2011,** *22* (5), 976-986.
361. Chae, S. Y.; Choi, Y. G.; Son, S.; Jung, S. Y.; Lee, D. S.; Lee, K. C., The fatty acid conjugated exendin-4 analogs for type 2 antidiabetic therapeutics. *J. Controlled Release* **2010,** *144* (1), 10-16.
362. Jonassen, I.; Havelund, S.; Ribel, U.; Plum, A.; Loftager, M.; Hoeg-Jensen, T.; Volund, A.; Markussen, J., Biochemical and Physiological Properties of a Novel Series of Long-Acting Insulin Analogs Obtained by Acylation with Cholic Acid Derivatives. *Pharm. Res.* **2006,** *23* (1), 49-55.
363. Chuang, Y.-M.; He, L.; Pinn, M. L.; Tsai, Y.-C.; Cheng, M. A.; Farmer, E.; Karakousis, P. C.; Hung, C.-F., Albumin fusion with granulocyte-macrophage colony-stimulating factor acts as an immunotherapy against chronic tuberculosis. *Cell. Mol. Immunol.* **2021,** *18* (10), 2393-2401.
364. Otsuka, H.; Nagasaki, Y.; Kataoka, K., PEGylated nanoparticles for biological and pharmaceutical applications. *Adv. Drug Delivery Rev.* **2003,** *55* (3), 403-419.
365. Han, Y.; Yuan, Z.; Zhang, P.; Jiang, S., Zwitterlation mitigates protein bioactivity loss in vitro over PEGylation. *Chem. Sci.* **2018,** *9* (45), 8561-8566.
366. Keefe, A. J.; Jiang, S., Poly(zwitterionic)protein conjugates offer increased stability without sacrificing binding affinity or bioactivity. *Nat. Chem.* **2012,** *4* (1), 59-63.
367. Shao, Q.; He, Y.; White, A. D.; Jiang, S., Different effects of zwitterion and ethylene glycol on proteins. *J. Chem. Phys.* **2012,** *136* (22), 225101.
368. Prendiville, J.; Thatcher, N.; Lind, M.; McIntosh, R.; Ghosh, A.; Stern, P.; Crowther, D., Recombinant human interleukin-4 (rhu IL-4) administered by the intravenous and subcutaneous routes in patients with advanced cancer—A phase I toxicity study and pharmacokinetic analysis. *Eur. J. Cancer* **1993,** *29* (12), 1700-1707.
369. Li, B.; Yuan, Z.; Hung, H. C.; Ma, J.; Jain, P.; Tsao, C.; Xie, J.; Zhang, P.; Lin, X.; Wu, K.; Jiang, S., Revealing the Immunogenic Risk of Polymers. *Angew. Chem. Int. Ed. Engl.* **2018,** *57* (42), 13873-13876.
370. McCallen, J.; Prybylski, J.; Yang, Q.; Lai, S. K., Cross-Reactivity of Select PEG-Binding Antibodies to Other Polymers Containing a C-C-O Backbone. *ACS Biomater. Sci. Eng.* **2017,** *3* (8), 1605-1615.
371. Fitton A.O., H. J., Jane D.E., Millar R., Synthesis of Simple Oxetanes Carrying Reactive 2-Substituents. *Synthesis* **1987,** *12*, 1140-1142.
372. Weinhart, M.; Grunwald, I.; Wyszogrodzka, M.; Gaetjen, L.; Hartwig, A.; Haag, R., Linear Poly(methyl glycerol) and Linear Polyglycerol as Potent Protein and Cell Resistant Alternatives to Poly(ethylene glycol). *Chem. Asian J.* **2010,** *5* (9), 1992-2000.
373. Pozsgay, V., Synthesis of Glycoconjugate Vaccines against Shigella dysenteriae Type 1. *The Journal of Organic Chemistry* **1998,** *63* (17), 5983-5999.
374. Dong, C.; Fu, T.; Ji, J.; Li, Z.; Gu, Z., The role of interleukin-4 in rheumatic diseases. *Clin Exp Pharmacol Physiol* **2018,** *45* (8), 747-754.
375. Joosten, L. A.; Lubberts, E.; Durez, P.; Helsen, M. M.; Jacobs, M. J.; Goldman, M.; van den Berg, W. B., Role of interleukin-4 and interleukin-10 in murine collagen-induced arthritis. Protective effect of interleukin-4 and interleukin-10 treatment on cartilage destruction. *Arthritis Rheum.* **1997,** *40* (2), 249–260.
376. Veronese, F. M.; Pasut, G., PEGylation, successful approach to drug delivery. *Drug Discovery Today* **2005,** *10* (21), 1451–1458.
377. Dodt, K.; Driessen, M. D.; Lamer, S.; Schlosser, A.; Lühmann, T.; Meinel, L., A Complete and Versatile Protocol: Decoration of Cell-Derived Matrices with Mass-Encoded Peptides for Multiplexed Protease Activity Detection. *ACS Biomater Sci Eng* **2020,** *6* (12), 6598-6617.
378. Dodt, K.; Lamer, S.; Drießen, M.; Bölch, S.; Schlosser, A.; Lühmann, T.; Meinel, L., Mass-Encoded Reporters Reporting Proteolytic Activity from within the Extracellular Matrix. *ACS Biomater. Sci. Eng.* **2020,** *6* (9), 5240-5253.
379. Savoca, M. P.; Tonoli, E.; Atobatele, A. G.; Verderio, E. A. M., Biocatalysis by Transglutaminases: A Review of Biotechnological Applications. *Micromachines (Basel)* **2018,** *9* (11).

380. Früh, S. M.; Spycher, P. R.; Mitsi, M.; Burkhardt, M. A.; Vogel, V.; Schoen, I., Functional modification of fibronectin by N-terminal FXIIIa-mediated transamidation. *ChemBiochem* **2014,** *15* (10), 1481–1486.
381. Hu, B.-H.; Messersmith, P. B., Rational design of transglutaminase substrate peptides for rapid enzymatic formation of hydrogels. *J. Am. Chem. Soc.* **2003,** *125* (47), 14298–14299.
382. Lühmann, T.; Hänseler, P.; Grant, B.; Hall, H., The induction of cell alignment by covalently immobilized gradients of the 6th Ig-like domain of cell adhesion molecule L1 in 3D-fibrin matrices. *Biomaterials* **2009,** *30* (27), 4503-4512.
383. Mosiewicz, K. A.; Kolb, L.; van der Vlies, A. J.; Martino, M. M.; Lienemann, P. S.; Hubbell, J. A.; Ehrbar, M.; Lutolf, M. P., In situ cell manipulation through enzymatic hydrogel photopatterning. *Nat Mater* **2013,** *12* (11), 1072-8.
384. Lorentz, K. M.; Kontos, S.; Frey, P.; Hubbell, J. A., Engineered aprotinin for improved stability of fibrin biomaterials. *Biomaterials* **2011,** *32* (2), 430-8.
385. Zisch, A. H.; Schenk, U.; Schense, J. C.; Sakiyama-Elbert, S. E.; Hubbell, J. A., Covalently conjugated VEGF–fibrin matrices for endothelialization. *J. Controlled Release* **2001,** *72* (1), 101-113.
386. Sato, H.; Ikeda, M.; Suzuki, K.; Hirayama, K., Site-specific modification of interleukin-2 by the combined use of genetic engineering techniques and transglutaminase. *Biochemistry* **1996,** *35* (40), 13072–13080.
387. GRIFFIN, M.; CASADIO, R.; BERGAMINI, C. M., Transglutaminases: Nature's biological glues. *Biochem. J* **2002,** *368* (2), 377-396.
388. Schense, J. C.; Hubbell, J. A., Cross-linking exogenous bifunctional peptides into fibrin gels with factor XIIIa. *Bioconjugate Chem.* **1999,** *10* (1), 75–81.
389. Baumann, A.; Piel, I.; Hucke, F.; Sandmann, S.; Hetzel, T.; Schwarz, T., Pharmacokinetics, excretion, distribution, and metabolism of 60-kDa polyethylene glycol used in BAY 94-9027 in rats and its value for human prediction. *Eur. J. Pharm. Sci.* **2019,** *130*, 11-20.
390. Sellaturay, P.; Nasser, S.; Islam, S.; Gurugama, P.; Ewan, P. W., Polyethylene glycol (PEG) is a cause of anaphylaxis to the Pfizer/BioNTech mRNA COVID-19 vaccine. *Clin Exp Allergy* **2021**.
391. Woodle, M. C.; Engbers, C. M.; Zalipsky, S., New amphipatic polymer-lipid conjugates forming long-circulating reticuloendothelial system-evading liposomes. *Bioconjugate Chem.* **1994,** *5* (6), 493–496.
392. Knop, K.; Hoogenboom, R.; Fischer, D.; Schubert, U. S., Poly(ethylene glycol) in Drug Delivery: Pros and Cons as Well as Potential Alternatives. *Angew. Chem., Int. Ed.* **2010,** *49* (36), 6288-6308.
393. Gaertner, F. C.; Luxenhofer, R.; Blechert, B.; Jordan, R.; Essler, M., Synthesis, biodistribution and excretion of radiolabeled poly(2-alkyl-2-oxazoline)s. *J. Controlled Release* **2007,** *119* (3), 291-300.
394. Sedlacek, O.; Van Driessche, A.; Uvyn, A.; De Geest, B. G.; Hoogenboom, R., Poly(2-methyl-2-oxazoline) conjugates with doxorubicin: From synthesis of high drug loading water-soluble constructs to in vitro anti-cancer properties. *J. Controlled Release* **2020,** *326*, 53-62.
395. Mero, A.; Fang, Z.; Pasut, G.; Veronese, F. M.; Viegas, T. X., Selective conjugation of poly(2-ethyl 2-oxazoline) to granulocyte colony stimulating factor. *J. Controlled Release* **2012,** *159* (3), 353-361.
396. Castells, M. C.; Phillips, E. J., Maintaining Safety with SARS-CoV-2 Vaccines. *N. Engl. J. Med.* **2021,** *384* (7), 643-649.
397. Bivona, L.; Zou, Z.; Stutzman, N.; Sun, P. D., Influence of the second amino acid on recombinant protein expression. *Protein Expression Purif.* **2010,** *74* (2), 248-256.
398. Wingfield, P. T., N-Terminal Methionine Processing. *Curr. Protoc. Protein Sci.* **2017,** *88* (1), 6.14.1-6.14.3.
399. Schneider, C. A.; Rasband, W. S.; Eliceiri, K. W., NIH Image to ImageJ: 25 years of image analysis. *Nat. Methods* **2012,** *9* (7), 671-675.
400. Waterhouse, A.; Bertoni, M.; Bienert, S.; Studer, G.; Tauriello, G.; Gumienny, R.; Heer, F. T.; de Beer, T. A. P.; Rempfer, C.; Bordoli, L.; Lepore, R.; Schwede, T., SWISS-MODEL: homology modelling of protein structures and complexes. *Nucleic Acids Res.* **2018,** *46* (W1), W296-w303.
401. Powers, R.; Garrett, D. S.; March, C. J.; Frieden, E. A.; Gronenborn, A. M.; Clore, G. M., Three-Dimensional Solution Structure of Human Interleukin-4 by Multidimensional Heteronuclear Magnetic Resonance Spectroscopy. *Science* **1992,** *256* (5064), 1673-1677.

402. wyffels, L.; Verbrugghen, T.; Monnery, B. D.; Glassner, M.; Stroobants, S.; Hoogenboom, R.; Staelens, S., μPET imaging of the pharmacokinetic behavior of medium and high molar mass 89Zr-labeled poly(2-ethyl-2-oxazoline) in comparison to poly(ethylene glycol). *J. Controlled Release* **2016,** *235*, 63-71.
403. Lühmann, T.; Spieler, V.; Werner, V.; Ludwig, M.-G.; Fiebig, J.; Mueller, T. D.; Meinel, L., Interleukin-4-Clicked Surfaces Drive M2 Macrophage Polarization. **2016,** *17* (22), 2123–2128.
404. Germershaus, O.; Schultz, I.; Luhmann, T.; Beck-Broichsitter, M.; Hogger, P.; Meinel, L., Insulin-like growth factor-I aerosol formulations for pulmonary delivery. *Eur. J. Pharm. Biopharm.* **2013,** *85* (1), 61-8.
405. Roushan, A.; Wilson, G. M.; Kletter, D.; Sen, K. I.; Tang, W.; Kil, Y. J.; Carlson, E.; Bern, M., Peak Filtering, Peak Annotation, and Wildcard Search for Glycoproteomics. *Mol. Cell. Proteomics* **2021,** *20*, 100011.
406. Simms, D., TRIzol: A new reagent for optimal single-step isolation of RNA. *Focus* **1993,** *4* (15), 532.
407. Roche, Fachinformation Roferon A®, https://www.roche.de/dok/Roferon-reg-A-Fertigspritze-fachinfo-0-na-attach.pdf (accessed january 2022). **2018**.
408. EMA, Plegridy 125 micrograms solution for injection in pre-filled syringe, https://www.ema.europa.eu/en/documents/product-information/plegridy-epar-product-information_en.pdf (accessed january 2022).
409. Schulz, K. S.; Mossman, K. L., Viral Evasion Strategies in Type I IFN Signaling – A Summary of Recent Developments. *Front. Immunol.* **2016,** *7* (498).
410. Gutmann, M.; Braun, A.; Seibel, J.; Lühmann, T., Bioorthogonal Modification of Cell Derived Matrices by Metabolic Glycoengineering. *ACS Biomater. Sci. Eng.* **2018,** *4* (4), 1300-1306.
411. Wang, G.; Hu, J.; Gao, W., Tuning the molecular size of site-specific interferon-polymer conjugate for optimized antitumor efficacy. *Science China Materials* **2017,** *60* (6), 563-570.
412. Shu, J. Y.; Tan, C.; DeGrado, W. F.; Xu, T., New Design of Helix Bundle Peptide−Polymer Conjugates. *Biomacromolecules* **2008,** *9* (8), 2111-2117.
413. Treetharnmathurot, B.; Ovartlarnporn, C.; Wungsintaweekul, J.; Duncan, R.; Wiwattanapatapee, R., Effect of PEG molecular weight and linking chemistry on the biological activity and thermal stability of PEGylated trypsin. *Int. J. Pharm.* **2008,** *357* (1), 252-259.
414. Lawrence, P. B.; Price, J. L., How PEGylation influences protein conformational stability. *Current opinion in chemical biology* **2016,** *34*, 88-94.
415. Lawrence, P. B.; Gavrilov, Y.; Matthews, S. S.; Langlois, M. I.; Shental-Bechor, D.; Greenblatt, H. M.; Pandey, B. K.; Smith, M. S.; Paxman, R.; Torgerson, C. D.; Merrell, J. P.; Ritz, C. C.; Prigozhin, M. B.; Levy, Y.; Price, J. L., Criteria for Selecting PEGylation Sites on Proteins for Higher Thermodynamic and Proteolytic Stability. *J. Am. Chem. Soc.* **2014,** *136* (50), 17547-17560.

Authorship statement

This section contains a list of the individual contribution for each author in percent (%) to the publication(s) reprinted in this thesis titled “Site directed molecular design and performances of Interferon-α2a and Interleukin-4 bioconjugates with PEG alternative polymers”. Unpublished manuscripts are handled, accordingly. All authors are informed and have agreed to their contribution.

1 Title: “*Bioconjugation strategies and clinical implications of Interferon-bioconjugates”*, Niklas Hauptstein (NH), Lorenz Meinel (LM), Tessa Lühmann (TL) journal: European Journal of Pharmaceutics and Biopharmaceutics, year: 2022, volume: 176, pages: 157-167, DOI: 10.1016/j.ejpb.2022.02.006

Autor	NH	LM	TL	Σ (%)
Concept	2	2	2	6
Design of figures	15			15
Literature research	39			39
Publication writing	15	5	10	30
Coordination		3	7	10
	71	10	19	100

2 Title: *"Molecular Insights into Site-Specific Interferon-α2a Bioconjugates Originated from PEG, LPG, and PEtOx"*, Niklas Hauptstein (NH), Paria Pouyan (PP), Josef Kehrein (JK), Michael Dirauf (MD), Marc D. Drießen (MDD) Martina Raschig (MR), Kai Licha (KL), Michael Gottschaldt (MG), Ulrich S. Schubert (US), Rainer Haag (RH), Lorenz Meinel (LM), Christoph Sotriffer (CS), Tessa Lühmann (TL), journal: Biomacromolecules, year: 2021, volume: 22, pages: 4521–4534, DOI: 10.1021/acs.biomac.1c00775

Autor	NH[#]	PP	JK	MD	MDD	MR	KL	MG	US	RH	LM	CS	TL	Σ (%)
Synthesis and characterization (SEC, NMR) of LPG		6												6
Synthesis and characterization (NMR) of PEG		5												5
Synthesis and characterization (SEC, NMR) of PEtOx				5										5
Design and cloning of IFN mutants	1													1
Synthesis and batch release of N^6-((2-azidoethoxy)carbonyl)-L-lysine	0.8					1.2								2
Upstream processing of Interferon-α2a and azide mutants in *E. coli*	8													8
Downstream processing of Interferon-α2a, azide mutants and bioconjugates	10													10
Characterization of Interferon-α2a, azide mutants and bioconjugates (SDS-PAGE, Native-PAGE, CD-Spectroscopy, MALDI-TOF MS, RP-HPLC, DSF, biopotency)	11													11
Thermal stability analysis using *in silico* methods			3											3
Molecular modelling of polymer density hotspots on tested bioconjugates			3											3
Limited Proteolysis Assay development, execution, data analysis and evaluation	3				3									6
Publication writing	7.5	4.5	3	2	2		0.5	0.5	0.5	0.5	1	2	4.5	28.5
Coordination	1						0.5	0.5	0.5	0.5	3.5	0.5	4.5	11.5
	42.3	15.5	9	7	5	1.2	1	1	1	1	4.5	2.5	9	100

[#]Parts of the credited work were already performed during the master thesis of NH. This included the cloning and production of one batch of IFN-α2a WT and IFNK31N_3 on a 500 µg scale. IFNK31N_3 was initially characterized for its suitability using a commercially available DBCO-PEG 10 kDa. IFN-α2a WT and IFNK31N_3 were characterized with CD-spectroscopy and tested on its bioactivity using a Dual-Glo Luciferase assay, that is based on a transient transfection of Huh-7 cells with two reporter plasmids. Additionally, one initial experiment of the LIP assay was performed to test the method. All described protocols were further optimized during the thesis.

3 Title: "Polymer selection impacts the pharmaceutical profile of site specifically conjugated Interferon-α2a", Niklas Hauptstein (NH), Paria Pouyan (PP), Kevin Witwer (KW), Josef Kehrein (JK), Gizem Cinar (GC), Oliver Scherf-Clavel (OC) Martina Raschig (MR), Kai Licha (KL), Tessa Lühmann (TL), Ivo Nischang (IN), Ulrich S. Schubert (US), Christian Pfaller (CP), Rainer Haag (RH), Lorenz Meinel (LM), journal: Journal of Controlled Release, year: 2022, volume: 348, pages: 881-892, DOI: 10.1016/j.jconrel.2022.05.060

Autor	NH	PP	KW	GC	OC	MR	KL	TL	IN	US	CP	RH	LM	Σ (%)
Synthesis and characterization (SEC, NMR) of LPG		12												12
Synthesis and characterization (NMR) of PEG		4												4
Analytical Ultracentrifugation of polymers, proteins and bioconjugates				2					2					4
Upstream processing of Interferon-α2a and mutants	7													7
Downstream processing of Interferon-α2a, azide mutants and bioconjugates	12													12
Synthesis and batch release of N^6-((2-azidoethoxy)carbonyl)-L-lysine	0.2					0.8								1
Characterization of Interferon-α2a, azide mutants and bioconjugates (SDS-PAGE, MALDI-TOF MS, RP-HPLC, DLS, DSF, biopotency)	9.5	0.5												10
Writing of animal testing proposal	0.8		0.4								0.4		0.4	2
Execution of *in vivo* pharmacokinetic study			8											8
ELISA experiments	2													2
Calculation of *in vivo* data and model fitting					1.5									1.5
FACS analysis of murine bone marrow cells by Interferon-α2a			1.5											1.5
Publication writing	9	4	1	2	1		0.5	0.5	0.5	0.5	0.5	0.5	5	25
Coordination	1						0.5	1.5	0.5	0.5	0.5	0.5	5	10
	41.5	20.5	10.9	4	2.5	0.8	1	2	3	1	1.4	1	10.4	100

4 Title: "PEtOxylated Interferon-α2a bioconjugates addressing H1N1 influenza A virus infection", Niklas Hauptstein (NH), Michael Dirauf (MD), Kevin Wittwer (KW), Bevan Sawatsky (BS), Gizem Cinar (GC), Oliver Siering (OS), Oliver Scherf-Clavel (OC), Martina Raschig (MR), Tessa Lühmann (TL), Ivo Nischang (IN), Ulrich S. Schubert (US), Christian Pfaller (CP), Lorenz Meinel (LM), journal: Biomacromolecules, year: 2022, volume: To be determined, pages: to be determined, DOI: 10.1021/acs.biomac.2c00358

Autor	NH	MD	KW	BS	GC	OS	OC	MR	TL	IN	US	CP	LM	Σ (%)
Synthesis and characterization (SEC, NMR, turbidity) of poly(2-ethyl-2-oxazolines)		12												12
AUC and SEC-MALLS of polymers					1.5					1.5				3
Upstream processing of Interferon-α2a and mutants	7													7
Downstream processing of Interferon-α2a, azide mutants and bioconjugates	10													10
Synthesis and batch release of N^6-((2-azidoethoxy)carbonyl)-L-lysine	0.2							0.8						1
Characterization of Interferon-α2a, azide mutants and bioconjugates (SDS-PAGE, RP-HPLC, DSF, biopotency)	12													12
Execution of *in vivo* pharmacokinetic study			5											5
ELISA experiments	1													1
Calculation of *in vivo* data and model fitting							1							1
Execution and analysis of *in vivo* ferret influenza study			4	4		4								12
Publication writing	9	2	0.5	1.5	1.5		1		1	1	0.5	0.5	7	25.5
Coordination	0.8								1.5	0.2	1	1	6	10.5
	40	14	9.5	5.5	3	4	2	0.8	2.5	2.7	1.5	1.5	13	100

5 Title: "Linear Polyglycerol for N-terminal-selective modification of Interleukin-4", Michael Tully (MT), Niklas Hauptstein (NH), Kai Licha (KL), Lorenz Meinel (LM), Tessa Lühmann (TL), Rainer Haag (RH), journal: Journal of pharmaceutical sciences, year: 2021, volume: 111, pages: 1642-1651, DOI: 10.1016/j.xphs.2021.10.032

Autor	MT	NH	KL	LM	TL	RH	Σ (%)
Synthesis of linear aldehyde functionalized polyglycerols	10						10
Synthesis of linear aldehyde functionalized polyethylene glycols	7						7
Upstream processing of Interleukin-4 in *E. coli*		6.5					6.5
Downstream processing of Interleukin-4		12					12
Downstream processing of bioconjugates	5.5						5.5
Characterization of bioconjugates (SDS-PAGE, CD-Spectroscopy, RP-HPLC, DLS, Glu-C digest, MALDI-TOF, SEC-MALLS, biopotency, plasma stability, MST, SPR, Anti-PEG ELISA)	10.5	11.5					22
Publication writing	8	8	1	1	1	7	26
Coordination	1	1	1	1	1	6	11
	42	39	2	2	2	13	100

6 Title: "Chemo-enzymatic PEGylation/ POxylation of murine Interleukin-4", Dorothee Haas (DH), Niklas Hauptstein (NH), Michael Dirauf (MD), Marc D. Driessen (MDD), Matthias Ruopp (MR), Ulrich S. Schubert (US), Tessa Lühmann (TL), Lorenz Meinel (LM), journal: Bioconjugate Chemistry, year: 2022, volume 33, pages: 97–104, DOI: 10.1021/acs.bioconjchem.1c00495

Autor	DH	NH	MD	MDD	MR	US	TL	LM	Σ (%)
Synthesis and characterization of poly(2-ethyl-2-oxazolines)			8						8
Linker peptide synthesis and purification	4								4
Upstream processing of proteins	8								8
Downstream processing of proteins and bioconjugates	16								16
Characterization of proteins and bioconjugates (SDS-PAGE, RP-HPLC, WST-1 assay, macrophage polarization, DSF)	11.5	7.5			1				20
LC MS/MS analysis of peptide conjugation sites				4					4
Publication writing	9	7	3	2.5		0.5	1	7	30
Coordination		1.5				0.5	2	6	10
	48.5	16	11	6.5	1	1	3	13	100

7 Title: "Bioresponsive release of Interferon-α2a by Matrix Metallopeptidase 9 from Extracellular Matrix after Transglutaminase enabled immobilization", Niklas Hauptstein (NH), Benedikt Gantert (BG) Marc D. Driessen (MDD), Tessa Lühmann (TL), Lorenz Meinel (LM), [unpublished]

Autor	NH	BG	MDD	TL	LM	Σ (%)
Gene design and cloning	5					5
Upstream processing of proteins	10					10
Downstream processing of proteins	19					19
Characterization of proteins (MALDI-TOF MS, biopotency, SDS-PAGE)	10					10
Synthesis and purification of model peptide		3				3
Western blotting	5					5
Enzymatic assays inkl. ECM (FXIIIa, MMP-9)	8	2				10
Mass spectrometric analysis			3			3
Scientific writing	15			5	5	25
Coordination	2			4	4	10
	74	5	3	9	9	100

Acknowledgements

First of all, I would like to thank Prof. Dr. Dr. Lorenz Meinel for his constant support and guidance during the 4.5 years of my PhD in his laboratories and research group. He has always supported me and the project with good advice when things went in the wrong direction.

The same gratitude goes to Prof. Dr. Tessa Lühmann as my second supervisor during this time. I have always appreciated the scientific advice and critical discussions during my PhD.

Additionally, I would like to thank all my dear colleagues for their help and support during my time at the institute. A PhD is never a one man show and always relies on the selfless assistance of good colleagues and friends, to support one in times of need.

I am also very grateful to my PhD colleagues Paria Pouyan and Michael Tully from the Free University of Berlin in the group of Prof. Dr. Rainer Haag as well as Michael Dirauf from the Friedrich Schiller University Jena in the group of Prof. Dr. Ulrich S. Schubert, for their supply of excellent polymers in our great collaboration.

I would also like to thank Josef Kehrein and Prof. Dr. Christoph Sotriffer for their collaboration, who have supported our experimental data with their computational analysis and expertise.

I would further like to thank Kevin Wittwer, Oliver Siering, Bevan Sawatsky and Dr. Christian Pfaller from the Paul Ehrlich institute in Langen for their support, time and expertise regarding the animal experiments.

I would additionally like to thank Dr. Andreas Schlosser, Stephanie Lamer (Rudolf Virchow Zentrum, University of Würzburg, Germany), as well as Juliane Adelmann and Antje Gerlinde Heckmann (Institute of Organic Chemistry, University of Würzburg) for their support in mass spectrometry analysis. The same appreciation goes to the groups of Prof. Dr. Schindelin and Prof. Dr. Kisker (Rudolf-Virchow-Zentrum, University of Würzburg, Germany) for their help with thermal shift assays and CD spectroscopy measurements.

At last, I would like to thank my family, especially my wife Julia, who kept me motivated over the years and listened uncomplainingly to all my complaints and sorrows.